

A LIPIDOMICS STUDY OF DIABETIC RETINOPATHY REVEALS A NOVEL ROLE FOR  
FATTY ACID ELONGASE ELOVL4 IN THE MAINTENANCE OF RETINAL VASCULAR  
INTEGRITY

By

Todd A. Lydic

A DISSERTATION

Submitted to  
Michigan State University  
in partial fulfillment of the requirements  
for the degree of

DOCTOR OF PHILOSOPHY

Physiology

2012

## ABSTRACT

### A LIPIDOMICS STUDY OF DIABETIC RETINOPATHY REVEALS A NOVEL ROLE FOR FATTY ACID ELONGASE ELOVL4 IN THE MAINTENANCE OF RETINAL VASCULAR INTEGRITY

By

Todd A. Lydic

Diabetic retinopathy (DR) is a blinding microvascular complication of diabetes mellitus for which no cure or preventative intervention exists. Chronic retinal inflammation is thought to play a major role in the development of diabetic retinal lesions, including endothelial injury and subsequent dysfunction of the blood-retinal barrier. Dyslipidemia is a major complication of diabetes which has been positively associated with the development of DR, yet no potential link between retinal lipid profiles and diabetes induced retinal vascular degeneration has been explored. We developed a mass spectrometry based lipidomics platform suitable for sensitive analysis and structural elucidation of diverse classes of complex retinal lipid species, and applied this lipidomics approach to the study of diabetic animal models to identify novel pathways involved in the development of diabetic retinal lesions. Lipidomics analysis of retina lipids in a streptozotocin (STZ) rat model of type 1 diabetes revealed multiple aberrations of retinal lipid metabolism at both early (six weeks) and late (36 weeks) time points of experimental diabetes. Dysregulated lipid metabolism in diabetic retina included a significant decrease in retinal glycerophospholipid polyunsaturated fatty acid (PUFA) content, including decreased docosahexaenoic acid (DHA, 22:6n3) and 32:6n3 very long chain PUFA (VLCPUFA). Investigation of the potential mechanisms of altered retinal lipid profiles in diabetes led to the

novel finding that diabetes decreases the expression of several retinal fatty acid elongases, including dramatic downregulation of the most abundant retinal elongase, elongation of very long chain fatty acids 4 (ELOVL4). The alteration of rat retina elongases and glycerophospholipid content was coupled with increased retinal gene expression of inflammatory markers including pro-inflammatory cytokines and intracellular adhesion molecule-1 (ICAM-1).

Decreased ELOVL4 expression or function has been associated with multiple retinal disorders, including blood-retinal barrier breakdown, in animal and human studies. This led us to hypothesize that ELOVL4 modulates diabetes-induced retinal vascular degeneration. The exact role of ELOVL4 in fatty acid synthesis has remained nebulous; however, ELOVL4 has been suggested to produce VLCPUFA. Using an adenovirus and capsid-modified Adeno-Associated Virus serotype 2 (AAV2) to overexpress ELOVL4 in human retinal pigment epithelial (RPE) and human retinal endothelial cell (HREC) culture models of the blood-retinal barrier, we found that ELOVL4 did not affect glycerophospholipid VLCPUFA content. Instead, ELOVL4 increased levels of saturated C26 fatty acids incorporated into ceramide while decreasing shorter chain ceramides in these cells. Altered sphingolipid content by ELOVL4 decreased RPE cell activation in response to stimulation by the pro-inflammatory cytokine IL-1 $\beta$ . Intravitreal delivery of ELOVL4-AAV2 to retinas of STZ diabetic rats reduced retinal vascular activation, blunted diabetes-induced retinal vascular permeability, and increased endothelial expression of blood-retinal barrier components despite having no mitigating effect on retinal inflammation. Taken together these data indicate that ELOVL4 prevents early stage vascular degeneration in diabetic retina through modulation of sphingolipid metabolism. Retinal delivery of ELOVL4 by AAV2 vectors may represent an effective intervention to prevent early vascular lesions of DR.

## DEDICATION

This dissertation is dedicated to Erin, Dylan, and Colin. Without you none of this would have been possible, and this dissertation would probably not have been attempted.

Or drooled on.

Or invaded by birds, bugs, and squirrels. Or stolen out of our driveway. Or severely dislocated twice. Or operated on to repair an old volleyball injury. Or found in the backyard with all of those socks. Or anxiously headed back to the hospital for the 100<sup>th</sup> time. Or lost somewhere in the Atlanta airport. Or forced to say goodbye to far too many people forever. Or taken on a bus, then a train, then a plane, then another plane, then a boat, and then another boat. Or tested the limits of Benadryl. Or bared witness to the growth of the Urban Family. Or gained three nieces. Or missed all of those Masters classes because you fell asleep rocking the baby again. Or developed a very strong preference for giving birth at a particular time in August. Or taught how to put on a diaper, then immediately left for the first class of Biochem 801. Or fallen asleep during 5 hour physiology 827 exams at night. Or been accused of being at the bar, rather than taking a 5 hour physiology 827 exam at night. Or been trapped on the floor of a small cramped room for four hours waiting for D to fall asleep. Or gained expertise about dinosaurs. Or put off in favor of playing with trains. Or T-ball. Or puzzles. Or stories. Or bouncing. This dissertation has seen a lot. Thank you for being there through it all.

As promised, the word “nefarious” appears in here somewhere. So does a reference to a dinosaur. You are going to have to look for them, though.

## ACKNOWLEDGEMENTS

It would be impossible to spend four-plus years doing something as challenging, fun, and crazy as this undertaking has been without compiling a huge list of people who deserve to be thanked for helping me out in one way or another. First and foremost I would like to thank my Advisor Extraordinaire Dr. Julia Busik. The fact that I am working on a dissertation right now is due in large part to her refusal to take “no” or “absolutely not” or “I just found a job after two years of searching and now you want me to QUIT?!?!” for an answer. Since the day I swallowed hard and enrolled in the doctoral program, she has been unfailing in her support, available at any time, and willing to help with an amazing array of issues. I have learned as much about life and parenting from her as I have about science, and I will be grateful to her for the rest of my life- which is fitting, since she played as large a role as anyone in changing the course of my life. As modest thanks I have included the word “complimentary” once in this dissertation. She’s going to have to look for it, though.

I would like to thank the members of my thesis committee: Dr. Karl Olson, Dr. Nara Parameswaran, Dr. Ron Meyer, Dr. Walter Esselman, and Dr. Gavin Reid. I appreciate the guidance, advice, and constructive criticism they have passed along over the course of committee meetings, classes, and talks during chance meetings in the hallway. Thank you for taking time out of your busy schedules to listen to my weird ideas about lipids, and to help me learn how to be critical of my own weird ideas.

I owe a special debt of gratitude to Dr. Gavin Reid, as my project literally would not have been possible without his willingness (and the required patience) to teach a biologist how to

navigate the world of bioanalytical chemistry. He also had the inexplicable willingness to let me grind up animal parts and shoot them into his half-million dollar mass spectrometers just to see what we would find. I pretty much lived in his lab for a couple of years while he taught me everything I know about mass spectrometry and lipidomics analysis. I will benefit from that experience forever.

I would also like to thank Dr. Walter Esselman for hiring me into Julia's lab six years ago to do some "lipid stuff." Look how that turned out! Since then, he has always taken the time to stop and talk and give his advice even though he is constantly pulled in 1000 different directions. He also has the uncanny ability to get straight to the heart of an idea and I learn something every time I talk to him.

Dr. Susanne Mohr has been a great lab neighbor and I have learned a lot from her about That Other Metabolic Disturbance in diabetes, as well as about how to present ideas in a useful way that doesn't confuse everybody. She has also been great to my kids, and Dylan still associates her with Gummi Bears.

I have been fortunate during this whole experience to work with a great group of people. Svetlana Bozack has selflessly helped out in so many ways I can't even name them all. When designing experiments, the number one parameter I usually considered was "what would be the least annoying to Svetlana?" because she does so much for all of us. As the person seated next to me in the lab, she also took the brunt of my venting and she always had something helpful to say or some sound advice to give. Maria Tikhonenko has been a great friend, and it was nice to have someone to suffer through those classes with. She also put up with my endless teasing about Russia and was more than willing to dish it back. Madalina Opreanu, Qi Wang, and Harshini

Chakravarthy all made the lab fun and were always willing to help when asked. I am also especially grateful to Kelly McSorely and Matt Faber. Kelly worked tirelessly on the projects during the early part of my work and was kind enough to listen to my insane rantings every day before politely saying “okay I should probably get back to work now.” She became a great friend. Good luck being a Veterinarian to the Stars, Kelly! Similarly, Matt helped me out on the work that became the last chapter in my dissertation, and he threw himself into it impressively. He is a great guy and a tireless worker, and I would STILL be doing experiments if not for him. I’m also a little bit astonished that he and Svetlana and I got through that whole final animal study as smoothly as we did, which is a testament to both of them. Good luck in med school, Matt!

## TABLE OF CONTENTS

<b>LIST OF TABLES</b>	<b>xiv</b>
<b>LIST OF FIGURES</b>	<b>xvi</b>
<b>LIST OF ABBREVIATIONS</b>	<b>xix</b>
<b>I. LITERATURE REVIEW</b>	<b>1</b>
1.1 Diabetes Mellitus	1
1.1.1 Overview	1
1.1.2 Societal impact	2
1.2 Diabetic retinopathy: Clinical aspects	3
1.2.1 Overview	3
1.2.2 Clinical presentation of DR	3
1.2.3 Current treatments	4
1.3 Diabetic retinopathy: Insights from animal models	6
1.3.1 Animal models of DR	6
1.3.2 Blood-retinal barrier dysfunction in diabetic retinopathy	7
1.3.3 Inflammation and diabetic retinopathy	11
1.4 Dyslipidemia	14
1.4.1 Overview	14
1.4.2 Fatty acid remodelling in dyslipidemia	16
1.5 Lipid metabolism in the retina	18
1.5.1 Overview	18
1.5.2 Fatty acid elongase ELOVL4	19
1.5.3 Very long chain saturated and monounsaturated fatty acids	22

1.5.4 Very long chain polyunsaturated fatty acids	23
1.5.5 Pathology of excess very long chain fatty acids	24
1.6 Enhanced methods for lipid analysis	25
1.6.1 Limitations of traditional methods of lipid analysis	25
1.6.2 Lipidomics	26
1.7 Objectives and hypothesis of dissertation	29
1.8 Overview of chapters	34
1.9 References	36

## **II. GLOBAL ANALYSIS OF RETINA LIPIDS BY COMPLEMENTARY PRECURSOR ION AND NEUTRAL LOSS MODE TANDEM MASS SPECTROMETRY** **51**

2.1 Abstract	51
2.2 Introduction	51
2.3 Results	54
2.3.1 Mass spectrum of a rat retina lipid extract	54
2.3.2 Complementary sets of precursor ion and neutral loss scans for global lipid Analysis	56
2.3.3 Complementary precursor ion and neutral loss scan mode analysis of rat retina SM and GPCho lipids	56
2.3.4 Complementary precursor ion and neutral loss scan mode analysis of rat retina GPEtn and GPIIns lipids	64
2.3.5 Complementary precursor ion and neutral loss scan mode analysis of rat retina GPSer lipids	67
2.3.6 Complementary neutral loss scan mode analysis of rat retina DG/TG lipids	71
2.4 Discussion	73
2.5 Conclusions	77
2.6 References	101

**III. ANALYSIS OF RETINA AND ERYTHROCYTE GLYCEROPHOSPHOLIPID ALTERATIONS IN A RAT MODEL OF TYPE 1 DIABETES 106**

3.1 Abstract	106
3.2 Introduction	107
3.3 Results	113
3.3.1 Analysis of GPCho lipids in retina and erythrocytes at 6 weeks of diabetes	113
3.3.2 Analysis of GPEtn lipids in retina and erythrocytes at 6 weeks of diabetes	116
3.3.3 Analysis of GPSer and GPIIns lipids in retina and erythrocytes at 6 weeks of diabetes	118
3.3.4 Analysis of GPCho and GPEtn lipids in retina and erythrocytes at 36 weeks of diabetes	119
3.3.5 Analysis of Amadori-GPEtn lipids in retina and erythrocytes at 36 weeks of diabetes	123
3.4 Discussion	123
3.5 Conclusions	124
3.6 References	147

**IV. REMODELING OF RETINAL FATTY ACIDS IN AN ANIMAL MODEL OF DIABETES: A DECREASE IN LONG CHAIN POLYUNSATURATED FATTY ACIDS IS ASSOCIATED WITH A DECREASE IN ELONGASES ELOVL2 AND ELOVL4 155**

4.1 Abstract	155
4.2 Introduction	156
4.3 Results	158
4.3.1 Body weight gain and blood glucose concentration of experimental animals	158
4.3.2 Elongase and desaturase expression level in control and diabetic animals	158
4.3.3 Plasma fatty acid profiles of control and diabetic animals	159

4.3.4 Liver fatty acid profiles of control and diabetic animals	159
4.3.5 Retinal fatty acid profiles of control and diabetic animals	160
4.3.6 Retinal and erythrocyte phospholipid profiles of control and diabetic animals	160
4.3.7 Inflammatory marker expression in control and diabetic retinas	161
4.4 Discussion	161

**V. INTRAVITREAL DELIVERY OF FATTY ACID ELONGASE ELOVL4 PREVENTS RETINAL VASCULAR DEGENERATION IN DIABETES THROUGH MODULATION OF SPHINGOLIPID METABOLISM** **182**

5.1 Abstract	182
5.2 Introduction	184
5.3 Results	187
5.3.1 Overexpression of ELOVL4 mitigates IL-1 $\beta$ induced activation of retinal pigment epithelial cells	187
5.3.2 ELOVL4 does not mediate phospholipid VLCPUFA incorporation in RPE cells	188
5.3.3 ELOVL4 mediates C26:0 ceramide production in cells of the blood-retinal barrier	189
5.3.4 AAV2-mediated expression of ELOVL4 in diabetic rat retina	190
5.3.5 Retinal vascular expression of ELOVL4 does not affect retinal lipid profile	191
5.3.6 Retinal delivery of ELOVL4 prevents blood-retinal barrier dysfunction in diabetic animals	191
5.3.7 Retinal delivery of ELOVL4 reduces markers of vascular activation, but not retinal inflammation	192
5.3.8 Retinal delivery of ELOVL4 alters expression of vascular tight junction components	193
5.3.9 Retinal delivery of ELOVL4 decreases caveolin-1 expression	194

5.4 Discussion	195
5.5 Conclusions	198
5.6 References	216
<b>VI. METHODS</b>	<b>224</b>
6.1 Materials and reagents	224
6.2 Methods	224
6.2.1 Culture of HREC and RPE cells	224
6.2.2 Animals and Induction of STZ diabetes	224
6.2.3 Fatty acid composition of the animal diet	225
6.2.4 Isolation of rat retina	226
6.2.5 RNA extraction	226
6.2.6 Quantitative real time PCR and primers used in these studies	226
6.2.7 Western blot analysis	228
6.2.8 Lipid extraction from retina	228
6.2.9 Lipid extraction from liver and plasma	229
6.2.10 Lipid extraction from erythrocytes	229
6.2.11 Lipid extraction from cultured cells	230
6.2.12 Mass spectrometry conditions for lipid analysis	231
6.2.13 Identification of lipid molecular species by mass spectrometry	232
6.2.14 Quantitation of lipid molecular species by tandem mass spectrometry	232
6.2.15 Analysis of saponified fatty acids by RP-HPLC	234
6.2.16 Viral Vectors	235
6.2.17 Adenoviral infections in RPE cells	236

6.2.18 hELOVL4-AAV2 mut quad infections in HREC	236
6.2.19 Fatty acid treatments in cultured cells	236
6.2.20 IL-1 $\beta$ treatment in RPE cells	237
6.2.21 Intravitreal injection of AAV2 mut quad vectors in diabetic rats	237
6.2.22 Assessment of retinal vascular permeability	238
6.2.23 Retinal histology and immunohistochemistry	239
6.2.24 Statistical analysis	239
6.3 References	241
<b>VII. CONCLUSIONS AND FUTURE PERSPECTIVES</b>	<b>243</b>
7.1 Conclusions	243
7.2 Future perspectives	248

## LIST OF TABLES

<b>Table 2.1.</b> Description of the precursor ion and neutral loss scan mode MS/MS experiments employed for the class-specific identification of lipid molecular species	78
<b>Table 2.2.</b> Rat retina SM and GPCho molecular species	81
<b>Table 2.3.</b> Rat retina GPEtn species detected by complementary positive and negative ion mode MS/MS analysis	84
<b>Table 2.4.</b> Rat retina GPIns species detected by complementary positive and negative ion mode MS/MS analysis	86
<b>Table 2.5.</b> Rat retina GPSer molecular species detected by complementary positive and negative ion mode MS/MS analysis	87
<b>Table 2.6.</b> Rat retina DG and TG molecular species detected as $[M+NH_4]^+$ ions	89
<b>Table 4.1.</b> Body weight gain and blood glucose concentrations of experimental animals	167
<b>Table 4.2.</b> Plasma fatty acid profiles of control and diabetic animals	168
<b>Table 4.3.</b> Liver fatty acid profiles of control and diabetic animals	169
<b>Table 4.4.</b> Retinal fatty acid profiles of control and diabetic animals	170



## LIST OF FIGURES

Figure 1.1. Broad objectives and initial guiding hypothesis of the dissertation	32
Figure 1.2. The proposed role of fatty acid elongase ELOVL4 in diabetic retinopathy	33
Figure 2.1. Full mass spectra of rat retina lipids	92
Figure 2.2. Negative ion mode analysis of GPCho and SM	93
Figure 2.3 Complementary negative ion mode MS/MS analysis of rat retina SM and GPCho species	94
Figure 2.4 Positive ion mode analysis of GPCho and SM	95
Figure 2.5. Complementary positive ion mode MS/MS analysis of rat retina SM and GPCho species	96
Figure 2.6. Complementary positive and negative ion mode MS/MS analysis of rat retina GPEtn and GPIIns species	97
Figure 2.7. Product ion mode MS/MS spectrum of synthetic GPSer(14:0/14:0) [M+H] <sup>+</sup> ions	98
Figure 2.8. Complementary positive and negative ion mode MS/MS analysis of rat retina GPSer species	99

Figure 2.9. Complementary positive ion mode MS/MS analysis of rat retina DG and TG species	100
Figure 3.1. Positive ion mode nESI-MS/MS analysis of GPCho in retina and erythrocytes at 6 weeks of diabetes	126
Figure 3.2. Ratiometric GPCho analysis in retina and erythrocytes at 6 weeks of diabetes	130
Figure 3.3. Ratiometric GPEtn analysis in retina and erythrocytes at 6 weeks of diabetes	131
Figure 3.4. Ratiometric GPSer analysis in retina and erythrocytes at 6 weeks of diabetes	134
Figure 3.5. Ratiometric GPIns analysis in retina and erythrocytes at 6 weeks of diabetes	136
Figure 3.6. Ratiometric GPCho analysis in retina at 36 weeks of diabetes, with or without an internal standard	138
Figure 3.7. Ratiometric GPCho analysis in erythrocytes at 36 weeks of diabetes, with or without an internal standard	140
Figure 3.8. Ratiometric GPEtn analysis in retina and erythrocytes at 36 weeks of diabetes with or without an internal standard	122
Figure 3.9. Positive ion mode nESI-MS/MS analysis of GPEtn and Amadori-GPEtn lipids in retina at 36 weeks of diabetes	142
Figure 3.10. Ratiometric Amadori-GPEtn analysis in retina and erythrocytes at 36 weeks of diabetes	146
Figure 4.1. <i>De novo</i> lipogenesis and polyunsaturated fatty acid remodeling pathways	171

Figure 4.2. Expression levels of elongases and desaturases in retinas and livers of control and diabetic animals	172
Figure 4.3. Retina fatty acid analysis by RP-HPLC and tandem mass spectrometry analysis of GPCho lipids in retina and erythrocytes at 3-6 weeks of diabetes	174
Figure 4.4. Expression levels of inflammatory markers in retinas of control and diabetic animals	176
Figure 5.1. Inverse relationship of ELOVL4 expression and cellular activation in RPE cells	201
Figure 5.2. Comparison of GPCho species containing VLCPUFA in retina and RPE cells	204
Figure 5.3. Biochemical function of ELOVL4 in cells of the blood-retinal barrier	205
Figure 5.4. Localization of AAV2 mut quad in diabetic retinas	209
Figure 5.5. hELOVL4 increases very long chain ceramide in diabetic retina	210
Figure 5.6. Expression levels of inflammatory markers in retinas of control and diabetic animals	211
Figure 5.7. Expression levels of blood-retinal barrier components in retinas of control and diabetic animals	213
Figure 5.8. Expression levels of transcellular transport components in retinas of control and diabetic animals	215

## LIST OF ABBREVIATIONS

AD	adenovirus
AAV	adeno-associated virus
ALA	alpha-linolenic acid, an 18:3n3 fatty acid
ASM	acid sphingomyelinase
BHT	butylated hydroxyl toluene
BRB	blood-retinal barrier
BSA	bovine serum albumin
BBZDR	Bio-Breeding Zucker diabetic rat
CBV	choroidal blood vessels
CER	ceramide
CMV	cytomegalovirus
DG	diglyceride
DR	diabetic retinopathy
DHA	docosahexaenoic acid, a 22:6n3 fatty acid
DPA	docosapentaenoic acid, a 22:5n3 fatty acid
ELOVL	elongation of very long chain fatty acids
ELSD	evaporative light scattering detection
EPA	eicosapentaenoic acid, a 20:5n3 fatty acid
ESAM	endothelial cell-specific adhesion molecule

ESI	electrospray ionization
FITC	fluorescein isothiocyanate
GCL	ganglion cell layer
GFP	green fluorescent protein
GPCho	glycerophosphocholine
GPEtn	glycerophosphoethanolamine
GPIIns	glycerophosphoinositol
GPSer	glycerophosphoserine
HPLC	high performance liquid chromatography
HREC	human retinal endothelial cells
IL-	interleukin-
IDL	intermediate density lipoprotein
INL	inner nuclear layer
IPL	inner plexiform layer
ICAM-1	intracellular adhesion molecule-1
LDL	low density lipoprotein
MS	Mass spectrometry or mass spectrum
MOI	multiplicity of infection
MS/MS	tandem mass spectrometry

MALDI	matrix-assisted laser desorption ionization
MUFA	monounsaturated fatty acid
n3	omega-3
n6	omega-6
NOD	non-obese diabetic
nESI	nano-electrospray ionization
NFκB	nuclear factor κB
ONL	outer nuclear layer
OPL	outer plexiform layer
PBS	phosphate buffered saline
POS	photoreceptor outer segments
PPAR	peroxisome proliferator-activated receptor
PUFA	polyunsaturated fatty acid (C22 or less)
qPCR	quantitative real time polymerase chain reaction
RP	reverse phase
RAGE	receptor for advanced glycation end products
RPE	retinal pigment epithelial cells
SM	sphingomyelin
STZ	streptozotocin

STGD3	Stargardt-like macular dystrophy
TG	triglyceride
TNF	tumor necrosis factor
T.REX	tyrannosaurus rex
UV	ultraviolet
VE-	vascular endothelila
VAMP	vesicle associated membrane protein
VEGF	vascular endothelial growth factor
VLDL	very low density lipoprotein
VCAM-1	vascular cell adhesion molecule-1
VLCPUFA	very long chain polyunsaturated fatty acid (>C22)
ZO-1	zonula occludens-1

## *1.1 Diabetes Mellitus*

### **1.1.1 Overview**

Diabetes mellitus is a disease characterized by insufficient insulin secretion or insulin action which results in chronically elevated blood glucose levels (hyperglycemia), with concomitant defects in the metabolism of carbohydrates, proteins, and fats (1). The American Diabetes Association defines diabetes as a fasting plasma glucose concentration greater than or equal to 126 mg/dL (or 7.0 mmol/L) (2). Depending on the nature of the central insulin defect, diabetes mellitus is commonly categorized as either type 1 or type 2. Type 1 diabetes is an autoimmune disease directed against the insulin producing beta cells located in the pancreatic islets of Langerhans, leading to progressive loss of both beta cells and insulin secretion (3). T-cells specific for beta cell antigens are currently thought to be the primary culprit driving beta cell loss in type 1 diabetes (4). The onset of type 1 diabetes usually occurs before adulthood, and insulin injections are typically required to manage hyperglycemia and prolong lifespan in type 1 diabetic patients (5). Type 1 accounts for approximately 10% of all cases of diabetes worldwide (6).

Type 2 diabetes is characterized by inadequate insulin action, notably diminished insulin-stimulated disposal of glucose in skeletal muscle and decreased suppression of hepatic glucose production, termed insulin resistance (6). Insulin resistance causes chronic hyperglycemia in type 2 diabetes, and beta cell dysfunction subsequently renders the body unable to compensate for increased glucose load (6). Although causes of Type 2 diabetes are likely multifactorial (6-8),

disease onset typically occurs in adults and is usually associated with obesity and inactive lifestyle (8). Type 2 accounts for nearly 90% of all cases of diabetes worldwide (6).

### **1.1.2 Societal impact**

Approximately 285 million people were diagnosed with either type 1 or type 2 diabetes in 2010, the last year for which data are available, and the number of expected total cases is anticipated to grow to 438 million by 2030 (9). The United States Centers for Disease Control and Prevention estimates that in 2010, approximately 26 million Americans had some form of diabetes with nearly 80 million additional adults at risk of developing the disease (10). Thus the number of Americans with diabetes has the potential to increase very rapidly.

Diabetes is associated with significant personal costs such as decreased quality of life and lost income due to increased absence from work (10), as well as extensive health care costs incurred while managing the disease over the course of decades of life. Such costs, along with the considerable morbidity and mortality which accompany diabetes, are related to the development of diabetic complications. These complications can be generalized as macrovascular or microvascular in nature. Macrovascular complications include stroke, coronary artery disease, and peripheral artery disease, while microvascular complications comprise retinopathy, nephropathy, and neuropathy (9). In 2007, expenditures for the treatment of diabetes and all related complications accounted for one out of every ten dollars spent on healthcare in the United States, as costs associated with both type 1 and type 2 diabetes totaled more than \$174 billion (10). Clearly, the impending increase in total cases of diabetes and its complications will

have serious ramifications on the future allocation of health care resources nationally and globally.

## *1.2 Diabetic Retinopathy: Clinical Aspects*

### **1.2.1 Overview**

Diabetic retinopathy (DR) is a nefarious complication of diabetes that can lead to impaired vision or total blindness and decreased quality of life. Evidence of DR is present in 65% of all type 1 and type 2 diabetic patients after 10 years of disease (11). The risk of developing DR increases with increasing duration of diabetes (11), therefore the aging of recently diagnosed diabetic patients coupled with the anticipated boom in new diabetes diagnosis is expected to cause a significant expansion of the number of cases of DR over the next few decades. At present diabetic retinopathy is already the leading cause of blindness and visual impairment in the global population of working-age adults (12). Currently there is no cure or effective preventative strategy.

### **1.2.2 Clinical presentation of DR**

Diabetic retinopathy has been classically defined as a neovascular disease of the retina. In early stage (background) DR, apoptosis of endothelial cells within retinal capillaries leads to formation of degenerate non-perfused acellular capillaries, causing downstream tissue anoxia that drives subsequent pathologic neovascularization during late stage (proliferative) DR (12).

Blindness subsequently arises from proliferative vessel growth or the leakage of blood into the field of vision and/or vitreous (12). Additionally, nascent blood vessels may grow into the vitreous and cause a significant degree of traction, resulting in complete retinal detachment (13). The initial stages of DR are diagnosed clinically by the appearance of retinal blood vessel microaneurysms and hemorrhages, as well as local points of retinal ischemia (12). Diabetes also induces noticeable changes in retinal blood vessel calibre, resulting in smaller retinal arterioles and venules (14). Chronic diabetes causes some structural changes in the retinal capillaries of nearly all patients with disease duration of more than 15 years (15).

Structural alterations to the retinal blood vessels induced by diabetes may also lead to diabetic macular edema, a thickening of the macula which results in decreased visual acuity and loss of central vision (16). Clinically significant macular edema occurs when retinal thickening occurs close to or within the central macula (17), which comprises the highest density of cone photoreceptors found in the retina (12). Macular edema that arises from blood vessel microaneurysms is termed focal diabetic macular edema, while diffuse diabetic macular edema is due to dysfunction of the blood–retinal barrier (16). Macular edema occurs more frequently in type 2 diabetes than in type 1 diabetes, while type 1 diabetes is associated with a higher incidence of proliferative diabetic retinopathy (13). However, proliferative diabetic retinopathy in type 2 diabetes almost always presents concomitantly with macular edema (13).

### **1.2.3 Current Treatments**

Tight control of blood glucose levels (acetylated hemoglobin < 7%) has emerged as a standard paradigm for preventing the onset and progression of diabetic retinopathy (13).

However, achieving such a level of blood glucose management often proves difficult therapeutically, and in many cases fails to prevent retinopathy altogether. Laser photocoagulation is currently the primary treatment for both proliferative diabetic retinopathy and diabetic macular edema (18). However, laser photocoagulation often fails to prevent further vision loss (13), and the treatment itself results in reduced color vision, visual field, and contrast sensitivity due to destruction of retinal tissue (12; 13).

Recently a new class of drug has become available for treatment of proliferative DR and diabetic macular edema. Multiple anti-vascular endothelial growth factor (VEGF) antibodies, including Bevacizumab and ranibizumab, are now available to block VEGF-mediated induction of blood vessel permeability and retinal neovascularization (16). Unfortunately, anti-VEGF therapies require frequent injections into the eye, leading to high costs, significant pain for the patient, and occasionally ocular hypertension (16; 19). Importantly, inhibition of VEGF may slow retinopathy progression, but does not always prevent eventual retinal neovascularization (20). Moreover, the ratio of VEGF to other growth factors including connective tissue growth factor may be critical to promoting pro-angiogenic conditions in the retina (21). Patients receiving intravitreal injections of anti-VEGF agents have been reported to have increased levels of retinal fibrosis due in part to the altered balance of VEGF and connective tissue growth factor (21). Given the limited treatment options for diabetic retinopathy, the identification of novel preventative strategies which mitigate the appearance of clinical symptoms of DR is imperative.

### *1.3 Diabetic retinopathy: Insights from animal models*

#### **1.3.1 Animal models of DR**

Due to the duration of time needed to evaluate the onset of human diabetic complications, and therefore the effectiveness of potential interventions, animal models of diabetes play an essential role in advancing knowledge of the progression of DR. Type 1 diabetic rat models, particularly those induced chemically by streptozotocin (STZ) or alloxan, are among the most commonly used animal models of diabetic retinopathy. Genetic models include spontaneous autoimmune diabetic rats such as BBDP/Wor, originally derived in Worcester, MA, (22) and non-obese diabetic (NOD) mice. All of these rodent models exhibit loss of pancreatic beta cells and subsequent hyperglycemia, and typically develop both macrovascular and microvascular complications (22). There are, however, important limitations of these models as they relate to human type 1 diabetes. Chemically induced type 1 diabetic rodent models fail to mimic the autoimmune response that ultimately drives beta cell destruction in humans, while development of diabetes in NOD mice strictly requires the absence of immune stimulation by foreign pathogens (22). Spontaneous autoimmune rats have now been derived from numerous colonies originating in locations other than Worcester, MA, and some studies have suggested that comparisons across colonies cannot be made due to genetic and phenotypic differences (23).

Among the most popular rat model of type 2 diabetes is the inbred Bio-Breeding Zucker diabetic (BBZDR)/Wor rat. These obese animals spontaneously develop diabetes at 70-80 days of age (24). Similarly, db/db (leptin receptor mutation) and ob/ob (leptin gene mutation) mice exhibit obesity that predisposes them to type 2 diabetes (25). While many aspects of these models closely resemble accelerated human type 2 diabetes, it should be noted that mouse models in particular do not share all aspects of islet pathology observed in humans (25). Additionally, BBZDR/Wor rats must be maintained on a diet containing n3 polyunsaturated fatty

acid (PUFA)-rich fish oil for a considerable length of time to prevent death of the animals at 6 to 8 months of age, limiting their utility in studies of lipid metabolism.

Importantly, neither type 1 nor type 2 diabetic animals live long enough to develop advanced proliferative (late stage) retinopathy, restricting their collective use to investigations of early stages of DR. However, it has been shown that these animals accurately model many cellular processes characteristic of early retinopathy seen in human diabetic patients, including the formation of nonperfused acellular retinal capillaries (26-28) after 6-9 months of diabetes. The formation of acellular retinal capillaries is now considered to be a hallmark of retinopathy in animal models, and quantitation of these degenerate capillaries is often used as a readout for the effects of diabetes and potential interventions (29). Together these animal models have led to the discovery of most of the known pathogenesis and associated features of diabetic retinopathy (30-33) including the early stage breakdown of the blood-retinal barrier, and the potential role of inflammation in the development of diabetic retinal lesions.

### **1.3.2 Blood-retinal barrier dysfunction in diabetic retinopathy**

Normal functioning of the retina is absolutely dependent on a selective diffusion barrier to separate retinal neurons, glia, and microglia from the systemic circulation. Disruption of vascular barrier function is associated with many neovascular diseases (34), and increased blood vessel permeability may be a key step in the initiation of new vessel growth (35). Moreover, nascent blood vessels formed during pathological tissue neovascularization in humans and animal models of accelerated retinal vessel growth also typically exhibit increased permeability due to decreased vascular barrier function (35). In the retina, separate barriers exist at each of

two distinct blood supplies. The outer blood-retinal barrier (BRB) consists only of tight junctions between retinal pigmented epithelial (RPE) cells, and regulates delivery of nutrients from the fenestrated choroidal blood vessels to the retinal photoreceptors (36). The inner BRB consists of both tight junctions and adherens junctions between adjacent endothelial cells of the retinal blood vessels which emerge from the optic disc to provide nutrients to the inner retinal cell layers (37). Interlinked junctional structures between adjacent endothelial cells greatly restrict the paracellular flow of water, lipids, proteins, and leukocytes into the retina (38; 39). The inner barrier receives perivascular support from retinal pericytes, Müller glial cells, and astrocytes, which form physical contacts with the retinal vasculature and may secrete barrier-inducing factors that upregulate junctional proteins (37). Investigations of the regulation of endothelial barrier formation, and subsequent breakdown of the blood-brain barrier in models of ischemic stroke, implicate sphingolipid metabolites as key barrier-inducing signals (40).

In addition to regulating paracellular flux, the BRB also tightly controls transcellular movement of solutes and macromolecules in part by regulation of caveolae (20). Caveolae are invaginations of the cell membrane which are enriched in the structural protein caveolin-1, cholesterol, sphingolipids, and phospholipids containing esterified saturated fatty acids, rendering them biochemically distinct from the remainder of the cell membrane (41). Caveolae of the retinal vascular endothelium serve as important sites of vesicle-mediated uptake of proteins and lipids (20). Accordingly, strict control of the quantity of these membrane microdomains may contribute to BRB regulation of transcellular permeability (20). Interestingly, membrane microdomains with lipid composition similar to caveolae (collectively termed ‘lipid rafts’) have also been shown to play key roles in the organization of both transcellular transport

proteins and tight junction proteins in brain microvascular endothelial cells (41). However, the potential contribution of lipids to retinal barrier function has not been addressed.

Cultured monolayers of retinal endothelial or pigmented epithelial cells serve as established *in vitro* models the inner and outer BRB, respectively (42). Growth of cells on porous transwell inserts creates upper and lower chambers in each cell culture well, enabling use of a voltmeter/ohmmeter for measurement of transendothelial or transepithelial resistance as an indicator of barrier integrity (36). Alternatively, the passage of a labelled macromolecule, such as fluorescent fluorescein isothiocyanate (FITC)-dextran, through the monolayer may be used to assess BRB properties (42). Measurement of BRB integrity *in vivo* is typically achieved by injection of a labelled marker, such as FITC-albumin or Evans blue dye, into the blood of an animal model of interest (43). After allowing for sufficient circulation of the labelled marker, the animal is perfused and the retina is isolated for quantitation of marker leakage into the retinal tissue relative to circulation time and plasma marker content (43).

Outer blood-retinal barrier breakdown is associated with choroidal neovascularization in the “wet” form of age-related macular degeneration (44), and the outer barrier may be impaired in diabetes as well (45). Numerous studies have indicated that retinas of diabetic animal models primarily exhibit increased vascular permeability due to dysfunction of the inner BRB, which precedes death of vascular endothelial cells and acellular capillary formation (34; 42; 43; 46). Assessment of vascular barrier function in diabetic retina may therefore be utilized as an early indicator of endothelial injury. Retinas of diabetic rats exhibit dysregulated vascular expression and altered localization of the tight junction associated protein occludin, which may directly increase paracellular permeability in the vascular endothelium (47). In addition to occludin, decreased mRNA and/or protein levels of other endothelial tight junction components including

claudin-5 and zonula occludens (ZO)-1 and -2 have been observed in diabetic rat retina (46; 48). Vascular endothelial (ve)-cadherin, a major structural protein of endothelial adherens junctions, undergoes increased tyrosine phosphorylation and subsequent turnover in early stages of experimental diabetes (42). Multiple studies have indicated that increased retinal VEGF-associated signaling in diabetic retina may account for decreased occludin and ve-cadherin levels and function (34; 49), and increased retinal levels of pro-inflammatory cytokines may be partly responsible for negative regulation of other junctional components as well (34). Together these findings indicate that diabetes compromises regulation of paracellular solute movement through the inner blood-retinal barrier.

Increased expression of transcellular transport components may also contribute to greater transcellular permeability in diabetic retina. Streptozotocin diabetic rats exhibit up to a 3-fold increase in the retinal expression of caveolin-1 and associated vesicular transport proteins between 6 weeks and 12 weeks of diabetes (48). In an oxygen-induced (nondiabetic) retinopathy mouse model of retinal neovascularization, increased caveolin-1 expression was also observed in hyperpermeable newly formed blood vessels (20). siRNA knockdown of caveolin-1 reduced vascular leakage by 56%, with a concomitant reduction in new vessel growth of 51% (20). Conversely, complete ablation of caveolae in caveolin-1 knockout mice has also been associated with increased vascular permeability and adhesion of the retina to the retinal pigmented epithelium (50). Together these findings imply that tight control of transcellular permeability is critical for normal retinal function, and dysregulation of caveolae constituents may contribute to early diabetic retinal pathology.

Diabetic patients presenting with diffuse macular edema due to impaired vascular barrier function do not always progress to proliferative DR. This implies that BRB breakdown is not

necessarily sufficient to drive retinal neovascularization in humans, although it may predispose patients to higher risk of tissue neovascularization (45). While most investigations of BRB failure in diabetic animal models have focused on increased paracellular permeability, diabetes-induced changes in hemodynamic factors could affect *in vivo* measurements of retinal vascular permeability. For example, increased capillary pressure or blood flow could lead to increased retinal accumulation of a labeled marker injected into the systemic circulation and lead to the appearance of increased vascular permeability in the presence of an intact barrier (51). Yet overall, studies from diabetic animal models have consistently shown altered expression of vascular barrier components that are consistent with increased paracellular and/or transcellular permeability. These molecular changes to blood-retinal barrier components imply that early endothelial damage occurs well before apoptosis of endothelial cells, and the subsequent formation of degenerate acellular capillaries.

### **1.3.3 Inflammation and diabetic retinopathy**

Early stage diabetic retinopathy exhibits characteristics of a low-grade chronic inflammatory disease (52-60). Diabetes increases retinal expression of numerous cytokines and growth factors including interleukin-1 (IL-1) $\beta$ , IL-6, tumor necrosis factor (TNF)- $\alpha$ , and vascular endothelial growth factor (VEGF) (61). Cytokines and VEGF directly upregulate vascular cell adhesion molecule-1 (VCAM-1) in cultured human retinal endothelial cells (HREC) via nuclear translocation of the nuclear factor  $\kappa$ B (NF $\kappa$ B) transcription factor, which is widely known to play a role in inflammatory signaling (62; 63). Cytokines have also been shown to upregulate intracellular adhesion molecule-1 (ICAM-1) in multiple retinal cell types (27), and both VCAM-

1 and ICAM-1 are upregulated in diabetic retinas (56). Diabetes-induced upregulation of ICAM-1 and VCAM-1 in retina contributes to leukocyte adhesion to the retinal vasculature (56). In turn, leukocyte adhesion may facilitate vessel occlusion and transmigration of leukocytes through the endothelium and into the retinal tissue, potentially promoting endothelial cell injury, apoptosis, and nonperfusion of affected capillaries (27; 53; 55; 57; 58; 60). Thus retinal inflammation, particularly upregulated levels of cytokines and VEGF, is thought to be a primary instigator of blood-retinal barrier dysfunction (34).

Sources of retinal pro-inflammatory factors at the onset of DR, as well as their respective mechanisms of action, are an area of ongoing research. NF $\kappa$ B and other transcription factors including specificity protein 1, hypoxia inducible factor 1- $\beta$ , and activator protein 1 may all contribute to increased transcription of various inflammatory mediators including inducible nitric oxide synthase, cyclooxygenase 2, receptor for advanced glycation end products (RAGE), and numerous cytokines and growth factors (27; 64). In Müller glial cells, activation of caspase-1 in response to hyperglycemia is known to drive production of the pro-inflammatory cytokine IL-1 $\beta$  (65), and hyperglycemia in general is thought to drive production of many retinal cytokines (12). VEGF is also secreted by Müller cells, as well as retinal pericytes and ganglion cells (27). Knockdown of many of these pro-inflammatory proteins, cytokines, and growth factors by pathway specific (i.e., cyclooxygenase-2 or VEGF) inhibitors (27; 66) or by administration of broad spectrum anti-inflammatory agents such as aspirin (26) or minocycline (65) have yielded decreases in degenerate capillary formation in diabetic animal models.

Several of the enzymes that have been shown to promote retinal inflammation, such as inducible nitric oxide synthase, as well as receptors for cytokines and growth factors upregulated in diabetic retina, are localized to endothelial cell caveolae (41; 67). Acid sphingomyelinase

(ASM), an enzyme that hydrolyzes cell membrane sphingomyelin to produce ceramide in response to many stress stimuli, is also localized to sphingomyelin-rich caveolae in endothelial cells (68). Many studies indicate that turnover of sphingomyelin to generate large ceramide-rich microdomains by activated ASM may be a critical factor for receptor clustering and signal propagation during inflammatory cytokine signaling (69-71). Moreover, altered sphingolipid turnover has been found to play a central role in diabetes induced loss of retinal vascular endothelial cells and ganglion cells (29; 72). Collectively these data indicate that propagation of diverse inflammatory signals in diabetic retina may depend on altered sphingolipid metabolism, and implicate caveolae as potentially important sites for inflammatory signal transduction.

However, elevated levels of circulating cytokines found in conditions such as obesity (73) are not sufficient to cause retinal degeneration and proliferative neovascularization in the absence of overt diabetes. Despite the efficacy of aspirin and other anti-inflammatory agents for prevention of diabetic retinal lesions in both animal models and small-scale human studies (27; 74), the largest study to date that assessed the ability of aspirin to improve retinopathy outcomes found that a daily regimen of 650 mg had no effect on the development of retinal microaneurysms relative to placebo in a group of 3711 diabetes patients (74). These data could indicate that inflammation alone may not be sufficient or absolutely required for the development of diabetic retinal vascular lesions, or that local factors in the retinal tissue are of greater importance than systemic pro-inflammatory factors. However, it is unclear whether the dose of aspirin used in the aforementioned trial was sufficient to produce the intended anti-inflammatory effect in the retina.

Interestingly, a mouse model utilizing endothelium-specific knockout of platelet-derived growth factor-B, a growth factor that supports capillary pericytes, exhibited retinal capillary

occlusion and acellular capillary formation that mimicked diabetic retinal lesions that correlated with the extent of pericyte loss (75). These animals also showed initial signs of proliferative new blood vessel growth (75). This indicates that perhaps changes in growth factor levels are sufficient to drive diabetic retinal lesions independent of retinal inflammation. Similarly, decreased levels of nerve growth factor have been observed in STZ diabetic rat retinas, and treatment of diabetic rats with nerve growth factor over the course of 14 weeks reduced loss of retinal ganglion cells and Müller cells, and prevented loss of retinal pericytes and the formation of degenerate acellular capillaries (15). While markers of inflammation were not assessed in this study, the data indicates that altering levels of retinal trophic factors could be sufficient to prevent early stage retinal vascular damage. Yet taken as whole, a preponderance of data gathered from animal models of DR suggests a role for diabetes-induced retinal inflammation in the onset and progression of retinopathy, despite the existence of some evidence to the contrary.

## *1.4 Dyslipidemia*

### **1.4.1 Overview**

The initiating events that promote retinal sequelae such as inflammation and BRB dysfunction in diabetic retinopathy are likely to stem from hyperglycemia and dyslipidemia that constitute two major metabolic abnormalities of diabetes mellitus. The role of hyperglycemia in the development of retinal inflammation and DR has been very well illustrated over decades of research, as reviewed in (12; 76). Nevertheless, to date no effective cure or preventative strategy for DR exists. Because the potential effects of diabetic dyslipidemia on retinal degeneration have not been explored in detail, lipid metabolism in diabetic retina merits further study.

Dyslipidemia is a broadly defined term generally applied to abnormalities of circulating lipid levels. Altered serum lipid profiles have been tied to the development of macrovascular and microvascular complications in both type 1 and type 2 diabetes (77-79). However, the presentation of dyslipidemia in patients with type 1 diabetes typically differs from those with type 2 diabetes. In type 1 diabetes that is tightly controlled by insulin therapy, patients exhibit plasma levels of cholesterol, free fatty acids, and triglycerides that are equal to, or even slightly decreased from, levels of nondiabetic subjects (78). Yet type 1 diabetes leads to increased Apo B lipoprotein content, as well as smaller, denser, pro-atherogenic low density lipoprotein (LDL) particles than control subjects (78) regardless of insulin therapy. Additionally, the presence of confounding poor insulin management of hyperglycemia in type 1 diabetes leads to overall increases in total serum cholesterol and LDL cholesterol, and a decrease in the ratio of high density lipoprotein (HDL) to LDL relative to control subjects (78). In a study of serum lipid profiles in a large cohort of patients with type 1 diabetes, the severity of diabetic retinopathy was correlated with increased triglyceride levels within the cohort, and even stronger correlations were found between retinopathy progression and decreased diameter of very low density lipoprotein (VLDL), LDL and HDL particles (77).

In type 2 diabetes, dyslipidemia typically develops prior to the appearance of overt diabetes, following the onset of insulin resistance (80). An insulin resistant state promotes dyslipidemia in the form of elevated total free fatty acids, total cholesterol and triglycerides, and decreased HDL cholesterol (81). A decrease in the diameter and increase in density of serum LDL cholesterol is also present in type 2 diabetes (81). The Fenofibrate Intervention and Event Lowering in Diabetes (FIELD) trial measured the ability of the lipid-lowering drug fenofibrate to decrease both macrovascular and microvascular events in type 2 diabetic patients with well-

managed blood glucose levels (average 6.9% acetylated haemoglobin) (82). While fenofibrate exhibits pleiotropic effects (83; 84), it acts in part by reducing serum triglyceride levels 20-30% while increasing levels of HDL by up to 10% (79). Use of fenofibrate in the FIELD study reduced the need for laser photocoagulation treatment for diabetic retinopathy by 37%, with a reduction of 31% in the need for first time laser treatment (79). While the underlying mechanism(s) remain uncertain, it is clear that dyslipidemia is strongly correlated with the onset and progression of diabetic retinopathy in both type 1 and type 2 diabetes.

#### **1.4.2 Fatty acid remodeling in dyslipidemia.**

Increased content of shorter (less elongated), more saturated fatty acid chains has been associated with decreased diameter and increased density of serum lipoprotein particles; conversely, increased content of longer chain, polyunsaturated fatty acids increases lipoprotein diameter and decreases density (85-87). Evidence of altered elongation or desaturation of serum fatty acids has been observed in both type 1 and type 2 diabetic patients (88; 89). Elongation and desaturation (remodeling) of fatty acids produced *de novo* or obtained from the diet is achieved by a group of enzymes acting in close physical proximity in the endoplasmic reticulum, termed fatty acid elongases and desaturases, respectively. It has been previously demonstrated that diabetes results in dysregulated desaturase activity (90-92). Stearoyl-CoA (SCD) and fatty acid desaturase (FAD) enzymes catalyze the introduction of fatty acid double bonds (desaturation) to acyl-CoA chains in a cytochrome b5 and cytochrome b5 reductase-dependent mechanism (93). Several recent studies indicate that diabetes also dysregulates elongase expression and activity

(94-98), although to date the role of elongases in diabetes and diabetic complications has received relatively little attention.

The seven known fatty acid elongases are designated *elongation of very long chain fatty acids* (ELOVL) 1-7 (93). Elongases perform the rate-limiting NADPH dependent condensation step of fatty acid elongation to extend a fatty acyl-CoA chain by two carbon units, utilizing malonyl-CoA as a carbon source (99). Elongases are physically associated with the enzymes 3-ketoacyl-CoA reductase, 3-hydroxyacyl-CoA dehydratase, and trans-2,3,-enoyl-CoA reductase, which complete the necessary dehydration and NADPH-dependent reductions of the elongated fatty acyl-CoA, suggesting that these enzymes exist as an elongation complex *in vivo* (100). Co-immunoprecipitation studies indicate that most elongases form additional physical interactions with other elongases (100), although the biochemical consequences of putative elongase hetero-oligomerization has not been elucidated. Moreover, certain elongases may directly interact with, and be regulated by, individual ceramide synthase enzymes, indicating that newly elongated fatty acids may be shuttled directly into sphingolipid metabolites (101; 102). Direct coordination of elongase activity and sphingolipid metabolism to date has been suggested for ELOVL1 and ELOVL4, via interaction with ceramide synthases 2 and 3 respectively (101; 102). While saturated fatty acids and monounsaturated fatty acids (MUFA) may be elongated through the action of several elongases in series, flux of PUFA into the fatty acid remodeling (Sprecher) pathway is gated by desaturase activity, necessitating coordination of the elongation and desaturation processes. Given the multifaceted nature of mammalian fatty acid remodeling and its association with the production of more complex membrane lipid species, any perturbation of the system by diabetes would be expected to impart wide-ranging consequences on systemic or tissue-specific lipid profiles.

## 1.5 Lipid Metabolism in the Retina

### 1.5.1 Overview

The retina is uniquely dependent on robust lipid metabolism to maintain proper function. Relative to other tissues, the retina is highly enriched in both omega-6 (n6) and omega-3 (n3) PUFA, especially arachidonic acid (ARA, 20:4n6) and docosahexaenoic acid (DHA, 22:6n3) (103-105). Retina also contains the highest concentration of very long chain polyunsaturated fatty acids (VLCPUFA), ranging in length from 28-36 carbons, found in the body (106), although VLCPUFA represent a relatively small proportion of total retina fatty acids. To date, VLCPUFA have been shown to be exclusively incorporated in retinal phosphatidylcholine, although indirect evidence suggests VLCPUFA may also partition into complex carbohydrate-bearing sphingolipids such as gangliosides (106). Additionally, retina also contains unique very long chain saturated and monounsaturated fatty acids (VLCFA) ranging in length from 26 to 30 carbons incorporated into sphingolipids including ceramide and gangliosides (106).

Alterations in retinal lipid metabolism have now been associated with visual impairment in several retinal disorders including diabetes (29; 72) age-related macular degeneration (107), Stargardt-like macular dystrophy (108), glaucoma (109), and Smith-Lemli-Opitz syndrome (110). Retina obtains fatty acids via *de novo* lipogenesis (111), uptake from the systemic circulation (112), and through elongation and desaturation of dietary precursor fatty acids (113). Elongation and desaturation is known to occur in endothelial cells of the retinal vasculature (114), retinal pigmented epithelial cells (113), ganglion cells and photoreceptor cell bodies (108). Uptake of dietary fatty acids as well as transport of newly synthesized or remodeled fatty acids

and other lipids between disparate retinal tissue layers requires proper functioning of the intra-retinal lipid transport system (115), which uses HDL-based particles as retinal lipid shuttles. Disruption of endogenous cholesterol metabolism, as occurs in Smith-Lemli-Opitz syndrome, leads to visual deficits associated with decreased retinal polyunsaturated fatty acid levels (110), which may be due in part to disrupted intra-retinal lipid transport. Retinal function absolutely requires all facets of lipid metabolism and transport to work in concert. Therefore the altered lipoprotein density and lipid content, HDL/LDL ratio, hypercholesterolemia, and reduced fatty acid remodeling that constitute diabetic dyslipidemia may be expected to have pronounced effects on retinal lipid composition and, subsequently, retinal physiology.

### **1.5.2 Fatty acid elongase ELOVL4**

Elongation of very long chain fatty acids 4 (ELOVL4) is the most highly expressed fatty acid elongase in the retina (116). Of the elongases, ELOVL4 remains among the least studied in terms of its biochemistry and role in mammalian physiology. ELOVL4 exhibits fairly broad tissue distribution, with highest levels reported in retina, thymus, brain, testes, and skin, and relatively lower expression detected in pancreas, skeletal muscle, heart, lymph node, spleen, small intestine, colon, prostate, placenta, and ovary (101; 116-118). No expression of ELOVL4 has been detected in liver (117). In retina, ELOVL4 protein has been detected in all tissue layers in neonatal mice (119), while in adult mammals, ELOVL4 protein was previously reported to primarily localize to mouse retina photoreceptor cell bodies, with moderate localization to the ganglion cell layer (108; 116). However, recent studies in porcine retina (120) have shown strongest ELOVL4 expression in the ganglion cell layer (adjacent to retinal capillaries) and inner nuclear layer, with lesser expression of ELOVL4 in photoreceptors. Factors that control

ELOVL4 expression have not been thoroughly evaluated, although positive regulation of ELOVL4 by the vitamin D receptor and its coactivators Steroid Receptor Coactivator (SRC) 1 and SRC2 has been demonstrated in human epidermal keratinocytes (121).

Several dominant-negative mutations in the human *ELOVL4* gene have been identified as sufficient to cause Stargardt-like macular dystrophy (STGD3), a juvenile-onset form of macular degeneration that leads to blindness (116; 122; 123). Homozygous *Elovl4* loss-of-function mice exhibit neonatal lethality, confounding attempts to discern the physiological and pathological functions of ELOVL4 (124). Several heterozygous mouse knock-in models of STGD3 have been developed carrying various dominant negative alleles of human *ELOVL4* variants under the control of photoreceptor-specific promoters, several of which exhibited truncated and mislocalized ELOVL4 protein leading to endoplasmic reticulum stress (108). Moreover, *ELOVL4* transgenic mice exhibit accumulation of the fluorophore A2E to toxic levels, abnormal electroretinogram responses, and progressive loss of rod and cone photoreceptors similar to that observed in STGD3 and the dry form of age-related macular degeneration (123; 125; 126). Retinal degeneration was independent of retinal DHA(22:6n3) content in ELOVL4 transgenic animals, and DHA(22:6n3) supplementation did not prevent pathology (127).

Knowledge of the fatty acid products of ELOVL4 has remained elusive and obfuscated by conflicting data obtained in a variety of systems. ELOVL4 was previously thought to play a role in the synthesis of PUFA (128). *ELOVL4* knock-in mouse models exhibited diverse fatty acid deficiency phenotypes, including reduced retinal C16-C24 fatty acids, (125) reduced retinal C18-C24 unsaturated and polyunsaturated fatty acids, (126) and reduced levels of retinal phosphatidylcholine containing omega-3 C32-C36 VLCPUFA (129). However, recent experiments utilizing siRNA knockdown of ELOVL4 in a retinal neuronal cell line revealed no

role for ELOVL4 in the metabolism of C20 and C22 fatty acids, including 22:6n3 (130). Conversely, introduction of ELOVL4 to yeast lead to accumulation of C22 saturated fatty acids, while ELOVL4 expression in Chinese hamster ovary cells had no discernible effect on fatty acid metabolism (131). A recent study in which mouse ELOVL4 was over expressed in cardiomyocytes provided evidence that ELOVL4 participates in the synthesis of very long chain C28 saturated and polyunsaturated fatty acids, and is likely to be involved in the synthesis of >C28 VLCPUFA (108). However, *in vitro* biochemical elongation assays performed with ELOVL4-enriched microsomes and controlled introduction of acyl-CoA substrates suggest that ELOVL4 is most efficient at elongating C24 saturated fatty acids to form C26 products, with lesser activity toward the elongation of C26 fatty acids to form C28 products (101); production of >C28 fatty acids was not verified. In subsequent studies, it has been shown that ELOVL4 does not directly bind 20:5n3 (100), which has been demonstrated to be the optimal substrate for VLCPUFA formation (132). Moreover, fatty acid elongase ELOVL2 expression has been determined to control levels of 28:5n6 and 30:5n6 VLCPUFA in testes independent of ELOVL4, despite robust levels of ELOVL4 in testes (133). Thus it is conceivable that VLCPUFA synthesis requires ELOVL2 activity upstream of ELOVL4, and ELOVL4 function may vary depending on the tissue or cellular context. As ELOVL4 is the most abundant retinal elongase, any diabetes-induced alterations in ELOVL4 function could be expected to impart a diverse array of retinal lipid phenotypes.

Since the original identification of dominant negative ELOVL4 mutations as causative for Stargardt-like macular dystrophy, recent reports have associated ELOVL4 with other retinal disorders as well. Interestingly, decreased retinal expression of ELOVL4 was associated with retinal vascular degeneration due to ischemia-reperfusion injury in mice (134), indicating that

ELOVL4 fatty acid products may effect retinal vascular homeostasis. Additionally, decreased VLCPUFA were associated with impaired vision due to aging and age-related macular degeneration in post-mortem human retinas (135), possibly implicating decreased ELOVL4 function. Reduction of VLCPUFA has also been observed in one mouse model of STGD3 retinal degeneration in the absence of the endoplasmic reticulum stress response and ELOVL4 protein mislocalization and aggregation observed in most models of STGD3, indicating that a decrease in ELOVL4 function may be causative for blindness (129). Based on these recent data, it is conceivable that ELOVL4 plays an important role in maintaining retinal homeostasis.

### **1.5.3 Very long chain saturated and monounsaturated fatty acids**

The physiological roles of many important lipids found in the retina, particularly PUFA such as DHA and ARA, have been thoroughly studied and are reviewed in (105; 107). However, the physiological roles of putative ELOVL4 products such as very long chain saturated and monounsaturated fatty acids greater than 24 carbons in length, have received virtually no attention in retina. Yet, the essential function of these unique fatty acids has been fairly well described in the skin. Lipid vesicles secreted by differentiated epidermal keratinocytes form “lipid sheet” structures in the stratum corneum, the outer layer of the epidermis (136; 137). These lipid sheets play a critical role in preventing water infiltration and infection by pathogens (121). Epidermal lipid sheets primarily contain free fatty acids, cholesterol, and ceramide species containing fatty acids ranging in length from 26 carbons to >30 carbons (121). Production of lipid sheets begins in the stratum granulosum with the synthesis of precursor lipids including glucosylceramide and sphingomyelin, which contain very long chain saturated or

monounsaturated fatty acids derived from elongases ELOVL3 and ELOVL4 (121). Glucosylceramide and sphingomyelin are then respectively hydrolyzed in the stratum corneum by  $\beta$ -glucocerebrosidase and acid sphingomyelinase or neutral sphingomyelinase to give rise to ceramides enriched in very long chain fatty acids (121). Accordingly, dysfunction of the epidermal permeability barrier has been observed upon inhibition or genetic ablation of elongases ELOVL3 and ELOVL4, or the enzymes involved in sphingolipid production and turnover (102; 121; 136; 137). Importantly, recently published data demonstrated that skin-specific normalization of ELOVL4 levels in homozygous *Elovl4* knockout mice restored normal skin barrier function in tandem with increased levels of ceramide containing C28-C36 fatty acids (138), enabling several weeks of post-natal survival.

#### **1.5.4 Very long chain polyunsaturated fatty acids**

As described above, ELOVL4 has also been implicated in the synthesis of C28-C32 VLCPUFA, and this is thought to be its primary function in the retina (129; 139). Extant data concerning possible physiological roles of any PUFA greater than 22 carbons in length is extremely limited, and the function of these unique fatty acids in the retina is not known. One of the few studies to address a possible *in vivo* action of >C22 PUFA demonstrated that purified 24:6n3, which undergoes peroxisomal retroconversion to DHA(22:6n3) in mammals (140), was approximately equal in potency to DHA(22:6n3) in blocking leukotriene and histamine production in mouse mast cells (141). A separate study revealed that radiolabeled C26 very long chain PUFA injected into rat brain undergo both chain elongation and peroxisomal beta-oxidation, with subsequent formation of C22 and C24 PUFA, in addition to >C26 PUFA (142).

An evaluation of omega-6 VLCPUFA found in the brain addressed the ability of C20-C30 n6 PUFA to elicit calcium mobilization in human neutrophils (143). It was determined that the ability to induce calcium mobilization first declined with increasing fatty acid length beyond 20 carbons (i.e., 20:4n6), and then eventually increased as fatty acid length reached 30 carbons (i.e., 30:4n6) (143). Together, these results imply that VLCPUFA may be capable of participating in cell signaling or other physiological processes similar to those described for other PUFA, and could potentially serve as substrates for peroxisome-mediated retroconversion to shorter chain PUFA. As described above, the depletion of retinal VLCPUFA in Stargardt-like macular dystrophy may be sufficient to cause retinal dysfunction and photoreceptor degeneration even in the absence of mislocalized ELOVL4 protein (129), implying that VLCPUFA may be vital for photoreceptor viability. In addition to retina, VLCPUFA are normally found as N-linked constituents of sphingolipids, particularly sphingomyelin, in testes and sperm (102). Depletion of VLCPUFA in testes by disruption of sphingolipid metabolism or ELOVL2 leads to extremely impaired fertility in mice (102; 133; 144), indicating that VLCPUFA are critical for male reproductive function. Although no mechanistic understanding or direct proof of causality has been provided by these initial reports, it is clear that very long chain polyunsaturated fatty acids warrant further study as potential participants in diverse physiological processes.

### **1.5.5 Pathology of excess very long chain fatty acids**

While reductions in both saturated and polyunsaturated very long chain fatty acids have been associated with specific pathologies, increases in the levels these low abundance fatty acids above normal physiological levels have also been implicated in disease. Peroxisomal disorders

are marked by elevated levels of very long chain fatty acids in the blood and central nervous system (131; 145), as peroxisomal beta-oxidation normally degrades fatty acids greater than 18 carbons in length (140). X-linked (or childhood) adrenoleukodystrophy (ALD) is a rare demyelinating disorder which is characterized by progressive central nervous system failure, ataxia, visual deficits, and eventual death before the third decade of life (131). Increases in serum levels of 26:0 fatty acids are associated with disease progression, and elevated levels of 26:0 fatty acids may drive plaque formation in cerebral white matter by increasing 5-LOX mediated inflammatory signaling (146) . In a separate study that sought to identify the fatty acid elongase responsible for very long chain fatty acid production in ALD, elongase ELOVL1 was found to synthesize both saturated and monounsaturated C26 fatty acids based on studies of orthologous elongase expression in yeast and Chinese hamster ovary cells (131). Overall, it is clear that while tissue and serum very long chain fatty acids are normally maintained at very low concentrations, deviations from normal physiological levels in either the positive or negative direction may have severe pathological consequences.

## *1.6 Enhanced methods for retinal lipidome analysis*

### **1.6.1 Limitations of traditional methods of lipid analysis**

Given the potential breadth of lipid abnormalities diabetes could be expected to impose on the retina, the selected method for analysis of retinal lipid metabolism should be capable of providing readouts across a diverse group of chemically dissimilar lipids, while maximizing the amount of information contained within those readouts. Traditionally the analysis of intact complex lipids has been accomplished by thin layer chromatography (147), which typically

provides information pertaining only to the total abundances of particular lipid classes without facile means of positively identifying the lipids to be quantitated. High performance liquid chromatography (HPLC) and gas chromatography-mass spectrometry (GC-MS) have enabled the identification and quantification of fatty acid species from total cell or tissue lipid extracts, following the liberation of fatty acid constituents of complex lipids by saponification or trans-methylation, respectively (94; 135). HPLC typically enables analysis of saponified fatty acids up to 24 carbons in length, but longer chain fatty acids require separation as transmethylated derivatives by GC-MS (135). Neither method, however, provides direct information as to the identities of the complex lipid species from which the fatty acids were liberated. And despite the applicability of GC-MS to the analysis of a larger range of fatty acids than HPLC, the relatively poor sensitivity of this method typically precludes detailed fatty acid analysis from a single rodent retina. Importantly, the isolation of fatty acids for use in HPLC or GC-MS analysis by saponification or trans-methylation typically fails to liberate amide-linked fatty acids of sphingolipid species (106), limiting the utility of these methods to the study of phospholipid or neutral lipid-derived fatty acids.

### **1.6.2 Lipidomics**

Alternatively, recently developed “lipidomics” approaches to lipid analysis have enabled the simultaneous monitoring of hundreds of chemically diverse lipid metabolites with greatly improved sensitivity relative to traditional methods. Utilizing a broad range of mass spectrometry platforms, lipidomics facilitates the identification of lipid “molecular species” comprising unique combinations of fatty acids, typically linked to a lipid backbone, as well as a

headgroup in the case of polar lipids. Lipidomics approaches often allow the investigator to identify each component of a given lipid molecular species (148). Therefore, in addition to greatly enhanced analytical sensitivity (149; 150), the potential power of lipidomics lies in the amount of information contained in identified molecular species, as an individual lipid molecular species necessarily represents the convergence of multiple pathways involved in lipid headgroup and backbone synthesis, fatty acid *de novo* biosynthesis, fatty acid desaturation and elongation, esterification of fatty acids to lipid backbones, and potentially lipase-mediated cleavage of fatty acids (151). Comparison of lipid molecular species across tissues, biological treatments, or disease states may therefore elucidate underlying pathways of lipid metabolism associated with the phenomenon of interest.

Recently, electrospray ionization (ESI) and matrix assisted laser desorption/ionization (MALDI) techniques coupled with high-resolution mass spectrometry (MS) analysis have emerged as valuable tools to rapidly identify differences between the abundances of individual lipid molecular species within complex lipid mixtures extracted from limited quantities of sample tissue in different physiological or disease states (152-154). However, the resolution and mass accuracy obtainable from many mass spectrometry platforms precludes the unambiguous identification or characterization of individual lipid species with the same nominal masses, on the basis of their masses alone. Furthermore, numerous lipid species have isobaric masses that can all be present at a given  $m/z$  value, thereby limiting the general utility of this approach. Finally, the presence of many classes of low abundance lipid species, such as ceramides, cholesteryl esters, mono-, di- and tri-acylglycerols, that may often be present at or below the level of chemical noise in the mass spectra, can generally not be determined by MS measurements alone without sufficient resolution and analytical sensitivity. Thus, tandem mass

spectrometry (MS/MS) methods are typically required for the unambiguous identification and quantitative analysis of the individual species that may be present within a complex unfractionated lipid mixture (150; 155-157).

Extensive previous studies have demonstrated that collision-induced dissociation tandem mass spectrometry (CID-MS/MS) of lipid precursor ions results in the observation of characteristic product ions formed via cleavage of either the lipid head group or the fatty acyl chains esterified to the lipid backbone, from which information regarding the identity and structure of the lipid may be elucidated (158). The results of these studies have facilitated the development of ‘shotgun’ lipidomics approaches employing selective precursor ion (PI) and neutral loss (NL) scan mode MS/MS methods for rapid and sensitive monitoring of the molecular compositions and abundances of individual lipid species in complex lipid extracts. This approach significantly reduces the requirement for extensive sample preparation or fractionation (such as liquid chromatography) prior to analysis (155; 156; 159-161). Additionally, the introduction of automated nano-ESI ion sources has improved the sensitivity, dynamic range, and throughput of shotgun lipid analyses, enabling the acquisition of a large number of PI or NL CID-MS/MS experiments from minute amounts of cells or tissue (162).

However, the formation and abundance of the characteristic product ions that are required for these precursor ion and neutral loss scan mode MS/MS experiments are known to be highly dependent on the structure of the lipid, the polarity of the precursor ion (+ve versus -ve) and the nature of the ionizing charge ( $+H^+$ ,  $+Na^+$ ,  $+Li^+$ ,  $-H^-$ ,  $+Cl^-$ ,  $+CH_3OCO_2^-$ ), as well as the instrumentation and collisional activation conditions that are employed (158; 163). Multiple ionic forms of individual lipids within a given lipid class are commonly observed under typical

sample preparation and analysis conditions, potentially adding significant complexity to the mixture as the same lipid is observed at several m/z values. Yet, the different product ions formed upon fragmentation of these various precursor ions may allow the development of more selective or sensitive precursor ion and neutral loss scan mode MS/MS methods for use in comprehensive lipid class-specific identification and quantification. Improved methods for retinal lipid analysis capable of identifying and quantifying a broad array of chemically dissimilar lipids are an absolute prerequisite to the subsequent identification of specific biochemical pathways relevant to the onset and progression of diabetic retinopathy.

### *1.7 Objectives and hypothesis of dissertation*

Early diabetic retinopathy has been suggested to be a low-grade chronic inflammatory disease (12; 26; 27; 65), characterized by increased expression of vascular cell adhesion molecules, leukostasis, and endothelial cell injury leading to disruption of the blood-retinal barrier (12; 27; 34; 45; 54; 164). Dyslipidemia associated with diabetes has been positively correlated with the development of diabetic retinopathy (77). Disruption of fatty acid metabolism is a component of dyslipidemia (90; 165) and altered fatty acid metabolism may contribute to the propagation of retinal inflammatory signaling (29; 62; 166; 167). We therefore initially proposed the broad central hypothesis that disruption of retinal lipid metabolism by diabetes contributes to the development of diabetic retinal vascular lesions. We first set out to establish analytical methods capable of facilitating comprehensive evaluation of this hypothesis with the eventual goal of identifying specific metabolic pathways that may contribute to diabetic retinal pathology through novel mechanisms. The broad objectives of this dissertation are summarized in Figure 1.1.

Utilizing a refined lipidomics approach to assess the retinal lipid profile in a streptozotocin rat model of diabetes, we found that diabetes causes significant decreases in retinal glycerophospholipids containing polyunsaturated fatty acids (PUFA), including decreased docosahexaenoic acid (DHA, 22:6n3) and 32:6n3 very long chain PUFA. We have demonstrated that retina lipid remodeling in diabetes occurred concurrently with retinal inflammation and decreased expression of multiple retinal fatty acid elongases, including the most abundant retinal elongase ELOVL4, which may play a role in the synthesis of n3 very long chain polyunsaturated fatty acids (VLCPUFA) of 28-36 carbons in length (108).

Recently, decreased functional capacity of ELOVL4 and a subsequent decrease in retinal n3 VLCPUFA was shown to be sufficient to cause retinal degeneration in a mouse model of Stargardt-like macular dystrophy, a juvenile onset disease that leads to blindness (125). Importantly, retinal deterioration in *ELOVL4* transgenic mice was independent of retinal DHA(22:6n3) content (127). Additionally, ELOVL4 expression has been inversely correlated with retinal vascular deterioration in an ischemia/reperfusion mouse model of accelerated vascular injury (134), yet no studies have directly tested possible roles of ELOVL4 in maintenance of retinal vascular function. Moreover, no detailed functional studies of ELOVL4 have been performed in retinal cell types known to be affected by diabetes, and no physiological role has been defined for very long chain fatty acids, the putative products of ELOVL4 activity. Given the associations of decreased ELOVL4 function with inflammation in diabetic retina, and deterioration of retinal vasculature and photoreceptors in other disease models, we targeted the pathway of ELOVL4 mediated fatty acid metabolism for further functional studies and hypothesized that decreased ELOVL4 expression in diabetic retina promotes diabetes induced

retinal vascular degeneration. A preliminary schematic of the proposed role of ELOVL4 in the development of diabetic retinopathy is provided in Figure 1.2.

Using cell culture models of the blood-retinal barrier, primarily human retinal pigment epithelial cells and human retinal endothelial cells, as well as animal models of diabetic retinopathy, we will use broad-based lipidomics analysis to simultaneously analyze numerous and diverse lipid classes in cells overexpressing ELOVL4 to establish its biochemical function in cells known to be affected by diabetic retinopathy. We will also challenge ELOVL4 overexpressing cells with pro-inflammatory factors such as cytokines to determine whether ELOVL4 plays any role in modulating retinal inflammatory signaling and cellular activation. Finally, we will use a ‘gene therapy’ approach to normalize ELOVL4 levels in retinas of streptozotocin diabetic rats to enable *in vivo* assessment of potential ELOVL4 effects on retinal lipid metabolism and retinal vascular health. For this study, we will assess the permeability of the retinal vasculature in diabetic animals with or without ELOVL4 normalization as a measure of early stage vascular damage, while also monitoring molecular indicators of vascular integrity and retinal inflammation.

This dissertation will provide novel approaches for the evaluation of tissue or cellular lipid profiles, and detail strategies for the identification of lipid metabolic pathways relevant to a biological phenomenon of interest. Application of these strategies will lead to new information concerning possible roles of ELOVL4 mediated fatty acid metabolism in the onset and progression of diabetic retinopathy, and will assess potential mechanisms by which the fatty acid elongase ELOVL4 may play a central role in retinal health and function.

Initial hypothesis: Disruption of lipid metabolism by diabetes contributes to retinal vascular pathology

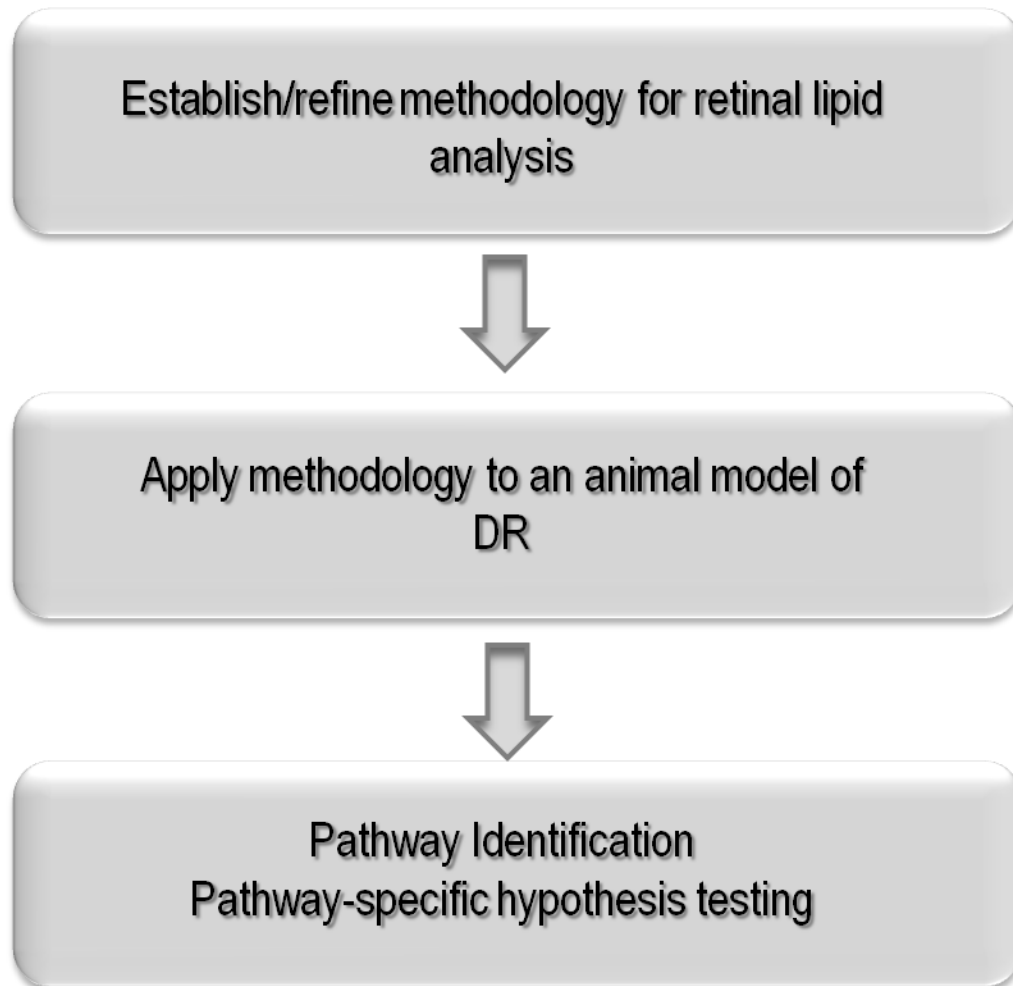


**Figure 1.1. Broad objectives and initial guiding hypothesis of the dissertation.**

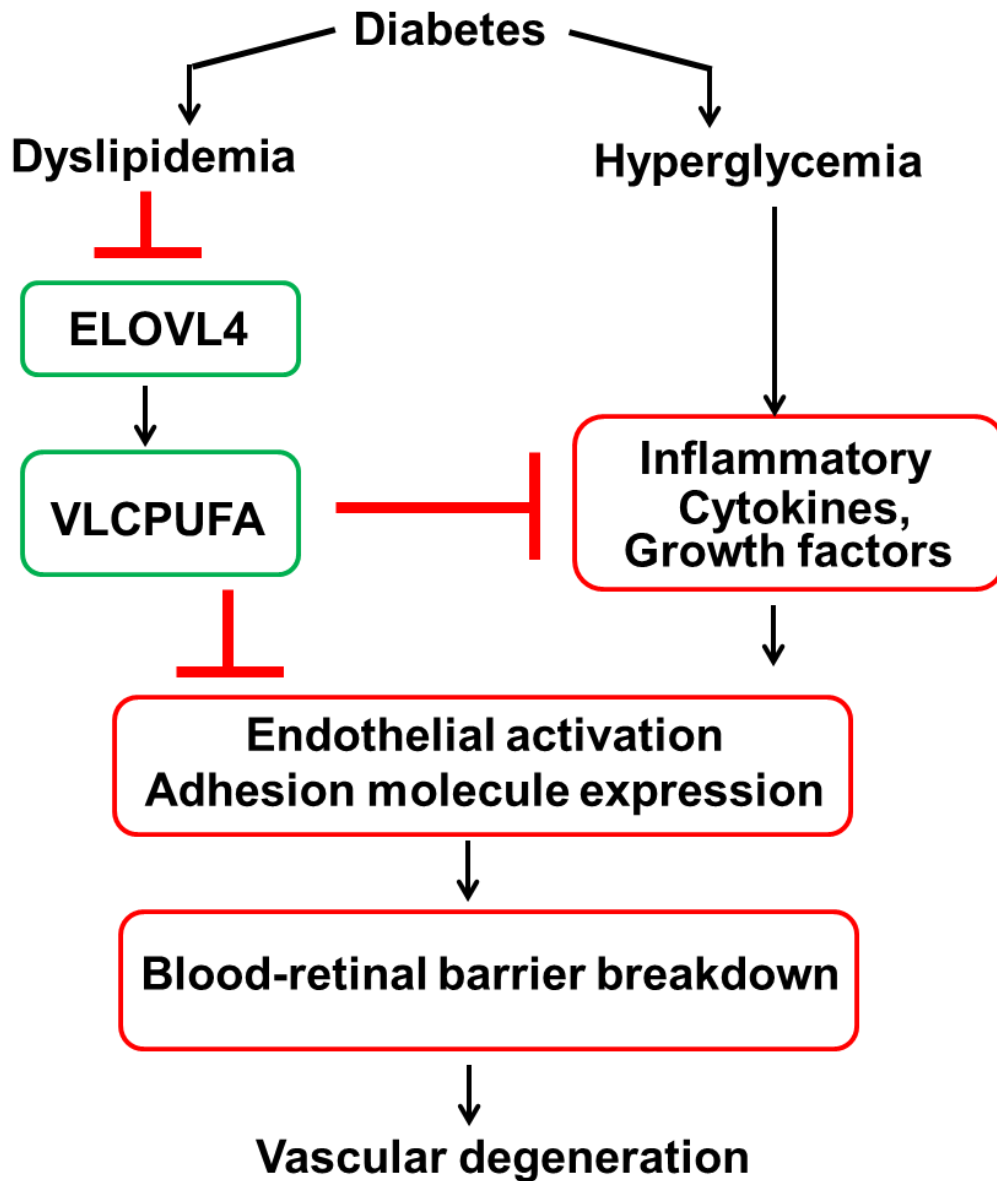


**Figure 1.2. The proposed role of fatty acid elongase ELOVL4 in diabetic retinopathy.** For interpretation of the references to color in this and all other figures, the reader is referred to the electronic version of this dissertation.

## *1.8 Overview of Chapters*

Chapter I is a review of literature encompassing diabetic retinopathy and the potential contribution of diabetic dyslipidemia to the onset of retinal inflammation and subsequent vascular injury, as well as methods relevant to the study of dyslipidemia in diabetic retinopathy.

Chapter II describes ‘lipidomics’ strategies for detailed analysis of retina lipid profiles, and provides in-depth information concerning the lipid profile of rat retina under normal physiological conditions.

Chapter III describes the application of the lipidomics platform outlined in Chapter II to the analysis of retina lipid profiles in a streptozotocin rat model of diabetic retinopathy, and reveals multiple diabetes-induced alterations of retinal lipid metabolism. Additionally, this chapter provides strategies for quantitative lipidome analysis and the discovery of disease biomarkers.

Chapter IV demonstrates that altered retinal lipid profiles in diabetes are associated with defects in retinal-specific lipid metabolism, and identifies decreased expression of fatty acid elongases as a major component of this phenomenon. This chapter also illustrates that the most dramatic downregulation of elongases in diabetes affects the elongase ELOVL4, which normally exhibits the highest expression among retinal elongases. Additionally this chapter establishes that altered retinal lipid profiles and elongase expression in diabetes are associated with increased markers of retinal inflammation.

Chapter V implicates ELOVL4 in the production of ceramides containing very long chain fatty acids in cells that constitute the inner and outer blood-retinal barriers, and postulates that modulation of sphingolipid metabolism by ELOVL4 is protective against pro-inflammatory

stimuli. This chapter illustrates the ability of ELOVL4 gene delivery to prevent diabetic retinal vascular lesions, and suggests that manipulation of retinal ELOVL4 levels may provide an effective therapeutic modality to prevent retinal vascular degeneration at the earliest stages of diabetic retinal disease.

Chapter VI details the methods used to acquire the data presented in this dissertation.

Chapter VII states the conclusions that can be drawn from the studies presented in this dissertation, addresses questions raised by the data, and suggests future areas of research related to the presented findings.

## References

## 1.9 References

1. Alberti KG, Zimmet PZ: Definition, diagnosis and classification of diabetes mellitus and its complications. Part 1: diagnosis and classification of diabetes mellitus provisional report of a WHO consultation. *Diabet Med* 15:539-553, 1998.
2. Report of the Expert Committee on the Diagnosis and Classification of Diabetes Mellitus. *Diabetes Care* 20:1183-1197, 1997.
3. Gianani R, Eisenbarth GS: The stages of type 1A diabetes: 2005. *Immunol Rev* 204:232-249, 2005.
4. Di Lorenzo TP, Peakman M, Roep BO: Translational mini-review series on type 1 diabetes: Systematic analysis of T cell epitopes in autoimmune diabetes. *Clin Exp Immunol* 148:1-16, 2007.
5. Mukherjee G, Diloranzo TP: The immunotherapeutic potential of dendritic cells in type 1 diabetes. *Clin Exp Immunol* 161:197-207.
6. Stumvoll M, Goldstein BJ, van Haeften TW: Type 2 diabetes: principles of pathogenesis and therapy. *Lancet* 365:1333-1346, 2005.
7. Pierce M, Keen H, Bradley C: Risk of diabetes in offspring of parents with non-insulin-dependent diabetes. *Diabet Med* 12:6-13, 1995.
8. Pradhan A: Obesity, metabolic syndrome, and type 2 diabetes: inflammatory basis of glucose metabolic disorders. *Nutr Rev* 65:S152-156, 2007.
9. Bakker SF, Tushuizen ME, von Blomberg ME, Mulder CJ, Simsek S: Type 1 diabetes and celiac disease in adults: glycemic control and diabetic complications. *Acta Diabetol*.
10. Economic costs of diabetes in the U.S. In 2007. *Diabetes Care* 31:596-615, 2008.
11. Klein R, Klein BE, Moss SE, Cruickshanks KJ: The Wisconsin Epidemiologic Study of diabetic retinopathy. XIV. Ten-year incidence and progression of diabetic retinopathy. *Arch Ophthalmol* 112:1217-1228, 1994.
12. Antonetti DA, Barber AJ, Bronson SK, Freeman WM, Gardner TW, Jefferson LS, Kester M, Kimball SR, Krady JK, LaNoue KF, Norbury CC, Quinn PG, Sandirasegarane L, Simpson IA: Diabetic retinopathy: seeing beyond glucose-induced microvascular disease. *Diabetes* 55:2401-2411, 2006.
13. Simo R, Hernandez C: Advances in the medical treatment of diabetic retinopathy. *Diabetes Care* 32:1556-1562, 2009.
14. Klein BE, Klein R, Myers CE, Lee KE: Complete blood cell count and retinal vessel diameters. *Arch Ophthalmol* 129:490-497.

15. Hammes HP, Federoff HJ, Brownlee M: Nerve growth factor prevents both neuroretinal programmed cell death and capillary pathology in experimental diabetes. *Mol Med* 1:527-534, 1995.
16. Karim R, Tang B: Use of antivascular endothelial growth factor for diabetic macular edema. *Clin Ophthalmol* 4:493-517.
17. Ting DS, Ng JQ, Morlet N, Yuen J, Clark A, Taylor HR, Keeffe J, Preen DB: Diabetic retinopathy management by Australian optometrists. *Clin Experiment Ophthalmol* 39:230-235.
18. Mohamed Q, Gillies MC, Wong TY: Management of diabetic retinopathy: a systematic review. *Jama* 298:902-916, 2007.
19. Jackson TL, Kirkpatrick L: Cost comparison of ranibizumab and bevacizumab. *Bmj* 343:d5058.
20. Tian XF, Xia XB, Xu HZ, Xiong SQ, Jiang J: Caveolin-1 expression regulates blood-retinal barrier permeability and retinal neovascularization in oxygen-induced retinopathy. *Clin Experiment Ophthalmol* 40:e58-66.
21. Van Geest RJ, Lesnik-Oberstein SY, Tan HS, Mura M, Goldschmeding R, Van Noorden CJ, Klaassen I, Schlingemann RO: A shift in the balance of vascular endothelial growth factor and connective tissue growth factor by bevacizumab causes the angiofibrotic switch in proliferative diabetic retinopathy. *Br J Ophthalmol* 96:587-590.
22. Mordes JP, Bortell R, Blankenhorn EP, Rossini AA, Greiner DL: Rat models of type 1 diabetes: genetics, environment, and autoimmunity. *Ilar J* 45:278-291, 2004.
23. Mordes JP: Autoimmune diabetes mellitus in the BB rat. In *animal models of diabetes: a primer*. Sima A, Shafir E, Eds. Warsaw, Harwood Academic Publishers, 2001.
24. Tirabassi RS, Flanagan JF, Wu T, Kislauskis EH, Birckbichler PJ, Guberski DL: The BBZDR/Wor rat model for investigating the complications of type 2 diabetes mellitus. *Ilar J* 45:292-302, 2004.
25. Cefalu WT: Animal models of type 2 diabetes: clinical presentation and pathophysiological relevance to the human condition. *Ilar J* 47:186-198, 2006.
26. Kern TS, Engerman RL: Pharmacological inhibition of diabetic retinopathy: aminoguanidine and aspirin. *Diabetes* 50:1636-1642, 2001.
27. Kern TS: Contributions of inflammatory processes to the development of the early stages of diabetic retinopathy. *Exp Diabetes Res* 2007:95103, 2007.

28. Kowluru RA, Tang J, Kern TS: Abnormalities of retinal metabolism in diabetes and experimental galactosemia. VII. Effect of long-term administration of antioxidants on the development of retinopathy. *Diabetes* 50:1938-1942, 2001.
29. Opreanu M, Tikhonenko M, Bozack S, Lydic TA, Reid GE, McSorley KM, Sochacki A, Perez GI, Esselman WJ, Kern T, Kolesnick R, Grant MB, Busik JV: The unconventional role of acid sphingomyelinase in regulation of retinal microangiopathy in diabetic human and animal models. *Diabetes* 60:2370-2378.
30. Aiello LP, Gardner TW, King GL, Blankenship G, Cavallerano JD, Ferris FL, 3rd, Klein R: Diabetic retinopathy. *Diabetes Care* 21:143-156, 1998.
31. King GL, Kunisaki M, Nishio Y, Inoguchi T, Shiba T, Xia P: Biochemical and molecular mechanisms in the development of diabetic vascular complications. *Diabetes* 45 Suppl 3:S105-108, 1996.
32. King GL, Ishii H, Koya D: Diabetic vascular dysfunctions: a model of excessive activation of protein kinase C. *Kidney Int Suppl* 60:S77-85, 1997.
33. Koya D, King GL: Protein kinase C activation and the development of diabetic complications. *Diabetes* 47:859-866, 1998.
34. Frey T, Antonetti DA: Alterations to the blood-retinal barrier in diabetes: cytokines and reactive oxygen species. *Antioxid Redox Signal* 15:1271-1284.
35. Dvorak HF, Brown LF, Detmar M, Dvorak AM: Vascular permeability factor/vascular endothelial growth factor, microvascular hyperpermeability, and angiogenesis. *Am J Pathol* 146:1029-1039, 1995.
36. Garcia-Ramirez M, Villarroel M, Corraliza L, Hernandez C, Simo R: Measuring permeability in human retinal epithelial cells (ARPE-19): implications for the study of diabetic retinopathy. *Methods Mol Biol* 763:179-194.
37. Runkle EA, Antonetti DA: The blood-retinal barrier: structure and functional significance. *Methods Mol Biol* 686:133-148.
38. Gardner TW, Antonetti DA, Barber AJ, Lieth E, Tarbell JA: The molecular structure and function of the inner blood-retinal barrier. Penn State Retina Research Group. *Doc Ophthalmol* 97:229-237, 1999.
39. Crane IJ, Liversidge J: Mechanisms of leukocyte migration across the blood-retina barrier. *Semin Immunopathol* 30:165-177, 2008.
40. Wacker BK, Freie AB, Perfater JL, Gidday JM: Junctional protein regulation by sphingosine kinase 2 contributes to blood-brain barrier protection in hypoxic preconditioning-induced cerebral ischemic tolerance. *J Cereb Blood Flow Metab*.

41. Dodelet-Devillers A, Cayrol R, van Horssen J, Haqqani AS, de Vries HE, Engelhardt B, Greenwood J, Prat A: Functions of lipid raft membrane microdomains at the blood-brain barrier. *J Mol Med (Berl)* 87:765-774, 2009.
42. Cai J, Wu L, Qi X, Li Calzi S, Caballero S, Shaw L, Ruan Q, Grant MB, Boulton ME: PEDF regulates vascular permeability by a gamma-secretase-mediated pathway. *PLoS One* 6:e21164.
43. Ramirez M, Wu Z, Moreno-Carranza B, Jeziorski MC, Arnold E, Diaz-Lezama N, Martinez de la Escalera G, Colosi P, Clapp C: Vasoinhibin gene transfer by adenoassociated virus type 2 protects against VEGF- and diabetes-induced retinal vasopermeability. *Invest Ophthalmol Vis Sci* 52:8944-8950.
44. Hou X, Hu D, Wang YS, Tang ZS, Zhang F, Chavakis T, Li Y, Li X: Targeting of junctional adhesion molecule-C inhibits experimental choroidal neovascularization. *Invest Ophthalmol Vis Sci* 53:1584-1591.
45. Trudeau K, Roy S, Guo W, Hernandez C, Villarroel M, Simo R, Roy S: Fenofibric acid reduces fibronectin and collagen type IV overexpression in human retinal pigment epithelial cells grown in conditions mimicking the diabetic milieu: functional implications in retinal permeability. *Invest Ophthalmol Vis Sci* 52:6348-6354.
46. Kim JH, Kim JH, Jun HO, Yu YS, Kim KW: Inhibition of protein kinase C delta attenuates blood-retinal barrier breakdown in diabetic retinopathy. *Am J Pathol* 176:1517-1524.
47. Antonetti DA, Barber AJ, Khin S, Lieth E, Tarbell JM, Gardner TW: Vascular permeability in experimental diabetes is associated with reduced endothelial occludin content: vascular endothelial growth factor decreases occludin in retinal endothelial cells. Penn State Retina Research Group. *Diabetes* 47:1953-1959, 1998.
48. Klaassen I, Hughes JM, Vogels IM, Schalkwijk CG, Van Noorden CJ, Schlingemann RO: Altered expression of genes related to blood-retina barrier disruption in streptozotocin-induced diabetes. *Exp Eye Res* 89:4-15, 2009.
49. Chen XL, Nam JO, Jean C, Lawson C, Walsh CT, Goka E, Lim ST, Tomar A, Tancioni I, Uryu S, Guan JL, Acevedo LM, Weis SM, Cheresch DA, Schlaepfer DD: VEGF-induced vascular permeability is mediated by FAK. *Dev Cell* 22:146-157.
50. Li X, McClellan ME, Tanito M, Garteiser P, Towner R, Bissig D, Berkowitz BA, Fliesler SJ, Woodruff ML, Fain GL, Birch DG, Khan MS, Ash JD, Elliott MH: Loss of Caveolin-1 Impairs Retinal Function Due to a Disturbance of the Subretinal Microenvironment. *J Biol Chem*.
51. Perrin RM, Harper SJ, Bates DO: A role for the endothelial glycocalyx in regulating microvascular permeability in diabetes mellitus. *Cell Biochem Biophys* 49:65-72, 2007.

52. Schroder S, Palinski W, Schmid-Schonbein GW: Activated monocytes and granulocytes, capillary nonperfusion, and neovascularization in diabetic retinopathy. *Am J Pathol* 139:81-100, 1991.
53. Jousseaume AM, Poulaki V, Mitsiades N, Kirchhof B, Koizumi K, Dohmen S, Adamis AP: Nonsteroidal anti-inflammatory drugs prevent early diabetic retinopathy via TNF-alpha suppression. *Faseb J* 16:438-440, 2002.
54. Jousseaume AM, Murata T, Tsujikawa A, Kirchhof B, Bursell SE, Adamis AP: Leukocyte-mediated endothelial cell injury and death in the diabetic retina. *Am J Pathol* 158:147-152, 2001.
55. McLeod DS, Lefer DJ, Merges C, Luttjohann GA: Enhanced expression of intracellular adhesion molecule-1 and P-selectin in the diabetic human retina and choroid. *Am J Pathol* 147:642-653, 1995.
56. Miyamoto K, Khosrof S, Bursell SE, Rohan R, Murata T, Clermont AC, Aiello LP, Ogura Y, Adamis AP: Prevention of leukostasis and vascular leakage in streptozotocin-induced diabetic retinopathy via intercellular adhesion molecule-1 inhibition. *Proc Natl Acad Sci U S A* 96:10836-10841, 1999.
57. Jousseaume AM, Poulaki V, Qin W, Kirchhof B, Mitsiades N, Wiegand SJ, Rudge J, Yancopoulos GD, Adamis AP: Retinal vascular endothelial growth factor induces intercellular adhesion molecule-1 and endothelial nitric oxide synthase expression and initiates early diabetic retinal leukocyte adhesion in vivo. *Am J Pathol* 160:501-509, 2002.
58. Adamis AP: Is diabetic retinopathy an inflammatory disease? *Br J Ophthalmol* 86:363-365, 2002.
59. Zheng L, Szabo C, Kern TS: Poly(ADP-ribose) polymerase is involved in the development of diabetic retinopathy via regulation of nuclear factor-kappaB. *Diabetes* 53:2960-2967, 2004.
60. Jousseaume AM, Huang S, Poulaki V, Camphausen K, Beecken WD, Kirchhof B, Adamis AP: In vivo retinal gene expression in early diabetes. *Invest Ophthalmol Vis Sci* 42:3047-3057, 2001.
61. Gariano RF, Gardner TW: Retinal angiogenesis in development and disease. *Nature* 438:960-966, 2005.
62. Chen W, Esselman WJ, Jump DB, Busik JV: Anti-inflammatory effect of docosahexaenoic acid on cytokine-induced adhesion molecule expression in human retinal vascular endothelial cells. *Invest Ophthalmol Vis Sci* 46:4342-4347, 2005.
63. Busik JV, Mohr S, Grant MB: Hyperglycemia-induced reactive oxygen species toxicity to endothelial cells is dependent on paracrine mediators. *Diabetes* 57:1952-1965, 2008.

64. Zong H, Ward M, Madden A, Yong PH, Limb GA, Curtis TM, Stitt AW: Hyperglycaemia-induced pro-inflammatory responses by retinal Muller glia are regulated by the receptor for advanced glycation end-products (RAGE). *Diabetologia* 53:2656-2666.
65. Vincent JA, Mohr S: Inhibition of caspase-1/interleukin-1beta signaling prevents degeneration of retinal capillaries in diabetes and galactosemia. *Diabetes* 56:224-230, 2007.
66. Ayalasmayajula SP, Kompella UB: Celecoxib, a selective cyclooxygenase-2 inhibitor, inhibits retinal vascular endothelial growth factor expression and vascular leakage in a streptozotocin-induced diabetic rat model. *Eur J Pharmacol* 458:283-289, 2003.
67. Stitt AW, Burke GA, Chen F, McMullen CB, Vlassara H: Advanced glycation end-product receptor interactions on microvascular cells occur within caveolin-rich membrane domains. *Faseb J* 14:2390-2392, 2000.
68. Bilderback TR, Gazula VR, Lisanti MP, Dobrowsky RT: Caveolin interacts with Trk A and p75(NTR) and regulates neurotrophin signaling pathways. *J Biol Chem* 274:257-263, 1999.
69. Kolesnick RN, Goni FM, Alonso A: Compartmentalization of ceramide signaling: physical foundations and biological effects. *J Cell Physiol* 184:285-300, 2000.
70. Smart EJ, Graf GA, McNiven MA, Sessa WC, Engelman JA, Scherer PE, Okamoto T, Lisanti MP: Caveolins, liquid-ordered domains, and signal transduction. *Mol Cell Biol* 19:7289-7304, 1999.
71. Holopainen JM, Subramanian M, Kinnunen PK: Sphingomyelinase induces lipid microdomain formation in a fluid phosphatidylcholine/sphingomyelin membrane. *Biochemistry* 37:17562-17570, 1998.
72. Fox TE, Han X, Kelly S, Merrill AH, 2nd, Martin RE, Anderson RE, Gardner TW, Kester M: Diabetes alters sphingolipid metabolism in the retina: a potential mechanism of cell death in diabetic retinopathy. *Diabetes* 55:3573-3580, 2006.
73. Gonzalez-Chavez A, Elizondo-Argueta S, Gutierrez-Reyes G, Leon-Pedroza JJ: Pathophysiological implications between chronic inflammation and the development of diabetes and obesity. *Cir Cir* 79:209-216.
74. Kohner EM: Aspirin for diabetic retinopathy. *Bmj* 327:1060-1061, 2003.
75. Enge M, Bjarnegard M, Gerhardt H, Gustafsson E, Kalen M, Asker N, Hammes HP, Shani M, Fassler R, Betsholtz C: Endothelium-specific platelet-derived growth factor-B ablation mimics diabetic retinopathy. *Embo J* 21:4307-4316, 2002.
76. Brownlee M: Biochemistry and molecular cell biology of diabetic complications. *Nature* 414:813-820, 2001.

77. Lyons TJ, Jenkins AJ, Zheng D, Lackland DT, McGee D, Garvey WT, Klein RL: Diabetic retinopathy and serum lipoprotein subclasses in the DCCT/EDIC cohort. *Invest Ophthalmol Vis Sci* 45:910-918, 2004.
78. Guy J, Ogden L, Wadwa RP, Hamman RF, Mayer-Davis EJ, Liese AD, D'Agostino R, Jr., Marcovina S, Dabelea D: Lipid and lipoprotein profiles in youth with and without type 1 diabetes: the SEARCH for Diabetes in Youth case-control study. *Diabetes Care* 32:416-420, 2009.
79. Steiner G: How can we improve the management of vascular risk in type 2 diabetes: insights from FIELD. *Cardiovasc Drugs Ther* 23:403-408, 2009.
80. Kreisberg RA: Diabetic dyslipidemia. *Am J Cardiol* 82:67U-73U; discussion 85U-86U, 1998.
81. Rader DJ: Effect of insulin resistance, dyslipidemia, and intra-abdominal adiposity on the development of cardiovascular disease and diabetes mellitus. *Am J Med* 120:S12-18, 2007.
82. Keech A, Simes RJ, Barter P, Best J, Scott R, Taskinen MR, Forder P, Pillai A, Davis T, Glasziou P, Drury P, Kesaniemi YA, Sullivan D, Hunt D, Colman P, d'Emden M, Whiting M, Ehnholm C, Laakso M: Effects of long-term fenofibrate therapy on cardiovascular events in 9795 people with type 2 diabetes mellitus (the FIELD study): randomised controlled trial. *Lancet* 366:1849-1861, 2005.
83. Kim J, Ahn JH, Kim JH, Yu YS, Kim HS, Ha J, Shinn SH, Oh YS: Fenofibrate regulates retinal endothelial cell survival through the AMPK signal transduction pathway. *Exp Eye Res* 84:886-893, 2007.
84. Goetze S, Eilers F, Bungenstock A, Kintscher U, Stawowy P, Blaschke F, Graf K, Law RE, Fleck E, Grafe M: PPAR activators inhibit endothelial cell migration by targeting Akt. *Biochem Biophys Res Commun* 293:1431-1437, 2002.
85. Adams TH, Walzem RL, Smith DR, Tseng S, Smith SB: Hamburger high in total, saturated and trans-fatty acids decreases HDL cholesterol and LDL particle diameter, and increases TAG, in mildly hypercholesterolaemic men. *Br J Nutr* 103:91-98.
86. Dolley G, Boisclair ME, Lamarche B, Despres JP, Bouchard C, Perusse L, Vohl MC: Interactions between dietary fat intake and FASN genetic variation influence LDL peak particle diameter. *J Nutrigenet Nutrigenomics* 4:137-145.
87. Kelley DS, Siegel D, Vemuri M, Mackey BE: Docosahexaenoic acid supplementation improves fasting and postprandial lipid profiles in hypertriglyceridemic men. *Am J Clin Nutr* 86:324-333, 2007.

88. Seigneur M, Freyburger G, Gin H, Claverie M, Lardeau D, Lacape G, Le Moigne F, Crockett R, Boisseau MR: Serum fatty acid profiles in type I and type II diabetes: metabolic alterations of fatty acids of the main serum lipids. *Diabetes Res Clin Pract* 23:169-177, 1994.
89. Tilvis RS, Taskinen MR, Miettinen TA: Effect of insulin treatment on fatty acids of plasma and erythrocyte membrane lipids in type 2 diabetes. *Clin Chim Acta* 171:293-303, 1988.
90. Brenner RR: Hormonal modulation of delta6 and delta5 desaturases: case of diabetes. *Prostaglandins Leukot Essent Fatty Acids* 68:151-162, 2003.
91. Nakamura MT, Nara TY: Gene regulation of mammalian desaturases. *Biochem Soc Trans* 30:1076-1079, 2002.
92. Rimoldi OJ, Finarelli GS, Brenner RR: Effects of diabetes and insulin on hepatic delta6 desaturase gene expression. *Biochem Biophys Res Commun* 283:323-326, 2001.
93. Guillou H, Zdravec D, Martin PG, Jacobsson A: The key roles of elongases and desaturases in mammalian fatty acid metabolism: Insights from transgenic mice. *Prog Lipid Res* 49:186-199.
94. Wang Y, Botolin D, Xu J, Christian B, Mitchell E, Jayaprakasam B, Nair MG, Peters JM, Busik JV, Olson LK, Jump DB: Regulation of hepatic fatty acid elongase and desaturase expression in diabetes and obesity. *J Lipid Res* 47:2028-2041, 2006.
95. Matsuzaka T, Shimano H, Yahagi N, Kato T, Atsumi A, Yamamoto T, Inoue N, Ishikawa M, Okada S, Ishigaki N, Iwasaki H, Iwasaki Y, Karasawa T, Kumadaki S, Matsui T, Sekiya M, Ohashi K, Hasty AH, Nakagawa Y, Takahashi A, Suzuki H, Yatoh S, Sone H, Toyoshima H, Osuga J, Yamada N: Crucial role of a long-chain fatty acid elongase, Elovl6, in obesity-induced insulin resistance. *Nat Med* 13:1193-1202, 2007.
96. Zdravec D, Brolinson A, Fisher RM, Carneheim C, Csikasz RI, Bertrand-Michel J, Boren J, Guillou H, Rudling M, Jacobsson A: Ablation of the very-long-chain fatty acid elongase ELOVL3 in mice leads to constrained lipid storage and resistance to diet-induced obesity. *Faseb J* 24:4366-4377.
97. Tripathy S, Torres-Gonzalez M, Jump DB: Elevated hepatic fatty acid elongase-5 activity corrects dietary fat-induced hyperglycemia in obese C57BL/6J mice. *J Lipid Res* 51:2642-2654.
98. Green CD, Olson LK: Modulation of palmitate-induced endoplasmic reticulum stress and apoptosis in pancreatic beta-cells by stearoyl-CoA desaturase and Elovl6. *Am J Physiol Endocrinol Metab* 300:E640-649.
99. Moon YA, Shah NA, Mohapatra S, Warrington JA, Horton JD: Identification of a mammalian long chain fatty acyl elongase regulated by sterol regulatory element-binding proteins. *J Biol Chem* 276:45358-45366, 2001.

100. Okuda A, Naganuma T, Ohno Y, Abe K, Yamagata M, Igarashi Y, Kihara A: Hetero-oligomeric interactions of an ELOVL4 mutant protein: implications in the molecular mechanism of Stargardt-3 macular dystrophy. *Mol Vis* 16:2438-2445.
101. Ohno Y, Suto S, Yamanaka M, Mizutani Y, Mitsutake S, Igarashi Y, Sassa T, Kihara A: ELOVL1 production of C24 acyl-CoAs is linked to C24 sphingolipid synthesis. *Proc Natl Acad Sci U S A* 107:18439-18444.
102. Sandhoff R: Very long chain sphingolipids: tissue expression, function and synthesis. *FEBS Lett* 584:1907-1913.
103. Lecomte M, Paget C, Ruggiero D, Wiernsperger N, Lagarde M: Docosahexaenoic acid is a major n-3 polyunsaturated fatty acid in bovine retinal microvessels. *J Neurochem* 66:2160-2167, 1996.
104. O'Brien JS, Sampson EL: Lipid composition of the normal human brain: gray matter, white matter, and myelin. *J Lipid Res* 6:537-544, 1965.
105. SanGiovanni JP, Chew EY: The role of omega-3 long-chain polyunsaturated fatty acids in health and disease of the retina. *Prog Retin Eye Res* 24:87-138, 2005.
106. Brush RS, Tran JT, Henry KR, McClellan ME, Elliott MH, Mandal MN: Retinal sphingolipids and their very-long-chain fatty acid-containing species. *Invest Ophthalmol Vis Sci* 51:4422-4431.
107. SanGiovanni JP, Chew EY, Clemons TE, Davis MD, Ferris FL, 3rd, Gensler GR, Kurinij N, Lindblad AS, Milton RC, Seddon JM, Sperduto RD: The relationship of dietary lipid intake and age-related macular degeneration in a case-control study: AREDS Report No. 20. *Arch Ophthalmol* 125:671-679, 2007.
108. Agbaga MP, Brush RS, Mandal MN, Henry K, Elliott MH, Anderson RE: Role of Stargardt-3 macular dystrophy protein (ELOVL4) in the biosynthesis of very long chain fatty acids. *Proc Natl Acad Sci U S A* 105:12843-12848, 2008.
109. Ren H, Magulike N, Ghebremeskel K, Crawford M: Primary open-angle glaucoma patients have reduced levels of blood docosahexaenoic and eicosapentaenoic acids. *Prostaglandins Leukot Essent Fatty Acids* 74:157-163, 2006.
110. Ford D, Monda J, Brush R, Anderson R, Richards M, Fliesler S: Lipidomic analysis of the retina in a rat model of Smith-Lemli-Opitz syndrome: alterations in docosahexaenoic acid content of phospholipid molecular species. *Journal of Neurochemistry* 105:1032-1047, 2008.
111. Rotstein NP, Aveldano MI: Synthesis of very long chain (up to 36 carbon) tetra, penta and hexaenoic fatty acids in retina. *Biochem J* 249:191-200, 1988.

112. Tserentsoodol N, Sztein J, Campos M, Gordiyenko NV, Fariss RN, Lee JW, Fliesler SJ, Rodriguez IR: Uptake of cholesterol by the retina occurs primarily via a low density lipoprotein receptor-mediated process. *Mol Vis* 12:1306-1318, 2006.
113. Wang N, Anderson RE: Synthesis of docosahexaenoic acid by retina and retinal pigment epithelium. *Biochemistry (Mosc)* 32:13703-13709, 1993.
114. Delton-Vandenbroucke I, Grammas P, Anderson RE: Polyunsaturated fatty acid metabolism in retinal and cerebral microvascular endothelial cells. *J Lipid Res* 38:147-159, 1997.
115. Tserentsoodol N, Gordiyenko NV, Pascual I, Lee JW, Fliesler SJ, Rodriguez IR: Intraretinal lipid transport is dependent on high density lipoprotein-like particles and class B scavenger receptors. *Mol Vis* 12:1319-1333, 2006.
116. Grayson C, Molday RS: Dominant negative mechanism underlies autosomal dominant Stargardt-like macular dystrophy linked to mutations in ELOVL4. *J Biol Chem* 280:32521-32530, 2005.
117. Umeda S, Ayyagari R, Suzuki MT, Ono F, Iwata F, Fujiki K, Kanai A, Takada Y, Yoshikawa Y, Tanaka Y, Iwata T: Molecular cloning of ELOVL4 gene from cynomolgus monkey (*Macaca fascicularis*). *Exp Anim* 52:129-135, 2003.
118. Lagali PS, Liu J, Ambasadhan R, Kakuk LE, Bernstein SL, Seigel GM, Wong PW, Ayyagari R: Evolutionarily conserved ELOVL4 gene expression in the vertebrate retina. *Invest Ophthalmol Vis Sci* 44:2841-2850, 2003.
119. Zhang XM, Yang Z, Karan G, Hashimoto T, Baehr W, Yang XJ, Zhang K: Elov14 mRNA distribution in the developing mouse retina and phylogenetic conservation of Elov14 genes. *Mol Vis* 9:301-307, 2003.
120. Sommer JR, Estrada JL, Collins EB, Bedell M, Alexander CA, Yang Z, Hughes G, Mir B, Gilger BC, Grob S, Wei X, Piedrahita JA, Shaw PX, Petters RM, Zhang K: Production of ELOVL4 transgenic pigs: a large animal model for Stargardt-like macular degeneration. *Br J Ophthalmol* 95:1749-1754.
121. Oda Y, Uchida Y, Moradian S, Crumrine D, Elias PM, Bikle DD: Vitamin D receptor and coactivators SRC2 and 3 regulate epidermis-specific sphingolipid production and permeability barrier formation. *J Invest Dermatol* 129:1367-1378, 2009.
122. Bernstein PS, Tammur J, Singh N, Hutchinson A, Dixon M, Pappas CM, Zabriskie NA, Zhang K, Petrukhin K, Leppert M, Allikmets R: Diverse macular dystrophy phenotype caused by a novel complex mutation in the ELOVL4 gene. *Invest Ophthalmol Vis Sci* 42:3331-3336, 2001.
123. Karan G, Lillo C, Yang Z, Cameron DJ, Locke KG, Zhao Y, Thirumalaichary S, Li C, Birch DG, Vollmer-Snarr HR, Williams DS, Zhang K: Lipofuscin accumulation, abnormal

electrophysiology, and photoreceptor degeneration in mutant ELOVL4 transgenic mice: a model for macular degeneration. *Proc Natl Acad Sci U S A* 102:4164-4169, 2005.

124. Vasireddy V, Uchida Y, Salem N, Jr., Kim SY, Mandal MN, Reddy GB, Bodepudi R, Alderson NL, Brown JC, Hama H, Dlugosz A, Elias PM, Holleran WM, Ayyagari R: Loss of functional ELOVL4 depletes very long-chain fatty acids (> or =C28) and the unique omega-O-acylceramides in skin leading to neonatal death. *Hum Mol Genet* 16:471-482, 2007.

125. McMahon A, Butovich IA, Mata NL, Klein M, Ritter R, 3rd, Richardson J, Birch DG, Edwards AO, Kedzierski W: Retinal pathology and skin barrier defect in mice carrying a Stargardt disease-3 mutation in elongase of very long chain fatty acids-4. *Mol Vis* 13:258-272, 2007.

126. Vasireddy V, Jablonski MM, Mandal MN, Raz-Prag D, Wang XF, Nizol L, Iannaccone A, Musch DC, Bush RA, Salem N, Jr., Sieving PA, Ayyagari R: Elov14 5-bp-deletion knock-in mice develop progressive photoreceptor degeneration. *Invest Ophthalmol Vis Sci* 47:4558-4568, 2006.

127. Li F, Marchette LD, Brush RS, Elliott MH, Le YZ, Henry KA, Anderson AG, Zhao C, Sun X, Zhang K, Anderson RE: DHA does not protect ELOVL4 transgenic mice from retinal degeneration. *Mol Vis* 15:1185-1193, 2009.

128. Wang Y, Botolin D, Christian B, Busik J, Xu J, Jump DB: Tissue-specific, nutritional, and developmental regulation of rat fatty acid elongases. *J Lipid Res* 46:706-715, 2005.

129. McMahon A, Jackson SN, Woods AS, Kedzierski W: A Stargardt disease-3 mutation in the mouse Elov14 gene causes retinal deficiency of C32-C36 acyl phosphatidylcholines. *FEBS Lett* 581:5459-5463, 2007.

130. Agbaga MP, Brush RS, Mandal MN, Elliott MH, Al-Ubaidi MR, Anderson RE: Role of Elov14 protein in the biosynthesis of docosahexaenoic acid. *Adv Exp Med Biol* 664:233-242.

131. Ofman R, Dijkstra IM, van Roermund CW, Burger N, Turkenburg M, van Cruchten A, van Engen CE, Wanders RJ, Kemp S: The role of ELOVL1 in very long-chain fatty acid homeostasis and X-linked adrenoleukodystrophy. *EMBO Mol Med* 2:90-97.

132. Yu M, Benham A, Logan S, Brush RS, Mandal MN, Anderson RE, Agbaga MP: ELOVL4 protein preferentially elongates 20:5n3 to very long chain PUFAs over 20:4n6 and 22:6n3. *J Lipid Res* 53:494-504.

133. Zadavec D, Tvrdik P, Guillou H, Haslam R, Kobayashi T, Napier JA, Capecchi MR, Jacobsson A: ELOVL2 controls the level of n-6 28:5 and 30:5 fatty acids in testis, a prerequisite for male fertility and sperm maturation in mice. *J Lipid Res* 52:245-255.

134. Abcouwer SF, Lin CM, Wolpert EB, Shanmugam S, Schaefer EW, Freeman WM, Barber AJ, Antonetti DA: Effects of ischemic preconditioning and bevacizumab on apoptosis and

vascular permeability following retinal ischemia-reperfusion injury. *Invest Ophthalmol Vis Sci* 51:5920-5933.

135. Liu A, Chang J, Lin Y, Shen Z, Bernstein PS: Long-chain and very long-chain polyunsaturated fatty acids in ocular aging and age-related macular degeneration. *J Lipid Res* 51:3217-3229.

136. van Smeden J, Hoppel L, van der Heijden R, Hankemeier T, Vreeken RJ, Bouwstra JA: LC/MS analysis of stratum corneum lipids: ceramide profiling and discovery. *J Lipid Res* 52:1211-1221.

137. Li W, Sandhoff R, Kono M, Zerfas P, Hoffmann V, Ding BC, Proia RL, Deng CX: Depletion of ceramides with very long chain fatty acids causes defective skin permeability barrier function, and neonatal lethality in ELOVL4 deficient mice. *Int J Biol Sci* 3:120-128, 2007.

138. McMahon A, Butovich IA, Kedzierski W: Epidermal expression of an Elovl4 transgene rescues neonatal lethality of homozygous Stargardt disease-3 mice. *J Lipid Res*.

139. McMahon A, Kedzierski W: Polyunsaturated extremely long chain C28-C36 fatty acids and retinal physiology. *Br J Ophthalmol*, 2009.

140. Sprecher H, Chen Q: Polyunsaturated fatty acid biosynthesis: a microsomal-peroxisomal process. *Prostaglandins Leukot Essent Fatty Acids* 60:317-321, 1999.

141. Ishihara K, Murata M, Kaneniwa M, Saito H, Shinohara K, Maeda-Yamamoto M, Kawasaki K, Ooizumi T: Effect of tetracosahexaenoic acid on the content and release of histamine, and eicosanoid production in MC/9 mouse mast cell. *Lipids* 33:1107-1114, 1998.

142. Robinson BS, Johnson DW, Poulos A: Metabolism of hexacosatetraenoic acid (C26:4,n-6) in immature rat brain. *Biochem J* 267:561-564, 1990.

143. Hardy SJ, Robinson BS, Ferrante A, Hii CS, Johnson DW, Poulos A, Murray AW: Polyenoic very-long-chain fatty acids mobilize intracellular calcium from a thapsigargin-insensitive pool in human neutrophils. The relationship between Ca<sup>2+</sup> mobilization and superoxide production induced by long- and very-long-chain fatty acids. *Biochem J* 311 ( Pt 2):689-697, 1995.

144. Furland NE, Zanetti SR, Oresti GM, Maldonado EN, Avelldano MI: Ceramides and sphingomyelins with high proportions of very long-chain polyunsaturated fatty acids in mammalian germ cells. *J Biol Chem* 282:18141-18150, 2007.

145. Poulos A, Sharp P, Singh H, Johnson D, Fellenberg A, Pollard A: Detection of a homologous series of C26-C38 polyenoic fatty acids in the brain of patients without peroxisomes (Zellweger's syndrome). *Biochem J* 235:607-610, 1986.

146. Khan M, Singh J, Gilg AG, Uto T, Singh I: Very long-chain fatty acid accumulation causes lipotoxic response via 5-lipoxygenase in cerebral adrenoleukodystrophy. *J Lipid Res* 51:1685-1695.
147. Riekhof WR, Ruckle ME, Lydic TA, Sears BB, Benning C: The sulfolipids 2'-O-acyl-sulfoquinovosyldiacylglycerol and sulfoquinovosyldiacylglycerol are absent from a *Chlamydomonas reinhardtii* mutant deleted in SQD1. *Plant Physiol* 133:864-874, 2003.
148. Han X, Gross RW: Shotgun lipidomics: multidimensional MS analysis of cellular lipidomes. *Expert Rev Proteomics* 2:253-264, 2005.
149. Han X, Cheng H: Characterization and direct quantitation of cerebroside molecular species from lipid extracts by shotgun lipidomics. *Journal of Lipid Research* 46:163-175, 2005.
150. Brugger B, Erben G, Sandhoff R, Wieland FT, Lehmann WD: Quantitative analysis of biological membrane lipids at the low picomole level by nano-electrospray ionization tandem mass spectrometry. *Proc Natl Acad Sci U S A* 94:2339-2344, 1997.
151. Gijon MA, Riekhof WR, Zarini S, Murphy RC, Voelker DR: Lysophospholipid acyltransferases and arachidonate recycling in human neutrophils. *J Biol Chem* 283:30235-30245, 2008.
152. Jones JJ, Borgmann S, Wilkins CL, O'Brien RM: Characterizing the phospholipid profiles in mammalian tissues by MALDI FTMS. *Anal Chem* 78:3062-3071, 2006.
153. Estrada R, Yappert MC: Alternative approaches for the detection of various phospholipid classes by matrix-assisted laser desorption/ionization time-of-flight mass spectrometry. *Journal of Mass Spectrometry* 39:412-422, 2004.
154. Jones JJ, Batoy SM, Wilkins CL: A comprehensive and comparative analysis for MALDI FTMS lipid and phospholipid profiles from biological samples. *Comput Biol Chem* 29:294-302, 2005.
155. Ejsing CS, Duchoslav E, Sampaio J, Simons K, Bonner R, Thiele C, Ekroos K, Shevchenko A: Automated identification and quantification of glycerophospholipid molecular species by multiple precursor ion scanning. *Anal Chem* 78:6202-6214, 2006.
156. Ekroos K, Chernushevich IV, Simons K, Shevchenko A: Quantitative profiling of phospholipids by multiple precursor ion scanning on a hybrid quadrupole time-of-flight mass spectrometer. *Anal Chem* 74:941-949, 2002.
157. Han X, Gross RW: Global analyses of cellular lipidomes directly from crude extracts of biological samples by ESI mass spectrometry: a bridge to lipidomics. *J Lipid Res* 44:1071-1079, 2003.

158. Pulfer M, Murphy RC: Electrospray mass spectrometry of phospholipids. *Mass Spectrom Rev* 22:332-364, 2003.
159. Han X, Gross RW: Shotgun lipidomics: electrospray ionization mass spectrometric analysis and quantitation of cellular lipidomes directly from crude extracts of biological samples. *Mass Spectrom Rev* 24:367-412, 2005.
160. Schwudke D, Hannich JT, Surendranath V, Grimard V, Moehring T, Burton L, Kurzchalia T, Shevchenko A: Top-down lipidomic screens by multivariate analysis of high-resolution survey mass spectra. *Anal Chem* 79:4083-4093, 2007.
161. Schwudke D, Oegema J, Burton L, Entchev E, Hannich JT, Ejsing CS, Kurzchalia T, Shevchenko A: Lipid profiling by multiple precursor and neutral loss scanning driven by the data-dependent acquisition. *Anal Chem* 78:585-595, 2006.
162. Ejsing C: Molecular characterization of the lipidome by mass spectrometry. Dresden, Technische Universitat Dresden, 2007, p. 104.
163. Zhang X, Reid GE: Multistage tandem mass spectrometry of anionic phosphatidylcholine lipid adducts reveals novel dissociation pathways. *International Journal of Mass Spectrometry* 252:242-255, 2006.
164. Jousen AM, Poulaki V, Le ML, Koizumi K, Esser C, Janicki H, Fauser S, Kern TS, Kirchof B, Adamis AP: Long-term leukocyte-mediated vascular pathology in the diabetic retina. *Invest Ophthalmol Vis Sci* 44:U221-U221, 2003.
165. Lydic TA, Tikhonenko M, Wang Y, Chen W, Opreanu M, Sochacki A, McSorley KM, Renis RL, Kern T, Jump DB, Reid GE, Busik JV: Remodeling of Retinal Fatty Acids in an Animal Model of Diabetes: a Decrease in Long Chain Polyunsaturated Fatty Acids is Associated with a Decrease in Fatty Acid Elongases Elovl2 and Elovl4. *Diabetes*, 2009.
166. Chen W, Jump DB, Esselman WJ, Busik JV: Inhibition of cytokine signaling in human retinal endothelial cells through modification of caveolae/lipid rafts by docosahexaenoic acid. *Invest Ophthalmol Vis Sci* 48:18-26, 2007.
167. Opreanu M, Lydic TA, Reid GE, McSorley KM, Esselman WJ, Busik JV: Inhibition of cytokine signaling in human retinal endothelial cells through downregulation of sphingomyelinases by docosahexaenoic acid. *Invest Ophthalmol Vis Sci* 51:3253-3263.

## Global Analysis of Retina Lipids by Complementary Precursor Ion and Neutral Loss

## Mode Tandem Mass Spectrometry

*2.1 Abstract*

Despite an increasing recognition of the causative and diagnostic role of lipids in the onset and progression of retinal disease, information on the global lipid profile of the normal retina is quite limited. Here, a “shotgun” tandem mass spectrometry approach involving the use of multiple lipid class-specific precursor ion and neutral loss scan mode experiments has been employed to analyze lipid extracts from normal rat retina, obtained with minimal sample handling prior to analysis. Redundant information for the identification and characterization of molecular species in each lipid class was obtained by complementary analysis of their protonated or deprotonated precursor ions, or by analysis of their various ionic adducts (e.g.,  $\text{Na}^+$ ,  $\text{NH}_4^+$ ,  $\text{Cl}^-$ ,  $\text{CH}_3\text{OCO}_2^-$ ). Notably, “alternative” precursor ion or neutral loss scan mode MS/MS experiments are introduced that were used to identify rat retina lipid molecular species that were not detected using “conventional” scan types typically employed in large-scale lipid-profiling experiments. This chapter outlines the principles and advantages of utilizing complementary/redundant identification of lipid species as a strategy to overcome inherent challenges and limitations of shotgun lipid analysis, and provides examples of the application of this strategy in the analysis of the retina lipidome.

*2.2 Introduction*

Retina has a unique fatty acid profile with the highest levels of long chain polyunsaturated fatty acids (LCPUFA), including docosahexaenoic acid (DHA22:6n3), and arachidonic acid (ARA20:4n6), observed in the body (1–5). Of these, DHA22:6n3 is the most abundant fatty acid in both neural and vascular elements of the retina (2), retinal pigment epithelial cells (6;7) and retinal photoreceptor outer segment disc membranes (8;9). Extensive studies clearly demonstrate the important role of lipids in retinal health and disease (5). However, most studies to date have focused on the role of LCPUFA's, and DHA in particular, measuring total fatty acid levels without obtaining structural information. The reason for this is likely methodological – LCPUFA are very abundant in the retina and relatively easy to measure by well developed high-performance liquid chromatography (HPLC) or gas chromatography (GC) techniques. The limitations of the traditional techniques have precluded comprehensive complex lipid analysis from the limited amount of retinal material that can be obtained from animal models such as rats and mice. Thus, there is surprisingly little information available regarding the lipid composition of the normal retina, and only limited information describing changes in global lipid profiles between normal and diseased retinal tissue.

Recent advances in the application of electrospray ionization (ESI) and matrix assisted laser desorption/ionization (MALDI) (10–20) techniques, coupled with the use of tandem mass spectrometry methods employing selective precursor ion and neutral loss scan mode analysis strategies, have enabled the development of “shotgun” lipidomics approaches for rapid and sensitive monitoring of the molecular compositions and abundances of individual lipid species in unfractionated lipid extracts (10–17). While shotgun approaches allow for high-throughput analysis of multiple lipid classes without prior chromatographic separation of lipid analytes, the large number of lipid molecular species present in crude extracts presents a significant challenge

for the analyst. In addition to possible overlap of the molecular ions and the  $^{13}\text{C}$  isotope peaks of numerous lipid species, even greater extract complexity can arise due to the presence of individual lipid species in multiple ionic forms, via adduction with a variety of cationic (e.g.,  $+\text{H}^+$ ,  $+\text{Na}^+$ ,  $+\text{NH}_4^+$ ) or anionic (e.g.,  $-\text{H}^-$ ,  $+\text{Cl}^-$ ) species in positive or negative ion modes, respectively, that may be present in small amounts following extraction of lipids from tissues or cells. Additional complexity may also be observed for certain lipids due to the presence of adducts formed by reaction of the solvents and buffer additives that are commonly employed for sample analysis. For example, phosphocholine-containing lipids are readily adducted with methylcarbonate ( $\text{CH}_3\text{OCO}_2^-$ ) anions (21), formed by the *in vitro* reaction of hydroxide or bicarbonate salts (22;23) with methanol, effectively increasing the number of lipid species observed in negative ion mode analysis.

In our studies, relatively limited tissue availability has prompted us to develop strategies for attaining a thorough accounting of the global lipid composition of retina without requirement for multiple sample fractionation or processing steps, such as chromatographic separation, or destruction of glycerophospholipids for enhanced sphingolipid analysis. Utilizing a triple quadrupole mass spectrometer to perform multiple precursor ion and neutral loss scan mode MS/MS experiments, we have found that complementary/redundant detection of a given lipid class based on the unique fragmentation behaviors of various ionic forms (e.g.,  $[\text{M} + \text{H}]^+$ ,  $[\text{M} - \text{H}]^-$ ,  $[\text{M} + \text{Na}]^+$ ,  $[\text{M} + \text{NH}_4]^+$ ,  $[\text{M} + \text{Cl}]^-$ ,  $[\text{M} + \text{CH}_3\text{OCO}_2]^-$ ) of various lipid classes facilitates (a) the ability to identify molecular lipid species that may not be detected when only one scan mode is used, (b) a more thorough accounting of the various lipid species that may be present in

multiple ionic forms when “absolute quantification” is desired, and (c) simplification of relative quantification by selection of an MS/MS scan mode in which lipid species are present in only one ionic form. Furthermore, the ability to identify lipids in more than one ionic form greatly increases the confidence for peak identification, even for ions observed at low (<5%) relative abundance.

Here, we outline the general approach and the results obtained by performing complementary precursor ion and neutral loss scan mode tandem mass spectrometry analyses. Although presented within the context of defining the normal rat retina lipidome, the analytical principles could benefit the analysis of virtually any tissue or cell lipid extract. In this chapter, our discussion will be limited to analysis of rat retina sphingomyelin (SM), glycerophosphatidylcholine (GPCho), glycerophosphatidylethanolamine (GPEtn), glycerophosphatidylinositol (GPIIns), glycerophosphatidylserine (GPSer), and diacylglycerol (DG) and triacylglycerol (TG) molecular lipid species. Complementary sets of precursor ion and neutral loss scan mode MS/MS experiments will be described for the analysis of these lipid classes. Analogous sets of complementary precursor ion and neutral loss experiments will also be suggested for additional lipid classes including ceramides, cholesteryl esters, glycerophosphatidylglycerol (GPGro), glycerophosphatidic acid (GPA), and monoacylglycerols. The results of the analyses for these additional lipid classes in rat retina lipid extracts may be obtained upon request from the authors.

## *2.3 Results*

### **2.3.1 Mass spectrum of a rat retina lipid extract**

The use of an animal model, such as the rat, for studying changes in global retina lipid profiles as a function of the onset and progression of disease is attractive for several reasons. These include the ability to control or systematically evaluate the effect of a number of variables, such as genetic background, environment, age, and diet that are known to alter the presence and abundance of particular lipid species at any given time. In order to obtain an initial “snapshot” of the global lipid profile of the normal rat retina, a crude lipid extract isolated from a whole retina was subjected to analysis by using nanoelectrospray ionization coupled to a triple quadrupole mass spectrometer in both positive and negative ionization modes. The mass spectra obtained from these analyses are shown in Fig. 2.1A and B respectively. Analysis of lipid extracts from three separate rat retinas resulted in essentially identical spectra to those shown in Fig. 2.1A and B, indicating that minimal biological variability was observed between these animals (data not shown). This was expected given that these samples were obtained from animals with identical genetic backgrounds that were maintained under essentially identical conditions.

The resolution and mass accuracy associated with the mass spectra shown in Fig. 2.1 precluded the identification of individual lipid species on the basis of their masses alone. Indeed, in many cases, the product ion scan mode MS/MS experiments and the precursor ion and neutral loss scan mode MS/MS experiments discussed below indicated that multiple lipid species having the same nominal mass values, as well as multiple lipids with isobaric masses, were present at a given  $m/z$  value. Furthermore, the presence and the identities of low abundance lipid species, such as mono-, di-, and tri-acylglycerols, ceramides, and cholesteryl esters that were present at or below the level of chemical noise in these spectra could not be determined.

### **2.3.2 Complementary sets of precursor ion and neutral loss scans for global**

#### **lipid analysis**

In order to obtain a more comprehensive profile of the lipid composition of the crude rat retina lipid extract, a series of 27 precursor ions and neutral loss scan mode MS/MS experiments were performed in both positive and negative ionization modes (11,13,14,21,26–30). A complete description of these scans, including the specific lipid class to be identified, the precursor ion type selected for each scan (e.g.,  $[M + H]^+$ ,  $[M + Na]^+$ ,  $[M + NH_4]^+$ ,  $[M - H]^-$ ,  $[M + Cl]^-$  and  $[M + CH_3OCO_2]^-$ ), the mass of the specific product ion or the neutral loss that was detected, and their identities, is given in Table 2.1. Specific examples of these experiments, for determining the presence of SM, GPCho, GPEtn, GPIIns, GPSer, DG, and TG lipids, are discussed below.

In each case, multiple precursor ion and neutral loss scan mode experiments were used to identify and characterize the individual components of a particular lipid class. The use of multiple scans enabled the compositions of the overlapping ions present at a particular  $m/z$  value in either the positive or negative ionization mode mass spectra to be more fully elucidated, and allowed the list of spectral features (i.e., molecular ions and their various adducts) that were observed in both the positive and negative ionization mode mass spectra to be significantly expanded. Particularly noteworthy was an observation that the use of complementary precursor ion and neutral loss scans enabled the identification and characterization of molecular species that were not detected using the 'typical' scan types that have been most commonly employed previously in the literature for lipid-profiling experiments.

### **2.3.3 Complementary precursor ion and neutral loss scan mode analysis of**

#### **rat retina SM and GPCho lipids**

The identification of abundant SM and GPCho species in negative ion mode is useful when it is necessary to (a) identify spectral features of a negative ion mass spectrum; (b) perform fatty acid analysis of lipid species by negative ion product ion tandem mass spectrometry or precursor ion scanning of  $m/z$  corresponding to deprotonated fatty acyls; and (c) identify  $m/z$  at which one or more lipid species may be present in a negative ion mass spectrum or tandem mass spectrum. Analysis of these two lipid classes is often complicated by overlap of a GPCho first  $^{13}\text{C}$  isotope peak with a putative SM molecular ion. This can be overcome by destruction of GPCho (and all glycerophospholipids) by alkaline hydrolysis (29). This approach is not useful, however, when analysis of both SM and GPCho species are needed from limited amounts of tissue. While algorithms to correct for  $^{13}\text{C}$  isotope abundances have been used to distinguish putative SM molecular ions from GPCho first  $^{13}\text{C}$  isotope peaks (25;31), the extremely low abundance of retinal SM molecular ions detected by typical positive ion analysis has precluded the successful reliance upon deisotoping algorithms alone for thorough analysis of rat retina SM species.

The ability of SM and GPCho species to form adducts with chloride ( $\text{Cl}^-$ ) and methyl carbonate ( $\text{CH}_3\text{OCO}_2^-$ ) anions enabled a convenient method for negative ion mode detection of SM and GPCho molecular species. Chloride ions are often present in small amounts in lipid extracts. While  $\text{Cl}^-$  ions may be minimized by multiple sample washing and desalting steps, we have found the presence of  $\text{Cl}^-$  to be beneficial for negative ion analysis of SM and GPCho. Figure 2.2A demonstrated negative ion mode collisionally induced dissociation (CID) of the  $[\text{M} + \text{Cl}]^-$  ion of a synthetic GPCho(14:0/14:0) species in the presence of 0.5 mM NaCl.

Collisionally induced dissociation of chloride adducts of GPCho species led to an abundant neutral loss of 50 Da, corresponding to loss of methyl chloride. Dissociation of this species also resulted in ions corresponding to the loss of the GPCho 14:0 fatty acid moieties as neutral ketene species, observed at  $m/z$  452, as well as abundant ions at  $m/z$  227 corresponding to the deprotonated fatty acids. By contrast, CID of chloride-adducted synthetic SM(d18:1/12:0) revealed the abundant neutral loss of 50 Da was the primary product ion observed over a wide range of collision energies (Fig. 2.2B). Dissociation of GPCho(14:0/14:0)  $[M + CH_3OCO_2]^-$  ions resulted in the spectra shown in Fig. 2.2C. Abundant neutral losses of 76 Da (loss of  $CH_3OCO_2 + H$ ), 135 Da (loss of  $CH_3OCO_2 + (CH_3)_3N$ ), and 161 Da (loss of  $CH_3OCO_2 + (CH_3)_3NCHCH_2$ ) were observed, as well as ions representing the loss of the neutral 14:0 fatty acid ( $m/z$  391) and the fatty acid anion ( $m/z$  227). Fragmentation of the methyl carbonate adduct of synthetic SM (d18:1/12:0) by CID Fig. (2.2D) revealed phosphocholine-derived ions similar to those observed for GPCho, however at significantly different abundances. Abundant neutral losses of 76, 135, and 161 Da were all observed, yet here the loss of 161 Da dominated, as opposed to the loss of 135 Da that was seen for GPCho.

The negative ion mode gas-phase fragmentation behavior of SM and GPCho species, as demonstrated in Figure 2.2, enable the use of neutral loss scan mode MS/MS for class-specific detection of SM and GPCho. Performing the conventionally used neutral loss scan (NLS) of 50 Da (scan number 1 in Table 2.1) in rat retina lipid extracts in the presence of 0.5 mM chloride resulted in detection of both SM and GPCho species (Figure 2.3A). From the NLS 50 scan a total of 8 SM peaks, highlighted with bold text in Figure 2.3A, were readily discernible from GPCho

species. As the neutral loss of 135 Da was the most abundant loss observed for GPCho  $[M+CH_3OCO_2]^-$  ions across a wide range of collision energies, it enabled negative ion detection of rat retina GPCho species as methyl carbonate adducts by performing NLS 135 (Figure 2.3B, scan number 2 in Table 2.1) when ammonium hydroxide was added to the rat retina lipid extract at a concentration of 20 mM. Five low abundance SM peaks, highlighted with bold text in Figure 2.3B, were also detected with this scan. We next employed the neutral loss of 161 Da (scan number 3 in Table 2.1) to detect SM and GPCho  $[M + CH_3OCO_2]^-$  ions in a rat retina lipid extract, which resulted in the spectrum shown in Figure 2.3C. Here, 7 additional SM peaks could be detected that were not observed in the NLS 135 scan, as well as 4 SM peaks not detected by NLS 50. Additionally, the relative abundances of SM species at  $m/z$  777 and 805 (corresponding to SM(d18:1/16:0) and SM(d18:1/18:0)  $[M + CH_3OCO_2]^-$  ions) were increased approximately 10-fold and 20-fold, respectively, compared to their relative abundances in the NLS 135 scan. The differential fragmentation behavior of methylcarbonate-adducted anions of SM and GPCho was thus exploited to preferentially detect either a predominance of GPCho ions via the neutral loss of 135 Da, or a predominance of SM ions via the neutral loss of 161 Da.

Both chloride and methylcarbonate adducts of GPCho species were suitable for performing negative ion mode product ion scans to confirm GPCho fatty acid assignments. Likewise, GPCho species were detected as both chloride and methylcarbonate-adducted anions when precursor ion scanning of  $m/z$  corresponding to deprotonated fatty acyls was performed in rat retina lipid extracts (scan number 18 in Table 2.1, data not shown.) Therefore, it was advantageous to assess rat retinal GPCho content by utilizing both NLS 135 and NLS 50 for detection of GPCho species as  $[M + CH_3OCO_2]^-$  and  $[M + Cl]^-$  ions respectively. Performing

the additional NLS 161 for detection of SM  $[M + \text{CH}_3\text{OCO}_2]^-$  ions allowed for the most thorough identification of rat retinal SM species. Under the conditions employed here, negligible formate, or acetate adducts of PC and SM lipids were observed (11; 32).

Fragmentation of GPCho and SM  $[M+H]^+$  ions yields an abundant characteristic product ion at  $m/z$  184 corresponding to the protonated phosphocholine headgroup. Product ion spectra of synthetic GPCho(14:0/14:0) and SM(d18:1/12:0) are shown in Figure 2.4A and 2.4B, respectively. As observed for chloride and methylcarbonate adducts of GPCho and SM, product ion spectra of synthetic GPCho(14:0/14:0) and SM(d18:1/12:0)  $[M+Na]^+$  ions yielded similar product ions, though at differing relative abundances (Figure 2.4B and 2.4C). Abundant ions corresponding to loss of 59 Da ( $\text{N}(\text{CH}_3)_3$ ), 183 Da (neutral phosphocholine), and an ion corresponding to sodiated cyclophosphane at  $m/z$  147 were observed in the product ion spectra of both GPCho and SM. In the case of GPCho, the ion at  $m/z$  147 was the most abundant ion observed in the product ion spectrum. In the case of SM, however, the neutral losses of 183 and 59 Da were more abundant than the ion at  $m/z$  147. Additionally, the loss of 205 Da (corresponding to the neutral loss of sodium choline phosphate), was abundant from dissociation of GPCho  $[M+Na]^+$  ions, yet was present at less than 1% relative abundance upon dissociation of SM  $[M+Na]^+$  ions.

The spectra obtained from various positive ionization mode precursor ion and neutral loss scan mode MS/MS experiments for the identification of SM and GPCho lipid ions from crude whole rat retina lipid extract are shown in Figure 2.5. The spectrum obtained from the conventional precursor ion scan (PIS) mode MS/MS experiment (scan number 4 in Table 2.1), to

monitor for the formation of the characteristic phosphocholine product ion at  $m/z$  184 from dissociation of SM and GPCho  $[M+H]^+$  ions, is shown in Figure 2.5A. After isotopic correction, only four SM peaks were identified ( $m/z$  703, 731, 759, and 815, corresponding to d18:1/16:0, d18:1/18:0, d18:1/20:0, and d18:1/24:0 species of SM, respectively), at low (<5%) relative abundance. However, PIS 184 provided excellent sensitivity for GPCho detection, as it provided the highest signal / noise observed for all methods of GPCho detection.

As sodium ( $Na^+$ ) ions are often present in lipid extracts due to carryover from the aqueous phase during lipid extraction, sample washing steps, and the mass spectrometer matrix, additional precursor ion and neutral loss scan mode MS/MS analyses of SM and GPCho  $[M+Na]^+$  ions were also performed (see Figure 2.5 B-D; scan numbers 5-7 in Table 2.1.) Notably, each scan type varied greatly in terms of utility for SM analysis, consistent with the analysis of product ion spectra from GPCho and SM  $[M+Na]^+$  ions. We found that PIS 147 (Figure 2.5B, scan number 5 in Table 2.1), resulted in relative abundances of SM and GPCho species that were overall very similar to those obtained by the PIS 184 scan; however, only two SM species could be identified with this MS/MS scan. Figure 2.5C demonstrates the virtually exclusive detection of GPCho species as  $[M+Na]^+$  ions with no detection of SM  $[M+Na]^+$  ions. This was achieved by utilizing the constant neutral loss of 205 Da (scan #6 in Table 2.1). Exclusive detection of GPCho species by NLS 205 was consistent with the expected result based on the product ion spectra of GPCho and SM  $[M+Na]^+$  ions. Conversely, the product ion spectra of GPCho and SM  $[M+Na]^+$  ions suggested that the neutral loss of 183 Da may allow preferential detection of SM ions relative to GPCho ions. The use of NLS 183 in rat retina lipid

extracts resulted in the spectrum shown in Figure 2.5D. Here, four SM species could be detected, and the relative abundances of SM and GPCho were similar to those observed for PIS 184. The same results were obtained when NLS 183 was performed across a wide range of collision energies, which implies that this MS/MS scan mode does not afford a significant improvement over PIS 184 in terms of detection of SM species. Additionally, the ion at  $m/z$  856 (corresponding to GPCho(18:0/22:6)) was observed at greater relative abundance in NLS 183 relative to the other MS/MS scans utilized, which may implicate an acyl chain contribution to the fragmentation behavior of these ions. All of the scans used to detect SM and GPCho as  $[M+Na]^+$  ions were equally useful in providing redundant identification of GPCho molecular species, yet none of these scans matched the PIS 184 MS/MS scan in terms of overall sensitivity.

As observed for negative ion analysis, complementary precursor ion and neutral loss scan mode MS/MS analysis of SM and GPCho in the positive ion mode enabled redundant detection of SM and GPCho species, and the use of NLS 205 enabled specific detection of only GPCho without lipid extract fractionation prior to analysis. The ability to redundantly detect multiple molecular species, especially in the case of GPCho, by using multiple lipid class-specific fragment ions increased confidence in peak identification for low abundance ions. It should be noted, however, that negative ion analysis of SM species as either  $[M+CH_3OCO_2]^-$  or  $[M+Cl]^-$  ions proved more useful than positive ion analysis in terms of readily identifying the greatest number of distinct SM molecular species. In contrast, positive ion analysis was more effective for identification of GPCho species in terms of overall sensitivity (signal / noise); however, negative ion analysis of GPCho was useful for determining fatty acid substituents by product ion scanning and/or precursor ion scanning of deprotonated fatty acyl species. If ‘absolute

quantitation' of retinal SM and GPCho were to be attempted here, it would be necessary to analyze all ionization forms of SM and GPCho relative to internal standards and sum the contributions of each ionization form of SM or GPCho molecular species. Relative comparisons of lipid species across numerous samples could be achieved by selecting optimal scan modes for the desired lipid classes (i.e., NLS 161 for analysis of SM and PIS 184 for analysis of GPCho).

The MS/MS spectra collected for analysis of SM and GPCho species described here were analyzed between  $m/z$  700-1200 for positive ion mode, and  $m/z$  700-1300 for negative ion mode. To allow these spectra to be viewed in greater detail, smaller mass ranges are shown in Figure 2.3 and Figure 2.5. However, it should be noted that complementary analysis of rat retina SM and GPCho species verified the presence of GPCho species containing 32:6 and 34:6 very long chain polyunsaturated fatty acids; in each case a 22:6 fatty acid was identified at the remaining glycerol position of the GPCho species. These species were observed as abundant ions in the positive ion MS spectrum (Figure 2.1A) at  $m/z$  1048 and 1046, respectively. These species were identified by all positive ion MS/MS scan modes employed here for the analysis of SM and GPCho. These high molecular weight GPCho species were also identified by NLS 50 as  $[M+Cl]^-$  ions, which subsequently were used for product ion mode MS/MS analysis to verify the identities of the fatty acid moieties. However, these GPCho species were not detected as methylcarbonate adducts by either NLS 135 or NLS 161. By combining both positive and negative ion mode shotgun MS/MS analyses of all phosphocholine-containing lipids, identification of 13 SM and 29 GPCho lipids was achieved in rat retina crude lipid extracts with a significant degree of redundancy. A summary of the SM and GPCho molecular species detected by all MS/MS scan modes described above is provided in Table 2.2

### 2.3.4 Complementary precursor ion and neutral loss scan mode analysis of rat retina GPEtn and GPIIns lipids

Pairs of complementary neutral loss and precursor ion scans were also employed for the identification and characterization of GPEtn and GPIIns lipid species. The detection of GPEtn lipids has typically been achieved by monitoring for the neutral loss of 141 Da (i.e., phosphoethanolamine) from their  $[M+H]^+$  precursor ions in positive ion mode MS/MS analysis (scan number 8 in Table 2.1). The spectrum obtained from analysis of the crude rat retina lipid extracts using this scan is shown in Figure 2.6A. After correction for  $^{13}\text{C}$  isotope contributions, a total of 20 GPEtn lipid species were identified in this experiment. The use of a complementary precursor ion scan to monitor for the presence of a characteristic  $m/z$  196 product ion, corresponding to a glycerol phosphoethanolamine derivative (Figure 2.6B) from the  $[M-H]^-$  precursor ions of GPEtn (scan number 9 in Table 2.1), enabled the detection of 3 additional GPEtn lipids. The observed discrepancy in identified GPEtn lipids between the two scan types was due in part to the fragmentation behavior of GPEtn alkenyl species. While collisionally induced decomposition of GPEtn alkenyl  $[M-H]^-$  ions gives rise to the GPEtn-specific fragment at  $m/z$  196, the neutral loss of 141 Da is virtually absent from CID of GPEtn alkenyl  $[M+H]^+$  ions (38). GPEtn alkenyl species detected by the negative ion PIS 196 included those at  $m/z$  748, 750, and 774 in Figure 2.6B (see Table 2.3). Although scanning for the constant neutral loss of 141 Da affords the most sensitivity for detection of GPEtn species in terms of signal / noise ratio and absolute ion abundance (data not shown), the utility of the positive ion NLS 141 is

effectively limited to detection of diacyl GPEtn species. Furthermore, GPEtn  $[M+Na]^+$  ions, if present, are also detected by NLS 141, further complicating spectrum interpretation and quantification against an internal standard.  $m/z$  814 and 858 in Figure 2.6A represent abundant ions corresponding to sodium adducts of GPEtn(18:0/22:6) and GPEtn(22:6/22:6), respectively. It is possible to decrease the abundance of  $[M+Na]^+$  ions in this scan mode by using low collision energy CID (<30V under the conditions employed); however, the use of lower collision energies in the analysis of rat retina GPEtn lipids resulted in underrepresentation of GPEtn species containing 22:6 fatty acid constituents due to the lower fragmentation efficiency of these species. While the negative ion precursor of  $m/z$  196 scan affords detection of both diacyl and alkyl/acyl GPEtn species, this scan mode may also detect GPEtn  $[M+Cl]^-$  ions formed when chloride is present in a lipid extract ( $m/z$  826 and 870 in figure 2.6B). It should be noted that the signal-to-noise associated with the spectrum obtained by negative ion mode PIS 196 was approximately two orders of magnitude lower than that of the positive ion mode neutral loss scan, thereby placing a limitation on the utility of this scan mode for the detection of additional low abundance GPEtn lipid ions. Due to the potential complications arising from the presence of various ionic adducts, as well as the differential fragmentation behavior of alkenyl GPEtn species in positive versus negative ionization mode, the use of both of these MS/MS scan modes to redundantly detect GPEtn lipids allowed for more thorough evaluation of GPEtn lipids and greater confidence in peak identification. The GPEtn lipids identified in rat retina are summarized in Table 2.3. Fatty acid constituents were analyzed in negative ion mode as described in Chapter VI, under the subheading “Identification of lipid molecular species.” In this

analysis, a total of 24 GPEtn species were identified in rat retina after accounting for isobaric species, with redundant identification achieved for all diacyl species.

The detection of GPIIns lipids is typically achieved using a negative ion precursor ion scan mode MS/MS experiment, by monitoring for the formation of a characteristic product ion at  $m/z$  241 (corresponding to a dehydrated phosphoinositol) from their  $[M-H]^-$  ions (scan number 10 in Table 2.1). The spectrum resulting from this scan, shown in Figure 2.6C, enabled the identification of 14 GPIIns lipids. The use of a complementary scan (number 11 in Table 2.1) to monitor for the characteristic neutral loss of 277 Da (corresponding to the combined losses of phosphoinositol+NH<sub>3</sub>) from the  $[M+NH_4]^+$  adducts of GPIIns (Figure 2.6D) enabled nine of the lipids observed in the negative ion mode precursor ion scan experiment to be confirmed. This was especially useful in confirming ions of relatively low abundance. For example, the ions at  $m/z$  909 and 929 in the spectrum shown in figure 2.6C represent putative GPIIns  $[M-H]^-$  (Total carbon : total double bond) 40:6 and 42:10 species, respectively. These ions were confirmed as likely GPIIns species by the presence of their corresponding  $[M+NH_4]^+$  ions after conducting NLS 277 ( $m/z$  928 and 948 in Figure 2.6D.) Further complementary negative ion mode fatty acid analysis by scanning for precursor ions corresponding to deprotonated fatty acyl groups (scan number 18 in Table 2.1) confirmed the fatty acid constituents of these GPIIns species as diacyl 18:0/22:6 and 20:4/22:6, respectively (data not shown.) Taken together, these complementary sets of data enabled confident identification of the ions in question despite their low relative abundance. A compilation of all rat retina GPIIns species identified by positive and negative ion mode analysis is provided in Table 2.4.

### 2.3.5 Complementary precursor ion and neutral loss scan mode analysis of rat retina

#### GPSer lipids

Detection of glycerophosphatidylserine (GPSer) lipid species is typically achieved in either positive or negative ion mode by the use of neutral loss scan mode MS/MS experiments. Figure 2.7A demonstrates the collisionally-induced decomposition of the  $[M+H]^+$  ion of synthetic GPSer(14:0/14:0) at  $m/z$  680. The fragmentation of this ion is dominated by the neutral loss of 185 Da corresponding to loss of the phosphoserine headgroup. Figure 2.7B shows the spectrum obtained from collisionally-induced decomposition of the  $[M+Na]^+$  ion of the same GPSer(14:0/14:0) species. While a neutral loss of 185 Da was observed, the fragmentation of the GPSer(14:0/14:0)  $[M+Na]^+$  ion was dominated by the formation of the ion at  $m/z$  208, corresponding to a sodium phosphoserine cation. Additionally, loss of neutral sodium phosphoserine (207 Da) was observed at  $m/z$  495. Figure 2.7C demonstrates CID of the GPSer(14:0/14:0)  $[M-H]^-$  ion observed at  $m/z$  678. The most abundant ion observed in this spectrum results from the loss of 87 Da, corresponding to a serine derivative. Additional abundant ions were observed at  $m/z$  381 and 363, corresponding to losses of the 14:0 fatty acids as ketene and neutral species, respectively;  $m/z$  227, corresponding to the deprotonated fatty acid ions; and  $m/z$  153, corresponding to a cyclic glycerolphosphate derivative.

As the neutral loss of 185 Da was observed from decomposition of both GPSer  $[M+H]^+$  and  $[M+Na]^+$  ions, performing the typical positive ion mode analysis of rat retina GPSer by

utilizing NLS 185 (scan number 12 in Table 2.1) resulted in detection of both GPSer  $[M+H]^+$  and  $[M+Na]^+$  ions (see Figure 2.8A). As observed in the positive ion analysis of GPETn lipids, the presence of GPSer species in two different ionization forms within the same spectrum complicated interpretation of the spectrum, as ions that differ by 22 mass units could represent a difference of an adducted sodium ion, or the mass difference represented by the addition of two fatty acid methylene groups and three double bonds. The spectrum in Figure 2.8A contains several sets of ions that differ by 22 mass units, such as  $m/z$  790 and  $m/z$  812;  $m/z$  812 and  $m/z$  834;  $m/z$  836 and  $m/z$  858;  $m/z$  858 and 880; and  $m/z$  880 and  $m/z$  902. In each case, the ion observed at an increase of 22 mass units could represent either a sodium-adducted species of the ion at the lower nominal mass, or a unique GPSer molecular species with one or more fatty acids that contain additional carbons and double bonds relative to the GPSer species at the lower nominal mass.

Additionally, the spectrum obtained by NLS 185 contained several ions of very low relative abundance (denoted by bold type), including  $m/z$  762,  $m/z$  790, and  $m/z$  936. In order to provide confirmation of low abundance rat retina GPSer species and clarify the identities and ionization forms of ions observed in the NLS 185 spectrum, we employed two additional complementary GPSer-specific MS/MS scans. Figure 2.8B demonstrates use of a precursor ion scan for  $m/z$  208 to detect formation of the sodium phosphoserine ion from GPSer  $[M+Na]^+$  ions (scan number 13 in Table 2.1.) The spectrum obtained by performing this scan contained ions of only a single ionization form and elucidated  $m/z$  at which sodium-adducted GPSer species contributed to total ion current of the NLS 185 spectrum. The use of this complementary precursor ion scan would be useful in any positive ion mode analysis of GPSer in order to

confirm the presence or absence of GPSer  $[M+Na]^+$  ions, or to simplify relative quantitation of GPSer species against an internal standard. Furthermore, the use of PIS 208 enabled redundant detection of the low-abundance ions observed in the spectrum obtained by scanning for the neutral loss of 185 Da. The ions in bold in Figure 2.8B at  $m/z$  784,  $m/z$  812, and  $m/z$  958 represent sodiated adducts of the protonated GPSer ions observed at  $m/z$  762,  $m/z$  790, and  $m/z$  936, respectively, detected by the neutral loss of 185 Da.

Negative ion mode analysis of rat retina GPSer was achieved by the commonly used neutral loss of 87 Da (scan number 14 in Table 2.1). The spectrum obtained from this neutral loss mode MS/MS experiment is shown in Figure 2.8C. Performing NLS 87 results in detection of GPSer molecular species in only one ionization form (i.e.,  $[M-H]^-$ ), which offers the same advantage as the positive ion mode PIS 208 in terms of spectrum simplification and ease of relative quantification against an internal standard. The detection of GPSer  $[M-H]^-$  ions by NLS 87 offers an additional advantage in that ions identified by this MS/MS scan may in turn be used for direct analysis of esterified fatty acid constituents by product ion mode MS/MS experiments, or by precursor ion scanning of individual fatty acid anions. The use of NLS 87 to detect rat retina GPSer also provided another means of confirming the presence of low abundance ions detected by positive ion GPSer analysis. The ions in bold in Figure 2.8C at  $m/z$  760,  $m/z$  788, and  $m/z$  934 represent deprotonated equivalents of the low abundance ions detected by NLS 185 and PIS 208. Subsequent analysis of the fatty acid constituents of these GPSer species from their deprotonated ions revealed that the identities of these low-abundance ions were diacyl GPSer(16:0/18:1), GPSer(18:0/18:1), and GPSer(24:6/24:6).

Notably, an abundant ion at  $m/z$  810 was observed in the spectrum obtained from the negative ion NLS 87 MS/MS experiment. This ion represents the deprotonated form of the protonated ion observed at  $m/z$  812 in the NLS 185 MS/MS experiment. However, an ion at  $m/z$  812 was also observed in the PIS 208 MS/MS experiment, indicating that a small contribution of the ion current for  $m/z$  812 in the NLS 185 spectrum was made by a GPSer sodium adduct of the ion at  $m/z$  790. The quantification of  $m/z$  812 in the NLS 185 spectrum against an internal standard would necessitate accommodation for the presence of underlying the GPSer  $[M+Na]^+$  ion; however, the presence of the underlying GPSer  $[M+Na]^+$  ion would not have been detected without performing the PIS 208 MS/MS scan. Furthermore, complementary positive and negative ion mode analysis of GPSer utilizing only NLS 185 and NLS 87, respectively, would have falsely confirmed that the ion detected at  $m/z$  812 in the NLS 185 MS/MS scan consisted entirely of GPSer  $[M+H]^+$  species. This analysis underscored the advantages of employing lipid class-specific MS/MS detection methods in which lipid species are detected as only one ion form.

The ability to redundantly detect low-abundance rat retina GPSer species in multiple ion forms enabled increased confidence in peak calling and subsequent inclusion of these ions in analysis of esterified fatty acid groups. The ability to identify both protonated and sodium-adducted GPSer molecular ions in positive ion mode MS/MS analysis expanded the number of spectral features that could be assigned in the spectrum obtained from the initial MS analysis. Importantly, the use of a precursor ion scan of  $m/z$  208 to identify GPSer  $[M+Na]^+$  ions simplified positive ion GPSer analysis by clarifying the identities of lipid species at  $m/z$  where potential overlap existed between protonated and sodiated GPSer ions of differing fatty acid

composition. Use of the negative ion NLS 87 scan for detection of GPSer enabled the identification of spectral features of the negative ion mode MS spectra, and provided additional confirmation of GPSer species observed at very low abundance. Relative quantification of GPSer would be most straightforward when using either the negative ion NLS 87 MS/MS experiment, or the positive ion PIS 208 MS/MS experiment when known amounts of exogenous salts have been added to a lipid extract; this scan is also useful for determining the presence of endogenous salts that may be present following lipid extraction. After taking into account the redundant lipid species identified in both the negative ion scan mode neutral loss experiment and the positive ion scan mode neutral loss and precursor ion experiments, a total of 29 GPSer molecular species could be identified in rat retina, with 22 redundant identifications. See Table 2.5 for a detailed catalog of all identified rat retina GPSer species. This example clearly highlights the utility of alternative or complementary MS/MS scans that are not commonly employed in lipidome profiling studies to provide more detailed insights into the composition of complex lipid mixtures.

### **2.3.6 Complementary neutral loss scan mode analysis of rat retina DG and TG lipids**

Nonpolar lipids, such as diacylglycerols (DG) and triacylglycerols (TG), have typically required derivatization and/or chromatographic separation prior to ESI-MS analysis (33-36). This limits the ability to analyze both polar and nonpolar lipid classes from limited sample amounts. We have applied the principle of complementary neutral loss scan mode MS/MS to the analysis of DG and TG species in the same unfractionated rat retina extract that was used for analysis of the polar lipid classes described above. The addition of ammonium hydroxide (other

other ammonium salts) to lipid extracts prior to mass spectrometry analysis provides abundant ammonium cations that readily adduct neutral lipids such as DG's and TG's. Redundant detection of DG and TG  $[M+NH_4]^+$  ions was achieved by neutral loss scanning for multiple  $m/z$  corresponding to the loss of a neutral fatty acid +  $NH_3$  (scan #15 in Table 2.1.) By comparing spectra obtained from neutral loss scans corresponding to multiple naturally occurring fatty acids, the fatty acid moieties esterified to the glycerol backbone of species at each  $m/z$  were elucidated. Additionally, we have found that mono- and diacylglycerol  $[M+NH_4]^+$  ions are readily identified by neutral loss scanning of 35 Da, corresponding to an abundant loss of  $NH_3+H_2O$  (scan number 17 in Table 2.1.) This neutral loss scan was advantageous when simultaneous comparison of all MG/DG species to an internal standard was desired. Use of the NLS 35 MS/MS experiment was also useful for identifying DG species present in the ammonium-adducted fatty acid neutral loss spectra, as scanning for loss of a fatty acid +  $NH_3$  may also detect cholesteryl esters present at very low abundance in rat retina. Thus, NLS 35 enabled differentiation between putative DG and cholesteryl ester ions detected by positive ion mode fatty acid analysis of neutral lipid species. This neutral loss mode MS/MS scan also provided another means of verifying low abundance putative DG peaks identified in one or more fatty acid neutral loss scan. The limitation of NLS 35 was that DG species were only identified in terms of total carbons : total double bonds, which could be deduced from the nominal mass of a given species.

Figure 2.9A shows the spectrum obtained from simultaneous analysis of all abundant rat retina DG species by scanning for a neutral loss of 35 Da between  $m/z$  580-700.  $m/z$  614 was

detected as a putative diglyceride in this scan, consistent with the mass of a 34:0 (TC:TDB) diglyceride as an  $[M+NH_4]^+$  ion. The fatty acid compositions of DG and TG species were then determined by scanning for the neutral loss of a 16:0 fatty acid +NH<sub>3</sub> (Figure 2.9B), loss of an 18:0 fatty acid +NH<sub>3</sub> (Figure 2.9C), and the loss of a 22:6 fatty acid +NH<sub>3</sub> (Figure 2.9D), over a wider mass range (m/z 580-980). m/z 614 was redundantly detected in scans for the neutral loss of 16:0 and 18:0 fatty acids, confirming the identification of this m/z as DG(16:0/18:0). Analysis of the high mass range of the spectra shown in Figure 2.9B-D also revealed the presence of m/z 924 in all three fatty acid neutral loss scans. This led to the identification of the TG species as TG(16:0/18:0/22:6). However, an ion at low relative abundance was observed at m/z 670 in the spectrum obtained from scanning for a neutral loss of an 18:0 fatty acid (Figure 2.9C) that was not observed in the NLS 35 MS/MS experiment used to identify DG species. While m/z 670 is within the expected mass range for putative DG molecular species, the lack of an ion at m/z 670 in the NLS 35 spectrum cast doubt that this particular ion represented an 18:0 fatty acid-containing diglyceride. Direct product ion MS/MS analysis of m/z 670 was precluded by the exceedingly low abundance of this ion relative to polar lipid ion abundances in the unfractionated rat retina lipid extract. As the expected mass range for cholesteryl esters is similar to the expected mass range of diglycerides, we conducted an additional precursor ion scan of m/z 369 (scan number 16 in Table 2.1) to detect cholesteryl esters as  $[M+NH_4]^+$  ions. A peak at m/z 670 was observed in the PIS 369 spectrum, corresponding to an 18:0 cholesteryl ester (data not shown). This was in agreement with the original observation of m/z 670 in a neutral loss scan of 18:0 fatty acid neutral species. Hence, the use of complementary precursor ion and neutral loss scan mode MS/MS experiments enabled detailed analysis and redundant confirmation of low

abundance ions corresponding to rat retina neutral lipids without chromatographic separation of polar and nonpolar analytes. Note that the fatty acids selected for analysis by neutral loss scanning presented here were for demonstrative purposes only; a thorough analysis was conducted by scanning for neutral losses of all naturally occurring fatty acids. From this set of complementary analyses we delineated a list of 29 diacylglycerol and 111 triacylglycerol distinct molecular species (see Table 2.6).

#### 2.4. Discussion

From the data described above, it is clear that crude lipid extracts from whole rat retinas contain an extremely complex mixture of molecular species, representing a wide array of lipid classes at varying abundances. The observation of multiple ionic adducts of a given lipid class in both positive (e.g.,  $[M+H]^+$ ,  $[M+Na]^+$  and  $[M+NH_4]^+$ ) and negative (e.g.,  $[M-H]^-$ ,  $[M+Cl]^-$  and  $[M+CH_3OCO_2]^-$ ) ionization modes adds further complexity, effectively increasing the number of ‘spectral features’ to the resultant mass spectra obtained by analysis of these extracts. However, the ability to identify specific lipid species in both positive and negative ionization modes, as well as in their multiple adducted forms, enables unambiguous lipid identification, particularly important when lipids were present at low abundance.

In many cases, multiple lipid species were found to be present at a single nominal  $m/z$  value. For example,  $m/z$  834 in the positive ion mode MS spectrum shown in Figure 2.1A, was found to contain diacyl GPCho(18:0/22:6)  $[M+H]^+$ , GPSer(18:1/22:6)  $[M+H]^+$ , and GPSer(18:0/20:4)  $[M+Na]^+$  ions. Likewise,  $m/z$  834 in the negative ionization mode spectrum

shown in Figure 2.1B was found to consist of the  $[M-H]^-$  ions of GPSer(18:0/22:6) and GPEtn(22:6/22:6), as well as the methyl carbonate adduct ( $[M+CH_3OCO_2]^-$ ) of GPCho(16:0/18:1). Detection of lipid classes in multiple ionization forms was necessary to fully elucidate the identities of ions present in both positive and negative ion mass spectra at numerous  $m/z$ . This point becomes especially important when comparisons must be made across numerous samples, such as comparisons between normal and disease states, in which case any observed change in ion abundance between two or more groups of samples must be accurately characterized.

To assist in the implementation of complementary analysis of major lipid classes within the lipidome, we have assembled multiple pairings of possible precursor ion and neutral loss scan mode MS/MS experiments to enable redundant detection of each lipid class. The advantages and disadvantages of many of these scan types have been discussed, and in several cases, the use of redundant detection of a lipid class minimized the shortcomings of one or more MS/MS experiments. For example, positive ion analysis of GPEtn  $[M+H]^+$  ions by neutral loss scan mode MS/MS was found to be more sensitive than negative ion mode precursor ion analysis of GPEtn  $[M-H]^-$  ions in terms of signal / noise and absolute ion abundance. The more sensitive positive ion neutral loss scan is therefore optimal for analysis of low abundance GPEtn ions. However, the additional presence of  $[M+Na]^+$  ions, even at very low abundance, complicates analysis of the resultant positive ion MS/MS spectra and necessitates complementary analysis of GPEtn  $[M-H]^-$  ions for clarity. Negative ion MS/MS analysis of GPEtn enables the identification of alkenyl species that are not observed in positive ion GPEtn MS/MS analysis; yet the

significantly lower sensitivity of the negative ion mode GPEtn precursor ion scan precludes analysis of lipid species that may be present at relatively low abundance.

Most of the individual MS/MS experiments we have paired for use in complementary analysis of rat retina lipid classes were obtained from the available literature. In several cases we have employed novel precursor ion and neutral loss scans derived from previously published gas-phase fragmentation pathways to detect lipid classes in various ionic forms or modification states. To our knowledge, this analysis of the rat retina lipidome was the first analysis to include the negative ion neutral loss of 135 Da for detection of SM and GPCho species as methylcarbonate adducts; likewise, it was the first analysis to explore differential detection of SM and GPCho as methylcarbonate adducts by use of the negative ion neutral loss of 161 Da for preferential detection of SM species; and it was the first analysis to include detection of sodiated GPCho and GPSer species by positive ion mode precursor ion scanning of  $m/z$  147 and  $m/z$  208, respectively. Additionally, we introduced the positive ion mode neutral loss of 35 Da for simultaneous detection of diglyceride species as ammonium adducts. In this chapter we have provided a preliminary outline of the possible benefits and shortcomings of each of these novel MS/MS experiments, although a more rigorous examination of each proposed scan would be beneficial for assessment of the viability of these scans for use in large scale lipid profiling experiments.

Clearly, the use of redundant identification of rat retina lipid classes from multiple precursor ion types enabled the identification of molecular species that would not have been observed if only one MS/MS scan mode had been employed in the analysis of each lipid class. This was especially true in the analysis of SM and GPCho species, in which only 4 rat retina SM species could be readily detected by the conventional positive ion precursor ion scan of  $m/z$  184;

4 SM species were detected by neutral loss of 183 Da from sodiated SM ions; 2 SM species were detected by PIS 147 from sodiated SM ions; and 12 SM species were detected by the negative ion neutral loss of 161 Da from SM methylcarbonate adducts.

We have provided, as a reference, pairings of MS/MS experiments in Table 2.1 that can be used in the complementary analysis of lipid classes that were not discussed in this chapter, including cholesteryl esters, glycerophosphatidic acid (GPA), glycerophosphatidylglycerol (GPGro), and ceramides. As these lipid classes are of low abundance in many tissues, and especially in rat retina, their analysis certainly benefits from complementary analysis of multiple ion forms where possible, or by redundant detection of the same ion form by multiple scans. The pairings suggested for complementary analysis of lipid classes are certainly not exhaustive, and other sets of complementary pairs could be substituted for analysis of various lipid classes. Furthermore, as the understanding of gas phase fragmentation pathways of lipid classes and their ionic adducts progresses, it will expand the ability to perform complementary analysis to lipid classes that have not been addressed in this chapter.

## *2.5 Conclusions*

Although disruption of lipid metabolism is known to play a key role in the onset and progression of a variety of retinal diseases, the use of retinal lipid profiles to identify relevant pathways of disease progression has not been sufficiently explored. This lack of knowledge is largely due to the diversity of lipids and to limits in the sensitivity of previously available analytical methods. The methodology described in this chapter for lipid profile analysis of normal retina will be further applied to various diseased retinal states to aid in developing effective therapeutic strategies for retinal disorders.

**Table 2.1.** Description of the precursor ion and neutral loss scan mode MS/MS experiments employed for the class-specific identification of lipid molecular species.

#	Lipid class	Precursor ion	MS/MS scan type <sup>a)</sup>	Product ion / Neutral loss	Ref
1	SM,GPCho	$[M+Cl]^-$	NLS 50	CH <sub>3</sub> Cl	21
2	SM, GPCho	$[M+CH_3OCO_2]^-$	NLS 135	CH <sub>3</sub> OCO <sub>2</sub> H+(CH <sub>3</sub> ) <sub>3</sub> N	21
3	SM, GPCho	$[M+CH_3OCO_2]^-$	NLS 161	CH <sub>3</sub> OCO <sub>2</sub> +(CH <sub>3</sub> ) <sub>3</sub> NCHCH <sub>2</sub> )	21
4	SM, GPCho	$[M+H]^+$	PIS 184	Phosphocholine	13
5	SM, GPCho	$[M+Na]^+$	PIS 147	Sodium cyclophosphane	37
6	GPCho	$[M+Na]^+$	NLS 205	Sodium cholinephosphate	13
7	SM, GPCho	$[M+Na]^+$	NLS 183	Neutral phosphocholine	37
8	GPEtn	$[M+H]^+, M+Na]^+$	NLS 141	Phosphoethanolamine	14
9	GPEtn	$[M-H]^-$	PIS 196	Glycerol phosphoethanolamine	13
10	GPIns	$[M-H]^-$	PIS 241	Dehydrated phosphoinositol	13
11	GPIns	$[M+NH_4]^+$	NLS 277	Phosphoinositol+NH <sub>3</sub>	38

Table 2.1 (cont'd)

12	GPSer	$[M+H]^+$ , $[M+Na]^+$	NLS 185	Phosphoserine	11
13	GPSer	$[M+Na]^+$	PIS 208	Sodium phosphoserine	-
14	GPSer	$[M-H]^-$	NLS 87	Serine	13
15	Di- / Triacylglycerols, Cholesteryl esters	$[M+NH_4]^+$	NLS (m/z varies)	Fatty acid+NH <sub>3</sub>	28
16	Cholesteryl esters	$[M+NH_4]^+$	PIS 369	Cholestane cation	13
17	Mono- / Diacylglycerols	$[M+NH_4]^+$	NLS 35	H <sub>2</sub> O+NH <sub>3</sub>	-
18	Glycerophospholipids	$[M-H]^-$ , $[M+Cl]^-$ , $[M+CH_3OCO_2]^-$	PIS (m/z varies)	Fatty acyl anion	13
19	GPGro	$[M+NH_4]^+$	NLS 189	Phosphoglycerol+NH <sub>3</sub>	38
20	GPA	$[M+NH_4]^+$	NLS 115	NH <sub>3</sub> +H <sub>3</sub> PO <sub>4</sub>	-
21	GPGro, GPA	$[M-H]^-$	PIS 153	Cyclic glycerophosphate	13
22	18:0-based ceramides	$[M+H]^+$	PIS 266	Sphinganine derivative	29

Table 2.1 (cont'd)

23	18:1-based ceramides	$[M+H]^+$	PIS 264	Sphingosine derivative	29
24	18:2-based ceramides	$[M+H]^+$	PIS 262	Sphingadienine derivative	27
25	18:0-based ceramides	$[M-H]^-$	NLS 258	16:0 aldehyde	30
26	18:1-based ceramides	$[M-H]^-$	NLS 256	16:1 aldehyde	30
27	18:2-based ceramides	$[M-H]^-$	NLS 254	16:2 aldehyde	30

**Table 2.2.** Rat Retina SM and GPCho molecular species.

Lipid species <sup>a</sup>	Scan #1	Scan #2	Scan #3	Scan #4	Scan #5	Scan #6	Scan #7
	NLS 50	NLS 135	NLS 161	PIS 184	PIS 147	NLS 205	NLS 183
	(m/z)						
SM(d18:1/16:1)	-	-	775	-	-	-	-
SM(d18:1/16:0)	737	777	777	703	725	-	725
GPCho(14:1/16:0)	738	-	778	704	-	-	726
GPCho(14:0/16:0)	-	-	780	706	728	-	-
SM(d18:1/18:1)	763	-	803	-	-	-	751
SM(d18:1/18:0)	765	805	805	731	753	-	753
GPCho(16:0/16:1)	766	806	806	732	754	-	754
GPCho(16:0/16:0)	768	808	808	734	756	756	756
SM(d18:1/19:0)	-	-	819	-	-	-	-
GPCho(O-18:0/16:0)	-	-	820	746	-	-	-
SM(d18:1/20:1)	-	-	831	-	-	-	-
GPCho(16:1/18:1)	-	832	832	758	780	780	780
GPCho(16:0/18:2)	-	832	832	758	780	-	780

Table 2.2 (cont'd)

SM(d18:1/20:0)	793	833	833	759	-	-	781
GPCho(16:0/18:1)	794	834	834	760	782	782	782
GPCho(16:0/18:0)	796	836	836	762	784	784	784
GPCho(O-18:0/18:0)	-	-	-	774	-	-	-
GPCho(16:0/20:4)	816	856	856	782	804	804	804
SM(d18:1/22:2)	-	857	857	-	-	-	-
SM(d18:1/22:1)	-	-	859	-	-	-	-
GPCho(18:1/18:1)	820	860	860	786	808	808	808
GPCho(18:0/18:2)	820	860	860	786	808	808	808
GPCho(18:0/18:1)	822	862	862	788	810	810	810
GPCho(18:0/18:0)	824	864	864	790	812	812	812
GPCho(16:0/22:6)	840	880	880	806	828	828	828
GPCho(16:1/22:5)	840	880	880	806	828	828	828
SM(d18:1/24:4)	841	881	881	-	-	-	-
GPCho(38:5)	-	-	-	808	-	830	830
GPCho(18:0/20:4)	844	884	884	810	832	832	832
SM(d18:1/24:2)	845	-	-	-	-	-	-

Table 2.2 (cont'd)

SM(d18:1/24:1)	847	-	887	-	-	-	-
SM(d18:1/24:0)	849	-	889	815	-	-	-
GPCho(18:1/20:0)	-	-	890	816	-	-	-
GPCho(18:1/22:6)	-	906	-	832	854	854	854
GPCho(18:0/22:6)	868	908	908	834	856	856	856
GPCho(18:1/22:5)	868	908	908	834	856	856	856
GPCho(40:4)	-	-	-	838	860	860	860
GPCho(42:10)	-	-	-	854	876	876	876
GPCho(42:4)	-	-	-	866	-	-	-
GPCho(22:6/22:6)	912	952	952	878	900	900	900
GPCho(22:6/32:6)	1052	-	-	1018	1040	1040	1040
GPCho(22:6/34:6)	1080	-	-	1046	1068	1068	1068

**Table 2.3.** Rat retina GPEtn species detected by complementary positive and negative ion mode MS/MS analysis.

Lipid species <sup>a</sup>	Scan #8 NLS 141 (m/z)	Scan #9 PIS 196 (m/z)
GPEtn(16:0/18:1)	718	716
GPEtn(16:0/18:0)	720	718
GPEtn(O-16:1/20:4)	-	722
GPEtn(16:0/20:4)	740	738
GPEtn(18:1/18:1)	744	-
GPEtn(18:0/18:1)	746	744
GPEtn(O-16:1/22:6)	-	746
GPEtn(O-16:0/22:6)	750	748
GPEtn(O-18:0/20:4)	752	750
GPEtn(16:0/22:6)	764	762
GPEtn(18:1/20:4)	766	764
GPEtn(18:0/20:4)	768	766
GPEtn(O-18:2/22:6)	774	772
GPEtn(O-18:1/22:6)	776	774
GPEtn(O-18:1/22:5)	778	776
GPEtn(O-18:0/22:6)		
GPEtn(O-20:1/20:4)	-	778
GPEtn(18:2/22:6)	788	786
GPEtn(18:1/22:6)	790	788

Table 2.3 (cont'd)

GPEtn(18:0/22:6)	792	790
GPEtn(20:0/20:4)	796	794
GPEtn(20:4/22:6)	812	810
GPEtn(22:6/22:6)	836	834
GPEtn(22:4:/22:6)	840	838

*a)* GPEtn fatty acid substituents were determined by negative ion mode MS/MS experiments as described in the Methods section. Alkenyl species are denoted by O- preceding the acyl chain. A dash indicates a species that was not detected.

**Table 2.4.** Rat retina GPIns species detected by complementary positive and negative ion mode MS/MS analysis.

Lipid species <sup>a</sup>	Scan #10 PIS 241 (m/z)	Scan #11 NLS 277 (m/z)
GPIns(16:0/18:1)	835	-
GPIns(16:1/20:4)	855	874
GPIns(16:0/20:4)	857	876
GPIns(18:2/20:4)	881	900
GPIns(16:0/22:6)	881	900
GPIns(18:1/20:4)	883	902
GPIns(18:0/20:4)	885	904
GPIns(18:2/22:6)	905	-
GPIns(18:1/22:6)	907	-
GPIns(18:0/22:6)	909	928
GPIns(20:0/20:4)	913	932
GPIns(20:4/22:6)	929	948
GPIns(20:4/22:6)	931	-
GPIns(22:6/22:6)	953	-

<sup>a)</sup> GPIns fatty acid substituents were determined by negative ion mode MS/MS experiments as described in the Methods section. A dash indicates a species that was not detected.

**Table 2.5.** Rat retina GPSer molecular species detected by complementary positive and negative ion mode MS/MS analysis.

Lipid species <sup>a</sup>	Scan #12 NLS 185 (m/z)	Scan #13 PIS 208 (m/z)	Scan #14 NLS 87 (m/z)
GPSer(16:0/18:1)	762	784	760
GPSer(16:1/18:0)	762	784	760
GPSer(16:0/18:0)	-	-	762
GPSer(18:0/18:1)	790	812	788
GPSer(16:1/20:4)	-	-	808
GPSer(16:0/20:4)	812	834	810
GPSer(16:0/22:0)	-	842	818
GPSer(18:0/20:0)	-	842	818
GPSer(O-18:0/22:6)	-	842	818
GPSer(18:1/22:6)	834	856	832
GPSer(18:0/22:6)	836	858	834
GPSer(18:0/22:5)	838	860	836
GPSer(18:0/22:4)	840	862	838
GPSer(20:0/20:4)	840	862	838
GPSer(20:4/22:6)	856	878	854
GPSer(20:4/22:5)	858	-	856
GPSer(20:4/22:4)	-	-	858
GPSer(20:0/22:6)	-	886	862
GPSer(20:0/22:5)	866	-	864
GPSer(22:6/22:6)	880	902	878
GPSer(22:5/22:6)	882	904	880

Table 2.5 (cont'd)

GPSer(22:4/22:6)	884	906	882
GPSer(22:3/22:6)	-	908	884
GPSer(22:6/24:6)	908	930	906
GPSer(22:5/24:6)	910	932	908
GPSer(22:4/24:6)	912	934	910
GPSer(22:3/24:6)	-	-	912
GPSer(24:6/24:6)	936	958	934
GPSer(24:5/24:6)	938	-	936

- a) GPSer fatty acid substituents were determined by negative ion mode MS/MS experiments as described in the Methods section. Alkenyl species are denoted by O- preceding the acyl chain. A dash indicates a species that was not detected.

**Table 2.6.** Rat retina DG and TG molecular species detected as  $[M+NH_4]^+$  ions by scan #15.

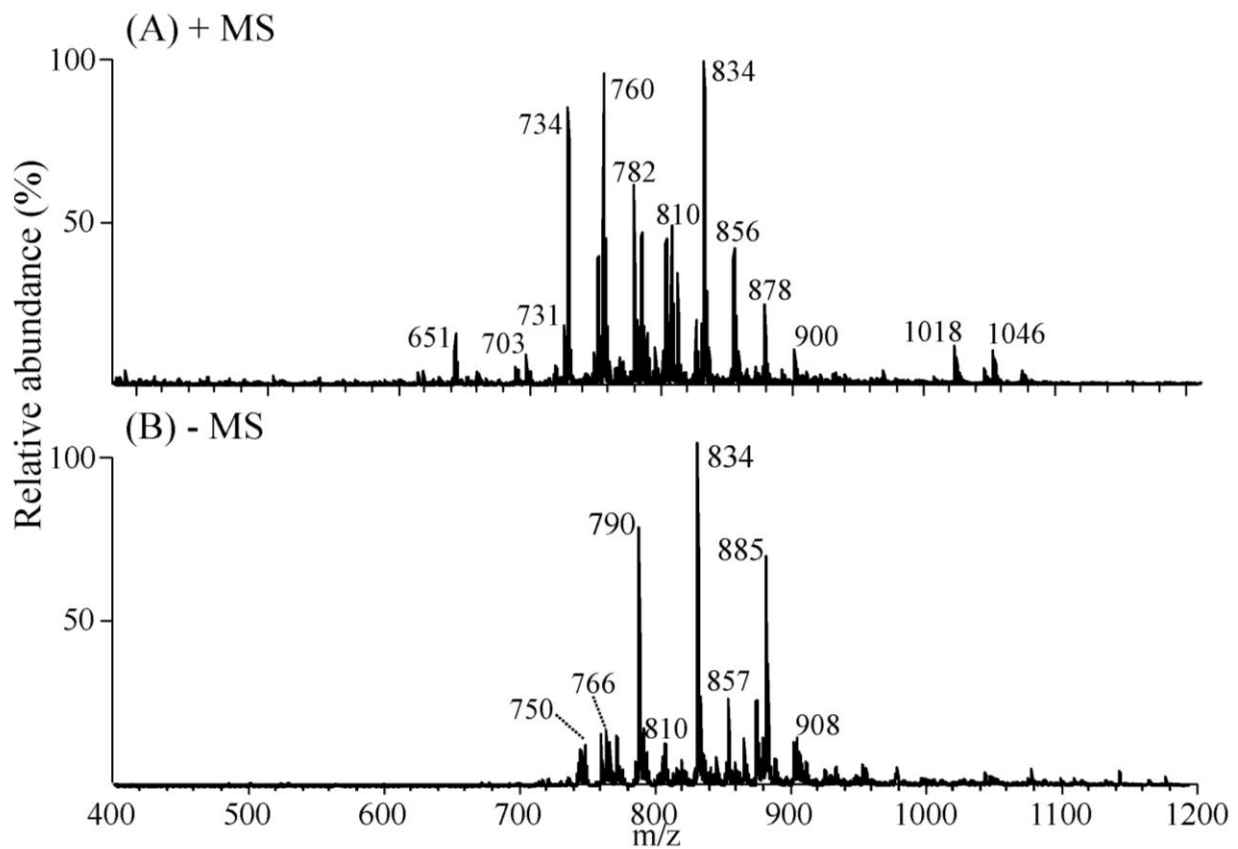
<u>m/z</u>	<u>Lipid species</u>						
584	DG(16:0/16:1)	820	TG(14:0/16:0/18:2)	876	TG(16:0/18:0/18:1)	922	TG(18:1/20:4/18:2)
586	DG(16:0/16:0)	820	TG(14:1/16:1/18:0)	876	TG(16:1/16:1/20:0)	924	TG(16:0/16:0/24:6)
612	DG(16:0/18:1)	820	TG(16:0/16:1/16:1)	878	TG(16:1/18:0/18:1)	924	TG(16:0/18:0/22:6)
612	DG(16:1/18:0)	822	TG(14:0/16:0/18:1)	878	TG(16:1/16:0/20:0)	924	TG(16:1/18:0/22:5)
614	DG(16:0/18:0)	822	TG(16:0/16:0/16:1)	880	TG(16:0/18:0/18:0)	926	TG(16:0/18:0/22:5)
634	DG(16:0/20:4)	824	TG(14:0/16:0/18:0)	894	TG(16:0/22:6/16:1)	926	TG(16:0/20:1/20:4)
638	DG(18:1/18:1)	824	TG(16:0/16:0/16:0)	894	TG(16:1/18:3/20:3)	926	TG(18:0/18:1/20:4)
640	DG(16:1/20:0)	844	TG(16:0/16:1/18:3)	894	TG(18:0/14:1/22:6)	928	TG(18:0/18:0/20:4)
640	DG(18:0/18:1)	844	TG(16:1/16:1/18:2)	894	TG(18:1/14:1/22:5)	944	TG(18:1/22:6/18:3)
642	DG(18:0/18:0)	844	TG(18:1/18:2/14:1)	896	TG(16:0/16:0/22:6)	946	TG(18:1/20:4/20:4)
642	DG(16:0/20:0)	844	TG(18:2/14:0/18:2)	896	TG(16:0/18:2/20:4)	948	TG(18:0/18:2/22:6)
658	DG(16:0/22:6)	846	TG(16:0/18:2/16:1)	896	TG(18:2/18:2/18:2)	948	TG(18:1/18:1/22:6)
660	DG(18:1/20:4)	846	TG(16:1/16:1/18:1)	898	TG(16:0/16:0/22:5)	950	TG(18:0/18:1/22:6)
660	DG(16:0/22:5)	846	TG(18:1/14:0/18:2)	898	TG(16:0/18:1/20:4)	950	TG(18:0/18:2/22:5)
662	DG(18:0/20:4)	846	TG(18:1/14:1/18:1)	898	TG(16:0/18:2/20:3)	952	TG(18:0/18:0/22:6)
664	DG(18:0/20:3)	848	TG(14:0/18:1/18:1)	898	TG(16:0/20:3/18:2)	956	TG(18:0/20:0/20:4)

Table 2.6 (cont'd)

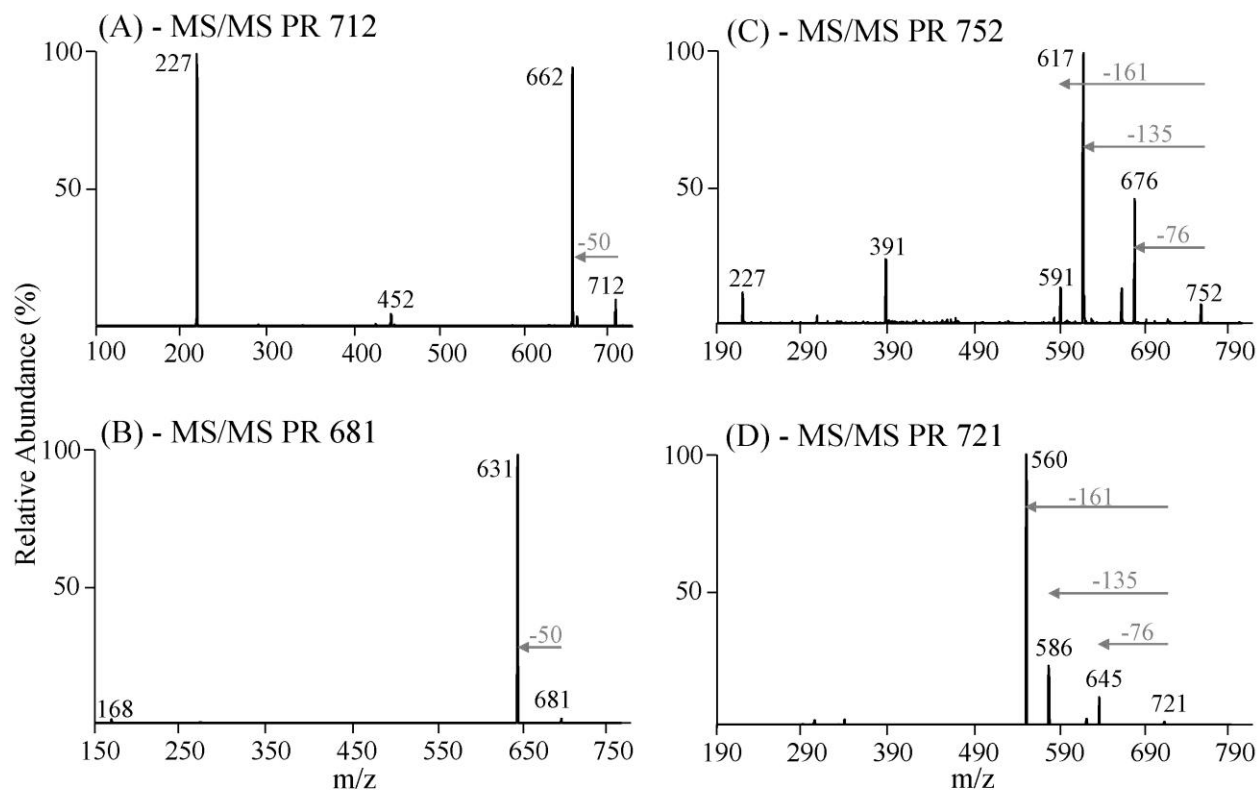
666	DG(18:2/20:0)	848	TG(16:0/16:0/18:2)	898	TG(16:1/20:1/18:3)	966	TG(20:4/20:4/20:5)
668	DG(18:1/20:0)	848	TG(16:0/16:1/18:1)	898	TG(16:1/20:3/18:1)	968	TG(18:2/22:6/20:4)
670	DG(18:0/20:0)	848	TG(18:1/14:0/18:1)	898	TG(18:2/18:2/18:1)	968	TG(18:3/20:3/22:6)
682	DG(20:4/20:4)	850	TG(16:0/16:0/18:1)	900	TG(16:0/18:0/20:4)	968	TG(22:6/22:6/16:0)
684	DG(18:1/22:6)	850	TG(16:0/18:0/16:1)	900	TG(16:0/18:1/20:3)	970	TG(16:1/22:5/22:5)
686	DG(18:0/22:6)	850	TG(18:0/14:0/18:1)	900	TG(18:0/18:1/18:3)	972	TG(18:0/20:4/22:6)
688	DG(18:0/22:5)	852	TG(16:0/16:0/18:0)	900	TG(18:0/18:2/18:2)	974	TG(18:0/20:4/22:5)
690	DG(20:0/20:4)	870	TG(16:0/20:4/16:1)	900	TG(18:1/18:1/18:2)	978	TG(18:2/22:5/20:0)
698	DG(20:0/20:0)	870	TG(16:1/16:1/20:3)	902	TG(18:1/18:1/18:1)		
706	DG(20:4/22:6)	870	TG(16:1/18:2/18:2)	902	TG(18:1/18:2/18:0)		
714	DG(20:0/22:6)	870	TG(16:1/18:3/18:1)	902	TG(18:2/20:1/16:0)		
720	DG(20:0/22:3)	870	TG(18:2/18:3/16:0)	904	TG(16:0/20:1/18:1)		
730	DG(22:6/22:6)	872	TG(16:0/16:0/20:4)	904	TG(18:0/18:0/18:2)		
		872	TG(16:0/18:1/18:3)	904	TG(18:0/18:1/18:1)		
768	TG(14:0/14:0/16:0)	872	TG(16:0/18:2/18:2)	906	TG(16:0/18:1/20:0)		
794	TG(14:0/14:0/18:1)	872	TG(16:0/20:3/16:1)	906	TG(16:0/18:0/20:1)		
794	TG(14:0/14:1/18:0)	872	TG(16:1/18:0/18:3)	906	TG(18:0/18:0/18:1)		
794	TG(14:0/16:1/16:0)	872	TG(16:1/18:1/18:2)	922	TG(16:0/18:1/22:6)		

Table 2.6 (cont'd)

818	TG(14:0/16:1/18:2)	874	TG(16:0/18:1/18:2)	922	TG(16:0/20:3/20:4)		
818	TG(16:1/14:1/18:1)	874	TG(16:1/18:0/18:2)	922	TG(16:0/16:1/24:6)		
818	TG(16:1/16:1/16:1)	874	TG(16:1/18:1/18:1)	922	TG(16:1/18:0/22:6)		
820	TG(14:0/16:0/18:2)	876	TG(16:0/18:0/18:2)	922	TG(16:1/20:2/20:4)		
820	TG(14:0/16:1/18:1)	876	TG(16:0/18:1/18:1)	922	TG(16:1/18:1/22:5)		



**Figure 2.1. Full mass spectra of rat retina lipids.** Mass spectra obtained from unfractionated rat retina lipid extract by scanning from  $m/z$  400 to  $m/z$  1200 in (A) positive ion or (B) negative ion mode.



**Figure 2.2. Negative ion mode analysis of GPCho and SM.** Negative ion mode product ion MS/MS spectra of  $[M+Cl]^-$  ions of synthetic GPCho(14:0/14:0) (A), SM(d18:1/12:0) (B), and  $[M+CH_3OCO_2]^-$  ions of synthetic GPCho(14:0/14:0) (C) and SM(d18:1/12:0) (D).

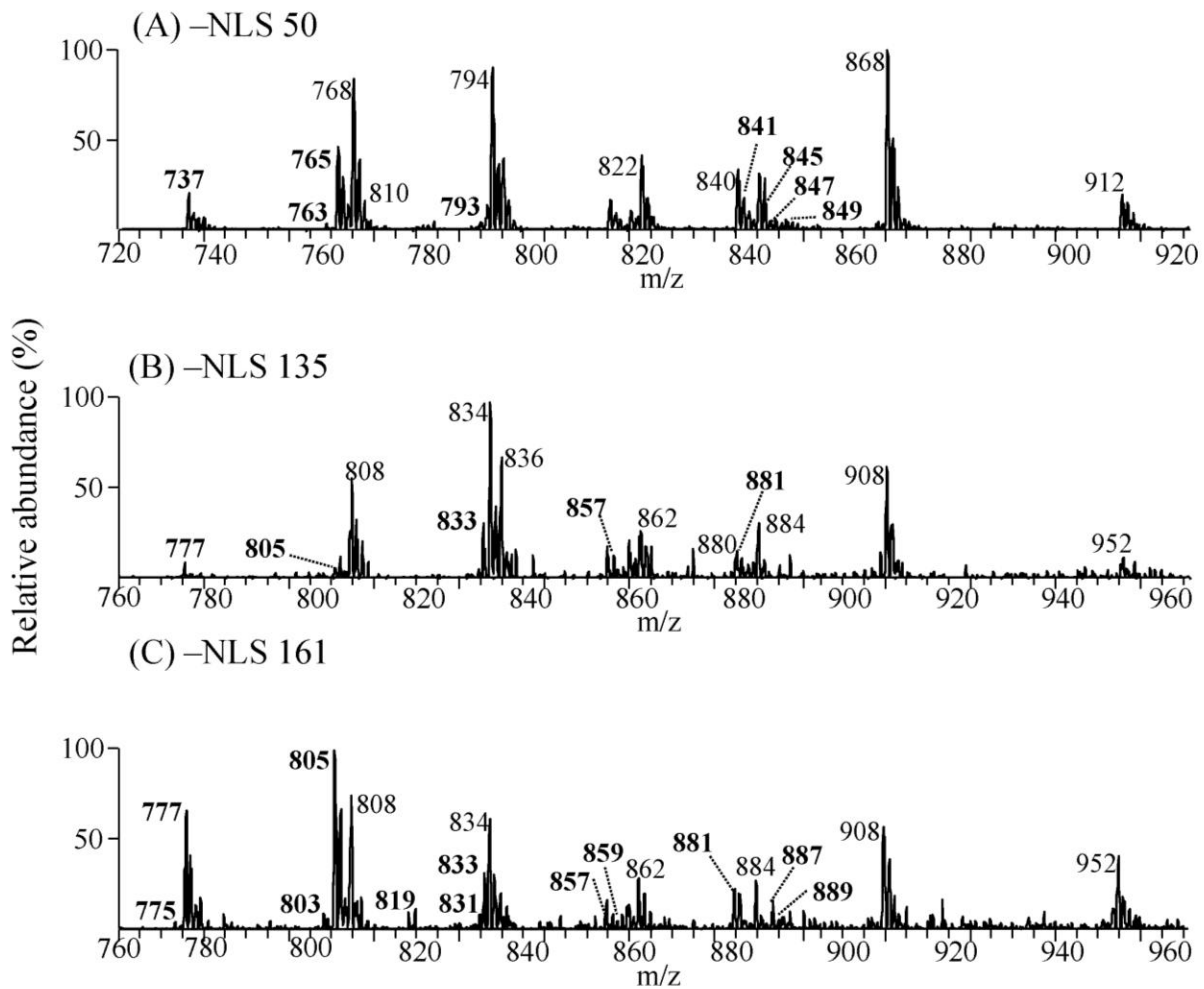


**Figure 2.3 Complementary negative ion mode MS/MS analysis of rat retina SM and GPCho species. Bold text indicates m/z of identified SM species.** (A) Detection of SM and GPCho as  $[M+Cl]^-$  ions by neutral loss scanning of 50 Da in the presence of 0.5 mM NaCl. (B) Detection of SM and GPCho as  $[M+CH_3OCOO]^-$  ions by neutral loss scanning of 135 Da. (C) Detection of SM and GPCho as  $[M+CH_3OCOO]^-$  ions by neutral loss scanning of 161 Da.

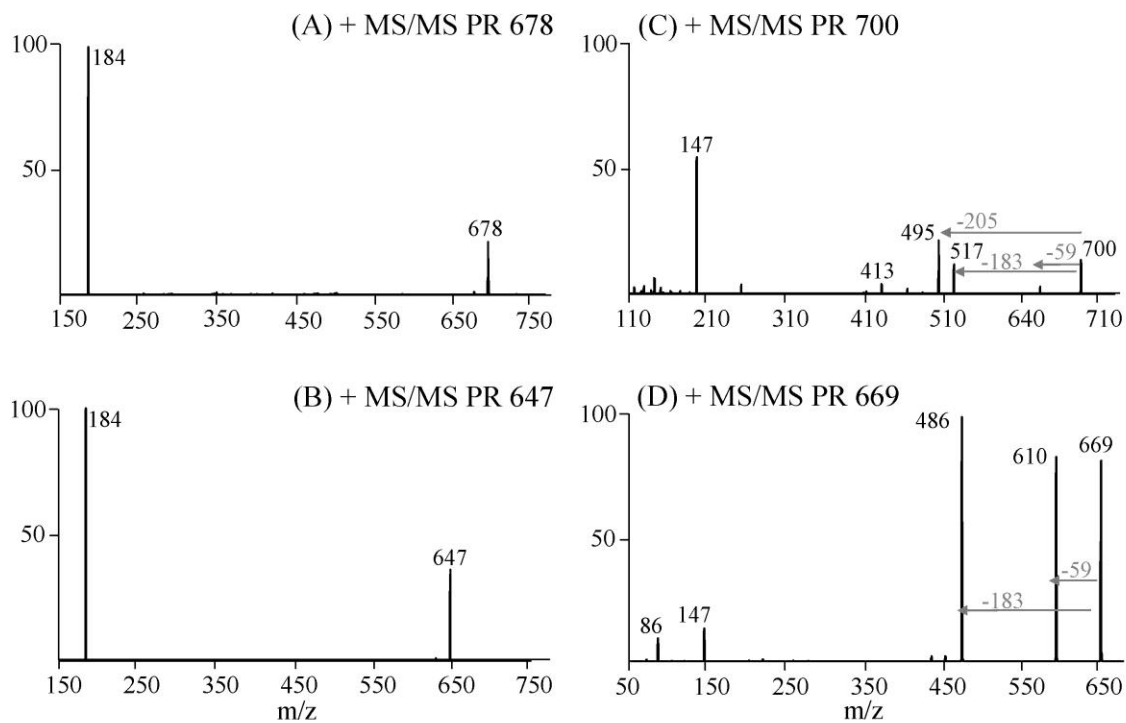


**Figure 2.4 Positive ion mode analysis of GPCho and SM.** Positive ion mode product ion MS/MS spectra of  $[M+H]^+$  ions of synthetic GPCho(14:0/14:0) (A), SM(d18:1/12:0) (B), and  $[M+Na]^+$  ions of synthetic GPCho(14:0/14:0) (C) and SM(d18:1/12:0) (D).

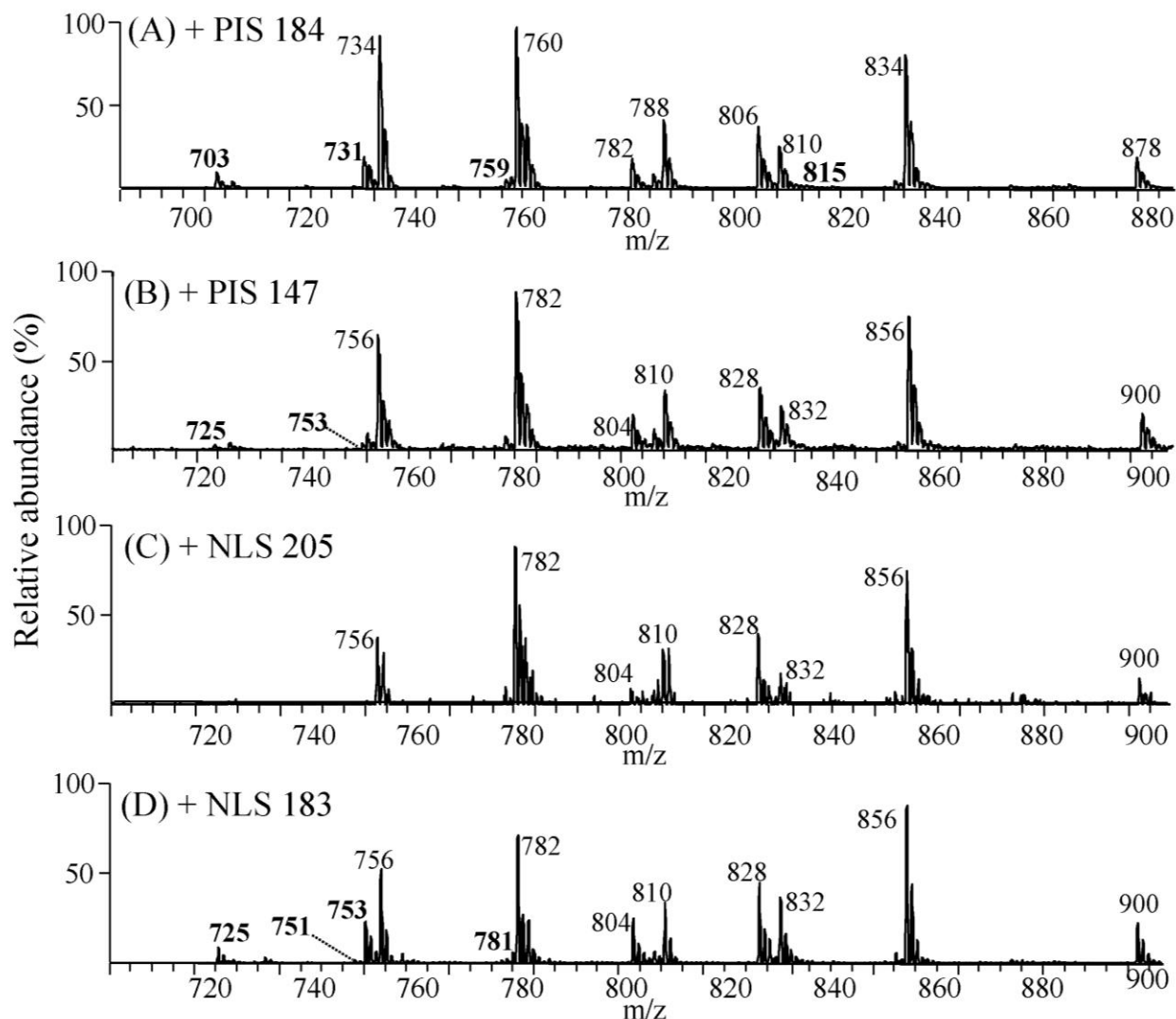


**Figure 2.5. Complimentary positive ion mode MS/MS analysis of rat retina SM and GPCho species.** Bold text indicates m/z of identified SM species. (A) Detection of SM and GPCho as  $[M+H]^+$  ions by precursor ion scanning of m/z 184. (B) Detection of SM and GPCho as  $[M+Na]^+$  ions by precursor ion scanning of m/z 147. (C) Detection of GPCho as  $[M+Na]^+$  ions by neutral loss scanning of 205 Da. (D) Detection of SM and GPCho as  $[M+Na]^+$  ions by neutral loss scanning of 183 Da.

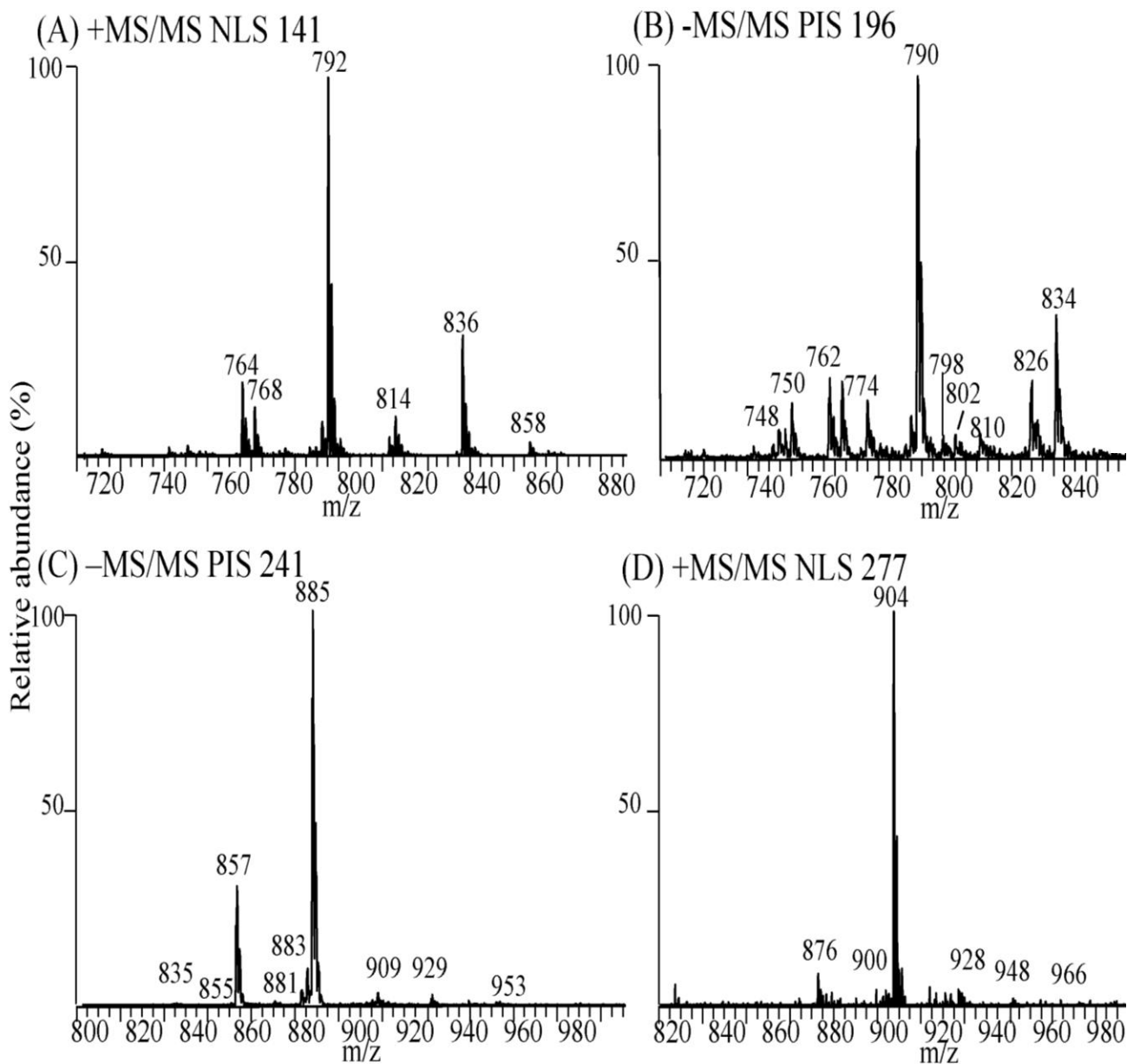


**Figure 2.6. Complementary positive and negative ion mode MS/MS analysis of rat retina GPEtn and GPIns species.** (A) Detection of GPEtn as  $[M+H]^+$  and  $[M+Na]^+$  ions by positive ion mode neutral loss scanning of 141 Da. (B) Detection of GPEtn as  $[M-H]^-$  ions by precursor ion scanning of m/z 196. (C) Detection of GPIns as  $[M-H]^-$  ions by negative ion mode precursor ion scanning of m/z 241. (D) Detection of GPIns as  $[M+NH_4]^+$  ions by positive ion mode neutral loss scanning of 277 Da.

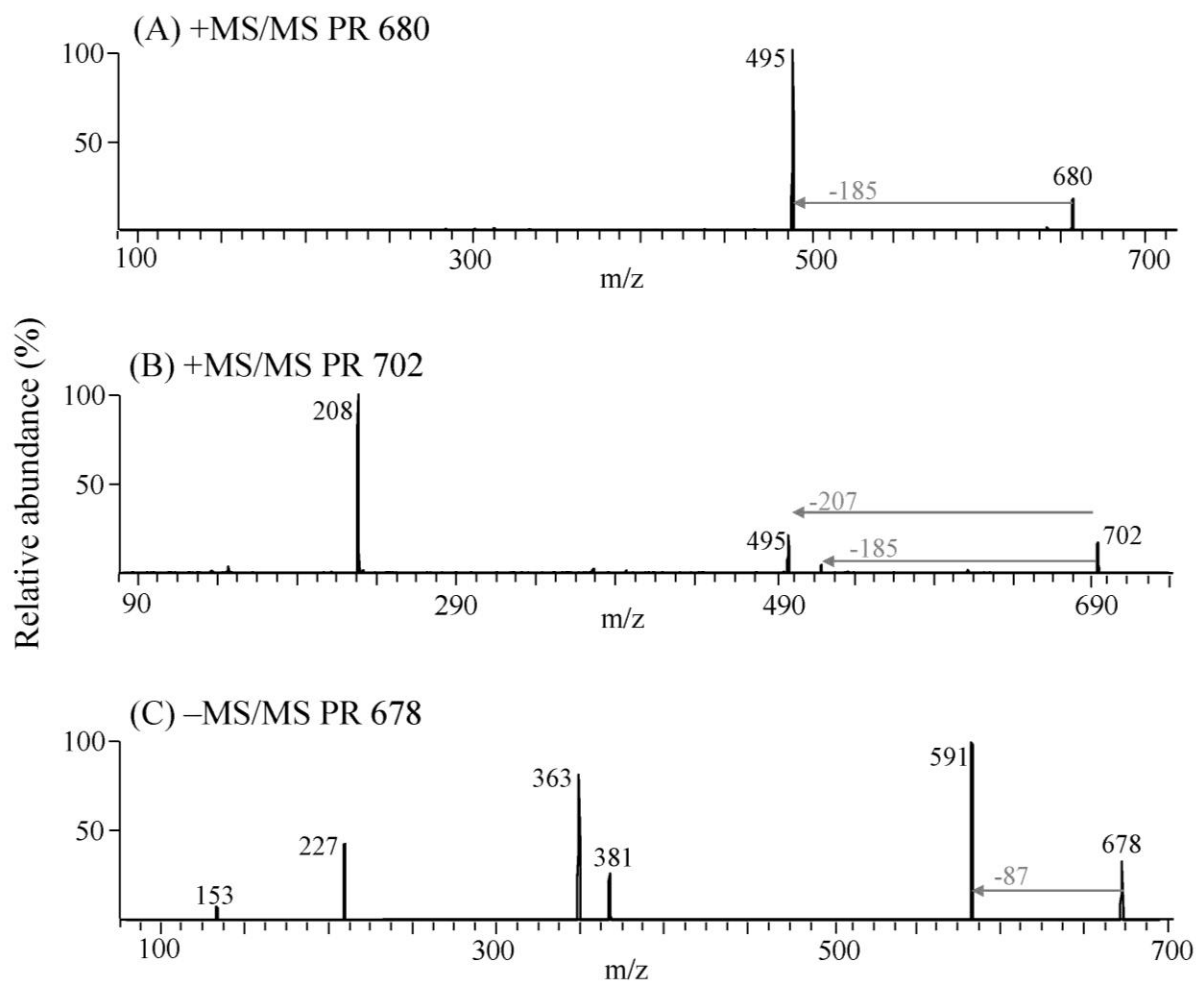


**Figure 2.7. Product ion mode MS/MS spectrum of synthetic GPSer(14:0/14:0)  $[M+H]^+$  ions. (A),  $[M+Na]^+$  ions (B), and  $[M-H]^-$  ions (C).**

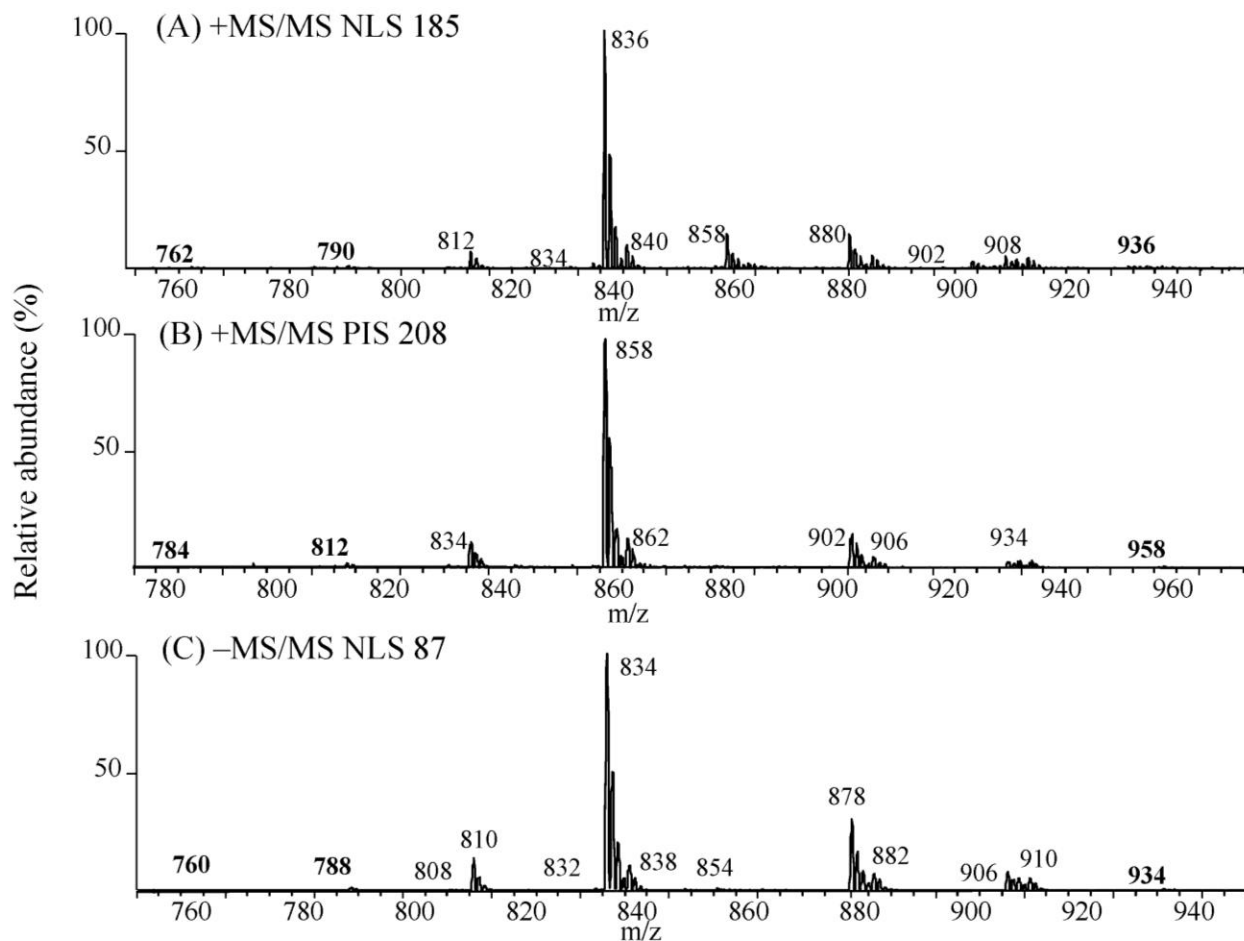


**Figure 2.8. Complementary positive and negative ion mode MS/MS analysis of rat retina GPSer species.** Bold text indicates m/z of species at very low relative abundance that were redundantly detected in multiple ion forms. (A) Detection of GPSer as  $[M+H]^+$  and  $[M+Na]^+$  ions by positive ion mode neutral loss scanning of 185 Da. (B) Detection of GPSer as  $[M+Na]^+$  ions by positive ion mode precursor ion scanning of m/z 208. (C) Detection of GPSer as  $[M-H]^-$  ions by negative ion mode neutral loss scanning of 87 Da.

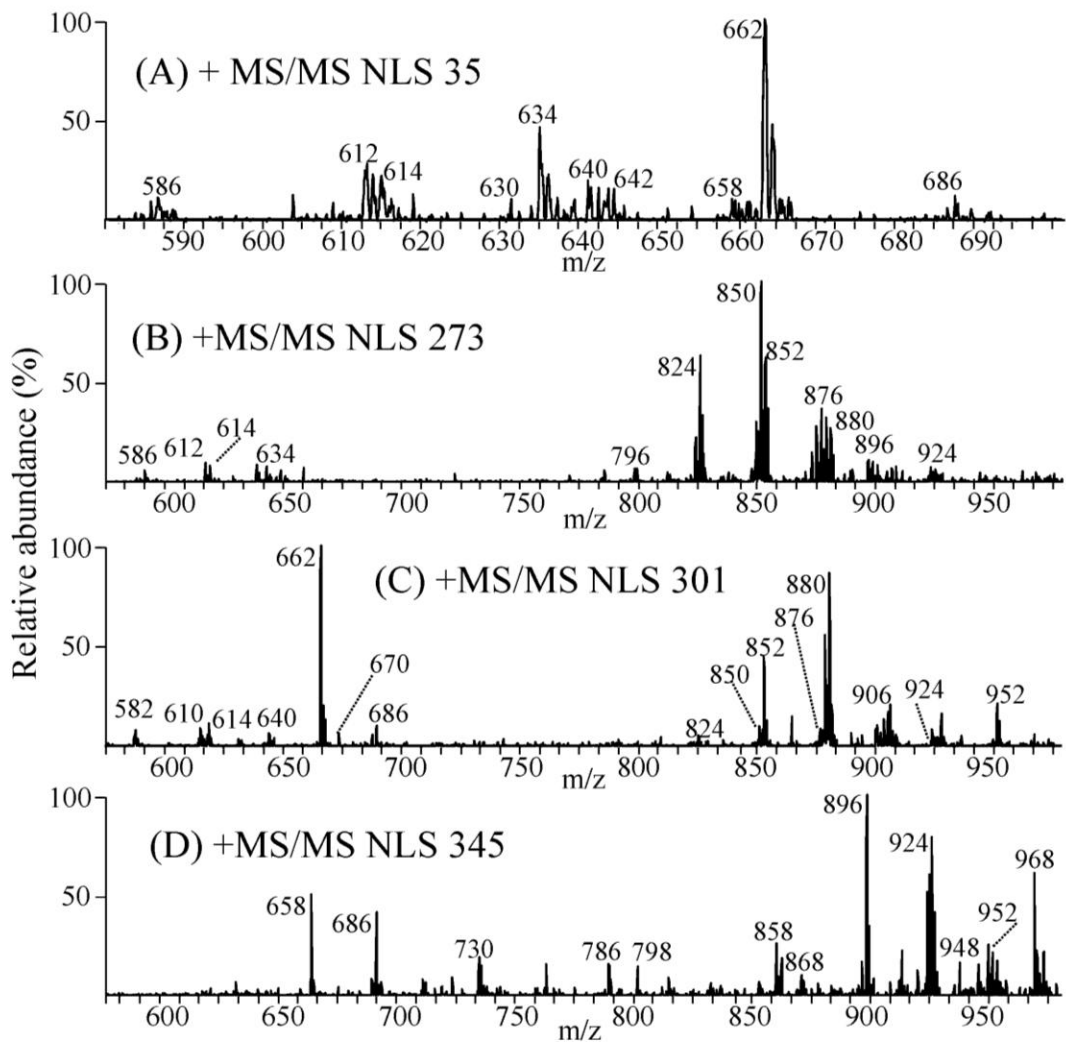


**Figure 2.9. Complementary positive ion mode MS/MS analysis of rat retina DG and TG species.** (A) Simultaneous detection of all abundant DG species as  $[M+NH_4]^+$  ions by neutral loss scanning of 35 Da. (B) Detection of all 16:0-containing DG and TG as  $[M+NH_4]^+$  ions by neutral loss scanning of 273 Da. (C) Detection of all 18:0- containing DG and TG as  $[M+NH_4]^+$  ions by neutral loss scanning of 301 Da. (D) Detection of all 22:6-containing DG and TG as  $[M+NH_4]^+$  ions by neutral loss scanning of 345 Da.

## References

## 2.6 References

1. Anderson RE. Lipids of ocular tissues. IV. A comparison of the phospholipids from the retina of six mammalian species. *Exp Eye Res* 1970;10(2):339-44.
2. Fliesler SJ, Anderson RE. Chemistry and metabolism of lipids in the vertebrate retina. *Prog Lipid Res* 1983;22(2):79-131.
3. Lecomte M, Paget C, Ruggiero D, Wiernsperger N, Lagarde M. Docosahexaenoic acid is a major n-3 polyunsaturated fatty acid in bovine retinal microvessels. *J Neurochem* 1996;66(5):2160-7.
4. O'Brien JS, Sampson EL. Fatty acid and fatty aldehyde composition of the major brain lipids in normal human gray matter, white matter, and myelin. *J Lipid Res* 1965;6(4):545-51.
5. SanGiovanni JP, Chew EY. The role of omega-3 long-chain polyunsaturated fatty acids in health and disease of the retina. *Progress in retinal and eye research* 2005;24(1):87-138.
6. Wang N, Anderson RE. Synthesis of docosahexaenoic acid by retina and retinal pigment epithelium. *Biochemistry (Mosc)* 1993;32(49):13703-9.
7. Wang N, Anderson RE. Transport of 22:6n-3 in the plasma and uptake into retinal pigment epithelium and retina. *Exp Eye Res* 1993;57(2):225-33.
8. Soubias O, Teague WE, Gawrisch K. Evidence for specificity in lipid-rhodopsin interactions. *J Biol Chem* 2006;281(44):33233-41.
9. Suh M, Wierzbicki AA, Clandinin MT. Dietary fat alters membrane composition in rod outer segments in normal and diabetic rats: impact on content of very-long-chain (C > or = 24) polyenoic fatty acids. *Biochimica et biophysica acta* 1994;1214(1):54-62.
10. Watson AD. Lipidomics: a global approach to lipid analysis in biological systems. *J Lipid Res* 2006;47(10):2101-11.
11. Brugger B, Erben G, Sandhoff R, Wieland FT, Lehmann WD. Quantitative analysis of biological membrane lipids at the low picomole level by nano-electrospray ionization tandem mass spectrometry. *Proc Natl Acad Sci U S A* 1997;94(6):2339-44.
12. Ejsing CS, Duchoslav E, Sampaio J, et al. Automated identification and quantification of glycerophospholipid molecular species by multiple precursor ion scanning. *Anal Chem* 2006;78(17):6202-14.

13. Han X, Gross RW. Shotgun lipidomics: electrospray ionization mass spectrometric analysis and quantitation of cellular lipidomes directly from crude extracts of biological samples. *Mass Spectrom Rev* 2005;24(3):367-412.
14. Pulfer M, Murphy RC. Electrospray mass spectrometry of phospholipids. *Mass Spectrom Rev* 2003;22(5):332-64.
15. Schwudke D, Oegema J, Burton L, et al. Lipid profiling by multiple precursor and neutral loss scanning driven by the data-dependent acquisition. *Anal Chem* 2006;78(2):585-95.
16. Welti R, Wang X, Williams TD. Electrospray ionization tandem mass spectrometry scan modes for plant chloroplast lipids. *Analytical biochemistry* 2003;314(1):149-52.
17. Welti R, Shah J, LeVine S, Esch SW, Williams TD, Wang X. High throughput lipid profiling to identify and characterize genes involved in lipid metabolism, signaling, and stress response. In: L. F, G.D. P, eds. *Functional Lipidomics*. New York: Marcel Dekker; 2005.
18. Jones JJ, Batoy SM, Wilkins CL. A comprehensive and comparative analysis for MALDI FTMS lipid and phospholipid profiles from biological samples. *Computational biology and chemistry* 2005;29(4):294-302.
19. Jones JJ, Borgmann S, Wilkins CL, O'Brien RM. Characterizing the phospholipid profiles in mammalian tissues by MALDI FTMS. *Anal Chem* 2006;78(9):3062-71.
20. Jones JJ, Stump MJ, Fleming RC, Lay JO, Jr., Wilkins CL. Strategies and data analysis techniques for lipid and phospholipid chemistry elucidation by intact cell MALDI-FTMS. *Journal of the American Society for Mass Spectrometry* 2004;15(11):1665-74.
21. Zhang X, Reid GE. Multistage tandem mass spectrometry of anionic phosphatidylcholine lipid adducts reveals novel dissociation pathways. *International Journal of Mass Spectrometry* 2006;252(3):242-55.
22. Koivusalo M, Haimi P, Heikinheimo L, Kostianen R, Somerharju P. Quantitative determination of phospholipid compositions by ESI-MS: effects of acyl chain length, unsaturation, and lipid concentration on instrument response. *J Lipid Res* 2001;42(4):663-72.
23. Zacarias A, Bolanowski D, Bhatnagar A. Comparative measurements of multicomponent phospholipid mixtures by electrospray mass spectroscopy: relating ion intensity to concentration. *Analytical biochemistry* 2002;308(1):152-9.
24. Folch J, Lees M, Sloane Stanley GH. A simple method for the isolation and purification of total lipides from animal tissues. *J Biol Chem* 1957;226(1):497-509.
25. Haimi P, Uphoff A, Hermansson M, Somerharju P. Software tools for analysis of mass spectrometric lipidome data. *Anal Chem* 2006;78(24):8324-31.

26. Callender HL, Forrester JS, Ivanova P, Preininger A, Milne S, Brown HA. Quantification of diacylglycerol species from cellular extracts by electrospray ionization mass spectrometry using a linear regression algorithm. *Anal Chem* 2007;79(1):263-72.
27. Colsch B, Afonso C, Popa I, et al. Characterization of the ceramide moieties of sphingoglycolipids from mouse brain by ESI-MS/MS: identification of ceramides containing sphingadienine. *J Lipid Res* 2004;45(2):281-6.
28. Murphy RC, James PF, McAnoy AM, Krank J, Duchoslav E, Barkley RM. Detection of the abundance of diacylglycerol and triacylglycerol molecular species in cells using neutral loss mass spectrometry. *Analytical biochemistry* 2007;366(1):59-70.
29. Merrill AH, Sullards MC, Allegood JC, Kelly S, Wang E. Sphingolipidomics: High-throughput, structure-specific, and quantitative analysis of sphingolipids by liquid chromatography tandem mass spectrometry. *Methods* 2005;36(2):207-24.
30. Han X. Characterization and direct quantitation of ceramide molecular species from lipid extracts of biological samples by electrospray ionization tandem mass spectrometry. *Analytical biochemistry* 2002;302(2):199-212.
31. Song H, Hsu F, Ladenson J, Turk J. Algorithm for processing raw mass spectrometric data to identify and quantitate complex lipid molecular species in mixtures by data-dependent scanning and fragment ion database searching. *J Am Soc Mass Spectrom* 2007;18:1848-58.
32. Houjou T, Yamatani K, Nakanishi H, Imagawa M, Shimizu T, Taguchi R. Rapid and selective identification of molecular species in phosphatidylcholine and sphingomyelin by conditional neutral loss scanning and MS3. *Rapid Commun Mass Spectrom* 2004;18(24):3123-30.
33. Liebisch G, Binder M, Schifferer R, Langmann T, Schulz B, Schmitz G. High throughput quantification of cholesterol and cholesteryl ester by electrospray ionization tandem mass spectrometry (ESI-MS/MS). *Biochimica et biophysica acta* 2006;1761(1):121-8.
34. Hvattum E. Analysis of triacylglycerols with non-aqueous reversed-phase liquid chromatography and positive ion electrospray tandem mass spectrometry. *Rapid Commun Mass Spectrom* 2001;15(3):187-90.
35. Li YL, Su X, Stahl PD, Gross ML. Quantification of diacylglycerol molecular species in biological samples by electrospray ionization mass spectrometry after one-step derivatization. *Anal Chem* 2007;79(4):1569-74.
36. Cai SS, Syage JA. Comparison of atmospheric pressure photoionization, atmospheric pressure chemical ionization, and electrospray ionization mass spectrometry for analysis of lipids. *Anal Chem* 2006;78(4):1191-9.

37. Han XL, Gross RW. Structural determination of picomole amounts of phospholipids via electrospray ionization tandem mass spectrometry. *J Am Soc Mass Spectr* 1995;6(12):1202-10.
38. Taguchi R, Houjou T, Nakanishi H, et al. Focused lipidomics by tandem mass spectrometry. *Journal of chromatography* 2005;823(1):26-36.

### III

## Analysis of Retina and Erythrocyte Glycerophospholipid Alterations in a Rat Model of Type 1 Diabetes

### *3.1 Abstract*

An automated tandem mass spectrometry based analysis employing precursor ion and neutral loss scans in a triple quadrupole mass spectrometer has been employed to identify and quantify changes in the abundances of glycerophospholipids extracted from retina and erythrocytes in a rat streptozotocin model of type 1 diabetes, 6 weeks and 36 weeks following induction of diabetes, compared to age matched nondiabetic controls. The utility of a 'label free' method compared to an 'internal standard' method for quantification of differences in the abundances of specific lipid ions was evaluated in both retina and erythrocyte lipid extracts. In retina, equivalent results were obtained by using the 'label free' and internal standard methods for quantification. In erythrocytes, the two methods of analysis yielded significantly different results, suggesting that factors intrinsic to particular sample types may influence the outcome of label-free lipidome quantification approaches.

Overall increases (~25% to ~35%) in the abundances of major retina glycerophospholipid classes were demonstrated in rats at 6 weeks of diabetes, relative to control animals. However, at 36 weeks of diabetes, subsequent overall decreases in retina glycerophosphocholine and glycerophosphoethanolamine abundances of 16% and 33%, respectively, were observed. Additionally, retina and erythrocyte glycerophosphocholine lipids at both 6 week and 36 weeks of diabetes exhibited increased incorporation of linoleic acid(18:2n6) and a decrease in docosahexaenoic acid (DHA(22:6n3)) content. Finally, an approximately 5-fold increase in the

abundances of specific glycated glycerophosphoethanolamine (Amadori-GPEtn) lipids were observed in the retina of 36 week diabetic rats, with a corresponding 1.6 fold increase of Amadori-GPEtn lipids in diabetic erythrocytes.

### *3.2. Introduction*

The identification of biomarkers that enable the early detection and prognosis of disease, or that facilitate measurement of the efficacy of response to a specific therapeutic intervention, hold great promise in advancing the capabilities of individualized medicine.(1-3) At this time however, there are only a few biomarkers for complex diseases, such as diabetes or cancer, which provide sufficient information for a variety of potential diagnostic decisions. Recent technological advances in mass spectrometry have enabled large scale biomarker discovery efforts to be initiated, particularly in the field of proteomics,(4) without prior requirement for detailed insights into the mechanisms responsible for the disease. However, there are a number of technical issues that currently limit the potential of mass spectrometry based protein biomarker identification approaches. Foremost among these is the analytical challenge presented by the enormous dynamic range associated with protein expression, particularly in plasma, which is in a constant state of spatial and temporal flux, as well as the great mixture complexity resulting from the diversity of transcriptional, translational and post translational modifications associated with protein expression throughout the cell cycle.(5) In recent years therefore, efforts have also been directed toward identification of other classes of biological molecules, including lipids, as potential biomarkers markers of specific disease states.(3; 6) Lipids are a diverse group of compounds, including fatty acyls, sterols, glycerolipids, glycerophospholipids and

sphingolipids, that play key biological roles as the main structural component of cell membranes, in energy storage and metabolism, and in cell signaling. A large number of studies have demonstrated that the disruption of lipid metabolism or signaling pathways can play a key role in the onset and progression of human disease.(7-12) Thus, a comprehensive analysis of the changes in lipid profiles that occur between normal and diseased cells, tissues or organs, and correlation of the changes observed in the end organs of the disease with those occurring in a more readily accessible blood fraction, such as erythrocytes, may enable the identification and characterization of specific lipids that can serve as effective biomarker signatures of disease.

Diabetic retinopathy is a debilitating complication of diabetes leading to blindness. Evidence of retinopathy is present in 65% of diabetic patients after 10 years of the disease.(13) It is widely accepted that diabetes-induced changes in the end organs of diabetic complications occur well before clinical manifestations of the complications can be observed. Moreover, using currently available treatment options, diabetes induced changes in the end organs are irreversible after a certain point, even after achievement of metabolic control. However, recent studies in animal models clearly demonstrate that there is both a circulating blood component and an end organ component of diabetic complications, and that correcting either of these components, at an early state in disease development, can ameliorate diabetic retinopathy.(14)

There is emerging evidence for a role of lipids in retinal pathology. Retina has the highest levels of long chain n3 and n6 polyunsaturated fatty acids (LCPUFA) including arachidonic acid (ARA(20:4n6)) and docosahexaenoic acid (DHA,22:6n3) observed in the body.(15-19) Numerous previous studies have recognized the important role of n3 and n6 LCPUFA's as key modulators of retinal development,(11; 12; 20; 21) and in the onset and progression of retinal diseases. For example, a case control study from the Age-Related Eye

Disease Study (AREDS) research group has demonstrated that total dietary n3 LCPUFA intake, including DHA(22:6n3), was inversely associated with neovascular age related macular degeneration (AMD), while the intake of n6 LCPUFA's, including ARA(20:4n6), was directly associated with the prevalence of the disease.(11) Another ocular disease, open angle glaucoma, has also been shown to be inversely associated with n3 PUFA levels. Compared with their healthy siblings, glaucoma patients had reduced eicosapentaenoic acid (EPA(20:5n3)) and DHA(22:6n3) in red blood cell phospholipids and triglycerides.(22) Low levels of DHA(22:6n3) in the erythrocytes of X-linked inherited Retinitis Pigmentosa (RP) patients have been shown to be negatively associated with the severity of the disease.(23-25) A recent study has demonstrated that the DHA(22:6n3) content of certain glycerophosphocholine (GPCho), glycerophosphoethanolamine (GPEtn) and glycerophosphoserine (GPSer) lipid molecular species were significantly lower in the retina of a rat model of Smith-Lemli-Opitz syndrome, relative to controls, and that these changes occurred in the absence of n3 fatty acid deficiency in plasma or liver.(9) DHA(22:6n3) deficiency has also been shown to result in a decrease in visual acuity during infant development,(20; 21) while a recent *in vivo* study has revealed that an increase in dietary DHA(22:6n3) intake can be protective against neovascularization in animal models of oxygen induced retinopathy of prematurity.(12)

Early stage diabetic retinopathy has been recognized as a low-grade chronic inflammatory disease.(26-31) Using a well established human retinal endothelial cell culture system, the primary cell type associated with diabetic retinopathy, it has recently been demonstrated that the n6 PUFA's linoleic acid(18:2n6) and ARA(20:4n6) induced inflammatory adhesion molecule expression and leukocyte adhesion,(32) whereas the n3 PUFA DHA22:6n3

exhibited an anti-inflammatory effect by inhibiting cytokine induced Nuclear Factor  $\kappa$ B (NF $\kappa$ B) activation and nuclear translocation, as well as adhesion molecule expression.(33; 34)

These studies clearly demonstrate the important role of lipids in retinal health and disease. However, there is surprisingly little information available that quantitatively describes the changes in global lipid profiles, or the specific molecular lipid species that undergo changes in abundance, upon development of diabetic complications in the retina.(35; 36)'(37) More importantly, there have been no studies carried out to date to correlate the lipid profile changes in the end organs of diabetic complications with those occurring in the blood cell or plasma of these subjects.

The limitations of techniques traditionally used for lipid analysis (e.g., thin-layer chromatography (TLC), gas-chromatography (GC)), have generally precluded comprehensive lipid analysis from the limited amount of material that can typically be obtained from either post-mortem human retina samples or the retinas obtained from animal models of the disease (e.g., rats and mice). However, the development of electrospray ionization (ESI) and matrix assisted laser desorption/ionization (MALDI) techniques,(38-46) coupled with the use of high-resolution mass spectrometry (MS) analysis,(47-49) or tandem mass spectrometry methods employing product ion scan or selective precursor ion and neutral loss scan mode analysis strategies,(39-43; 50-52) have enabled the application of 'shotgun' lipidomics approaches for rapid and sensitive monitoring of the molecular compositions and abundances of individual lipid species in complex lipid extracts obtained from limited quantities of sample tissue, and with minimal sample preparation. The application of selective precursor ion scan and neutral loss scan MS/MS methods, based on detection of the characteristic product ions formed via cleavage of either a

particular lipid head group or fatty acyl chain esterified to the glycerol backbone, from which information regarding the identity and structure of the lipid may be elucidated, have been particularly attractive for the rapid identification and characterization of multiple isobaric lipid species that may be present at a given  $m/z$  value. As the level of background noise is significantly reduced in precursor ion and neutral loss scan MS/MS spectra compared to a mass spectrum, these methods are also attractive for use in the rapid identification of low abundance lipid species, such as ceramides, cholesteryl esters, mono-, di- and tri-acylglycerols, or modified lipid species such as Amadori glycerophosphoethanolamine (Amadori-GPEtn) or glycerophosphoinositol (GPIs) mono-, bis- or tris-phosphate, that may often be present at or below the level of chemical noise in the mass spectra.

Quantitation of lipidomic data has typically been achieved by ratiometric comparison of the abundance of lipid ions of interest against that of a known exogenous lipid species added to the sample, following isotopic correction. The majority of approaches have entailed the use of synthetic exogenous lipid standards representative of a particular lipid class of interest. The synthetic lipids may be added during(41; 53; 54) or following(40; 43; 55) lipid extraction, and typically all lipid molecular species of a given class are quantified against a single synthetic internal standard of the same lipid class. While relatively straightforward, this approach does not take into account differences in ionization efficiency of lipids of differing acyl chain lengths and degree of unsaturation, which are pronounced in samples with a high total lipid concentration,(56; 57) or correct for different CID-MS/MS fragmentation efficiencies as a function of precursor ion mass under constant collision energy conditions. Correction for differences in ionization or dissociation efficiencies across the molecular species of a given lipid class may be performed by inclusion of several internal standards per lipid class, thereby

covering a wide range of fatty acyl total carbons and total double bonds, or through normalization to multiple external calibration curves.(56; 58; 59) The use of multiple internal standards consisting of stable isotope labeled lipid species has also been demonstrated to provide accurate quantitation of lipids with a high degree of variability in the number of total carbons and total double bonds.(60) However, the use of this strategy may not be feasible for analyzing large numbers of different molecular species across diverse lipid classes, as an untenable number of internal standards would be required.

In contrast to internal standard-dependent methods of lipidome quantification, the feasibility of obtaining statistical analysis based on comparative analysis of MS peak intensities and relative abundances from lipid extracts of experimental treatments relative to baselines obtained from control samples has been demonstrated.(61) Such “label free” approaches are critical when an internal standard for a lipid class of interest, such as modified lipids, is not readily (i.e., commercially) available. In proteomics based quantification, numerous studies in recent years have shown that label free methods, involving quantification of relative protein abundances based on precursor ion area intensity measurements using high resolution mass spectrometry, or by ‘spectral counting’ using the number of spectra identified for a given protein from multidimensional LC-MS/MS analyses of different biological samples, can provide comparable results to stable isotope labeling methods for abundant proteins.(62; 63)

### *3.3 Results*

Analyses of crude lipid extracts isolated from the whole retina and erythrocytes of age matched control and type 1 diabetic male *Wistar* rats, 6 weeks or 36 weeks after induction of diabetes with streptozotocin (STZ), were performed by introduction of the extracts to a triple

quadrupole (QqQ) mass spectrometer via infusion using a chip-based nano-electrospray ionization (nESI) source, followed by automated MS and MS/MS analysis in both positive and negative ion modes to identify and quantify GPCho, GPEtn, GPSer and GPIIns lipids. The use of an animal model, such as the rat, for studying changes in global retina lipid profiles as a function of the onset and progression of disease is attractive for several reasons, including the ability to control or systematically evaluate the effect of a number of variables, such as genetic background, environment, age and diet, that are known to alter the presence and abundance of particular lipid species at any given time.

### 3.3.1 Analysis of GPCho lipids in retina and erythrocytes at 6 weeks of diabetes

Representative mass spectra, obtained by using a precursor ion (PI) scan mode CID-MS/MS experiment in positive ion mode to identify the  $[M+H]^+$  precursor ions of glycerophosphatidylcholine (GPCho) lipids in whole retina and erythrocytes of age matched control and type 1 diabetic male *Wistar* rats, 6 weeks after treatment with STZ, via detection of the characteristic phosphocholine product ion at  $m/z$  184, are shown in Figure 3.1. The complementary information provided from the GPCho lipid class specific PI scan, as well as fatty acyl group specific precursor ion MS/MS scans or product ion MS/MS scan experiments of the  $[M+Cl]^-$  or  $[M+CH_3OCO_2]^-$  precursor ions in negative ion mode,<sup>(64)</sup> were employed to fully elucidate the identity of the head group, as well as the identities of the fatty acyl chains (number of total carbons and double bonds), within the lipid of interest (data not shown.) The most abundant GPCho lipid molecular species within the control rat retina (Figure 3.1A) was

found to contain the n3 polyunsaturated DHA(22:6n3) fatty acid (i.e., GPCho(18:0/22:6), m/z 834.4). Other abundant DHA(22:6n3) containing GPCho lipids were also observed, including GPCho(16:0/22:6) at m/z 806.4, a 44:12 GPCho species containing DHA(22:6n3) fatty acids at both the sn1 and sn2 positions of the lipid glycerol backbone (GPCho(22:6/22:6), m/z 878.4), and very long chain fatty acid-containing GPCho lipids (GPCho(32:6/22:6), m/z 1018.6 and GPCho(34:6/22:6), m/z 1046.6). A variety of n6 polyunsaturated linoleic acid(18:2n6) and ARA(20:4n6) containing GPCho lipids were also identified, including GPCho(16:0/18:2) at m/z 758.4, GPCho(18:0/18:2) at m/z 786.4, GPCho(16:0/20:4) at m/z 782.4 and GPCho(18:0/20:4) at m/z 810.4. Finally, several abundant GPCho lipids containing saturated palmitic acid(16:0) and stearic acid(18:0), and the n9 monounsaturated oleic acid(18:1) were observed, including GPCho(16:0/16:0) at m/z 734.4, GPCho(16:0/18:1) at m/z 760.4 and GPCho(18:0/18:1) at m/z 788.4.

Analysis of lipid extracts from three separate control rat retinas resulted in essentially identical spectra to those shown in Figure 3.1A, with percent standard deviations (% S.D.) ranging from 5-20% (with an average % S.D. of 11%), indicative of the minimal biological variability between these animals. This was expected given that these samples were obtained from animals with identical genetic backgrounds that were maintained under essentially identical conditions. However, in order to evaluate the variability introduced by the sample handling steps following initial lipid extraction, as well as the run-to-run variability associated with the mass spectrometry analysis, a series of experiments were also performed by triplicate dilution and analysis of a single control retina lipid extract, and by triplicate analysis of a single diluted control retina lipid extract. The % S.D.'s determined from these experiments, ranging from 6-14% with an average of 9% for the former, and from 4-12% with an average of 8% for the later,

were both smaller than the biological variability, indicating that the analysis methodology would be sufficiently reproducible and stable to enable quantitative determination of differences in the retina between control and diabetic sample groups (see below).

Although the molecular species identified from the diabetic rat retina (Figure 3.1B) were all consistent with those in the control retina, the relative abundances of individual lipids were observed to vary between control and diabetic states (compare Figures 3.1A and 3.1B, respectively, and Figure 3.2A). Changes in the relative abundances of individual lipids between control and diabetic erythrocyte lipid extracts were also observed (compare Figures 3.1C and 3.1D, respectively, and Figure 3.2B). Note, however, that the composition and abundances of the GPCho lipids from the erythrocyte extracts were quite different from those in the retina.

Interestingly, the average GPCho lipid ion abundances in the diabetic retina lipid extracts were found to be approximately 25% higher than the age matched control extracts (average ratio of diabetic/control of 1.2419 with a standard deviation of  $\pm 0.2259$ ) (Figure 3.2C). This increase is likely due to diabetes-induced upregulation of lipogenic gene expression, consistent with that previously reported by Brucklacher *et al.* (65) Notably, the average abundances of two n6 polyunsaturated linoleic acid containing GPCho lipids were significantly higher in the diabetic retina compared to the control retina (i.e., GPCho(16:0/18:2) with a 1.81 fold change, and GPCho(18:1/18:2) with a 1.67 fold change), where significance was defined as being outside the 90% confidence interval defined by  $\pm 1.645$  S.D., while one n3 polyunsaturated DHA<sub>22:6n3</sub> containing lipid (GPCho(22:6/22:6)) was found to undergo a significant decrease between diabetic and control retina samples, with a diabetic/control ratio of 0.86.

Comparison of the erythrocyte extract GPCho lipid ion abundances between age matched control and diabetic rats, 6 weeks after STZ treatment, determined that the average GPCho ion abundances remained essentially constant (Figure 3.2D). However, the level of one n6 PUFA containing GPCho lipid (GPCho(18:0/18:2)) was observed to give rise to a significant 1.41 fold increase, while a very low abundance GPCho(20:4/22:6) lipid was found to be lower in the diabetic erythrocyte (ratio of diabetic/control of 0.31). However, given the low abundance of this lipid in both control and diabetic extracts, we have not assigned any significance to this change in abundance. Overall, these results are consistent with previous studies that have found that the values of n6 PUFA's, linoleic acid(18:2n6) and ARA(20:4n6) in the plasma and erythrocyte membrane lipids in diabetic children and diabetic young adults versus age-matched healthy controls were significantly higher in diabetic subjects than in controls, while the n3 PUFA DHA<sub>22:6n3</sub> was significantly lower.(66; 67) Furthermore, the trends observed here are generally consistent between the GPCho lipids observed in the retina and erythrocyte samples, with an increase in the relative abundance of lipids containing oleic acid(18:1n9) and linoleic acid(18:2n6) fatty acids, and a decrease in lipids containing DHA<sub>22:6n3</sub> fatty acids.

### **3.3.2 Analysis of GPEtn lipids in retina and erythrocytes at 6 weeks of diabetes**

The identification and quantitative analysis of GPEtn lipids by CID-MS/MS represent a particular challenge. Both protonated ( $[M+H]^+$ ) and sodiated ( $[M+Na]^+$ ) GPEtn precursor ions are typically observed in a mass spectrum of a crude lipid extract, and sodiated GPEtn precursor ions may overlap at the same m/z value with protonated GPEtn precursors (e.g.,

$[\text{GPEtn}(18:0/20:4)+\text{Na}]^+$  at  $m/z$  788.5195 and  $[\text{GPEtn}(18:2/22:6)+\text{H}]^+$  at  $m/z$  788.5219). As both protonated and sodiated GPEtn precursor ions give rise to the neutral loss of phosphoethanolamine (141 Da) upon CID-MS/MS,(42)(68) a NL  $m/z$  141 scan cannot be used to differentiate between the presence of these two species. However, we have recently reported that the dissociation of sodiated ( $[\text{M}+\text{Na}]^+$ ) GPEtn precursor ions also give rise to a phosphoethanolamine+Na<sup>+</sup> product ion at  $m/z$  164, allowing the presence of the sodiated precursor ion to be readily determined by using a PI  $m/z$  164 scan.(69) Thus, in the analysis method employed here, both NL  $m/z$  141 and PI  $m/z$  164 scans were employed, as well as fatty acyl group specific PI scans in negative ion mode, to confirm the presence and identity of GPEtn lipids at specific  $m/z$  values. Only the identity of the most abundant GPEtn lipid that was found at a specific  $m/z$  value is reported.

The most abundant GPEtn lipid molecular species identified from the age matched control and diabetic rat retinas, 6 weeks following STZ treatment, were found to contain DHA(22:6n3) and ARA(20:4n6) (i.e., GPEtn(18:0/22:6) at  $m/z$  792.3, GPEtn(16:0/22:6) at  $m/z$  764.5, GPEtn(22:6/22:6) at  $m/z$  836.3 and GPEtn(18:0/20:4) at  $m/z$  768.5) (Figure 3.3A), while those in the control and diabetic rat erythrocytes were found to contain linoleic acid(18:2n6) and ARA(20:4n6) (i.e., GPEtn(16:0/18:2) at  $m/z$  716.5, GPEtn(16:0/20:4) at  $m/z$  740.5, GPEtn(18:1/18:2) at  $m/z$  742.5, GPEtn(18:0/18:2) at  $m/z$  744.5, GPEtn(18:1/20:4) at  $m/z$  766.5 and GPEtn(18:0/20:4) at  $m/z$  768.5) (Figure 3.3B). All of these are consistent with the acyl chain compositions found in the GPCho lipids described above. Also similar to that observed from the GPCho lipid analysis, an approximately 33% increase in the average GPEtn lipid ion abundance

was observed for the diabetic rat retina extracts compared to the control extracts (Figure 3.3C). A decrease in the abundance of the GPEtn(22:6/22:6) lipid was observed in the diabetic rat retina extracts (with a diabetic/control ratio of 0.77), consistent with the change in the abundance of the GPCho(22:6/22:6) lipid described above. However, the magnitude of this change was not found to be significant at this time. An increase in the abundance of a lipid identified as GPEtn(18:0/22:5), containing docosapentaenoic acid(22:5n3), was observed between diabetic and control retina extracts. However, as this lipid was very low in abundance, and could potentially overlap with the M+2 isotope peak from the highly abundant GPEtn(18:0/22:6) lipid, we have not assigned any significance to this change.

Comparison of the GPEtn lipid ion abundances determined from the erythrocyte extracts of age matched control and diabetic rats, 6 weeks after STZ treatment (Figure 3.3D), found that the average abundances were approximately 25% higher in the diabetic samples. This is in contrast to the results observed for the GPCho lipids extracted from erythrocytes. However, similar to that determined from the GPCho lipid analysis, the GPEtn(20:4/22:6) lipid was found to be lower in abundance in the diabetic erythrocyte (ratio of diabetic/control of 0.88). Once again however, due to the low abundance of this lipid, we have not assigned any significance to this change. Overall however, the trends observed were generally consistent between the GPEtn and GPCho lipids observed in the retina and erythrocyte samples, i.e., an increase in the relative abundance of lipids containing n6 PUFA and a decrease in the relative abundance of those containing n3 PUFA.

### **3.3.3 Analysis of GPSer and GPIIns lipids in retina and erythrocytes at 6 weeks of diabetes**

Similar to that found in the GPCho and GPEtn retina lipids, an increase in the average GPSer and GPIIns lipid ion abundances were observed between control and diabetic rat retina extracts (1.32 and 1.39 fold change, respectively) (Figures 3.4A,C and 3.5A,C, respectively). The average GPSer lipid ion abundances were observed to remain essentially unchanged between the control and diabetic rat erythrocyte extracts, while the average GPIIns erythrocyte lipid ion abundance increased (1.34 fold change) (Figures 3.4B,D and 3.5B,D, respectively). With the exception of the low abundance GPSer(18:0/18:2) lipid, that underwent a 1.31 fold increase between the control and diabetic erythrocyte extracts (see Figure 3.4B and 3.4D), consistent with that observed for the equivalent but more abundant GPCho(18:0/18:2) lipid species (see Figure 3.2D and 3.2B), none of the GPSer or GPIIns lipids in either the retina or erythrocyte extracts were found to undergo a significant change between control and diabetic states.

### **3.3.4 Analysis of GPCho and GPEtn lipids in retina and erythrocytes at 36 weeks of diabetes**

Given that the GPSer and GPIIns lipids were observed at very low abundance in both the retina and erythrocyte extracts at the 6 week time point following STZ treatment, and were not observed to yield significant changes between control and diabetic samples, all further analysis of retina and erythrocyte lipid extracts from control and diabetic rats, 36 weeks post STZ treatment, was performed only on the GPCho and GPEtn lipids. Prior to further dilution and subsequent mass spectrometry analysis of the lipid extracts, internal standards consisting of GPCho(14:0/14:0) and GPEtn(14:0/14:0) were added. This enabled a direct comparison of the

quantitative results obtained by analysis using the ‘label free’ method, with those obtained using an ‘internal standard’ method.

For the retina GPCho lipid extracts, essentially identical results were obtained from each method. The standard deviations obtained using the ‘internal standard’ method ranged from 12.0 - 27.7% with an average of 17.4% for the control extracts and from 10.2 - 23.6% with an average of 18.6% for the diabetic extracts (Figure 3.6A), while those from the ‘label free’ method ranged from 18.4 – 26.9 % with an average of 21.3 % for the control extracts and from 13.5 – 24.6 % with an average of 18.5 % for the diabetic extracts (Figure 3.6B). However, in contrast to the results obtained from the 6 week post STZ treatment GPCho retina lipid extracts (Figures 3.2A), where an approximately 24% increase in the average ion abundance was observed between diabetic and control samples, a decrease of approximately 16% in the average ion abundance between diabetic and control samples was observed at 36 weeks post STZ treatment, using both the internal standard and ‘label free’ approaches (Figures 3.6C and 3.6D, respectively). These data suggest that the increase in retina glycerophospholipid ion abundances observed at the 6 week time point following the onset of diabetes (postulated above to be due to diabetes-induced upregulation of lipogenic gene expression) are offset at the later time point, potentially due to an increase in retinal permeability associated with diabetic macular edema, which would decrease the ratio of lipid/water in the retina.<sup>(70)</sup> However, despite the overall decrease in average GPCho lipid abundances in the diabetic retina, the same molecular GPCho lipid species that were observed to be either significantly higher or lower in abundance in the diabetic retina compared to the control retina at the 6 week time point (i.e., GPCho(16:0/18:2), GPCho(18:1/18:2) and GPCho(22:6/22:6)) were also found to be significant at the 36 week time point.

In contrast to that determined from the retina samples, the results obtained from the extracted erythrocyte GPCho lipids, 36 weeks post STZ treatment, using the internal standard (Figure 3.7A) and the 'label free' (Figure 3.7B) methods yielded significantly different results. While the results obtained using the internal standard method indicated that the average GPCho lipid ion abundances were essentially unchanged between diabetic and control groups (Figure 3.7C), the 'label free' approach indicated an approximate increase in average ion abundances of 26% (Figure 3.7D). Diabetic ketoacidosis is known to result in a decrease in diabetic blood pH, and in the absence of buffering of tissue/cell homogenates, may affect extraction efficiencies or ionization efficiencies for lipids extracted from diabetic erythrocytes compared to control erythrocytes, or introduce other unanticipated matrix effects during mass spectrometry analysis. Note that the quantitative results obtained using the 'label free' and internal standard methods were both taken from the same experimental data sets, i.e., for the 'label free' method, each lipid extract contained the internal standard but this was not used for normalization of ion abundances. Thus, the observed differences between the 'label free' and internal standard quantification results may not be due to altered extraction efficiencies. Even though buffering of the lipid extracts prior to mass spectrometry analysis was performed via the inclusion of 20 mM  $\text{NH}_4\text{OH}$ , it was not determined whether the pH of the extracts were identical between diabetic and control erythrocyte lipid extracts. Thus, the differences in quantitative results that were determined using the two methods are likely due to higher electrospray ionization efficiencies or other matrix-related effects associated with the diabetic erythrocytes. Interestingly, as described above, no discrepancy in lipid ion abundances were observed between the internal standard and 'label free' methods for the 36 week retina samples. This is consistent with results from a previous study, suggesting that the retina is protected from perturbations due to diabetic ketoacidosis.(71)

Differences in the abundances of several individual GPCho molecular lipid species were determined between the diabetic and control erythrocyte extracts, 36 weeks post STZ treatment. For example, GPCho(18:1/22:6) was found to undergo a significant decrease using both ‘internal standard’ and ‘label free’ quantitative methods, while GPCho(16:0/18:1) was determined to undergo a significant increase, albeit only in the ‘label free’ quantitative method. However, the validity of the GPCho changes in the erythrocyte lipid profiles at the 36 week time point, determined using the ‘label free’ method, must be questioned.

Analysis of the GPEtn lipids extracted from retina and erythrocytes of control and diabetic rats, 36 weeks post STZ treatment, were also determined using both the internal standard and ‘label free’ methods. The results obtained from the retina and erythrocyte lipid extracts using the internal standard method are shown in Figures 3.8A and 3.8B, respectively. Similar to that described above for the GPCho lipids, analysis of the retina GPEtn lipids were found to yield essentially identical results from both methods, with an approximately 25% decrease in the average GPEtn lipid ion abundances observed between diabetic and control retina (Figure 3.8C), again indicating the utility of the label free method for quantitative analysis of lipids from retina tissue. However, none of the observed GPEtn molecular lipid species were found to be significantly different in abundance between the diabetic and control retina samples, consistent with that observed at the 6 week time point. Use of the label free method for analysis of the erythrocyte GPEtn lipids gave erroneously high results compared to those determined using the internal standard method (an 11% increase versus a 1% decrease in average GPEtn lipid ion abundances, respectively) (Figure 3.8D), similar to that determined by analysis of the GPCho lipids.

### 3.3.5 Analysis of Amadori-GPEtn lipids in retina and erythrocytes at 36 weeks of diabetes

As described above, quantitative mass spectrometry analysis determined that none of the individual GPEtn molecular lipid species were significantly different in abundance between the diabetic and control retina samples, at either the 6 week or 36 week time points following STZ treatment. However, a significant increase in abundance was observed between the diabetic and control retina for a modified (glycated) form of the GPEtn lipids (i.e., Amadori-PE or GPEtn(Glc)), determined by using a neutral loss scan to identify the characteristic loss of 303 m/z(72) (Figure 3.9). Representative mass spectra of the GPEtn lipids observed from control and diabetic retina extracts are shown in Figures 3.9A and 3.9B, respectively, while the spectra obtained for the Amadori-GPEtn lipids from the same samples are shown in Figures 3.9C and 3.9D, respectively. For the most abundant Amadori GPEtn lipid (i.e., Amadori-GPEtn(18:0/22:6)), a 4.8 fold increase ( $p < 0.05$ ) in the ratio of the Amadori-GPEtn to GPEtn lipid abundance was observed in the diabetic versus control retina lipid extracts (Figure 3.10A). Importantly, an increase in Amadori-GPEtn lipid abundance was also observed between the diabetic and control erythrocyte lipid extracts, where the most abundant Amadori-GPEtn lipid (GPEtn(18:10/20:4)) was observed to undergo a 1.6 fold increase ( $p < 0.05$ ).

### 3.4 Discussion

An increase in advanced glycation endproducts (AGE) in diabetes is well documented and has been extensively studied over the last decade.(73; 74) Moreover, serum levels of AGE's are known to be increased in patients with diabetic complications, compared to a complications-free cohort.(75; 76) However, AGE inhibitors have been shown to be effective in preventing the

development of diabetic complications in animal models.(77; 78) Although most prior studies have focused on AGE modified proteins, the free amino groups of aminophospholipids, such as GPEtn and GPSer, can also be targeted for non-enzymatic glycation, leading to the formation of glycated phospholipids.(79) Indeed, glycated GPEtn, referred to as Amadori-PE in the literature, has been shown to be increased approximately 2 fold in the blood plasma of type 2 diabetic patients compared to controls,(80) consistent with the results described above. Addition of synthetic Amadori-PE to human umbilical vein endothelial cell culture significantly increased angiogenic factors, including matrix metalloproteinase 2,(81) a pivotal enzyme in the initial step of angiogenesis.(82) Although the magnitude of the changes observed here in Amadori-GPEtn lipid abundances in both the retina and erythrocytes require further confirmation using an Amadori-GPEtn internal standard,(72) this data clearly demonstrates for the first time that increased Amadori-GPEtn levels are observed in the retinas of type 1 diabetic animals, indicating a potential role for this lipid in diabetic retinopathy. Furthermore, these changes are correlated with those observed in the erythrocytes of these animals, indicating that erythrocyte Amadori-GPEtn levels could potentially act as biomarkers for diabetic retinopathy.

### *3.5 Conclusions*

We have demonstrated for the first time that retina phospholipid metabolism is altered in a rat model of type 1 diabetes. While fluctuations in total retinal phospholipid levels at 6 and 36 weeks of STZ diabetes were not reflected in the abundances of erythrocyte phospholipids, a trend toward increased incorporation of linoleic acid(18:2n6) and decreased esterification of docosahexaenoic acid(22:6n3) was observed in GPCCho of both retina and erythrocytes at each time point. Furthermore, we have reported the first demonstration that glycated (Amadori)

phosphoethanolamine lipid species are increased in retinas of diabetic rats. The significant elevation of Amadori-GPEtn in both diabetic retina and erythrocytes may enable the future use of blood or plasma Amadori-GPEtn levels as a predictor of the onset of diabetic retinopathy.

To facilitate future lipidomic analyses, we have also compared two different methods of lipidome quantification. We found no difference in the results obtained for retina lipid analysis when quantification was performed against exogenously added internal standards, or through the use of a 'label free' comparison of MS/MS product ion abundances. However, the two quantitative methods did not provide identical results in the analysis of erythrocyte lipids, as the 'label-free' method may have been influenced by differences in ionization efficiencies across samples. This suggests that 'label-free' quantification of lipidomic data may be feasible as a simple and efficient alternative to 'absolute quantification' strategies; however, rigorous optimization of sample extraction, preparation, and analytical conditions must be considered imperative prior to 'label-free' analysis of diverse sample types. Overall, the automated tandem mass spectrometry based approach to lipidome analysis described in this study could facilitate future research in biomarker discovery across a wide spectrum of diseases, and assist in general comparative lipidomic analyses regardless of the desired application.

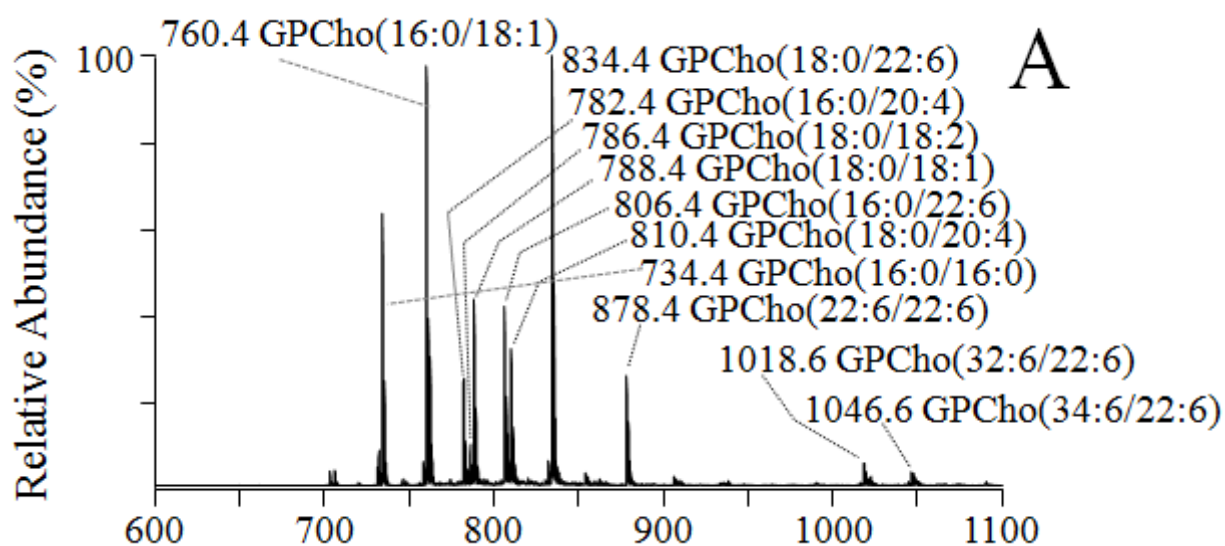


**Figure 3.1. Positive ion mode nESI-MS/MS analysis of GPCho in retina and erythrocytes at 6 weeks of diabetes.** (A) control retina, (B) diabetic retina, (C) control erythrocytes and (D) diabetic erythrocytes. Spectra were obtained by precursor ion scanning for the characteristic phosphocholine ion at  $m/z$  184 to identify  $[M+H]^+$  precursor ions. Selected regions from  $m/z$  600-1100 of representative spectra, obtained from control and diabetic lipid extracts, containing the major GPCho lipids, are shown.

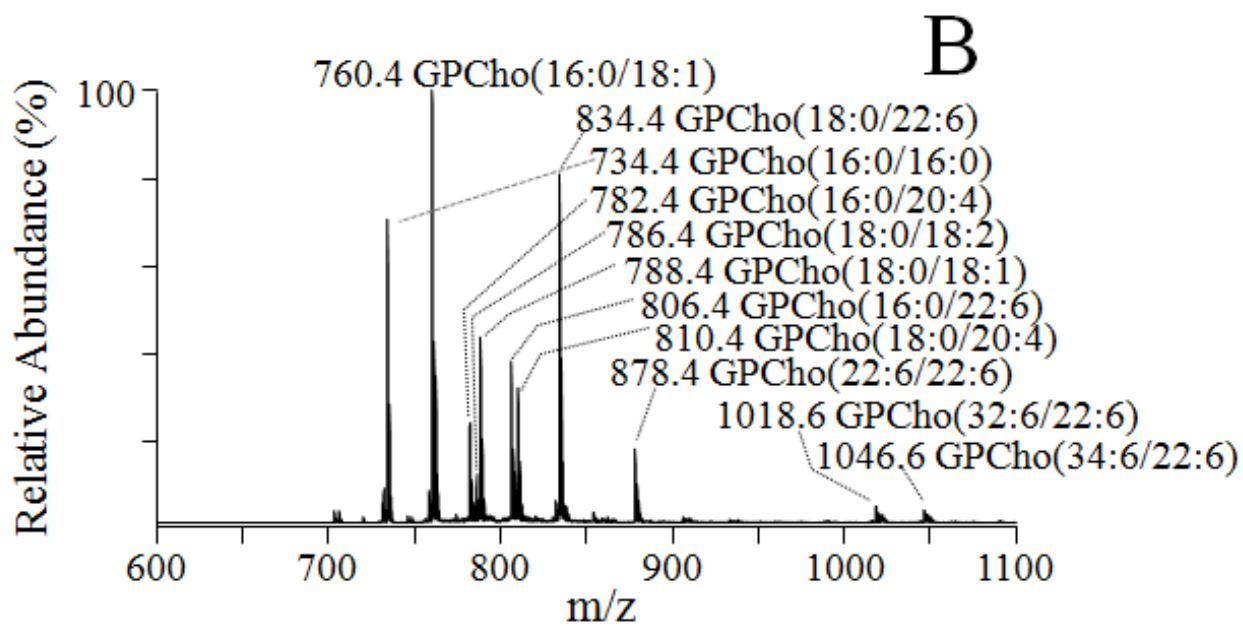


Figure 3.1 (cont'd).

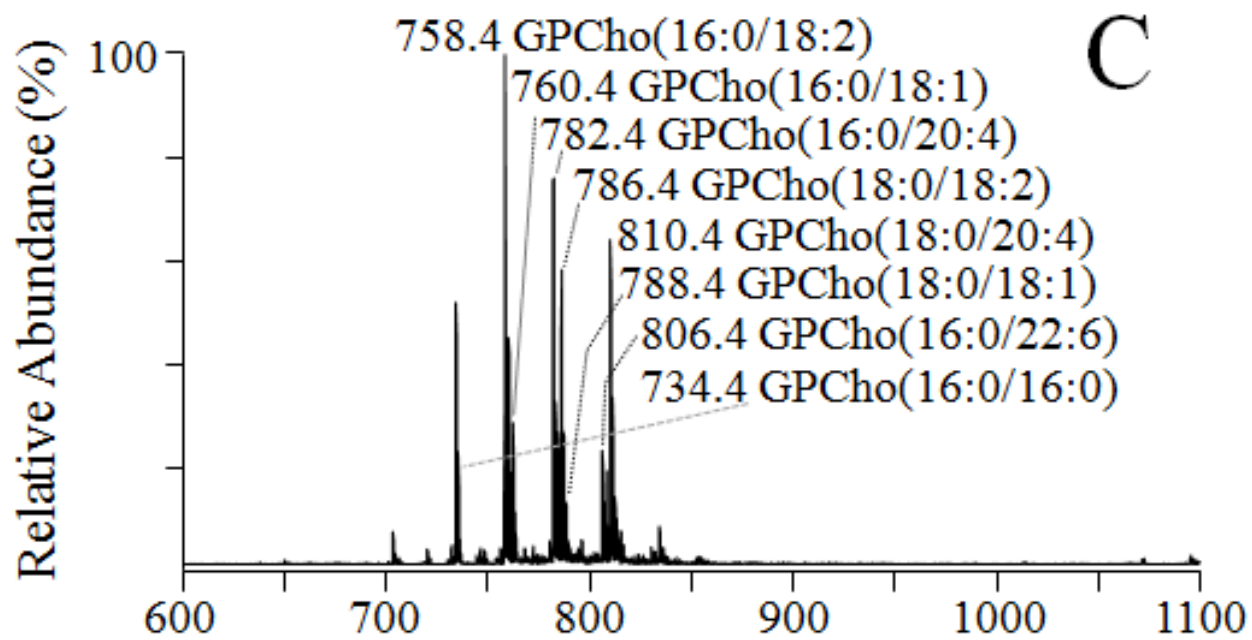


Figure 3.1 (cont'd).

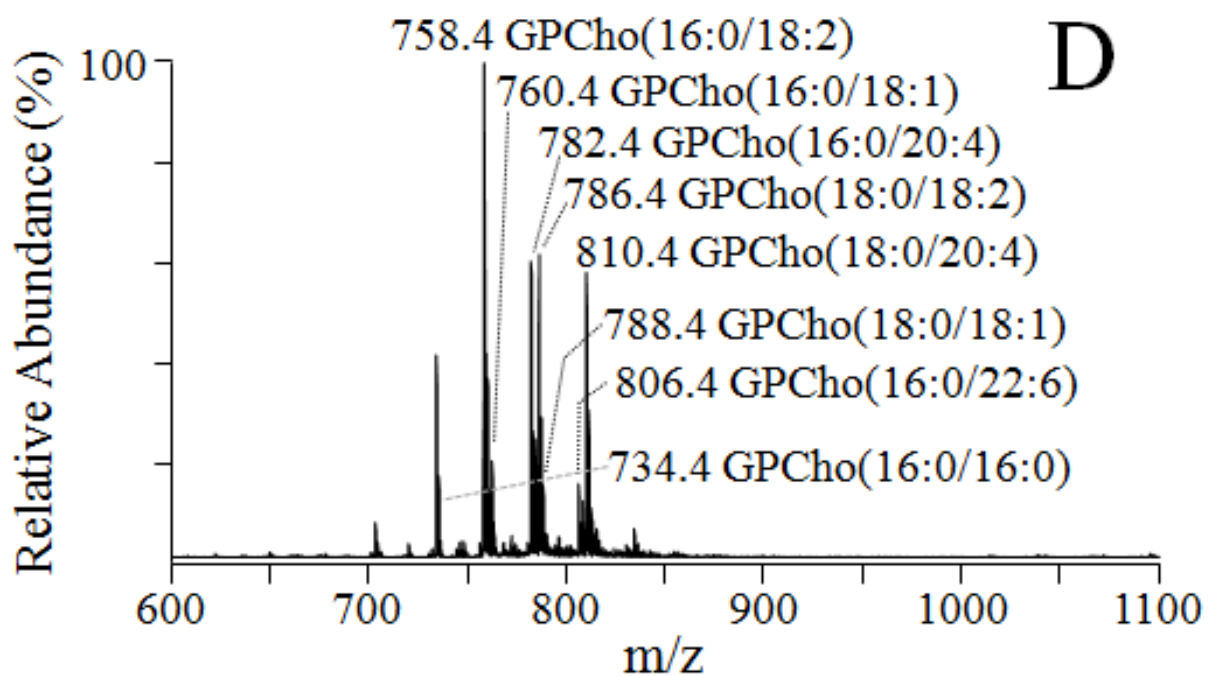
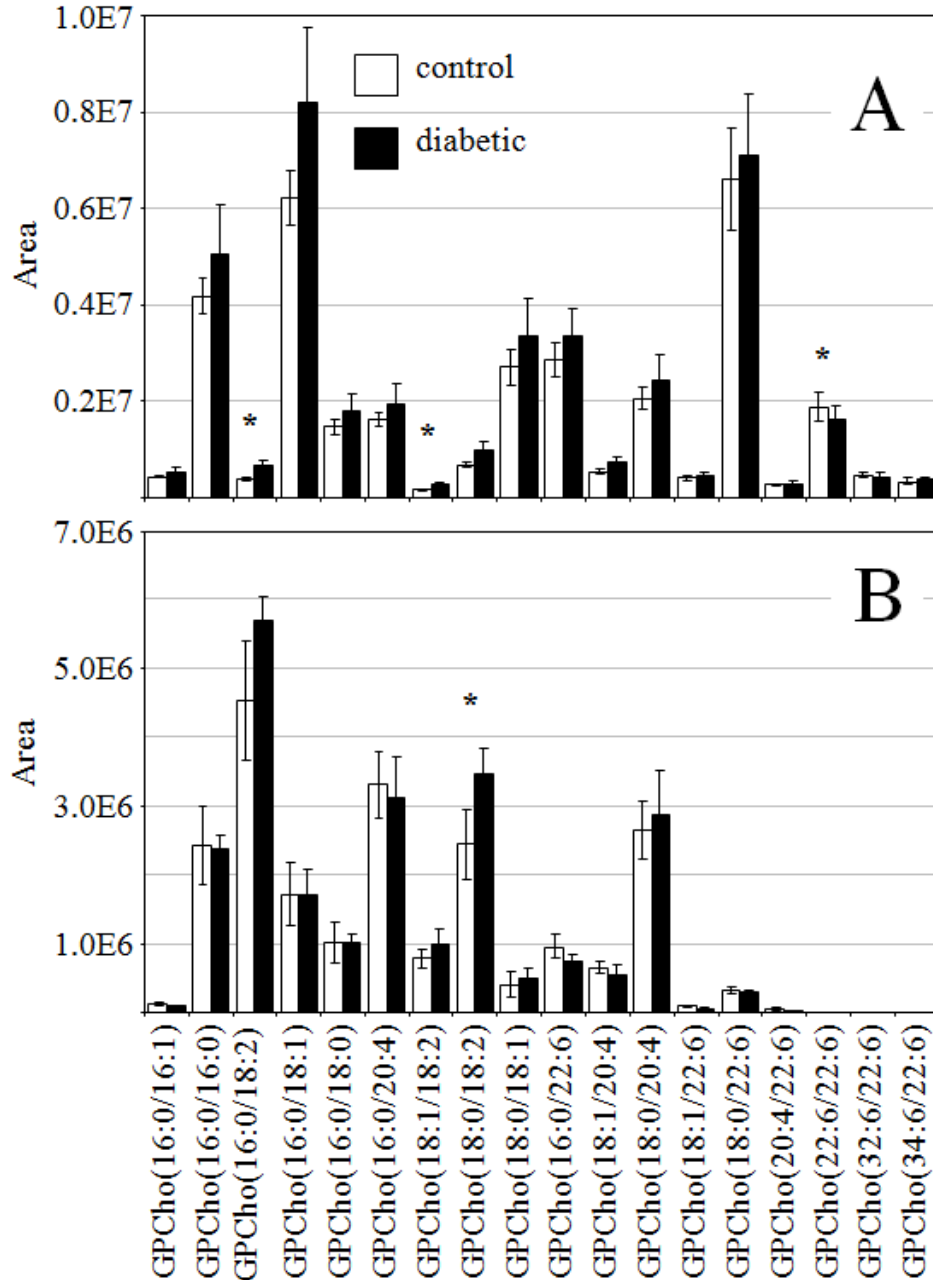


Figure 3.1 (cont'd).



**Figure 3.2. Ratiometric GPCho analysis in retina and erythrocytes at 6 weeks of diabetes.** Data values are displayed as mean  $\pm$  standard deviation (S.D.) from  $n=3$  control and  $n=4$  diabetic rats. (A) Comparison of age matched control and diabetic rat retina from Figures 3.1A and 3.1B. (B) Comparison of age matched control and diabetic rat erythrocytes from Figures 3.1C and 3.1D. (C) Visualization of the fold change (expressed as the ratio of diabetic/control lipid area intensity) observed for individual GPCho lipid ions between age matched control and diabetic rat retina from panel A. (D) Visualization of the fold change (expressed as the ratio of diabetic/control lipid area intensity) observed for individual GPCho lipid ions between age matched control and diabetic rat erythrocytes from panel B. The solid line indicates the mean of the measurements, while the dashed lines indicate  $\pm 1.645$  S.D. (i.e., 90% confidence intervals).

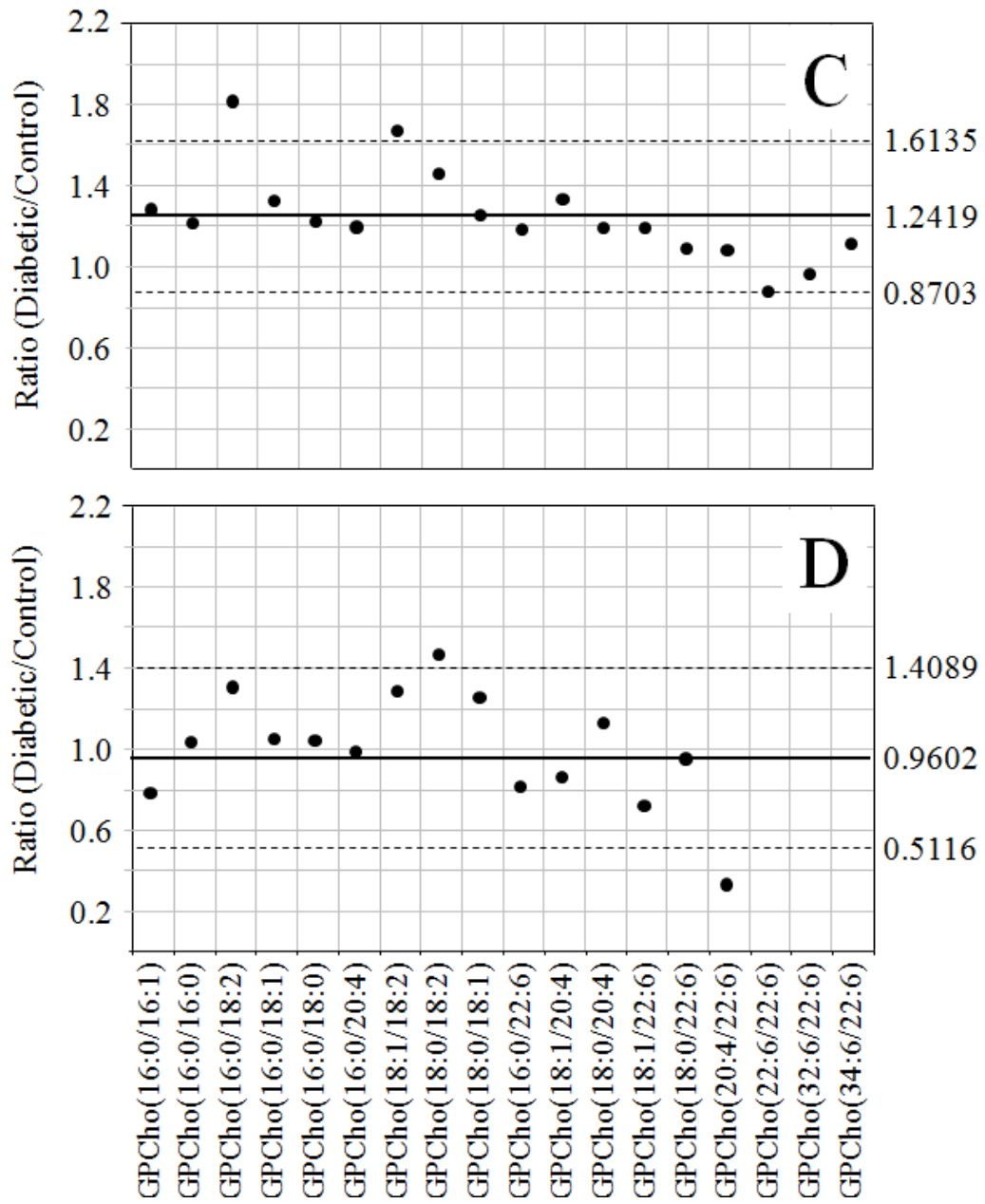
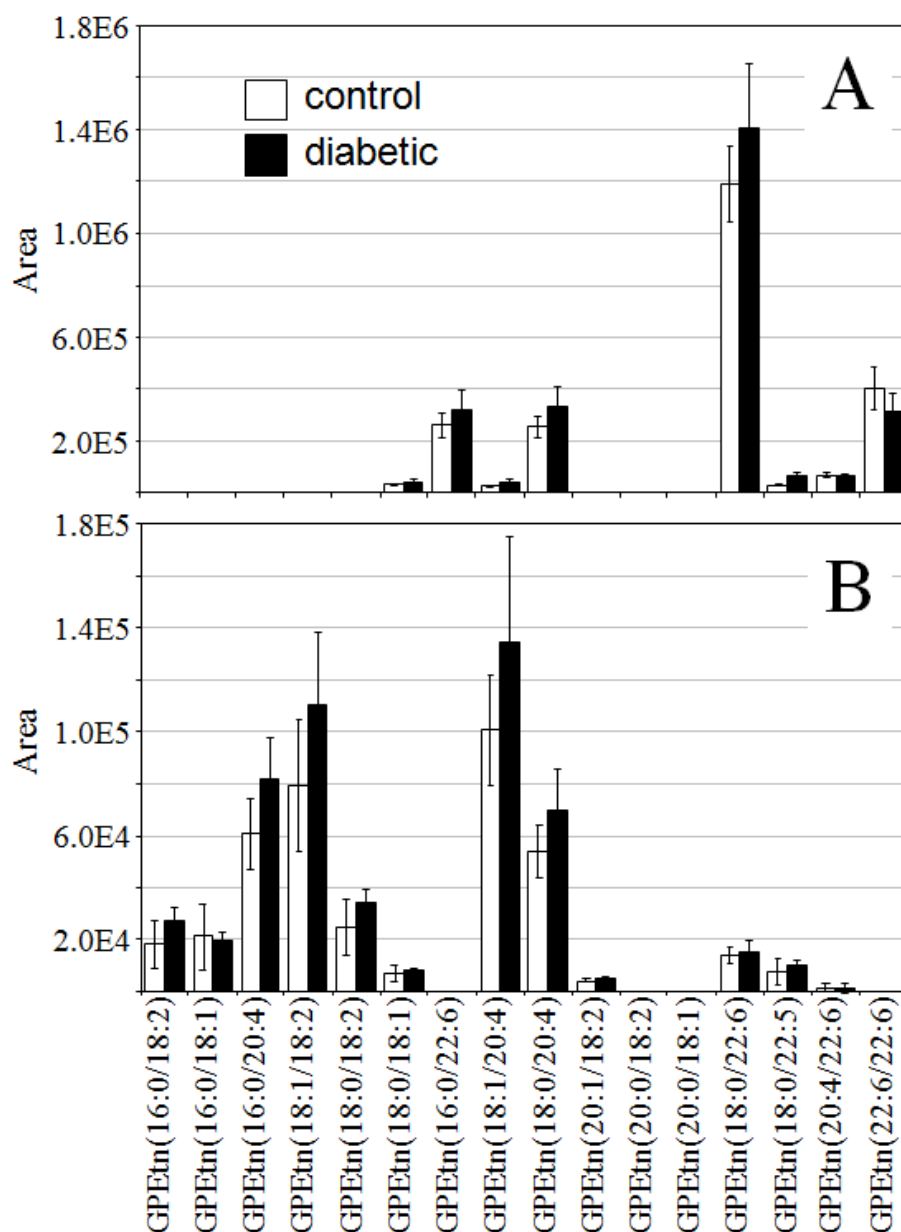


Figure 3.2 (cont'd).



**Figure 3.3. Ratiometric GPEtn analysis in retina and erythrocytes at 6 weeks of diabetes.** Data were obtained by positive ion mode ESI-MS/MS analysis, via scanning for the characteristic neutral loss of phosphoethanolamine ( $m/z$  141). Values are displayed as mean  $\pm$  standard deviation. (S.D.) from  $n=3$  control and  $n=4$  diabetic rats. (A) Comparison of age matched control and diabetic rat retina. (B) Comparison of age matched control and diabetic rat erythrocytes. (C) Visualization of the fold change (expressed as the ratio of diabetic/control lipid area intensity) observed for individual GPEtn lipid ions between age matched control and diabetic rat retina from panel A. (D) Visualization of the fold change (expressed as the ratio of diabetic/control lipid area intensity) observed for individual GPEtn lipid ions between age matched control and diabetic rat erythrocytes from panel B. The solid line indicates the mean of the measurements, while the dashed lines indicate  $\pm 1.645$  S.D. (i.e., 90% confidence intervals).

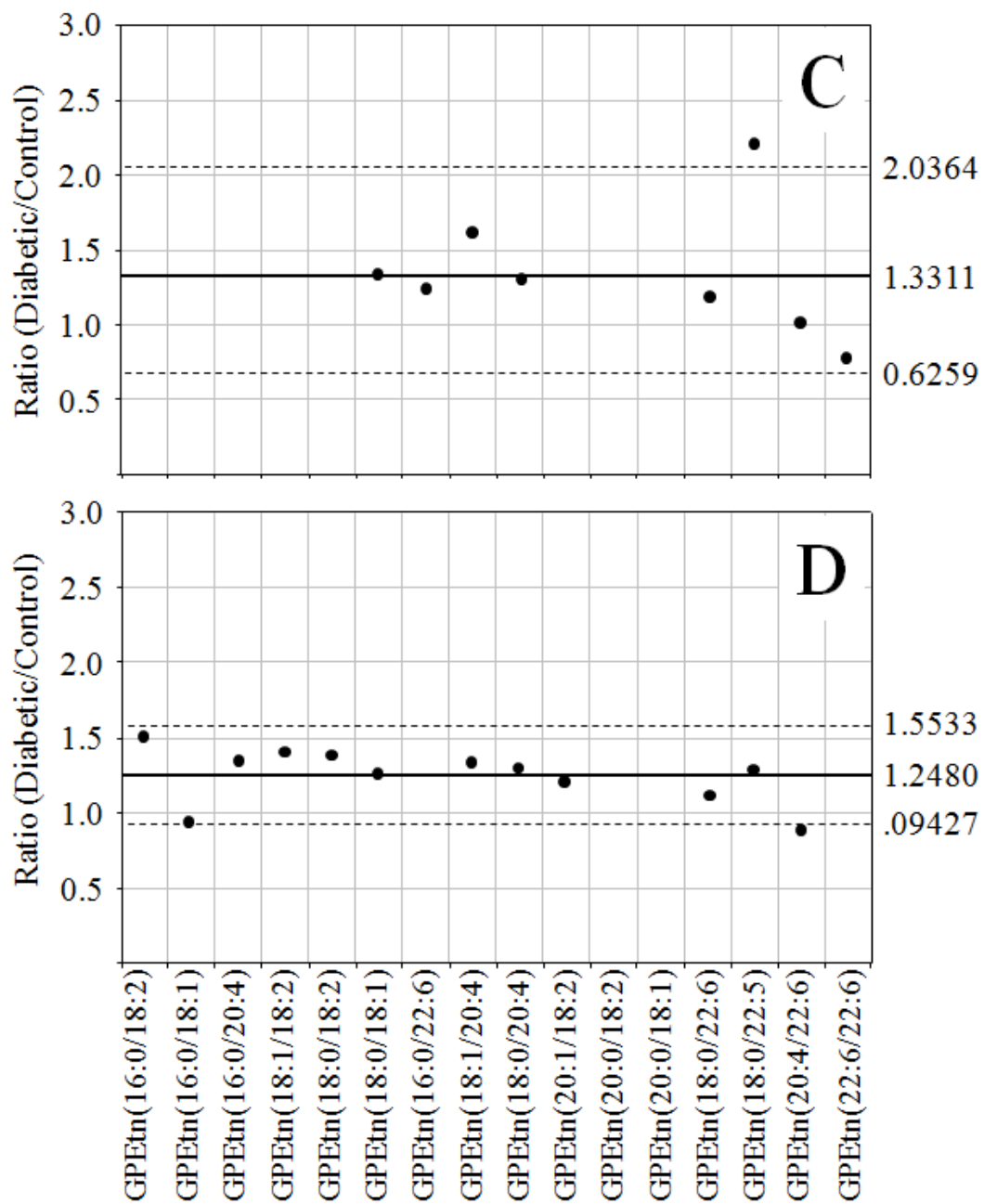
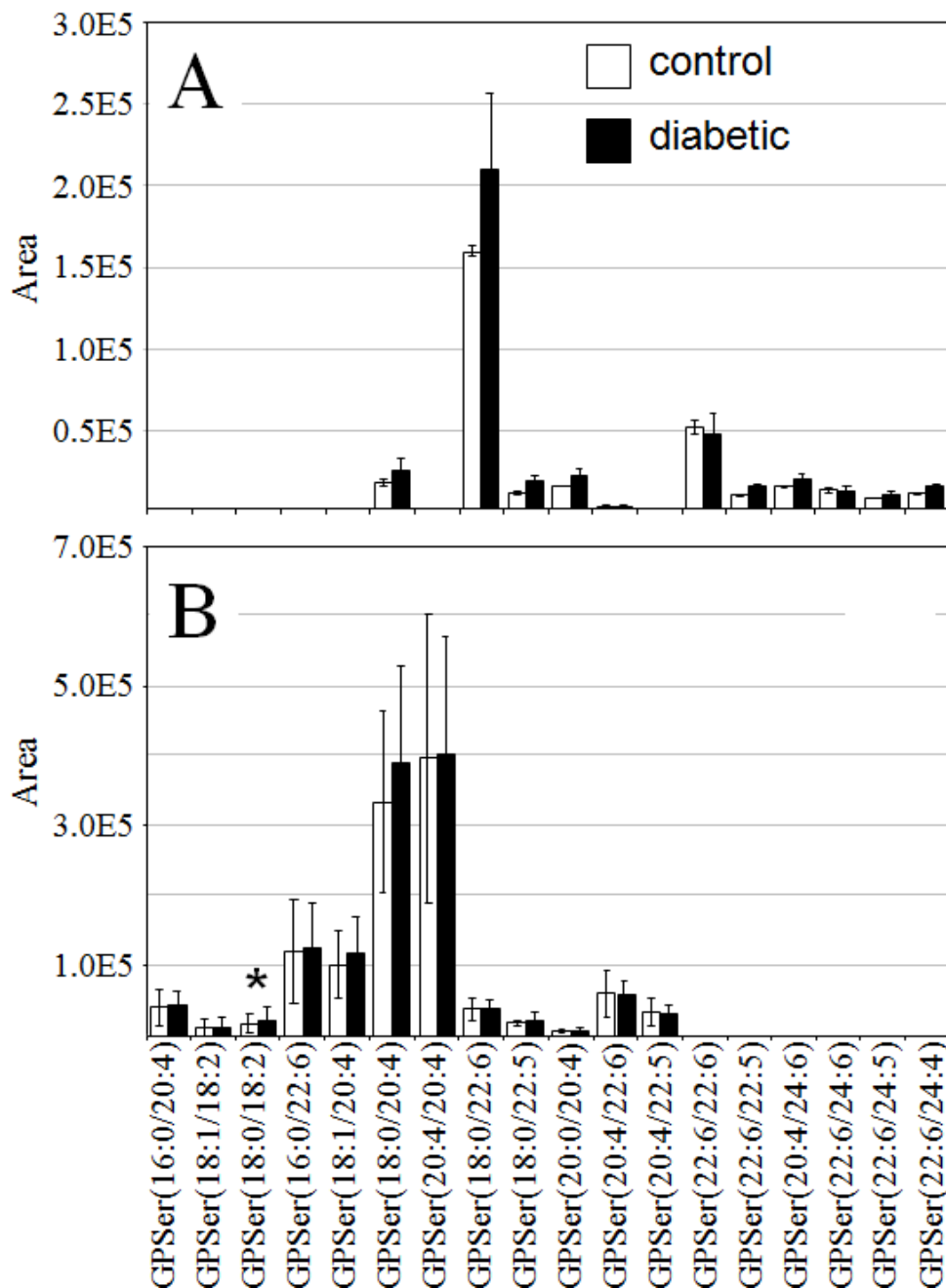
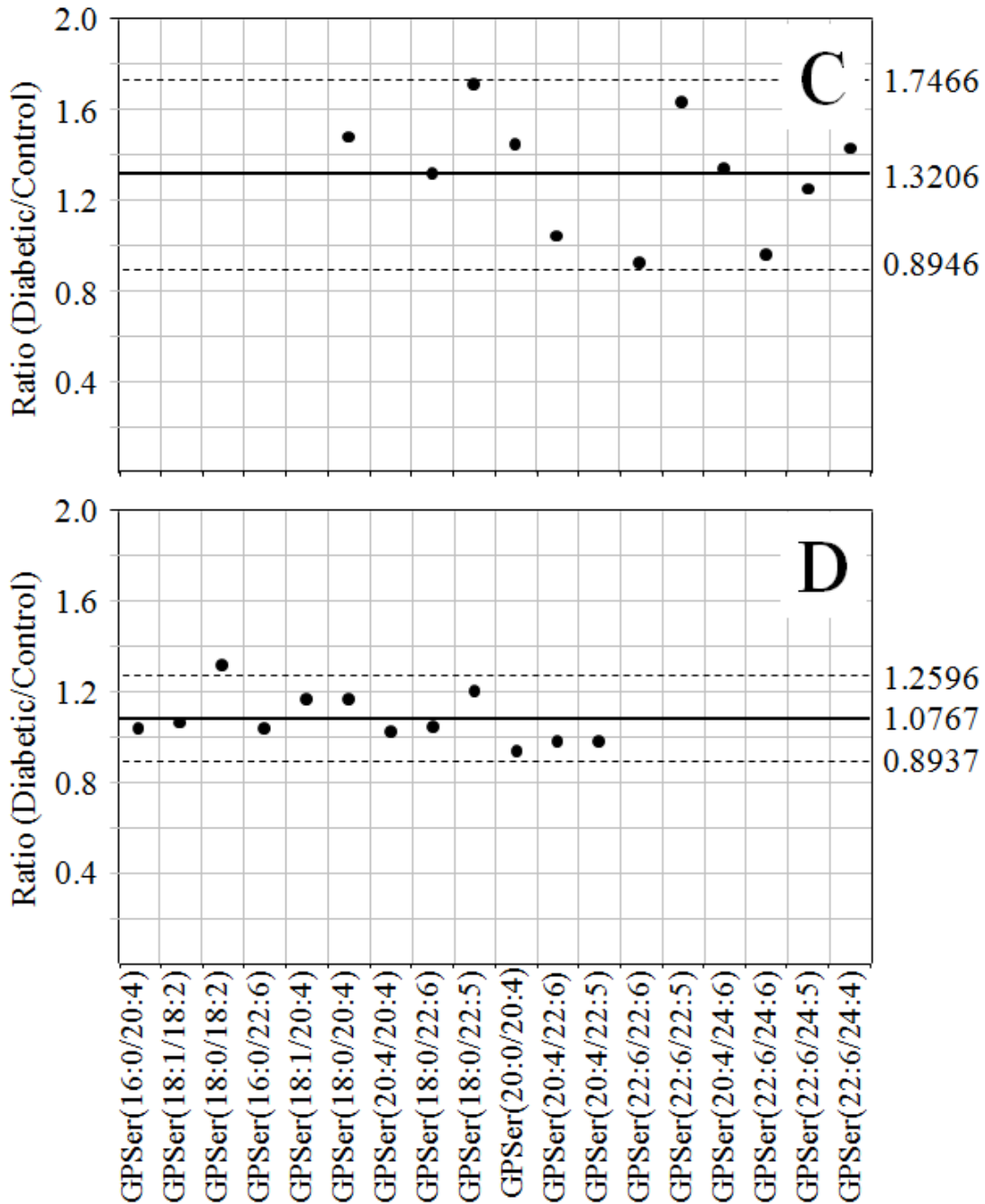


Figure 3.3 (cont'd).



**Figure 3.4. Ratiometric GPSer analysis in retina and erythrocytes at 6 weeks of diabetes.** Data were obtained by negative ion mode nESI-MS/MS analysis, via scanning for the characteristic neutral loss of dehydroalanine ( $m/z$  87) to identify  $[M-H]^-$  precursor ions. Data values are displayed as mean  $\pm$  standard deviation. (S.D.) from  $n=3$  control and  $n=4$  diabetic rats. (A) Comparison of age matched control and diabetic rat retina. (B) Comparison of age matched control and diabetic rat erythrocytes.



**Figure 3.4 (cont'd).** (C) Visualization of the fold change (expressed as the ratio of diabetic/control lipid area intensity) observed for individual GPSer lipid ions between age matched control and diabetic rat retina from panel A. (D) Visualization of the fold change (expressed as the ratio of diabetic/control lipid area intensity) observed for individual GPSer lipid ions between age matched control and diabetic rat erythrocytes from panel B. The solid line indicates the mean of the measurements, while the dashed lines indicate  $\pm 1.645$  S.D. (i.e., 90% confidence intervals).

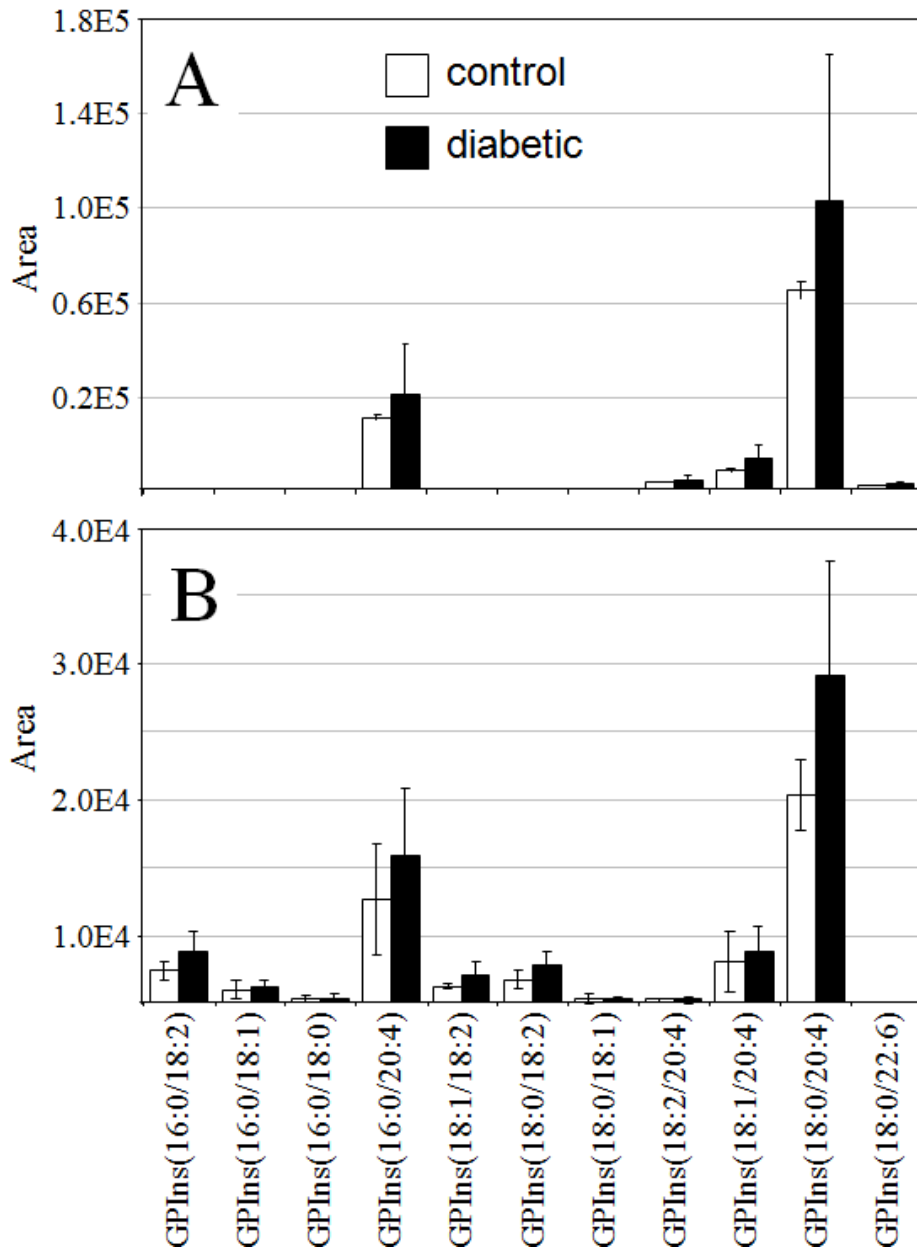


**Figure 3.5. Ratiometric GPIs analysis in retina and erythrocytes at 6 weeks of diabetes.** Values are displayed as mean  $\pm$  standard deviation. (S.D.) from n=3 control and n=4 diabetic rats. (A) Comparison of age matched control and diabetic rat retina. (B) Comparison of age matched control and diabetic rat erythrocytes. (C) Visualization of the fold change (expressed as the ratio of diabetic/control lipid area intensity) observed for individual GPIs lipid ions between age matched control and diabetic rat retina from panel A. (D) Visualization of the fold change (expressed as the ratio of diabetic/control lipid area intensity) observed for individual GPIs lipid ions between age matched control and diabetic rat erythrocytes from panel B. The solid line indicates the mean of the measurements, while the dashed lines indicate  $\pm 1.645$  S.D. (i.e., 90% confidence intervals).

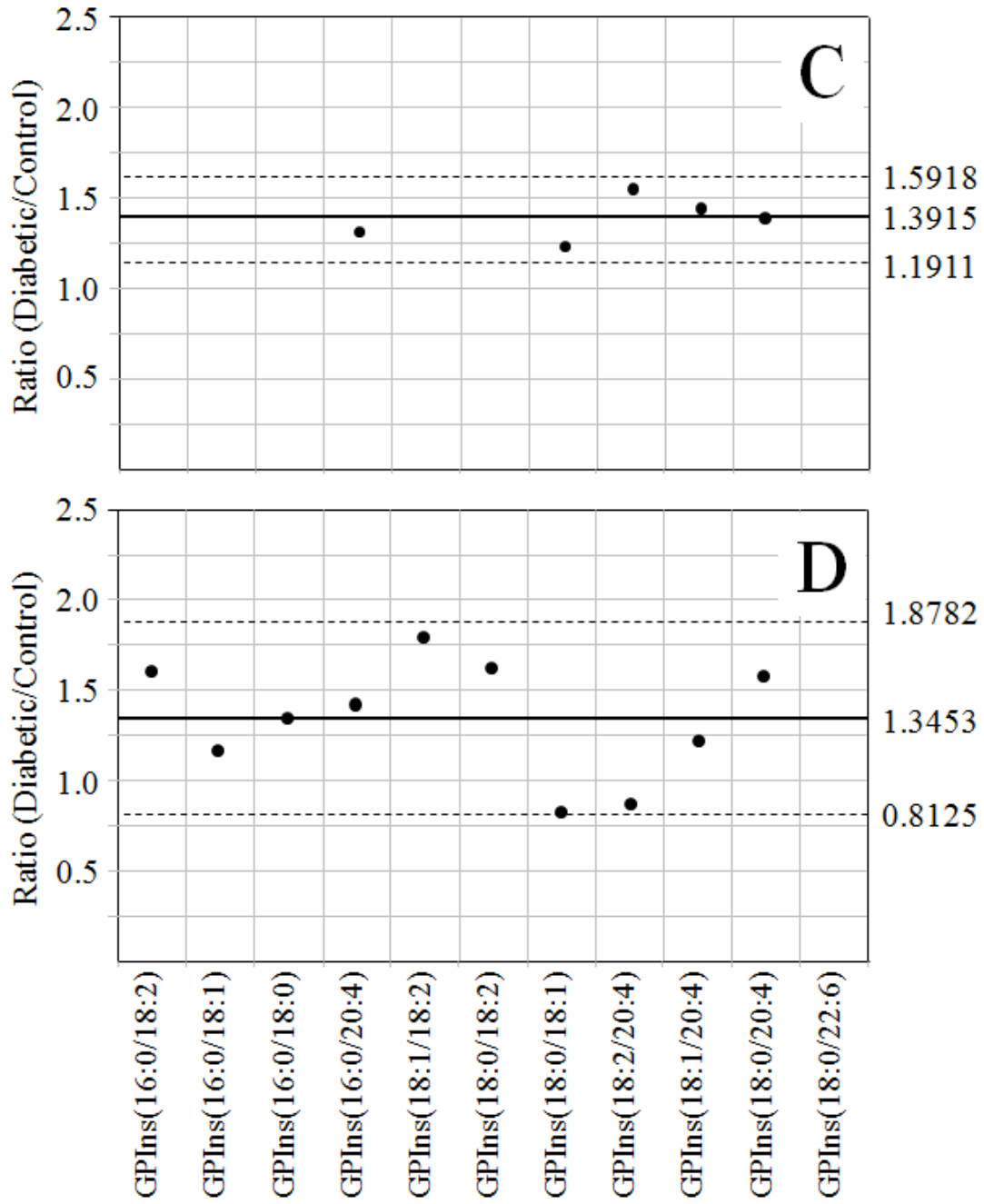
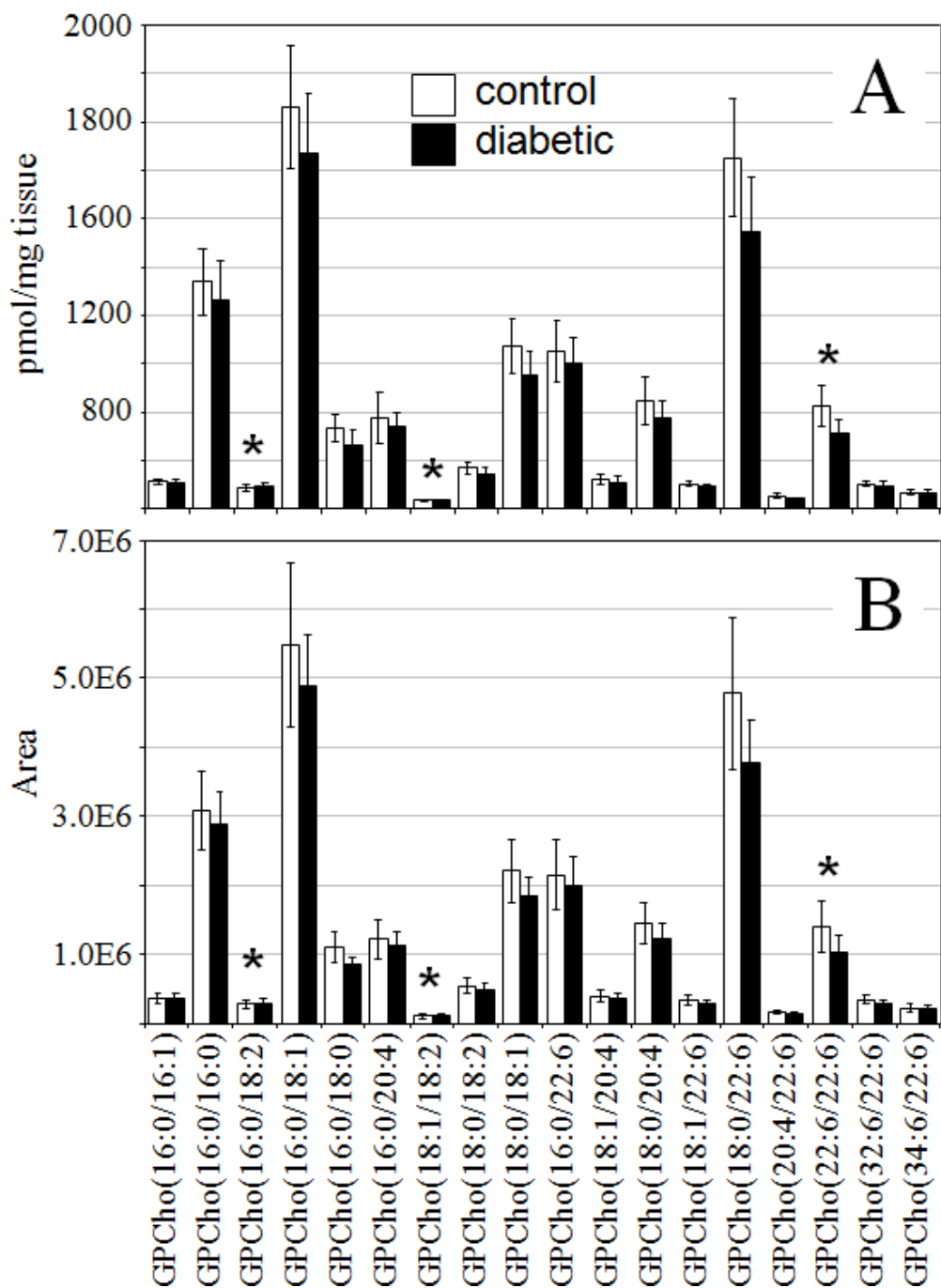
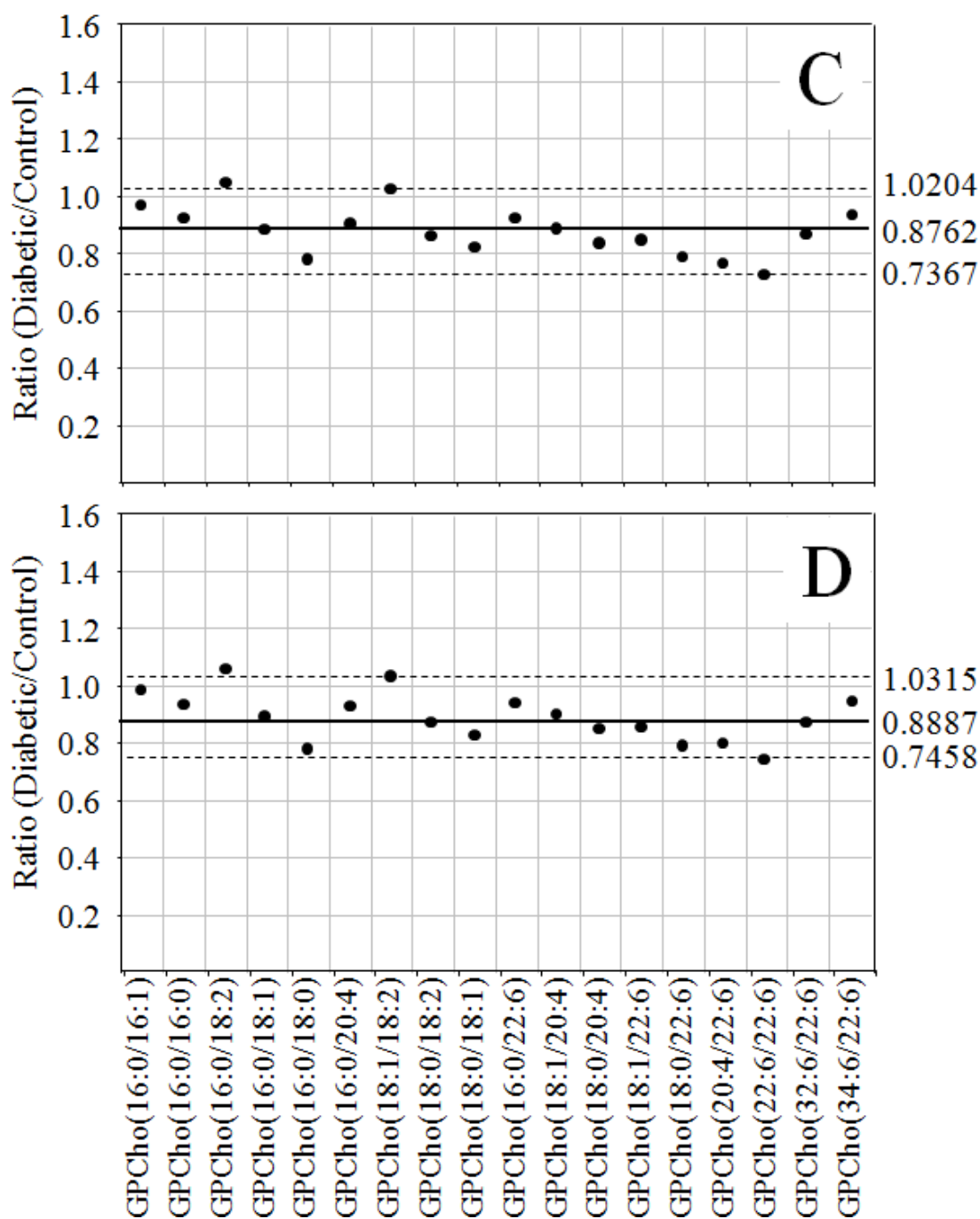


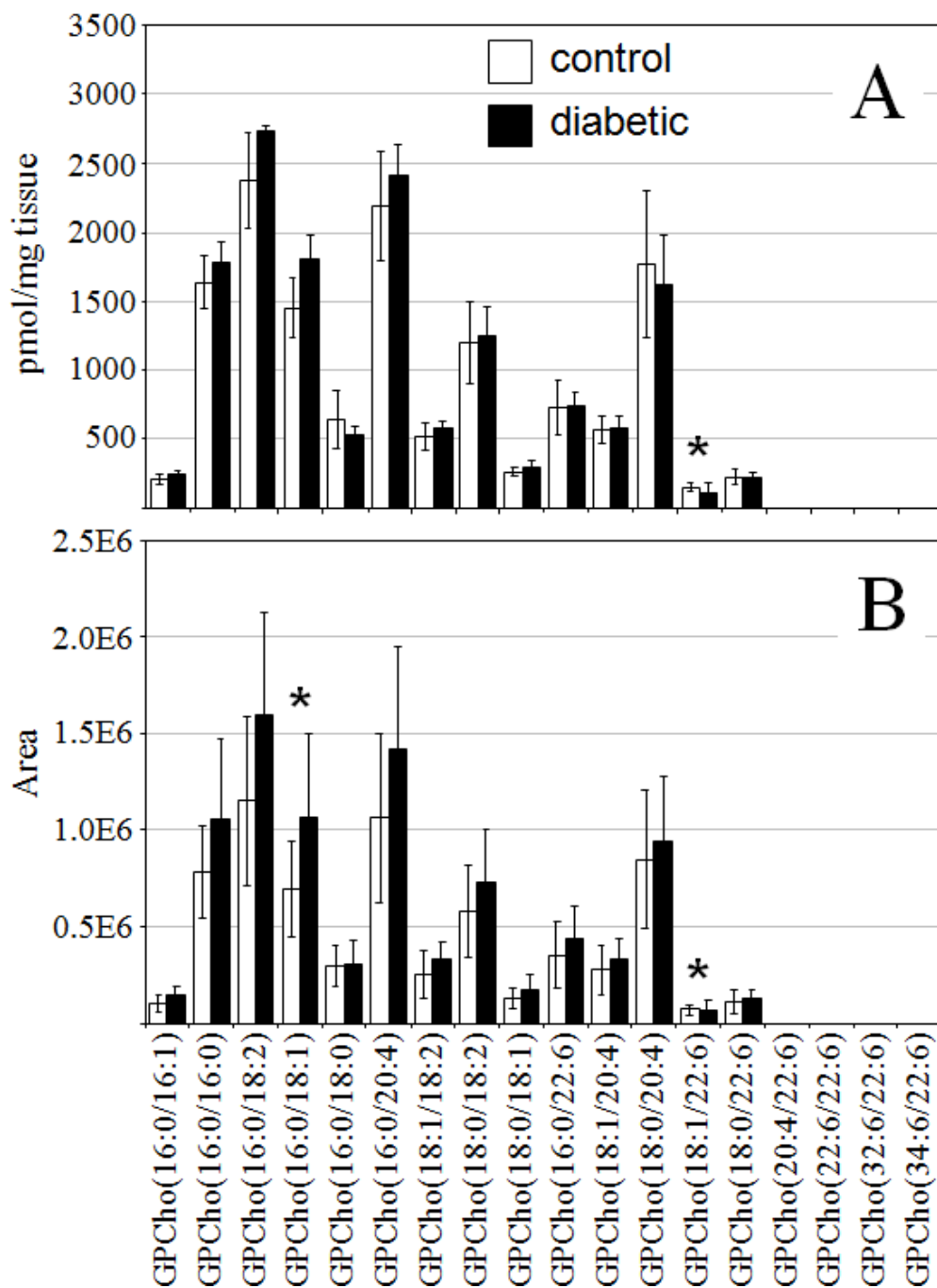
Figure 3.5 (cont'd).



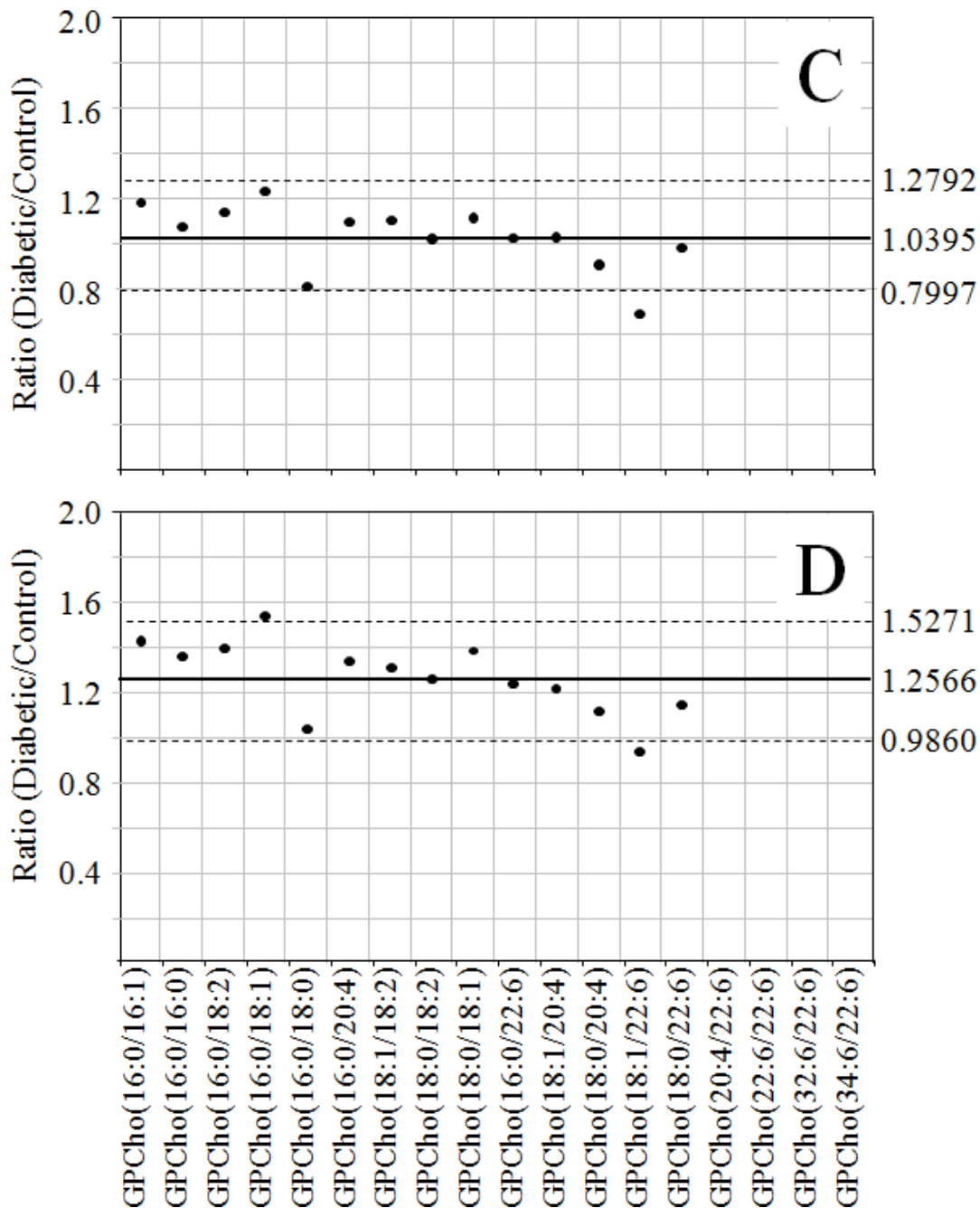
**Figure 3.6. Ratiometric GPCho analysis in retina at 36 weeks of diabetes, with or without an internal standard.** Data were obtained by positive ion mode nESI-MS/MS analysis, via precursor ion scanning for the characteristic phosphocholine ion at  $m/z$  184 to identify  $[M+H]^+$  precursor ions. Data values are displayed as mean  $\pm$  standard deviation. (S.D.) from  $n=6$  control and  $n=5$  diabetic rats. (A) Comparison of age matched control and diabetic rat retina (with internal standard). (B) Comparison of age matched control and diabetic rat retina (without internal standard).



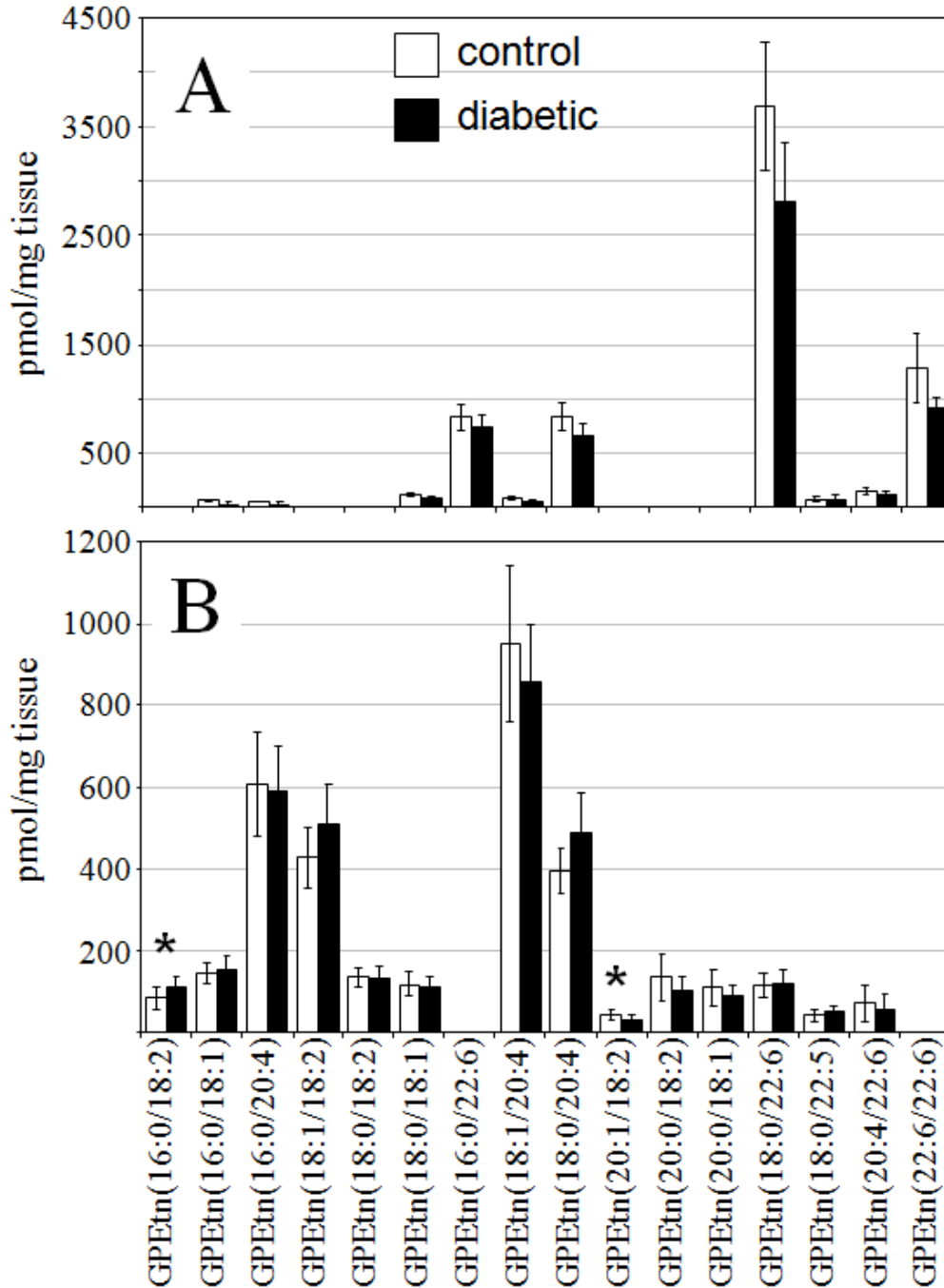
**Figure 3.6 (cont'd).** (C) Visualization of the fold change (expressed as the ratio of diabetic/control lipid area intensity) in the abundances of individual GPCho lipid ions observed between age matched control and diabetic rat retina from panel A. (D) Visualization of the fold change (expressed as the ratio of diabetic/control lipid area intensity) in the abundances of individual GPCho lipid ions observed between age matched control and diabetic rat retina from panel B. The solid line indicates the mean of the measurements, while the dashed lines indicate  $\pm 1.645$  S.D. (i.e., 90% confidence intervals).



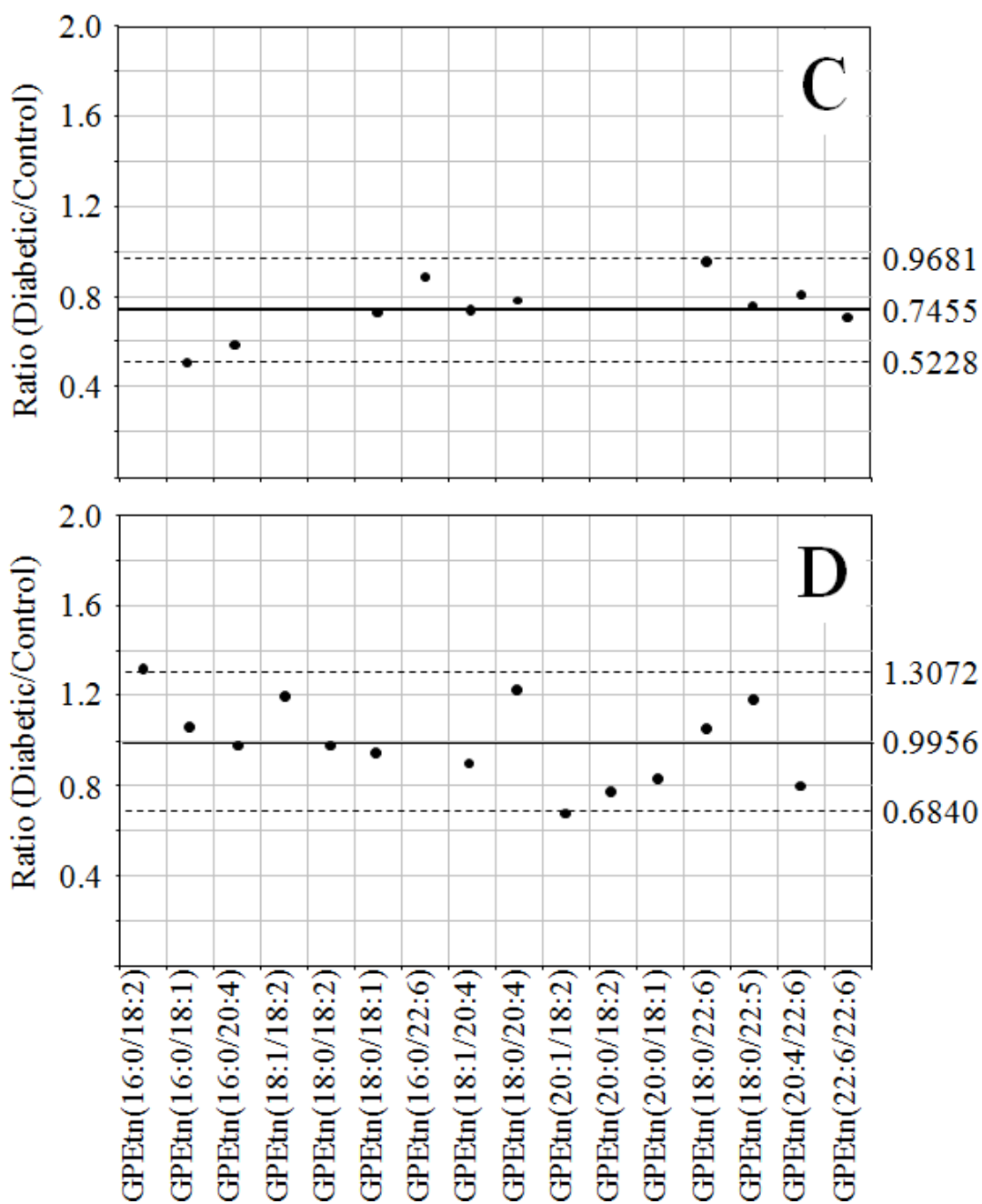
**Figure 3.7. Ratiometric GPCho analysis in erythrocytes at 36 weeks of diabetes, with or without an internal standard.** Data were obtained by positive ion mode nESI-MS/MS analysis, via precursor ion scanning for the characteristic phosphocholine ion at  $m/z$  184 to identify  $[M+H]^+$  precursor ions. Data values are displayed as mean  $\pm$  standard deviation. (S.D.) from  $n=5$  control and  $n=4$  diabetic rats. (A) Comparison of age matched control and diabetic rat erythrocytes (with internal standard). (B) Comparison of age matched control and diabetic rat erythrocytes (without internal standard).



**Figure 3.7 (cont'd).** (C) Visualization of the fold change (expressed as the ratio of diabetic/control lipid area intensity) in the abundances of individual GPCho lipid ions observed between age matched control and diabetic rat erythrocytes from panel A. (D) Visualization of the fold change (expressed as the ratio of diabetic/control lipid area intensity) in the abundances of individual GPCho lipid ions observed between age matched control and diabetic rat erythrocytes from panel B. The solid line indicates the mean of the measurements, while the dashed lines indicate  $\pm 1.645$  S.D. (i.e., 90% confidence intervals).



**Figure 3.8. Ratiometric GPEtn analysis in retina and erythrocytes at 36 weeks of diabetes with or without an internal standard.** Data were obtained by positive ion mode nESI-MS/MS analysis, via scanning for the characteristic neutral loss of phosphoethanolamine ( $m/z$  141) to identify  $[M+H]^+$  or  $[M+Na]^+$  precursor ions. Data values are displayed as mean  $\pm$  standard deviation. (S.D.) from  $n=6$  control and  $n=6$  diabetic rats. (A) Comparison of age matched control and diabetic rat retina. (B) Comparison of age matched control and diabetic rat erythrocytes.



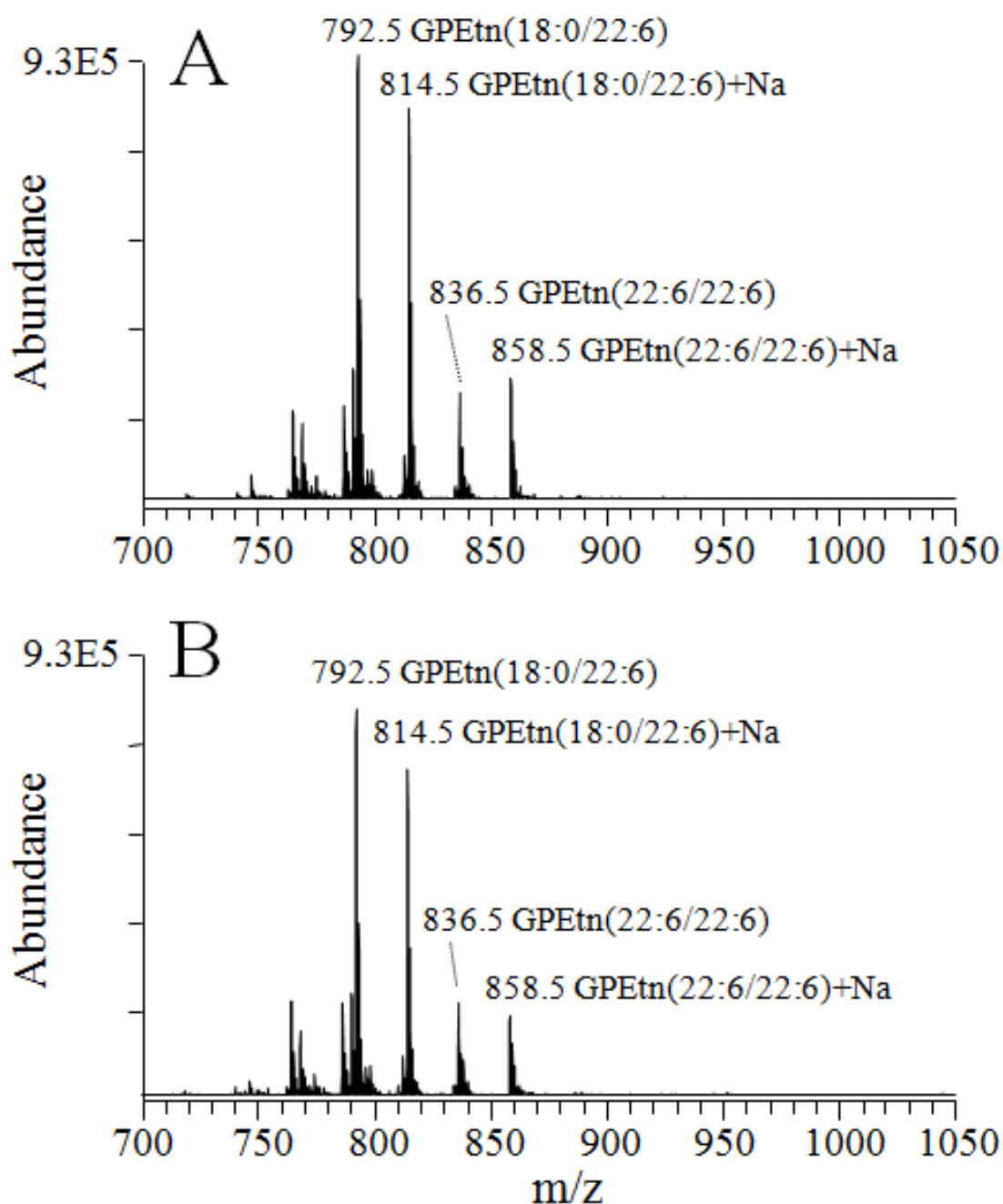


**Figure 3.9. Positive ion mode nESI-MS/MS analysis of GPEtn and Amadori-GPEtn lipids in retina at 36 weeks of diabetes.** (A) GPEtn lipids from control retina, (B) GPEtn lipids from diabetic retina, (C) Amadori-GPEtn lipids from control retina and (D) Amadori-GPEtn lipids from diabetic retina. GPEtn and Amadori-GPEtn spectra were obtained by scanning for the characteristic neutral losses of phosphoethanolamine ( $m/z$  141) and glycated phosphoethanolamine ( $m/z$  303), respectively, to identify  $[M+H]^+$  and  $[M+Na]^+$  precursor ions. Selected regions of representative spectra from  $m/z$  700-1050, containing the major GPEtn and Amadori-GPEtn lipids, are shown.

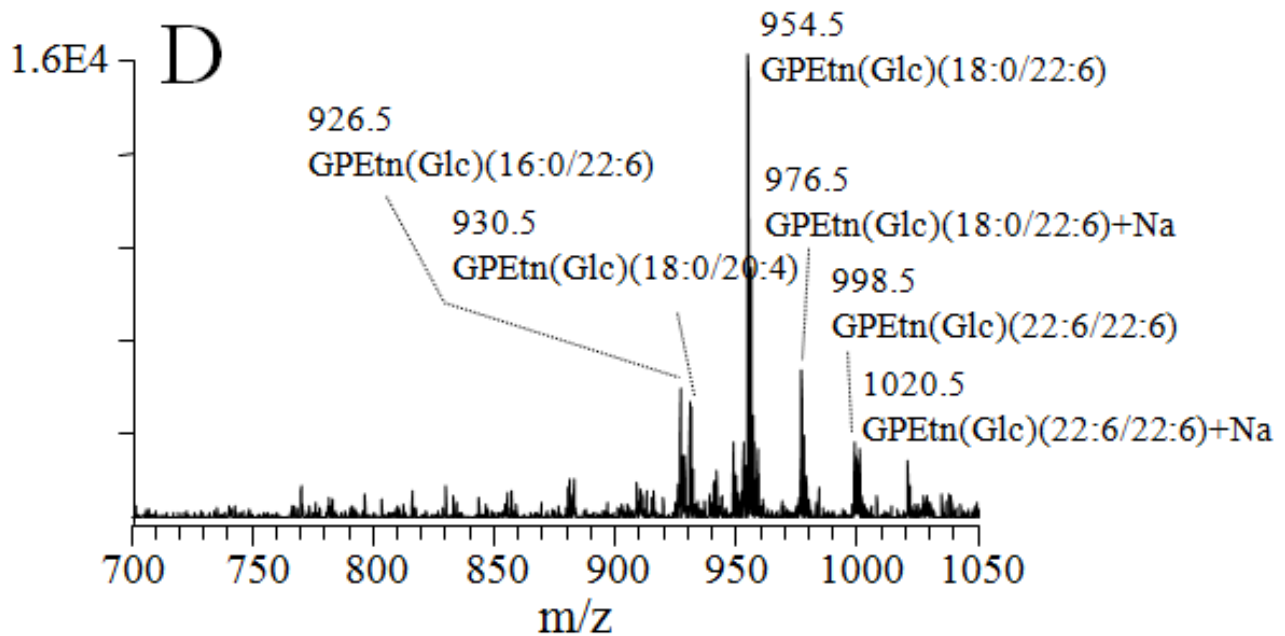
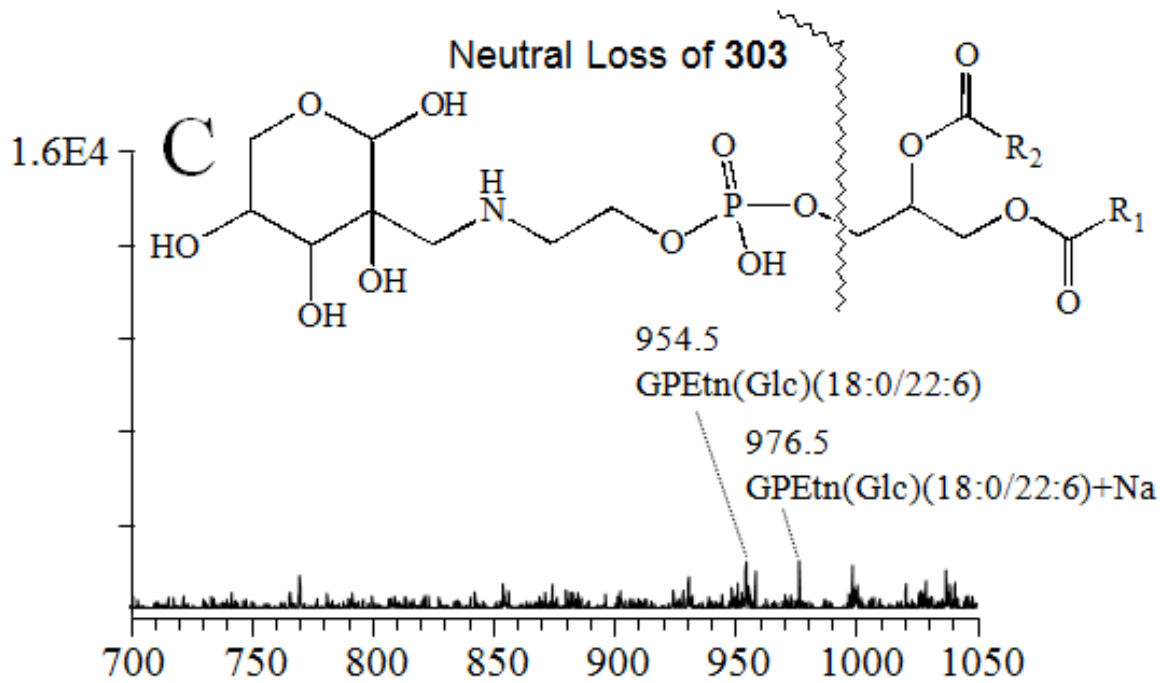
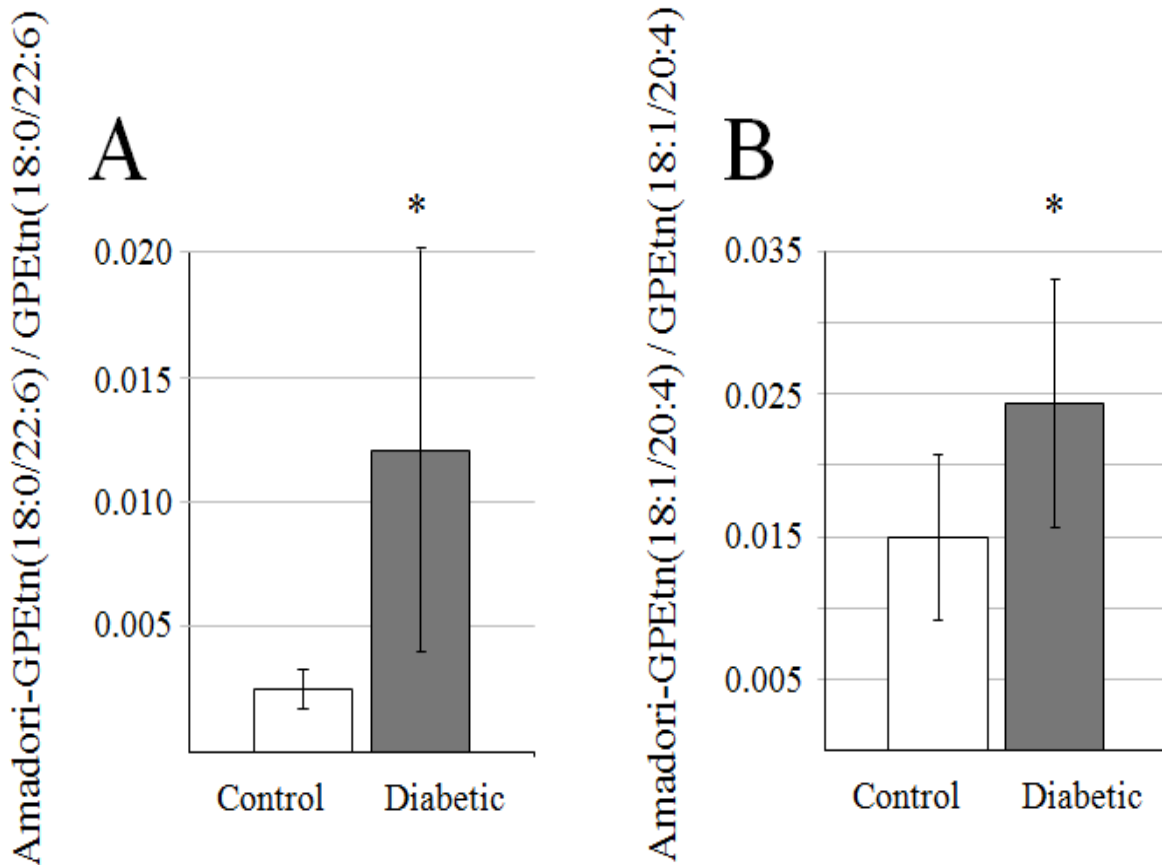


Figure 3.9 (cont'd).



**Figure 3.10. Ratiometric Amadori-GPEtn analysis in retina and erythrocytes at 36 weeks of diabetes.** (A) Ratios of the Amadori-GPEtn to GPEtn lipid abundances for the most abundant GPEtn(18:0/22:6) lipid observed in the control and diabetic retina lipid extracts. Data values are displayed as mean  $\pm$  standard deviation. (S.D.) from n=4 control and n=5 diabetic rats. \* p < 0.05 by Student's t-test. (B) Ratio of the Amadori-GPEtn to GPEtn lipid abundances for the most abundant GPEtn(18:10/20:4) lipid observed in the control and diabetic erythrocyte lipid extracts. Data values are displayed as mean  $\pm$  standard deviation. (S.D.) from n=5 control and n=6 diabetic rats \* p < 0.05 by Student's t-test.

## References

### 3.6 References

1. LaBaer J: So, you want to look for biomarkers (introduction to the special biomarkers issue). *J Proteome Res* 4:1053-1059, 2005.
2. Semmes OJ, Malik G, Ward M: Application of mass spectrometry to the discovery of biomarkers for detection of prostate cancer. *J Cell Biochem* 98:496-503, 2006.
3. Wenk MR: The emerging field of lipidomics. *Nat Rev Drug Discov* 4:594-610, 2005.
4. Metz T, Qian W-J, Jacobs JM, Gritsenko M, Moore R, Polpitiya A, Monroe M, Camp D, Mueller P, Smith R: Application of Proteomics in the Discovery of Candidate Protein Biomarkers in a Diabetes Autoantibody Standardization Program Sample Subset. *J. Prot. Res.* 7:698-707, 2008.
5. Anderson NL, Anderson NG: The human plasma proteome: history, character, and diagnostic prospects. *Mol Cell Proteomics* 1:845-867, 2002.
6. van Meer G: Cellular lipidomics. *Embo J* 24:3159-3165, 2005.
7. Han X, Gross R: Specific lipid alterations in Alzheimer's disease and diabetes: shotgun global cellular lipidome analyses by electrospray ionization mass spectrometry using intrasource separation. In *Functional Lipidomics* Feng L, Prestwich, G., Ed. Boca Raton, FL., CRC Press LLC, 2006, p. 286-306.
8. Han X, Yang J, Yang K, Zhongdan Z, Abendschein DR, Gross RW: Alterations in myocardial cardioliipin content and composition occur at the very earliest stages of diabetes: a shotgun lipidomics study. *Biochemistry* 46:6417-6428., 2007.
9. Ford D, Monda J, Brush R, Anderson R, Richards M, Fliesler S: Lipidomic analysis of the retina in a rat model of Smith-Lemli-Opitz syndrome: alterations in docosaehaenoic acid content of phospholipid molecular species. *Journal of Neurochemistry* 105:1032-1047, 2008.
10. Gross R, Han X: Lipidomics in diabetes and the metabolic syndrome. *Methods in Enzymology* 433:73-90, 2007.
11. SanGiovanni JP, Chew EY, Clemons TE, Davis MD, Ferris FL, 3rd, Gensler GR, Kurinij N, Lindblad AS, Milton RC, Seddon JM, Sperduto RD: The relationship of dietary lipid intake and age-related macular degeneration in a case-control study: AREDS Report No. 20. *Arch Ophthalmol* 125:671-679, 2007.
12. Connor KM, Sangiovanni JP, Lofqvist C, Aderman CM, Chen J, Higuchi A, Hong S, Pravda EA, Majchrzak S, Carper D, Hellstrom A, Kang JX, Chew EY, Salem N, Jr., Serhan CN, Smith LE: Increased dietary intake of omega-3-polyunsaturated fatty acids reduces pathological retinal angiogenesis. *Nat Med* 13:868-873, 2007.

13. Klein R, Klein BE, Moss SE, Cruickshanks KJ: The Wisconsin Epidemiologic Study of diabetic retinopathy. XIV. Ten-year incidence and progression of diabetic retinopathy. *Arch Ophthalmol* 112:1217-1228, 1994.
14. Joussen AM, Poulaki V, Le ML, Koizumi K, Esser C, Janicki H, Schraermeyer U, Kociok N, Fauser S, Kirchhof B, Kern TS, Adamis AP: A central role for inflammation in the pathogenesis of diabetic retinopathy. *Faseb J* 18:1450-1452, 2004.
15. Anderson RE: Lipids of ocular tissues. IV. A comparison of the phospholipids from the retina of six mammalian species. *Exp Eye Res* 10:339-344, 1970.
16. Fliesler SJ, Anderson RE: Chemistry and metabolism of lipids in the vertebrate retina. *Prog Lipid Res* 22:79-131, 1983.
17. Lecomte M, Paget C, Ruggiero D, Wiernsperger N, Lagarde M: Docosahexaenoic acid is a major n-3 polyunsaturated fatty acid in bovine retinal microvessels. *J Neurochem* 66:2160-2167, 1996.
18. O'Brien JS, Sampson EL: Lipid composition of the normal human brain: gray matter, white matter, and myelin. *J Lipid Res* 6:537-544, 1965.
19. SanGiovanni JP, Chew EY: The role of omega-3 long-chain polyunsaturated fatty acids in health and disease of the retina. *Prog Retin Eye Res* 24:87-138, 2005.
20. Weisinger HS, Armitage JA, Jeffrey BG, Mitchell DC, Moriguchi T, Sinclair AJ, Weisinger RS, Salem N, Jr.: Retinal sensitivity loss in third-generation n-3 PUFA-deficient rats. *Lipids* 37:759-765, 2002.
21. Birch EE, Garfield S, Castaneda Y, Hughbanks-Wheaton D, Uauy R, Hoffman D: Visual acuity and cognitive outcomes at 4 years of age in a double-blind, randomized trial of long-chain polyunsaturated fatty acid-supplemented infant formula. *Early Hum Dev* 83:279-284, 2007.
22. Ren H, Magulike N, Ghebremeskel K, Crawford M: Primary open-angle glaucoma patients have reduced levels of blood docosahexaenoic and eicosapentaenoic acids. *Prostaglandins Leukot Essent Fatty Acids* 74:157-163, 2006.
23. Hartong DT, Berson EL, Dryja TP: Retinitis pigmentosa. *Lancet* 368:1795-1809, 2006.
24. Hoffman DR, Birch DG: Docosahexaenoic acid in red blood cells of patients with X-linked retinitis pigmentosa. *Invest Ophthalmol Vis Sci* 36:1009-1018, 1995.
25. Schaefer EJ, Robins SJ, Patton GM, Sandberg MA, Weigel-DiFranco CA, Rosner B, Berson EL: Red blood cell membrane phosphatidylethanolamine fatty acid content in various forms of retinitis pigmentosa. *J Lipid Res* 36:1427-1433, 1995.
26. Schroder S, Palinski W, Schmid-Schonbein GW: Activated monocytes and granulocytes, capillary nonperfusion, and neovascularization in diabetic retinopathy. *Am J Pathol* 139:81-100, 1991.

27. Joussen AM, Poulaki V, Mitsiades N, Kirchhof B, Koizumi K, Dohmen S, Adamis AP: Nonsteroidal anti-inflammatory drugs prevent early diabetic retinopathy via TNF-alpha suppression. *Faseb J* 16:438-440, 2002.
28. Joussen AM, Poulaki V, Qin W, Kirchhof B, Mitsiades N, Wiegand SJ, Rudge J, Yancopoulos GD, Adamis AP: Retinal vascular endothelial growth factor induces intercellular adhesion molecule-1 and endothelial nitric oxide synthase expression and initiates early diabetic retinal leukocyte adhesion in vivo. *Am J Pathol* 160:501-509, 2002.
29. Joussen AM, Murata T, Tsujikawa A, Kirchhof B, Bursell SE, Adamis AP: Leukocyte-mediated endothelial cell injury and death in the diabetic retina. *Am J Pathol* 158:147-152, 2001.
30. McLeod DS, Lefer DJ, Merges C, Luty GA: Enhanced expression of intracellular adhesion molecule-1 and P-selectin in the diabetic human retina and choroid. *Am J Pathol* 147:642-653, 1995.
31. Miyamoto K, Khosrof S, Bursell SE, Rohan R, Murata T, Clermont AC, Aiello LP, Ogura Y, Adamis AP: Prevention of leukostasis and vascular leakage in streptozotocin-induced diabetic retinopathy via intercellular adhesion molecule-1 inhibition. *Proc Natl Acad Sci U S A* 96:10836-10841, 1999.
32. Chen W, Jump DB, Grant MB, Esselman WJ, Busik JV: Dyslipidemia, but not hyperglycemia, induces inflammatory adhesion molecules in human retinal vascular endothelial cells. *Invest Ophthalmol Vis Sci* 44:5016-5022, 2003.
33. Chen W, Esselman WJ, Jump DB, Busik JV: Anti-inflammatory effect of docosahexaenoic acid on cytokine-induced adhesion molecule expression in human retinal vascular endothelial cells. *Invest Ophthalmol Vis Sci* 46:4342-4347, 2005.
34. Chen W, Jump DB, Esselman WJ, Busik JV: Inhibition of cytokine signaling in human retinal endothelial cells through modification of caveolae/lipid rafts by docosahexaenoic acid. *Invest Ophthalmol Vis Sci* 48:18-26, 2007.
35. Futterman S, Kupfer C: The fatty acid composition of the retinal vasculature of normal and diabetic human eyes. *Invest Ophthalmol* 7:105-108, 1968.
36. Suh M, Wierzbicki AA, Clandinin MT: Dietary fat alters membrane composition in rod outer segments in normal and diabetic rats: impact on content of very-long-chain (C > or = 24) polyenoic fatty acids. *Biochim Biophys Acta* 1214:54-62, 1994.
37. Fox TE, Han X, Kelly S, Merrill AH, 2nd, Martin RE, Anderson RE, Gardner TW, Kester M: Diabetes alters sphingolipid metabolism in the retina: a potential mechanism of cell death in diabetic retinopathy. *Diabetes* 55:3573-3580, 2006.
38. Watson AD: Lipidomics: a global approach to lipid analysis in biological systems. *J Lipid Res* 47:2101-2111, 2006.

39. Brugger B, Erben G, Sandhoff R, Wieland FT, Lehmann WD: Quantitative analysis of biological membrane lipids at the low picomole level by nano-electrospray ionization tandem mass spectrometry. *Proc Natl Acad Sci U S A* 94:2339-2344, 1997.
40. Ejsing CS, Duchoslav E, Sampaio J, Simons K, Bonner R, Thiele C, Ekroos K, Shevchenko A: Automated identification and quantification of glycerophospholipid molecular species by multiple precursor ion scanning. *Anal Chem* 78:6202-6214, 2006.
41. Han X, Gross RW: Shotgun lipidomics: electrospray ionization mass spectrometric analysis and quantitation of cellular lipidomes directly from crude extracts of biological samples. *Mass Spectrom Rev* 24:367-412, 2005.
42. Pulfer M, Murphy RC: Electrospray mass spectrometry of phospholipids. *Mass Spectrom Rev* 22:332-364, 2003.
43. Schwudke D, Oegema J, Burton L, Entchev E, Hannich JT, Ejsing CS, Kurzchalia T, Shevchenko A: Lipid profiling by multiple precursor and neutral loss scanning driven by the data-dependent acquisition. *Anal Chem* 78:585-595, 2006.
44. Welti R, Wang X, Williams TD: Electrospray ionization tandem mass spectrometry scan modes for plant chloroplast lipids. *Anal Biochem* 314:149-152, 2003.
45. Welti R, Shah J, LeVine S, Esch SW, Williams TD, Wang X: High throughput lipid profiling to identify and characterize genes involved in lipid metabolism, signaling, and stress response. In *Functional Lipidomics* L. F, G.D. P, Eds. New York, Marcel Dekker, 2005.
46. Jones JJ, Stump MJ, Fleming RC, Lay JO, Jr., Wilkins CL: Strategies and data analysis techniques for lipid and phospholipid chemistry elucidation by intact cell MALDI-FTMS. *J Am Soc Mass Spectrom* 15:1665-1674, 2004.
47. Jones JJ, Batoy SM, Wilkins CL: A comprehensive and comparative analysis for MALDI FTMS lipid and phospholipid profiles from biological samples. *Comput Biol Chem* 29:294-302, 2005.
48. Jones JJ, Borgmann S, Wilkins CL, O'Brien RM: Characterizing the phospholipid profiles in mammalian tissues by MALDI FTMS. *Anal Chem* 78:3062-3071, 2006.
49. Estrada R, Yappert MC: Alternative approaches for the detection of various phospholipid classes by matrix-assisted laser desorption/ionization time-of-flight mass spectrometry. *Journal of Mass Spectrometry* 39:412-422, 2004.
50. Han X, Gross RW: Shotgun lipidomics: multidimensional MS analysis of cellular lipidomes. *Expert Rev Proteomics* 2:253-264, 2005.

51. Ekroos K, Chernushevich IV, Simons K, Shevchenko A: Quantitative profiling of phospholipids by multiple precursor ion scanning on a hybrid quadrupole time-of-flight mass spectrometer. *Anal Chem* 74:941-949, 2002.
52. Kerwin JL, Tuininga AR, Ericsson LH: Identification of molecular species of glycerophospholipids and sphingomyelin using electrospray mass spectrometry. *J Lipid Res* 35:1102-1114, 1994.
53. Han X, Gross RW: Global analyses of cellular lipidomes directly from crude extracts of biological samples by ESI mass spectrometry: a bridge to lipidomics. *J Lipid Res* 44:1071-1079, 2003.
54. Merrill AH, Sullards MC, Allegood JC, Kelly S, Wang E: Sphingolipidomics: High-throughput, structure-specific, and quantitative analysis of sphingolipids by liquid chromatography tandem mass spectrometry. *Methods* 36:207-224, 2005.
55. Welti R, Li W, Li M, Sang Y, Biesiada H, Zhou HE, Rajashekar CB, Williams TD, Wang X: Profiling membrane lipids in plant stress responses. Role of phospholipase D alpha in freezing-induced lipid changes in Arabidopsis. *J Biol Chem* 277:31994-32002, 2002.
56. Koivusalo M, Haimi P, Heikinheimo L, Kostianen R, Somerharju P: Quantitative determination of phospholipid compositions by ESI-MS: Effects of acyl chain length, unsaturation, and lipid concentration on instrument response. *J. Lipid Res.* 42:663-672., 2001.
57. DeLong CJ, Baker PR, Samuel M, Cui Z, Thomas MJ: Molecular species composition of rat liver phospholipids by ESI-MS/MS: the effect of chromatography. *J Lipid Res* 42:1959-1968, 2001.
58. Song H, Ladenson J, Turk J: Algorithms for automatic processing of data from mass spectrometric analyses of lipids. *J Chromatogr B Analyt Technol Biomed Life Sci*, 2008.
59. Ivanova PT, Milne SB, Byrne MO, Xiang Y, Brown HA: Glycerophospholipid identification and quantitation by electrospray ionization mass spectrometry. *Methods Enzymol* 432:21-57, 2007.
60. Murphy RC, James PF, McAnoy AM, Krank J, Duchoslav E, Barkley RM: Detection of the abundance of diacylglycerol and triacylglycerol molecular species in cells using neutral loss mass spectrometry. *Analytical Biochemistry* 366:59-70, 2007.
61. Ivanova PT, Milne SB, Forrester JS, Brown HA: LIPID arrays: new tools in the understanding of membrane dynamics and lipid signaling. *Mol Interv* 4:86-96, 2004.
62. Turck CW, Falick AM, Kowalak JA, Lane WS, Lilley KS, Phinney BS, Weintraub ST, Witkowska HE, Yates NA: The Association of Biomolecular Resource Facilities Proteomics Research Group 2006 study: relative protein quantitation. *Mol Cell Proteomics* 6:1291-1298, 2007.

63. Old WM, Meyer-Arendt K, Aveline-Wolf L, Pierce KG, Mendoza A, Sevinsky JR, Resing KA, Ahn NG: Comparison of label-free methods for quantifying human proteins by shotgun proteomics. *Mol Cell Proteomics* 4:1487-1502, 2005.
64. Zhang X, Reid GE: Multistage tandem mass spectrometry of anionic phosphatidylcholine lipid adducts reveals novel dissociation pathways. *International Journal of Mass Spectrometry* 252:242-255, 2006.
65. Brucklacher RM, Patel KM, VanGuilder HD, Bixler GV, Barber AJ, Antonetti DA, Lin CM, LaNoue KF, Gardner TW, Bronson SK, Freeman WM: Whole genome assessment of the retinal response to diabetes reveals a progressive neurovascular inflammatory response. *BMC Med Genomics* 1:26, 2008.
66. Decsi T, Minda H, Hermann R, Kozari A, Erhardt E, Burus I, Molnar S, Soltesz G: Polyunsaturated fatty acids in plasma and erythrocyte membrane lipids of diabetic children. *Prostaglandins Leukot Essent Fatty Acids* 67:203-210, 2002.
67. Decsi T, Szabo E, Burus I, Marosvolgyi T, Kozari A, Erhardt E, Soltesz G: Low contribution of n-3 polyunsaturated fatty acids to plasma and erythrocyte membrane lipids in diabetic young adults. *Prostaglandins Leukot Essent Fatty Acids* 76:159-164, 2007.
68. Han X, Gross R: Structural Determination of Picomole Amounts of Phospholipids Via Electrospray Ionization Tandem Mass Spectrometry. *Journal of the American Society for Mass Spectrometry* 6:1202-1210, 1995.
69. Lydic TA, Busik JV, Esselman WJ, Reid GE: Complementary precursor ion and neutral loss scan mode tandem mass spectrometry for the analysis of glycerophosphatidylethanolamine lipids from whole rat retina. *Anal Bioanal Chem*, 2009.
70. Viores SA, Derevjanik NL, Ozaki H, Okamoto N, Campochiaro PA: Cellular mechanisms of blood-retinal barrier dysfunction in macular edema. *Doc Ophthalmol* 97:217-228, 1999.
71. Martin SL, Hoffman WH, Marcus DM, Passmore GG, Dalton RR: Retinal vascular integrity following correction of diabetic ketoacidosis in children and adolescents. *J Diabetes Complications* 19:233-237, 2005.
72. Miyazawa T, Oak JH, Nakagawa K: Tandem mass spectrometry analysis of Amadori-glycated phosphatidylethanolamine in human plasma. *Ann N Y Acad Sci* 1043:280-283, 2005.
73. Ahmed N: Advanced glycation endproducts--role in pathology of diabetic complications. *Diabetes Res Clin Pract* 67:3-21, 2005.
74. Brownlee M: Lilly Lecture 1993. Glycation and diabetic complications. *Diabetes* 43:836-841, 1994.
75. Baynes JW, Thorpe SR: Glycooxidation and lipoxidation in atherogenesis. *Free Radic Biol Med* 28:1708-1716, 2000.

76. Jakus V, Rietbrock N: Advanced glycation end-products and the progress of diabetic vascular complications. *Physiol Res* 53:131-142, 2004.
77. Gardiner TA, Anderson HR, Stitt AW: Inhibition of advanced glycation end-products protects against retinal capillary basement membrane expansion during long-term diabetes. *J Pathol* 201:328-333, 2003.
78. Kern TS, Engerman RL: Pharmacological inhibition of diabetic retinopathy: aminoguanidine and aspirin. *Diabetes* 50:1636-1642, 2001.
79. Ravandi A, Kuksis A, Marai L, Myher JJ, Steiner G, Lewisa G, Kamido H: Isolation and identification of glycated aminophospholipids from red cells and plasma of diabetic blood. *FEBS Lett* 381:77-81, 1996.
80. Nakagawa K, Oak JH, Miyazawa T: Angiogenic potency of Amadori-glycated phosphatidylethanolamine. *Ann N Y Acad Sci* 1043:413-416, 2005.
81. Oak JH, Nakagawa K, Oikawa S, Miyazawa T: Amadori-glycated phosphatidylethanolamine induces angiogenic differentiations in cultured human umbilical vein endothelial cells. *FEBS Lett* 555:419-423, 2003.
82. Navaratna D, McGuire PG, Menicucci G, Das A: Proteolytic degradation of VE-cadherin alters the blood-retinal barrier in diabetes. *Diabetes* 56:2380-2387, 2007.

Remodeling of Retinal Fatty Acids in an Animal Model of Diabetes: a Decrease in Long Chain Polyunsaturated Fatty Acids is Associated with a Decrease in Fatty Acid Elongases ELOVL2 and ELOVL4.

*4.1 Abstract*

The results of the DCCT/EDIC revealed a strong association between dyslipidemia and the development of diabetic retinopathy. However, there are no experimental data on retinal fatty acid (FA) metabolism in diabetes. This study determined retinal specific FA metabolism in control and diabetic animals.

Tissue gene and protein expression profiles were determined by qRT-PCR and western blot in control and STZ diabetic rats at 3-6 weeks of diabetes. Fatty acid profiles were assessed by RP-HPLC, and phospholipid analysis was performed by nESI-MS/MS.

We found a dramatic difference between retinal and liver elongase and desaturase profiles with high elongase and low desaturases gene expression in the retina compared to liver. ELOVL4, an elongase expressed in the retina, but not in the liver, showed the greatest expression level among retinal elongases, followed by ELOVL2, ELOVL1 and ELOVL6. Importantly, early stage diabetes induced a marked decrease in retinal expression levels of ELOVL4, ELOVL2 and ELOVL6. Diabetes-induced downregulation of retinal elongases translated into a significant decrease in total retinal docosahexaenoic acid, as well as decreased incorporation of very long chain polyunsaturated fatty acids, particularly 32:6n3, into retinal phosphatidylcholine. This decrease in n3 PUFA was coupled with inflammatory status in diabetic retina, reflected by an increase in gene expression of pro-inflammatory markers IL-6, VEGF, and ICAM-1.

This is the first comprehensive study demonstrating diabetes-induced changes in retinal FA metabolism. Normalization of retinal FA levels by dietary means or/and modulating expression of elongases could represent a potential therapeutic target for diabetes-induced retinal inflammation.

#### 4.2. Introduction

Early diabetic retinopathy has been suggested to be a low-grade chronic inflammatory disease (1-3) with a number of inflammatory markers such as VEGF (4; 5), ICAM-1 (6; 7), TNF $\alpha$  (8) and IL-6 (9) shown to be upregulated in diabetic retina. The individual molecular steps leading to inflammation in the retina are not well resolved, but likely involve hyperglycemia and dyslipidemia associated with diabetes mellitus.

Dyslipidemia is a major metabolic disorder of diabetes mellitus and the DCCT/EDIC cohort study revealed that dyslipidemia was significantly associated with the development of diabetic retinopathy (10). Diabetic dyslipidemia is the result of an imbalance in the complex regulation of lipid uptake, metabolism, release by adipocytes, and clearance from circulation (11; 12). Perturbation of fatty acid metabolism in diabetes is an important part of diabetic dyslipidemia (13).

To understand the effects of diabetes on plasma and tissue fatty acid composition, two metabolic routes have to be considered: *de novo* lipogenesis, and the polyunsaturated fatty acid (PUFA) remodeling Sprecher pathway (14). Saturated (SFA), mono- (MUFA) and polyunsaturated fatty acids are synthesized from dietary precursors (glucose, palmitic[16:0], oleic[18:1n9], linoleic[18:2n6],  $\alpha$ -linolenic[18:3n3], eicosapentaenoic acid [EPA20:5n3], and docosahexaenoic acid [DHA22:6n3]) through a series of desaturation ( $\Delta$ 5-desaturase [ $\Delta$ 5D],  $\Delta$ 6-

desaturase [ $\Delta 6D$ ] or  $\Delta 9$ -desaturase [ $\Delta 9D$ ]) and elongation (ELOVL1-7) reactions. In the recent work by Agbaga et al. (15), the Sprecher pathway was expanded to include very long chain polyunsaturated fatty acids (VLCPUFA), up to 38 carbon fatty acids in which elongation of shorter chain fatty acid precursors is performed by ELOVL4 (see Figure 4.1). ELOVL4 has very limited tissue specificity. It is highly expressed in the retina (16-18), thymus and skin (17) as well as at lesser levels in the brain (17; 18) and testis (18). ELOVL4 is not expressed in the liver (17; 18). In human retina ELOVL4 was shown to be primarily expressed in the inner segment of photoreceptors extending to photoreceptor cell bodies in the outer nuclear layer (19). Moderate labeling was also observed in the ganglion cells (19). ELOVL4 has received much attention recently as an autosomal dominant Stargardt-like macular dystrophy was linked to several dominant negative mutations in ELOVL4 (19-21). The role of VLCPUFA produced by ELOVL4 is not known, but because of their localization in retinal outer segment membranes and ability to span both leaflets of the lipid bilayer, they are suggested to play a role in stabilizing cellular membranes with high curvature, such as the rims of photoreceptor disks (15). Fatty acid desaturase enzymes are known to be inhibited in diabetes (22-24) and there is emerging information suggesting that certain elongases might also be affected (25). Thus, diabetes may result in reduced FA remodeling and, consequently, lead to an accumulation of the substrates and depletion of the products. The elongases ELOVL2 and ELOVL6 are ubiquitously expressed in most tissues; however, retina expresses ELOVL2 at a very high level. ELOVL2 is involved in several steps of DHA22:6n3 biosynthesis (26). Retina has a unique fatty acid profile with one of the highest levels of long chain PUFA, especially DHA22:6n3, in the body (27). We have previously demonstrated that DHA22:6n3 has a pronounced anti-inflammatory effect on cytokine induced activation of the NF $\kappa$ B pathway and adhesion molecule expression in human

retinal endothelial cells (HREC) (28). Thus perturbation of lipid metabolism in diabetes with a subsequent decrease in DHA22:6n3 could create pro-inflammatory conditions in the retina potentially contributing to the development of diabetic retinopathy. The effect of diabetes on retinal fatty acid elongases and desaturases and diabetes-induced changes in retinal fatty acid remodeling has not been analyzed, and represents one of the goals of this study.

### *4.3. Results*

#### **4.3.1 Body weight gain and blood glucose concentration of experimental animals**

As presented in Table 4.1, body weight gain was significantly slower in diabetic animals compared to control animals. Blood glucose levels were almost 5 times higher in diabetic animals compared to control. As this was a short term diabetes study, Hb<sub>A1C</sub> levels were not measured.

#### **4.3.2 Elongase and desaturase expression level in control and diabetic animals**

The gene expression levels of elongases and desaturases in control retinas were determined by qRT-PCR and compared to the levels found in the livers of the same animals. Retinal-specific elongase, ELOVL4, had the highest expression level among all the elongases in the retina and was not expressed in the liver. Retinas also had high levels of ELOVL2 expression (Figure 4.2A). Livers exhibited higher levels of ELOVL5, and  $\Delta$ 5,  $\Delta$ 6 and  $\Delta$ 9 desaturases than retina (Figure 4.2A), and the liver profile of all elongases and desaturases agreed with our previous study (25).

In the liver, diabetes induced a 25% decrease in ELOVL2 and a 33% decrease in ELOVL6 expression, as well as an 85% decrease in  $\Delta$ 9-desaturase (Figure 4.2B), compared to

controls. In the retina, diabetes induced a 40% reduction in ELOVL4 and 50% reduction in ELOVL2 expression levels (Figure 4.2C). There was no significant effect of diabetes on the retinal desaturases (Figure 4.2C). A decrease in ELOVL4 protein level was confirmed by western blot as shown in Figure 4.2D.

#### **4.3.3 Plasma fatty acid profiles of control and diabetic animals**

The control and diabetic plasma fatty acid profiles 3 weeks after STZ injection are presented in Table 4.2. There was a tendency towards higher total fatty acids level in diabetic vs. control plasma. We observed changes in the plasma fatty acid profile consistent with inhibition of fatty acid remodeling in diabetes that leads to a lower end product-to-precursor fatty acid ratio. There was a decrease in two major end products of the PUFA synthesis pathway, arachidonic20:4n6 acid and DHA22:6n3, relative to their precursors, linoleic18:2n6 and  $\alpha$ -linolenic18:3n3 acid, respectively (Table 4.2). As a result of these changes we observed a decrease in the unsaturation index (the number of double bonds per fatty acyl residue) and a decrease in the long chain/short chain PUFA ratio in diabetic vs. control animals (Table 4.2).

#### **4.3.4 Liver fatty acid profiles of control and diabetic animals**

The control and diabetic liver fatty acid profiles 3 weeks after STZ injection are presented in Table 4.3. There was an increase in the linoleic acid18:2n6 level in the livers of diabetic vs. control animals that led to a decrease in long chain/short chain PUFA ratio (Table 4.3). There were no other significant changes in liver fatty acid profiles in diabetic vs. control animals. The liver unsaturation index and PUFA synthesis pathway end product to precursor ratios did not change in diabetic vs. control animals (Table 4.3).

#### **4.3.5 Retinal fatty acid profiles of control and diabetic animals**

Retina has a unique fatty acid profile with the highest content of long chain PUFA in the body. In agreement with other studies, retinal profiles were very rich in DHA<sub>22:6n3</sub> and arachidonic<sub>20:4n6</sub> acid (Table 4.4). The levels of linoleic<sub>18:2n6</sub> and  $\alpha$ -linolenic<sub>18:3n3</sub> acid in the retina were very low, thus we did not calculate the PUFA synthesis pathway end product to precursor ratios. Importantly, the retinas of diabetic animals had 28% less DHA<sub>22:6n3</sub> compared to control. As a result, we observed a decrease in unsaturation index, a decrease in long chain/short chain PUFA ratio and a decrease in the n<sub>3</sub>/n<sub>6</sub> PUFA ratio in the retinas of diabetic vs. control animals (Table 4.4). Representative RP-HPLC chromatograms of saponified fatty acids from control and diabetic retina are presented in Figure 4.3A.

#### **4.3.6 Retinal and erythrocyte phospholipid profiles of control and diabetic animals**

In agreement with saponified fatty acid profile data, nano-electrospray ionization (nESI) coupled with tandem mass spectrometry (MS/MS) analysis of the retina lipid extracts of diabetic animals (n=3) showed a significant (up to 34%) decrease in the abundance of glycerophospholipids containing DHA<sub>22:6n3</sub> compared to the control animals (n=3). For example, compare the abundance of the GPCho(18:0/22:6) and GPCho(22:6/22:6) lipids in the ratiometric analysis shown in Figure 4.3B. Similar decreases in the abundances of DHA<sub>22:6n3</sub> containing lipids were also observed for glycerophosphoethanolamine and glycerophosphoserine lipids (data not shown). In contrast, an increase (37%) in the abundance of the linoleic<sub>18:2n6</sub> acid-containing GPCho(16:0/18:2) lipid was observed for the same samples as shown in Figure 4.3B. In addition to known fatty acids identified by HPLC analysis, nESI-MS/MS analysis

revealed several VLCPUFA, primarily 32:6n3 and 34:6n3, esterified to GPCho in the retina. Interestingly, GPCho(32:6/22:6) was significantly decreased (24%) in diabetic retinas compared to control, and there was a non-significant decrease (9%) of GPCho(34:6/22:6).

In erythrocyte lipid extracts, an increase in the abundance of linoleic18:2n6 acid-containing lipids, namely GPCho(16:0/18:2) and GPCho(18:0/18:2), was observed between the diabetic and control samples, consistent with the changes in retina lipids, as shown in Figure 4.3C. Erythrocytes had very low levels of DHA-containing phospholipid species and there was no effect of diabetes on these species. There was no detectable GPCho(32:6/22:6) or GPCho(34:6/22:6) in the erythrocytes, or in liver and plasma (data not shown).

#### **4.3.7 Inflammatory marker expression in control and diabetic retinas**

As n3 PUFA are known to have anti-inflammatory properties, we hypothesized that a decrease in n3 PUFA would be associated with a pro-inflammatory state in diabetic retinas. As shown in Figure 4.4, diabetic retinas had increased expression levels of several inflammatory markers including adhesion molecules (ICAM-1), cytokines (IL-6), and growth factors (VEGF).

#### *4.4 Discussion*

The association of dyslipidemia with the development of diabetic retinopathy has been underscored by the DCCT/ EDIC cohort study (8). In spite of this evidence the experimental data on diabetes induced changes in lipid profile and lipid metabolism in the retina are not

available. This is the first comprehensive study to analyze retinal- specific FA profiles and metabolism and to compare them to liver and blood plasma in control and diabetic animals.

In this study utilizing STZ diabetic rats we found a decreased level of DHA<sub>22:6n3</sub>, the major retinal long chain PUFA, in diabetic retina. This finding confirmed earlier studies showing a decrease in relative percentage of DHA<sub>22:6n3</sub> in the diabetic retina (29). In addition to DHA<sub>22:6n3</sub>, VLCPUFA including 32:6n3 and 34:6n3 were detected as substituents of retina GPCho. VLCPUFA were not detected in lipid classes other than GPCho, and were only detected in retina. Three weeks of diabetes reduced retinal levels of 32:6n3-GPCho compared to controls. As a result of these changes, the diabetic retina had a lower unsaturation index and lower long chain/short chain PUFA ratio. Moreover, there was a shift toward n3 PUFA deficient, n6 PUFA rich profile in the diabetic retina.

In general, n6 PUFA induce, while n3 PUFA inhibit the inflammation and the relative amount of these PUFA plays important role in the regulation of immunity (30). Our previous studies indicated that treatment of a cell type affected by diabetic retinopathy, human retinal endothelial cells (HREC), with n6 PUFA leads to a lipoxygenase-dependent increase in ICAM-1/VCAM-1 expression (31). Conversely, we have demonstrated that DHA<sub>22:6n3</sub> inhibited cytokine induced activation of NFκB signaling pathway and adhesion molecule expression in HRECs (28). Thus a decrease in the n3/n6 PUFA ratio in the diabetic retina observed in this study would create pro-inflammatory conditions potentially contributing to the development of diabetic retinopathy. Indeed, previous studies demonstrated an upregulation in a number of inflammatory markers in the retina early in diabetes: VEGF(4; 5), ICAM-1 (7; 32) TNFα (8) and IL-6 (33). ICAM-mediated leukostasis was detected within one week of diabetes in rats (6; 32).

VEGF was shown to increase ICAM expression in retinas of non-diabetic mice (32) and vitreal VEGF levels were found to be correlated with that of IL-6 and severity of diabetic retinopathy in diabetic patients (9) .

In this study we chose a cytokine (IL-6), a growth factor (VEGF), and an adhesion molecule (ICAM-1) as readout of an inflammatory status in the retinas of diabetic animals with decreased n3/n6 PUFA. mRNA levels of all three markers were elevated in diabetic retinas as compared to controls.

Importantly, diabetes induced the most pronounced changes in the retinal fatty acid profile, whereas liver fatty acid profile was only slightly affected, indicating that the disruption of retinal fatty acid metabolism in diabetes might not simply be a result of altered liver metabolism. Moreover, VLCPUFA-containing phospholipids detected in the retina were not present in the liver or erythrocyte total lipids. The fatty acid profile in a particular peripheral tissue depends on two factors: a) the profile in circulation due to the diet and liver metabolism and b) the ability of a local tissue to remodel fatty acids. Retina has a unique fatty acid profile characterized by one of the highest levels of DHA22:6n3 in the body and by the presence of VLCPUFA (27; 34). While the expression level of retinal desaturases was relatively low compared to retinal elongases, it has been reported that retina can synthesize DHA22:6n3 from  $\alpha$ -linolenic18:3n3 acid and EPA20:5n3 (35). Although retina may obtain additional DHA22:6n3 by uptake from the circulation, changes in the retinal fatty acid profiles of diabetic animals did not mirror changes observed in liver and plasma fatty acid profiles. Thus a retina-specific decrease in DHA22:6n3 in diabetes is likely to be due to changes in retinal fatty acid metabolism.

To determine the effect of diabetes on retinal fatty acid metabolism, we analyzed the level of fatty acid elongase and desaturase gene expression in control and diabetic animals. Retinas had a very high expression level of the retinal specific elongase, ELOVL4, as well as high expression levels of long chain PUFA elongase ELOVL2. Delta 5, 6 and 9 desaturase levels were low compared to the liver expression levels. The high levels of ELOVL4 and ELOVL2 and low levels of desaturases suggest that the retina is preferentially involved in production of very long chain fatty acids and exhibits a low level of de-novo lipogenesis. The retinal elongase expression profile that we observed likely explains the high level of long chain PUFA in the retina compared to liver and plasma levels. ELOVL2 elongates C20-22 fatty acids (36-38). ELOVL4 was recently shown to be involved in VLCPUFA synthesis with substrate specificity for C26-36 fatty acids (15). The role of VLCPUFA is not known. Because of their specific presence in tissues with high membrane curvature and their ability to span both leaflets of the lipid bilayer, VLCPUFA are suggested to play the role of an anchor stabilizing high curvature cellular membranes (15). In the retina VLCPUFA are mainly present in the rod outer segment membrane (15) where they are suggested to play a role in stabilizing the rims of photoreceptor disks. This specific localization might explain the low abundance of VLCPUFA in the total retinal lipids extracted in this study. At the same time, their specific localization in rod outer segments suggests that VLCPUFA might play an important role in photoreceptor function. This study provides the first direct evidence that a significant decrease in ELOVL4 in diabetic retina is indeed associated with a decrease in VLCPUFA (i.e., 32:6n3) synthesis. Despite their lower abundance, the diabetes induced decrease in 32:6n3 containing GPCho (24%) was similar to the decrease in DHA22:6n3 containing GPChos (15-34%). ELOVL4 protein expression in diabetic retina was inhibited to a greater extent (73%) than the mRNA expression (40%)

suggesting control of ELOVL4 expression at both transcriptional and translational levels. Although the decrease of VLCPUFA is most likely to arise from ELOVL4 loss, another plausible explanation could be that this reduction was due to reduction in VLCPUFA precursor lipids, EPA20:5n3 and/or DHA22:6n3. This possibility can be tested in the future by determining whether downregulation of VLCPUFA in diabetes persists in animals supplemented with high EPA20:5n3/ DHA22:6n3 diet.

Another possibility could be that high level of reactive oxygen species in diabetic retina leads to degradation of the highly oxidation-prone DHA molecule. Previous studies using the same STZ diabetes model of similar duration, however, did not find oxidized DHA products in diabetic retina (39).

Several ELOVL4 gene mutations have been recently identified in the pathogenesis of another retinal disease, Stargardt-like macular dystrophy (19; 20; 21). Stargardt-like macular dystrophy is an autosomal dominant disorder due to a dominant negative effect of the mutated ELOVL4 on wild-type protein (19). As ELOVL4 is highly expressed in the photoreceptors (19; 21), it is not surprising that mutant ELOVL4 transgenic mice are characterized by lipofuscin accumulation, abnormal electrophysiology and photoreceptor degeneration (20). Although photoreceptors are not the primary site of diabetic retinopathy, several abnormalities in the neural retina have been associated with the development of diabetic retinopathy (40; 41). The decrease in ELOVL4 observed in this study would not be expected to have as dramatic an effect on photoreceptor viability as the dominant negative mutation in ELOVL4. However, the reduction in ELOVL4 in diabetic retina could be responsible for more subtle changes in photoreceptor/RPE cell function that could lead to metabolic changes in the whole retina, and eventually contribute to the pathology characteristic of diabetic retinopathy.

#### *4.5 Conclusions*

In conclusion, a decrease in the expression level of retinal fatty acid elongases ELOVL2 and ELOVL4 and concomitant decrease in the major n3 PUFA, DHA22:6n3, as well as the VLCPUFA 32:6n3, results in an increased n6-to-n3 PUFA ratio in the diabetic retina that likely creates a pro-inflammatory state contributing to the development of diabetic retinopathy. Increasing the gene expression of fatty acid elongases in the retina represents a potential therapeutic strategy for modulating fatty acid metabolism and altering the pathogenesis of diabetic retinopathy.

**Table 4.1.** Body weight gain and blood glucose concentrations of experimental animals.

	Weight gain, g/day	Blood Glucose (mM)
Control animals	4.05 ± 0.65	4.33 ± 0.29
Diabetic animals	2.32 ± 0.89	20.80 ± 1.16

**Table 4.2.** Plasma fatty acid profiles of control and diabetic animals.

Fatty acids	Control animals Mean±SD	Diabetic animals Mean±SD	Difference <i>p</i> value	
Total (nmol/mg protein)	2262.55 ± 639.64	3286.54 ± 766.69	0.0972	
Mole% of total fatty acids				
16:0 (palmitic)	2.19 ± 1.17	3.70 ± 0.46	↑	0.0362 *
18:0 (stearic)	2.25 ± 0.34	2.08 ± 0.40		0.5639
18:1n9 (oleic)	12.65 ± 1.03	13.43 ± 1.74		0.5126
18:2n6 (linoleic)	54.12 ± 2.31	57.44 ± 2.62		0.1207
18:3n3 (α-linolenic)□	1.93 ± 0.32	2.71 ± 0.36	↑	0.0214 *
18:3n6 (γ-linolenic)	0.31 ± 0.13	0.51 ± 0.37		0.4028
20:3n6 (dihomo-γ-linolenic)	0.84 ± 0.12	0.87 ± 1.15		0.9631
20:3n9 (mead)	0.52 ± 0.32	0.35 ± 0.30		0.4636
20:4n6 (arachidonic)	21.29 ± 2.70	15.90 ± 1.95	↓	0.0161 *
20:5n3 (eicosapentaenoic)	0.53 ± 0.08	0.51 ± 0.03		0.7449
22:5n3 (docosapentaenoic)	0.84 ± 0.22	0.54 ± 0.04	↓	0.0235 *
22:6n3 (docosahexaenoic)	2.78 ± 0.23	1.72 ± 0.25	↓	0.0010 *
Fatty acid ratios				
unsaturation index	61.58 ± 18.05	38.91 ± 5.56	↓	0.0342 *
LCPUFA/SCPUFA†	0.48 ± 0.06	0.33 ± 0.05	↓	0.0107 *
20:4n6/18:2n6	0.40 ± 0.07	0.28 ± 0.04	↓	0.0232 *
22:6n3/18:3n3	1.46 ± 0.17	0.64 ± 0.13	↓	0.0002 *

\*P < 0.05; †Long Chain Polyunsaturated Fatty Acids/Short Chain Polyunsaturated Fatty Acids

**Table 4.3.** Liver fatty acid profiles of control and diabetic animals.

Fatty acids	Control animals Mean±SD	Diabetic animals Mean±SD	Difference <i>p</i> value	
Total (nmol/mg protein)	1762.82 ± 480.50	1357.85 ± 241.19	0.1542	
Mole% of total fatty acids				
16:0 (palmitic)	26.73 ± 8.18	17.55 ± 3.25	0.0518	
18:0 (stearic)	11.25 ± 3.74	12.64 ± 3.55	0.9706	
18:1n9 (oleic)	3.11 ± 1.03	3.39 ± 1.04	0.4785	
18:2n6 (linoleic)	33.14 ± 5.34	39.90 ± 2.71	↑ 0.0161	*
18:3n3 (α-linolenic) □	0.49 ± 0.11	0.59 ± 0.11	0.2101	
18:3n6 (γ-linolenic)	0.13 ± 0.14	0.09 ± 0.04	0.2173	
20:3n6 (dihomo-γ-linolenic)	0.34 ± 0.04	0.43 ± 0.15	0.3942	
20:3n9 (mead)	0.62 ± 0.24	0.51 ± 0.14	0.9340	
20:4n6 (arachidonic)	19.87 ± 4.43	21.37 ± 2.50	0.4581	
20:5n3 (eicosapentaenoic)	0.15 ± 0.03	0.15 ± 0.05	0.7777	
22:5n3 (docosapentaenoic)	0.57 ± 0.15	0.44 ± 0.07	0.2388	
22:6n3 (docosahexaenoic)	3.60 ± 0.92	2.94 ± 0.35	0.2294	
Fatty acid ratios				
unsaturation index	5.05 ± 1.82	6.56 ± 1.31	0.0911	
LCPUFA/SCPUFA †	0.74 ± 0.07	0.64 ± 0.02	↓ 0.0123	*
20:4n6/18:2n6	0.60 ± 0.07	0.53 ± 0.03	0.1211	
22:6n3/18:3n3	7.74 ± 2.96	5.11 ± 1.05	0.0979	

\*P < 0.05; †Long Chain Polyunsaturated Fatty Acids/Short Chain Polyunsaturated Fatty Acids

**Table 4.4.** Retinal fatty acid profiles of control and diabetic animals.

Fatty acids	Control animals Mean±SD	Diabetic animals Mean±SD	Difference <i>p</i> value	
Total (nmol/mg protein)	488.96±17.64	460.32±27.82	0.43	
n3 fatty acids	225.1±4.23	166.34±20.66	↓ 0.0495	*
n6 fatty acids	38.67±4.71	40.59±3.9	0.7693	
Mole% of total fatty acids				
16:0 (palmitic)	15.51±0.8	18.32±1.67	0.2046	
18:0 (stearic)	18.61±0.97	21.98±2.	0.2046	
18:1n9 (oleic)	10.58±0.2	12.9±0.77	↑ 0.0441	*
18:2n6 (linoleic)	0.44±0.06	0.88±0.05	↑ 0.0051	*
18:3n3 ( $\alpha$ -linolenic □)	0.24±0.06	0.17±0.02	0.3556	
20:3n6 (dihomo- $\gamma$ -linolenic)	0.11±0.02	0.04±0.01	0.0819	
20:3n9 (mead)	0.97±0.06	1.09±0.2	0.6103	
20:4n6 (arachidonic)	7.33±0.75	7.9±0.64	0.6004	
20:5n3 (eicosapentaenoic)	0.04±0.02	0.01±0.01	0.2910	
22:5n3 (docosapentaenoic)	0.47±0.08	0.28±0.05	0.1129	
22:6n3 (docosahexaenoic)	45.37±1.32	35.47±2.71	↓ 0.0305	*
Fatty acid ratios				
unsaturation index	20.77±1.63	14.9±2.57	0.1259	
LCPUFA/SCPUFA	80.39±4.86	42.53±3.94	↓ 0.0038	*
%n3 fatty acids of total	46.12±1.41	35.93±2.77	↓ 0.0306	*

\*P &lt; 0.05

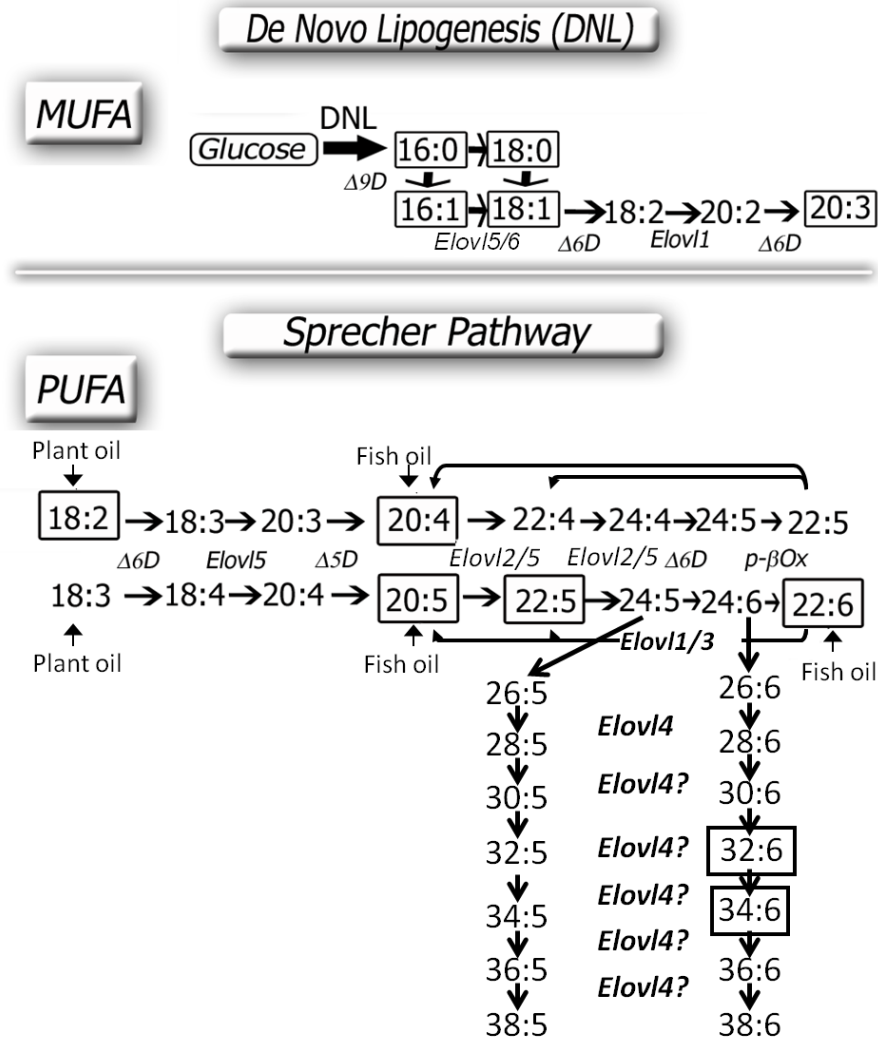


**Figure 4.1. De novo lipogenesis and polyunsaturated fatty acid remodeling pathways.** Fatty acids are synthesized from glucose through de novo lipogenesis or converted from dietary palmitic(16:0), oleic(18:1n9), linoleic(18:2n6),  $\alpha$ -linolenic(18:3n3) acids to long chain unsaturated fatty acids *in vivo* by a series of desaturation ( $\Delta$ -5-desaturase [ $\Delta$ 5D],  $\Delta$ -6-desaturase [ $\Delta$ 6D] or  $\Delta$ -9-desaturase [ $\Delta$ 9D]) and elongation (Elovl-1-7) reactions. Fatty acids that accumulate in animal and human tissues are in solid boxes. Dietary linoleic(18:2n6) and  $\alpha$ -linolenic(18:3n3) are obtained from plants, EPA(20:5n3) and DHA(22:6n3) are rich in fish oil. A recent study demonstrated ELOVL4 is necessary for synthesis of C26 and C28 VLCPUFA from 24:5n3 and 24:6n3 fatty acid precursors, and suggests ELOVL4 is also required for synthesis of >C28 VLCPUFA. There is no inter-conversion between n3, n6 and n9 fatty acids in animals.

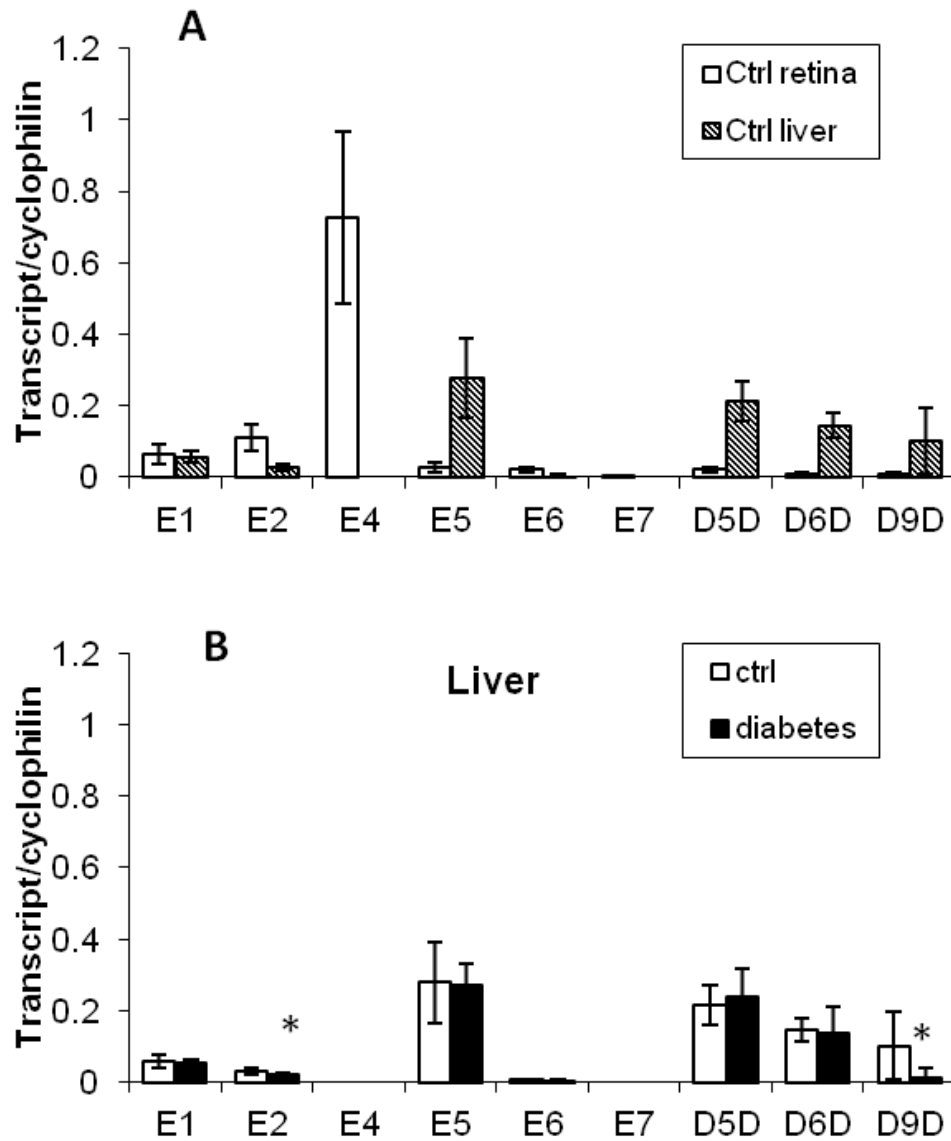


**Figure 4.2. Expression levels of elongases and desaturases in retinas and livers of control and diabetic animals.** Total RNA was extracted from retinas and livers of normal control (n=4) and STZ diabetic animals (n=5) after 3-6 weeks of diabetes and analyzed by real-time PCR for elongases 1-7 (E1-7) and delta 5, 6 and 9 desaturase (D5D, D6D and D9D) expression level. A comparison of the expression levels in retina (white bars) and liver (hatched bars) of normal control animals is presented in A. Diabetes induced changes in liver elongase and desaturase expression levels are presented in B (control – white bars, diabetes – black bars).

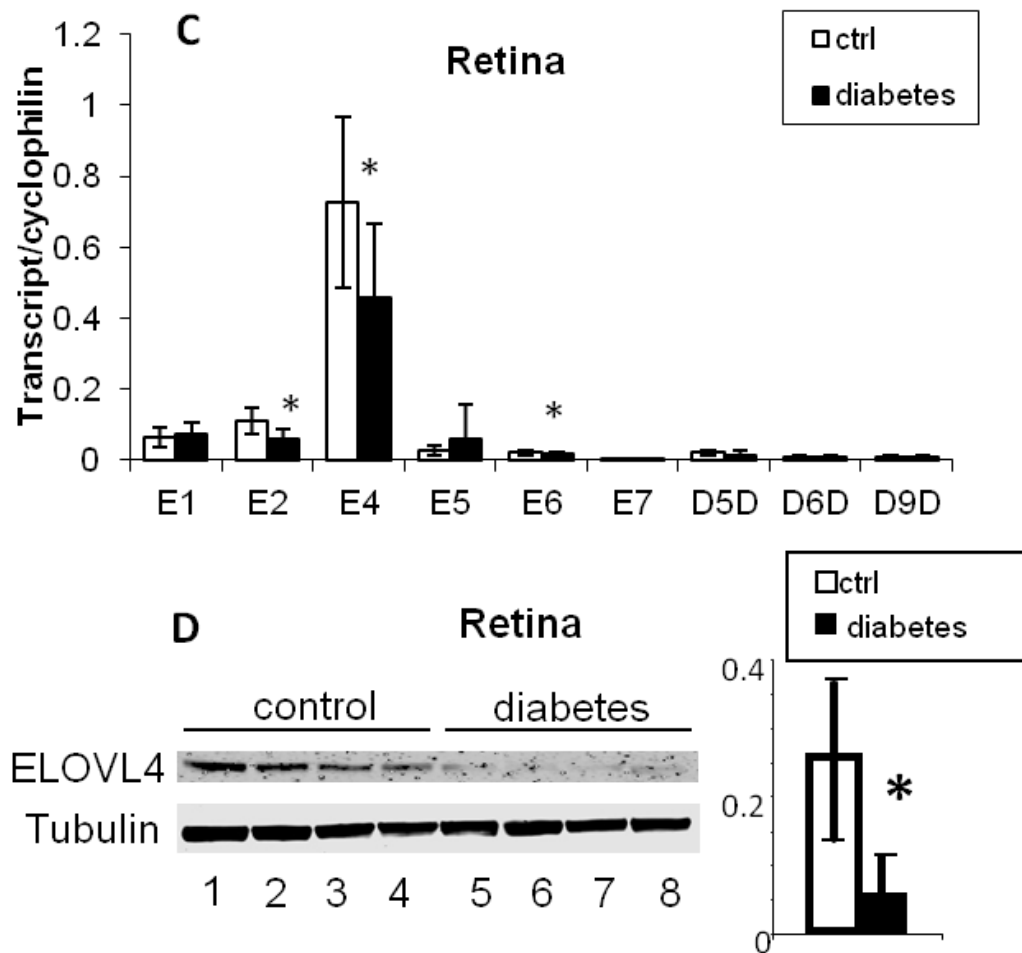


**Figure 4.2 (cont'd).** Diabetes induced changes in retinal expression levels are presented in C (control – white bars, diabetes – black bars). A Western blot of diabetes induced changes in retina ELOVL4 protein level (lanes 1-4 control, lanes 5-8 diabetic), and quantification by ratiometric comparison to tubulin, are presented in D (control - white bars, diabetes – black bars). Data are presented as mean  $\pm$  SD of 5 independent experiments. Asterisk indicates statistical significance at  $P < 0.05$ .

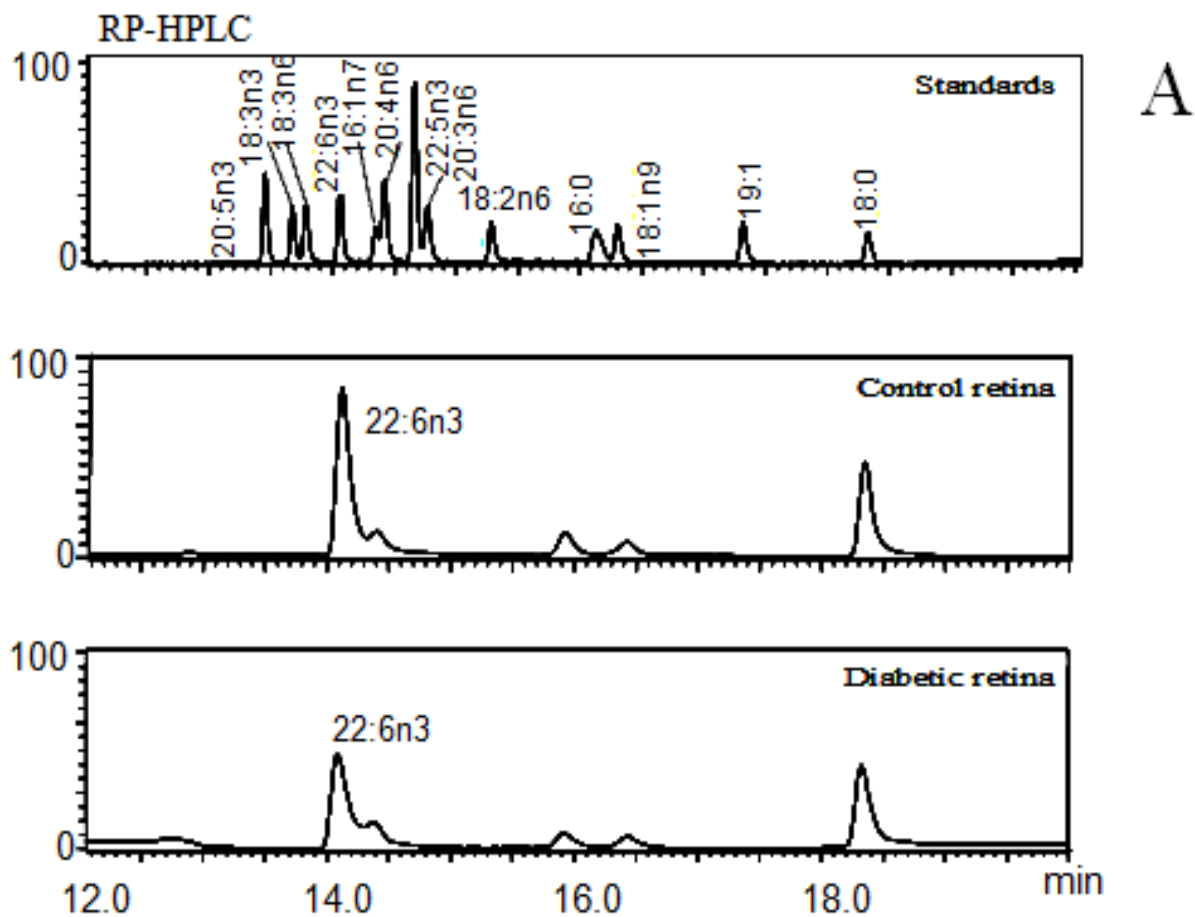


**Figure 4.3. Retina fatty acid analysis by RP-HPLC and tandem mass spectrometry analysis of GPCho lipids in retina and erythrocytes at 3-6 weeks of diabetes.** (A) Identification and quantification of diabetes-induced changes in total retina saponified fatty acids. Top, RP-HPLC chromatogram of a mixture of authentic fatty acid standards. Middle, control retina saponified fatty acids. Bottom, diabetic retina saponified fatty acids. Y-axis represents ELSD signal (%).

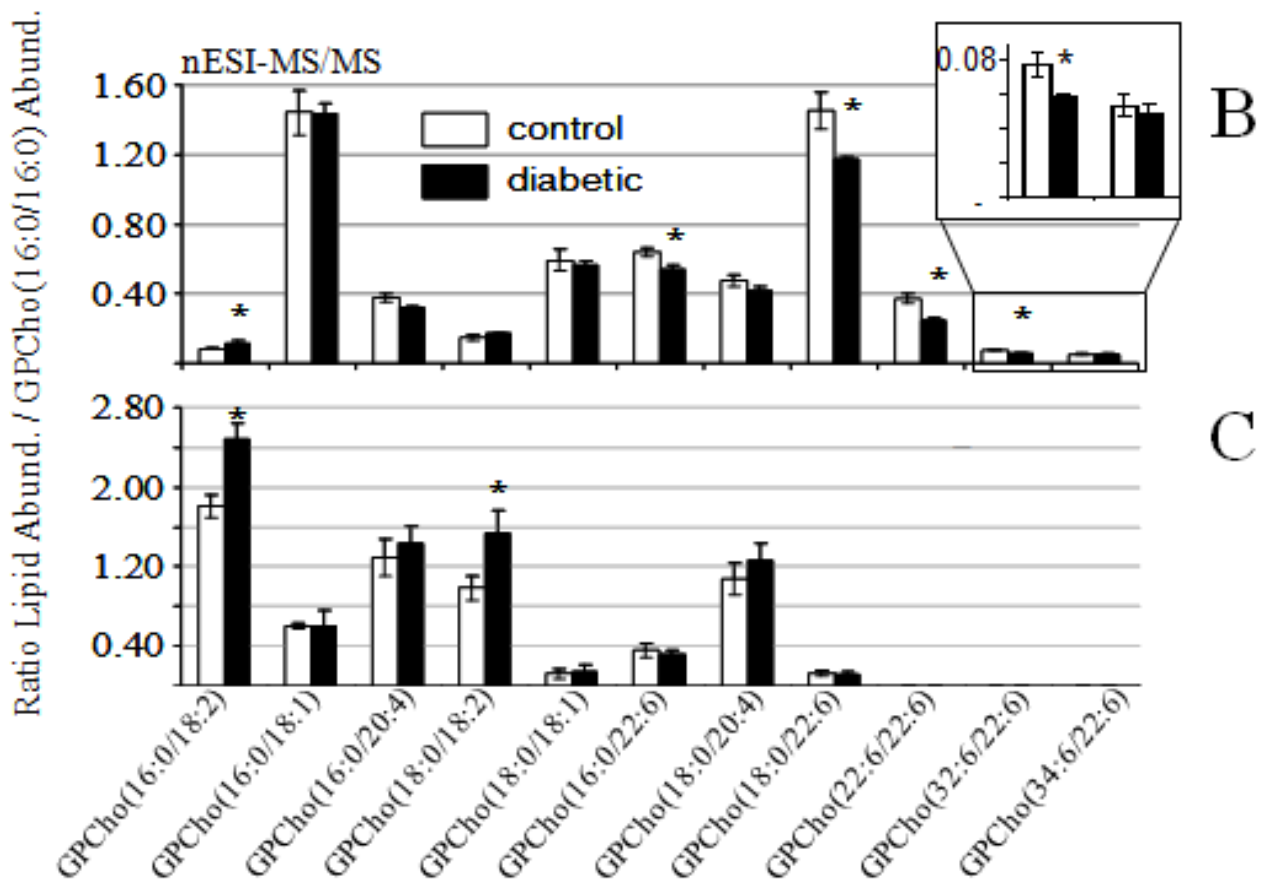


**Figure 4.3 (cont'd).** (B) Ratiometric analysis of changes in GPCho lipid abundance between control and diabetic retina. GPCho species were detected by nESI-MS/MS using PI  $m/z$  184 and further characterized as described in *Chapters II and VI*. (C) Ratiometric analysis of changes in GPCho lipid abundance between control and diabetic erythrocytes. Data are presented as mean  $\pm$  SD. Asterisk indicates statistical significance at  $P < 0.05$ .  $n = 3$  animals per group.

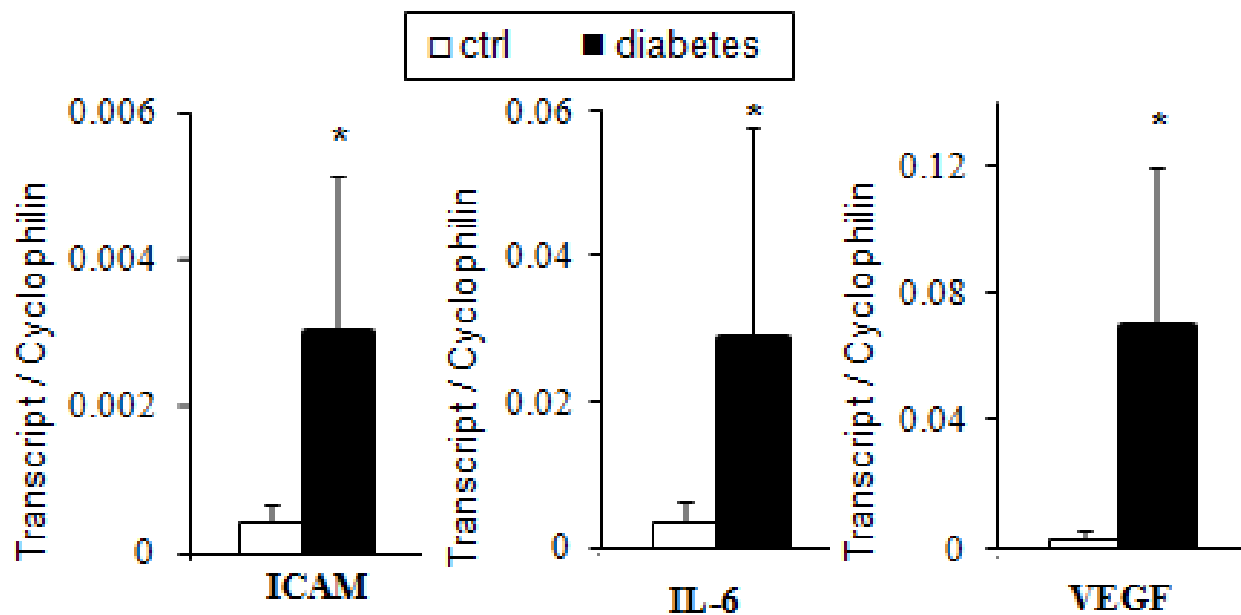


**Figure 4.4. Expression levels of inflammatory markers in retinas of control and diabetic animals.** Total RNA was extracted from retinas of control and diabetic animals after 3-6 weeks of diabetes and analyzed by real-time PCR. Diabetes induced changes in retinal ICAM-1, IL-6 and VEGF expression are shown (control – white bars, diabetes – black bars). Data are presented as mean  $\pm$  SD of at least 4 independent experiments. Asterisk indicates statistical significance at  $P < 0.05$ .  $n = 7$  animals per group.

## References

#### 4.6 References

1. Schroder S, Palinski W, Schmid-Schonbein GW: Activated monocytes and granulocytes, capillary nonperfusion, and neovascularization in diabetic retinopathy. *Am J Pathol* 139:81-100, 1991.
2. Miyamoto K, Khosrof S, Bursell SE, Rohan R, Murata T, Clermont AC, Aiello LP, Ogura Y, Adamis AP: Prevention of leukostasis and vascular leakage in streptozotocin-induced diabetic retinopathy via intercellular adhesion molecule-1 inhibition. *Proc Natl Acad Sci U S A* 96:10836-10841, 1999.
3. Adamis AP: Is diabetic retinopathy an inflammatory disease? *Br J Ophthalmol* 86:363-365, 2002.
4. Antonetti DA, Barber AJ, Khin S, Lieth E, Tarbell JM, Gardner TW: Vascular permeability in experimental diabetes is associated with reduced endothelial occludin content: vascular endothelial growth factor decreases occludin in retinal endothelial cells. Penn State Retina Research Group. *Diabetes* 47:1953-1959, 1998.
5. Antonetti DA, Lieth E, Barber AJ, Gardner TW: Molecular mechanisms of vascular permeability in diabetic retinopathy. *Semin Ophthalmol* 14:240-248, 1999.
6. Jousen AM, Murata T, Tsujikawa A, Kirchhof B, Bursell SE, Adamis AP: Leukocyte-mediated endothelial cell injury and death in the diabetic retina. *Am J Pathol* 158:147-152, 2001.
7. Al-Shabrawey M, Rojas M, Sanders T, Behzadian A, El-Remessy A, Bartoli M, Parpia AK, Liou G, Caldwell RB: Role of NADPH oxidase in retinal vascular inflammation. *Invest Ophthalmol Vis Sci* 49:3239-3244, 2008.
8. Jousen AM, Poulaki V, Mitiades N, Kirchhof B, Koizumi K, Dohmen S, Adamis AP: Nonsteroidal anti-inflammatory drugs prevent early diabetic retinopathy via TNF-alpha suppression. *Faseb J* 16:438-440, 2002.
9. Funatsu H, Yamashita H, Shimizu E, Kojima R, Hori S: Relationship between vascular endothelial growth factor and interleukin-6 in diabetic retinopathy. *Retina* 21:469-477, 2001.
10. Lyons TJ, Jenkins AJ, Zheng D, Lackland DT, McGee D, Garvey WT, Klein RL: Diabetic retinopathy and serum lipoprotein subclasses in the DCCT/EDIC cohort. *Invest Ophthalmol Vis Sci* 45:910-918, 2004.
11. Coppack SW, Evans RD, Fisher RM, Frayn KN, Gibbons GF, Humphreys SM, Kirk ML, Potts JL, Hockaday TD: Adipose tissue metabolism in obesity: lipase action in vivo before and after a mixed meal. *Metabolism* 41:264-272, 1992.
12. Weinstock PH, Levak-Frank S, Hudgins LC, Radner H, Friedman JM, Zechner R, Breslow JL: Lipoprotein lipase controls fatty acid entry into adipose tissue, but fat mass is preserved by

endogenous synthesis in mice deficient in adipose tissue lipoprotein lipase. *Proc Natl Acad Sci U S A* 94:10261-10266, 1997.

13. Julius U: Influence of plasma free fatty acids on lipoprotein synthesis and diabetic dyslipidemia. *Exp Clin Endocrinol Diabetes* 111:246-250, 2003.

14. Sprecher H, Chen Q: Polyunsaturated fatty acid biosynthesis: a microsomal-peroxisomal process. *Prostaglandins Leukot Essent Fatty Acids* 60:317-321, 1999.

15. Agbaga MP, Brush RS, Mandal MN, Henry K, Elliott MH, Anderson RE: Role of Stargardt-3 macular dystrophy protein (ELOVL4) in the biosynthesis of very long chain fatty acids. *Proc Natl Acad Sci U S A* 105:12843-12848, 2008.

16. Lagali PS, Liu J, Ambasudhan R, Kakuk LE, Bernstein SL, Seigel GM, Wong PW, Ayyagari R: Evolutionarily conserved ELOVL4 gene expression in the vertebrate retina. *Invest Ophthalmol Vis Sci* 44:2841-2850, 2003.

17. Umeda S, Ayyagari R, Suzuki MT, Ono F, Iwata F, Fujiki K, Kanai A, Takada Y, Yoshikawa Y, Tanaka Y, Iwata T: Molecular cloning of ELOVL4 gene from cynomolgus monkey (*Macaca fascicularis*). *Exp Anim* 52:129-135, 2003.

18. Zhang XM, Yang Z, Karan G, Hashimoto T, Baehr W, Yang XJ, Zhang K: Elov14 mRNA distribution in the developing mouse retina and phylogenetic conservation of Elov14 genes. *Mol Vis* 9:301-307, 2003.

19. Grayson C, Molday RS: Dominant negative mechanism underlies autosomal dominant Stargardt-like macular dystrophy linked to mutations in ELOVL4. *J Biol Chem* 280:32521-32530, 2005.

20. Karan G, Lillo C, Yang Z, Cameron DJ, Locke KG, Zhao Y, Thirumalaichary S, Li C, Birch DG, Vollmer-Snarr HR, Williams DS, Zhang K: Lipofuscin accumulation, abnormal electrophysiology, and photoreceptor degeneration in mutant ELOVL4 transgenic mice: a model for macular degeneration. *Proc Natl Acad Sci U S A* 102:4164-4169, 2005.

21. Zhang K, Kniazeva M, Han M, Li W, Yu Z, Yang Z, Li Y, Metzker ML, Allikmets R, Zack DJ, Kakuk LE, Lagali PS, Wong PW, MacDonald IM, Sieving PA, Figueroa DJ, Austin CP, Gould RJ, Ayyagari R, Petrukhin K: A 5-bp deletion in ELOVL4 is associated with two related forms of autosomal dominant macular dystrophy. *Nat Genet* 27:89-93, 2001.

22. Brenner RR: Hormonal modulation of delta6 and delta5 desaturases: case of diabetes. *Prostaglandins Leukot Essent Fatty Acids* 68:151-162, 2003.

23. Nakamura MT, Nara TY: Gene regulation of mammalian desaturases. *Biochem Soc Trans* 30:1076-1079, 2002.

24. Rimoldi OJ, Finarelli GS, Brenner RR: Effects of diabetes and insulin on hepatic delta6 desaturase gene expression. *Biochem Biophys Res Commun* 283:323-326, 2001.
25. Wang Y, Botolin D, Xu J, Christian B, Mitchell E, Jayaprakasam B, Nair MG, Peters JM, Busik JV, Olson LK, Jump DB: Regulation of hepatic fatty acid elongase and desaturase expression in diabetes and obesity. *J Lipid Res* 47:2028-2041, 2006.
26. Joussen AM, Poulaki V, Le ML, Koizumi K, Esser C, Janicki H, Schraermeyer U, Kociok N, Fauser S, Kirchhof B, Kern TS, Adamis AP: A central role for inflammation in the pathogenesis of diabetic retinopathy. *Faseb J*, 2004.
27. Anderson RE: Lipids of ocular tissues. IV. A comparison of the phospholipids from the retina of six mammalian species. *Exp Eye Res* 10:339-344, 1970.
28. Chen W, Esselman WJ, Jump DB, Busik JV: Anti-inflammatory effect of docosahexaenoic acid on cytokine-induced adhesion molecule expression in human retinal vascular endothelial cells. *Invest Ophthalmol Vis Sci* 46:4342-4347, 2005.
29. Futterman S, Sturtevant R, Kupfer C: Effect of alloxan diabetes on the fatty acid composition of the retina. *Invest Ophthalmol* 8:542-544, 1969.
30. Harbige LS: Fatty acids, the immune response, and autoimmunity: a question of n-6 essentiality and the balance between n-6 and n-3. *Lipids* 38:323-341, 2003.
31. Chen W, Jump DB, Grant MB, Esselman WJ, Busik JV: Dyslipidemia, but not hyperglycemia, induces inflammatory adhesion molecules in human retinal vascular endothelial cells. *Invest Ophthalmol Vis Sci* 44:5016-5022, 2003.
32. Joussen AM, Poulaki V, Qin W, Kirchhof B, Mitsiades N, Wiegand SJ, Rudge J, Yancopoulos GD, Adamis AP: Retinal vascular endothelial growth factor induces intercellular adhesion molecule-1 and endothelial nitric oxide synthase expression and initiates early diabetic retinal leukocyte adhesion in vivo. *Am J Pathol* 160:501-509, 2002.
33. Mocan MC, Kadayifcilar S, Eldem B: Elevated intravitreal interleukin-6 levels in patients with proliferative diabetic retinopathy. *Can J Ophthalmol* 41:747-752, 2006.
34. Fliesler SJ, Anderson RE: Chemistry and metabolism of lipids in the vertebrate retina. *Prog Lipid Res* 22:79-131, 1983.
35. Delton-Vandenbroucke I, Grammas P, Anderson RE: Polyunsaturated fatty acid metabolism in retinal and cerebral microvascular endothelial cells. *J Lipid Res* 38:147-159, 1997.
36. Moon YA, Shah NA, Mohapatra S, Warrington JA, Horton JD: Identification of a mammalian long chain fatty acyl elongase regulated by sterol regulatory element-binding proteins. *J Biol Chem* 276:45358-45366, 2001.

37. Jakobsson A, Westerberg R, Jacobsson A: Fatty acid elongases in mammals: their regulation and roles in metabolism. *Prog Lipid Res* 45:237-249, 2006.
38. Leonard AE, Pereira SL, Sprecher H, Huang YS: Elongation of long-chain fatty acids. *Prog Lipid Res* 43:36-54, 2004.
39. Sunada S, Kiyose C, Kubo K, Takebayashi J, Sanada H, Saito M: Effect of docosahexaenoic acid intake on lipid peroxidation in diabetic rat retina under oxidative stress. *Free Radic Res* 40:837-846, 2006.
40. Barber AJ, Lieth E, Khin SA, Antonetti DA, Buchanan AG, Gardner TW: Neural apoptosis in the retina during experimental and human diabetes. Early onset and effect of insulin. *J Clin Invest* 102:783-791, 1998.
41. Gardner TW, Antonetti DA, Barber AJ, LaNoue KF, Nakamura M: New insights into the pathophysiology of diabetic retinopathy: potential cell-specific therapeutic targets. *Diabetes Technol Ther* 2:601-608, 2000.

Intravitreal Delivery of Fatty Acid Elongase ELOVL4 Prevents Retinal Vascular Degeneration  
in Diabetes Through Modification of Sphingolipid Metabolism

*5.1. Abstract*

Fatty acid elongase ELOVL4 is the most abundant elongase in the retina, and it has been reported to synthesize  $\geq$  C26 saturated and monounsaturated very long chain fatty acids, and  $\geq$  C28 very long chain polyunsaturated fatty acids (VLCPUFA). We have previously shown that dramatic diabetes-induced downregulation of ELOVL4 was associated with retinal-specific changes in lipid metabolism and retinal inflammation, and decreased ELOVL4 expression has also been correlated with retinal vascular degeneration in an ischemia/reperfusion model of accelerated retinal injury. However, to date no causal relationship has been established among ELOVL4, inflammation, and diabetes induced retinal lesions. The goal of this study was to determine whether restoration of retinal ELOVL4 levels is sufficient to prevent early diabetes induced retinal vascular degeneration.

To this end, human ELOVL4 was overexpressed in human retinal pigment epithelial (RPE) and human retinal endothelial (HREC) cells using an adenoviral vector, and an adeno-associated virus serotype 2 (AAV2) containing four capsid Y-F mutations (hELOVL4-AAV2 mut quad). Cells were challenged with the pro-inflammatory cytokine IL-1 $\beta$  or vehicle, and

ELOVL4 and intracellular adhesion molecule-1 (ICAM-1) mRNA were assessed by quantitative real-time PCR (qPCR). Streptozotocin (STZ) diabetic rats received intravitreal injection of hELOVL4-AAV2 mut quad or a similar AAV2 containing GFP, and retinal localization of AAV2 mediated transgene expression was determined by immunohistochemistry. Retinal vascular permeability was assessed in control and diabetic rats by measuring extravasation of FITC-albumin after 6-8 weeks of diabetes. qPCR was used to assess retinal levels of inflammatory markers, as well as the expression of genes related to paracellular and transcellular pathways of vascular permeability. Lipids were extracted from cultured cells and rat retinas and analyzed by tandem mass spectrometry.

Surprisingly, overexpression of ELOVL4 in cell culture models of the blood-retinal barrier did not affect phospholipid VLCPUFA content, but instead increased C26:0 ceramide levels relative to controls with concomitant relative decreases in shorter chain ceramides. Furthermore, ELOVL4 mediated alteration of sphingolipid metabolism reduced RPE ICAM-1 expression in response to the pro-inflammatory cytokine IL-1 $\beta$ . Intravitreal delivery of AAV2 mut quad vectors in STZ diabetic rats resulted in primarily vascular and perivascular localization of transgene expression. Interestingly, a 39% reduction in diabetes-induced retinal vascular permeability was observed in hELOVL4 transduced retinas 4-6 weeks after viral injection, while GFP had no effect on vascular permeability. Intravitreal delivery of hELOVL4 had no effect on ICAM-1 levels in the whole retina, and increased retinal IL-1 $\beta$  relative to diabetic retinas that received GFP. Yet hELOVL4 reduced vascular-specific markers of endothelial activation, particularly vascular cell adhesion molecule-1 and acid sphingomyelinase, relative to GFP. Moreover, assessment of endothelial blood-retinal barrier and transcellular transport components revealed that hELOVL4 activity resulted in augmented expression of several tight junction and

adherens junction proteins relative to controls and GFP, while decreasing retinal expression of caveolin-1.

In conclusion, intravitreal delivery of ELOVL4 mitigates early retinal vascular degeneration in diabetic animals by modulating retinal sphingolipid metabolism. Retinal gene delivery of ELOVL4 by capsid-modified AAV2 may represent a novel strategy for the prevention of diabetic visual impairment.

## *5.2. Introduction*

Diabetic retinopathy (DR) is a significant microvascular complication of diabetes that leads to impaired vision, blindness, and decreased quality of life. Chronic diabetes induced retinal inflammation is thought to contribute to early stage injury of the retinal vascular endothelium (1; 2). Elevated retinal levels of pro-inflammatory cytokines, such as IL-1 $\beta$ , and growth factors including vascular endothelial growth factor (VEGF) have been shown to increase endothelial expression of adhesion molecules (1; 3), promoting leukostasis and endothelial injury (4; 5). Eventually, degenerated vasculature promotes hypoxia driven proliferative neovascularisation of the retina, and blindness results from vessel growth or hemorrhage in the visual field (3). The primary treatment for DR is pan-retinal laser photocoagulation to inhibit retinal neovascularization, yet laser treatment destroys retinal tissue and leads to impaired visual acuity and central vision (3; 6), and often fails to prevent further neovascularization. As the worldwide diabetes epidemic continues to expand, the identification of novel therapies or effective preventative strategies for DR is imperative.

Early in the progression of DR, retinal vascular injury leads to dysregulation of endothelial tight junction and adherens junction components which comprise the inner blood-retinal barrier (7; 8), while tight junctions between retinal pigment epithelial cells that form the outer blood retinal barrier may also be compromised (9). This alteration of junctional organization results in increased paracellular permeability of both retinal barriers (9; 10). Additionally diabetes has been shown to upregulate the expression of retinal transcellular transporters and caveolin-1, the structural scaffolding protein of caveolae, which mediate endothelial uptake of nutrients from the circulation (11). Thus diabetes may also increase transcellular flux across the blood-retinal barrier (11; 12). This early stage disruption of the blood-retinal barrier leads to extravasation of fluid and proteins which results in edema, loss of visual acuity, and injury to the surrounding retinal tissue (8). Loss of retinal endothelial barrier function precedes endothelial cell apoptosis and capillary nonperfusion, and is considered a key indicator of early vascular damage in diabetic retina (8; 10; 13-15) .

Despite decades of research, the underlying causes of retinal inflammation and vascular dysfunction in diabetes are still incompletely understood. Along with hyperglycemia, dyslipidemia is a major metabolic perturbation of diabetes, and dyslipidemia is positively associated with the progression of DR (16). We previously explored the novel hypothesis that diabetic dyslipidemia contributes to retinal vascular degeneration through impaired retinal fatty acid metabolism and altered lipid remodelling (17-20). We found that diabetes decreased the expression of several retinal fatty acid elongases, including a dramatic downregulation of the most abundant elongase in the retina, elongation of very long chain fatty acids 4 (ELOVL4) (17). Diabetes induced downregulation of retinal elongases translated into significant remodeling of retinal lipid profiles, including reductions of retinal polyunsaturated fatty acids, as well as 32:6n3

very long chain polyunsaturated fatty acids (VLCPUFA) esterified to phosphatidylcholine (GPCCho) (17). Additionally we found that diabetes upregulated retinal expression of acid sphingomyelinase (ASM), the central enzyme in sphingolipid catabolism, and showed that ASM-dependent imbalance of endothelial sphingolipid metabolism plays a central role in retinal vascular pathology (20). These alterations of rat retina lipid metabolism were coupled with increased retinal gene expression of pro-inflammatory cytokines and adhesion molecules, and retinal vascular pathology (17; 20). Yet to date, no data exist that directly connect retinal fatty acid elongase activity with retinal sphingolipid metabolism, diabetes induced inflammation, and retinal vascular dysfunction.

Fatty acid elongases perform the rate limiting condensation step in the NADPH-dependent addition of two-carbon units to fatty-acyl CoAs (21). *In vitro* biochemical studies suggest that ELOVL4 most efficiently elongates 24 carbon saturated fatty acids to produce C26 fatty acids (22), and further elongates C26 fatty acids to produce C28 and possibly longer chain species. It has also been demonstrated that ELOVL4 mediates production of  $\geq$ C28 VLCPUFA, which are thought to localize almost exclusively to photoreceptor outer segments (23; 24), and production of VLCPUFA is thought to be the primary function of ELOVL4 in the retina (25). ELOVL4 expression has also been detected in numerous other mammalian tissues, organs, and cell types (22). However, VLCPUFA have only been detected at significant levels in retina, brain, and testes (26; 27).

Of the retinal elongases negatively regulated by diabetes, ELOVL4 stands out as having been recently associated with several retinal pathologies. Repressed ELOVL4 function through downregulation or somatic mutation accompanies increased retinal vascular permeability, juvenile onset blindness, and decreased visual acuity in animal and human models of retinal

ischemia-reperfusion injury, Stargardt-like macular dystrophy, age related macular degeneration, and ocular aging (23; 28-30). Thus a clear understanding of ELOVL4 function in the retina may be relevant to the study of a broad range of visual disorders, including diabetic retinopathy.

Despite the inverse associations of ELOVL4 expression with the onset of vascular permeability and diabetes induced inflammation in the retina, it is unclear whether ELOVL4 plays a direct role in either phenomenon. The goals of the present study were to determine the biochemical function of ELOVL4 in cell culture models relevant to the study of diabetic retinal degeneration *in vitro*, and to test the hypothesis that retinal delivery of ELOVL4 can modulate diabetes induced retinal vascular dysfunction *in vivo*.

### 5.3. Results

#### **5.3.1 Overexpression of ELOVL4 mitigates IL-1 $\beta$ induced activation of retinal pigment epithelial cells**

To establish whether there is an inverse relationship between ELOVL4 expression and inflammation in retinal cells, we initially examined ELOVL4 expression in human retinal pigment epithelial (RPE) cells, an established model of the outer blood-retinal barrier (14). The pro-inflammatory cytokine IL-1 $\beta$  was added to RPE cell culture media at 1 ng/ml for 48 hours, and ELOVL4 mRNA was assessed by quantitative real-time PCR (qRT-PCR). IL-1 $\beta$  significantly decreased ELOVL4 mRNA by 44% (Figure 5.1A), indicating that pro-inflammatory signaling negatively regulates ELOVL4 expression. Next we overexpressed ELOVL4 in RPE cells by using an adenoviral vector containing the human ELOVL4 cDNA (Ad-ELOVL4) under control of the CMV promoter, or an empty vector adenovirus (Ad-Null) as a

negative control. Infection of RPE cells with Ad-ELOVL4 resulted in moderate (1.7 fold) overexpression of ELOVL4 protein as determined by Western blot (Figure 5.1B) relative to cells infected with the control virus. Adenovirus-transduced cells were then challenged with 1 ng/ml IL-1 $\beta$  for 48 hours, and ICAM-1 levels were assessed by qPCR as a measure of cellular activation. As seen in Figure 5.1C, overexpression of ELOVL4 decreased ICAM-1 mRNA by 45% upon addition of IL-1 $\beta$ . These data are the first to indicate that increased pro-inflammatory cytokines present in diabetic retina may negatively regulate ELOVL4 expression, and that overexpression of ELOVL4 attenuates cytokine-induced activation of RPE cells.

### **5.3.2 ELOVL4 does not mediate phospholipid VLCPUFA incorporation in RPE cells**

To gain insight into how ELOVL4 mediated lipid metabolism may influence inflammatory signaling in RPE cells, we next performed tandem mass spectrometry based lipidomics analysis on total lipid extracts from cells infected with the ELOVL4 adenovirus or Null adenovirus. Surprisingly, overexpression of ELOVL4 did not affect incorporation of  $\geq$ C28 VLCPUFA or other fatty acids in phosphatidylcholine (GPCho) or other lipid classes. The lack of ELOVL4-derived VLCPUFA incorporation persisted when potential VLCPUFA precursor fatty acids 20:5n3 or 22:5n3 (23; 31) bound to BSA were added to culture media following infection with the ELOVL4 adenoviral vector. Figure 5.2A shows a mass spectrum of rat retina lipid species, with VLCPUFA-GPCho molecular ions labeled in the high m/z region. The lower spectra show GPCho species from a total lipid extract of RPE cells infected with the control adenovirus (Figure 5.2B) or Ad-ELOVL4 (Figure 5.2C) and supplemented with BSA-bound

20:5n3 for 72 hours. Adenoviral transduction experiments were performed using multiplicities of infection (MOIs) ranging from 50 to 20,000. An MOI of 100 was used in Figures 5.2B and 5.2C.

### **5.3.3 ELOVL4 mediates C26:0 ceramide production in cells of the blood-retinal barrier**

While lipidomics analysis did not identify any effect of ELOVL4 overexpression on RPE PUFA metabolism, short term adenoviral-mediated overexpression of ELOVL4 in RPE cells resulted in a 113% increase in the relative amount of cellular C26:0 ceramide compared to controls (See Figure 5.3A). Conversely, C16:0 ceramide was reduced by 43% in the ELOVL4-overexpressing cells, with similar decreases observed in other ceramide species relative to the controls. The observed increase in 26:0 fatty acid was not observed in sphingomyelin or other lipid classes (data not shown).

Primary cultures of human retinal endothelial cells (HREC) provide an ideal *in vitro* model of the inner blood-retinal barrier, the principle site of tissue injury in diabetic retinopathy. However, endothelial cells are resistant to infection by many commonly used viral vectors (32), limiting their utility for gene delivery studies. We therefore obtained human ELOVL4 cDNA packaged in an adeno-associated virus serotype 2 vector containing four capsid Y to F mutations (hELOVL4-AAV2 mut quad), with ELOVL4 under control of the strong constitutive truncated chimeric CMV-chicken  $\beta$ -actin (smCBA) promoter enabling efficient and stable transgene expression in most retinal cell types (33; 34). As shown in Figure 5.3B, transduction of HREC with hELOVL4-AAV2 mut quad led to a striking increase in HREC 26:0 ceramide content two weeks after transfection, which was not detected in control HREC. Four weeks after transfection, hELOVL4-AAV2 infected HREC exhibited decreased 16:0 ceramide relative to

controls, but no significant difference from control cells was observed in the level of 26:0 ceramide due to greatly increased levels of endogenous C26:0 ceramide in the control cells (Figure 5.3C), indicating that endogenous C26:0 ceramide normally accumulates in HREC with increasing duration of culture. Figure 5.3D demonstrates successful upregulation of ELOVL4 protein in HREC four weeks post infection with hELOVL4-AAV2. When transduced HREC were supplemented continuously with BSA-bound 20:5n3, no VLCPUFA incorporation was observed in any HREC phospholipid class up to four weeks post infection (Figure 5.3E). Taken together, these data strongly suggest that ELOVL4 drives very long chain ceramide production, but not phospholipid VLCPUFA incorporation, in both the inner and outer blood-retinal barrier.

#### **5.3.4 AAV2-mediated expression of ELOVL4 in diabetic rat retina**

As our *in vitro* data suggested that ELOVL4 overexpression may counteract cytokine induced inflammatory signaling by modulating sphingolipid metabolism in cells of the blood-retinal barrier, we hypothesized that gene delivery of ELOVL4 in diabetic retina may mitigate diabetes induced retinal vascular degeneration. Streptozotocin (STZ)-induced diabetic rats received intravitreal injections of  $1 \times 10^9$  viral genomes of either hELOVL4-AAV2 mut quad or GFP-AAV2 mut quad in confirmed diabetic animals two weeks after STZ injections as described in Chapter 6. Animals were sacrificed 4-6 weeks following viral injections (6-8 total weeks of diabetes). Body weight gain and blood glucose concentrations of the animals used in this study are described in Table 5.1. As expected, diabetes reduced the expression of endogenous rat ELOVL4 mRNA in both GFP and hELOVL4 transduced retinas (Figure 5.4A). To assess the localization of AAV2-delivered hELOVL4 and GFP within the retina, immunohistochemistry

analysis for GFP was performed on transverse retinal sections. Surprisingly, GFP expression was primarily limited to the ganglion cell layer in close proximity to retinal capillaries, with significant labeling in the RPE and choroidal blood vessels (see Figure 5.4B). Initial breakdown of the blood-retinal barrier has been reported to occur as little as two weeks following induction of diabetes in experimental animals (35), which probably enabled the AAV2 vector to enter retinal capillaries in the anterior retina and readily infect vascular endothelial cells in the retina and choroid. qPCR analysis of hELOVL4 mRNA revealed that retinal AAV2-derived hELOVL4 mRNA expression was equal to approximately 1% of total retinal ELOVL4 mRNA (data not shown.) This is consistent with primarily vascular transgene expression, as retinal capillaries constitute approximately 1-3% of total retinal tissue (3). The hELOVL4 transgene mRNA was not detected in liver, indicating the virus primarily infected endothelial cells within in the eye.

### **5.3.5 Retinal vascular expression of ELOVL4 does not affect total retinal lipid profile**

We next performed lipidomic analysis on total lipid extracts isolated from control, and diabetic retinas transduced with either GFP or hELOVL4. Given the mostly vascular and perivascular transgene localization in retina, major hELOVL4 effects on total retinal lipid composition were unlikely to be detected. Accordingly, no significant differences were observed in the abundances of any very long chain ceramide or VLCPUFA-GPCho molecular species, or lipid species of other lipid classes, across the three treatment groups (data not shown).

### **5.3.6 Retinal delivery of ELOVL4 prevents blood-retinal barrier dysfunction in diabetic animals**

To determine whether ELOVL4 modulation in retinal vasculature could prevent early degeneration of the retinal vasculature, we assessed retinal vascular permeability in control and diabetic rats by measuring extravasation of FITC-albumin in rat retina after 6-8 weeks of STZ diabetes. As demonstrated in Figure 5.5, diabetes significantly increased retinal vascular permeability 3.7 fold in retinas that received intravitreal injection of saline in the left eye (n=4), relative to control nondiabetic animals (n=4). Notably, intravitreal hELOVL4-AAV2 injected in the right eye of each animal (n=4) achieved an average 39% reduction in diabetes induced vascular permeability relative to the matched saline treated retinas from the contra-lateral eye, which was not statistically different from control retinas. In a separate group of animals, 6-8 weeks of diabetes increased retinal vascular permeability by 1.6 fold in retinas that received intravitreal saline (n=5), while intravitreal GFP-AAV2 administered in the contra-lateral eye did not reduce retinal vascular permeability. Overall this data demonstrates that hELOVL4-AAV2, but not GFP-AAV2, prevented early vascular degeneration in diabetic retina.

### **5.3.7 Retinal delivery of ELOVL4 reduces markers of vascular activation, but not retinal inflammation**

To determine whether reduced vascular permeability in hELOVL4-AAV2 transduced diabetic retinas was the result of reduced retinal inflammation, we examined the expression of markers of retinal inflammation and vascular endothelial cell activation by qPCR. Figure 5.6A clearly indicates that AAV2 mediated expression of hELOVL4 ablated the diabetes induced increase of acid sphingomyelinase (ASM), a key responder in retinal endothelial cell

inflammatory signaling (19; 20). Moreover, hELOVL4 expression completely blocked the upregulation of vascular cell adhesion molecule-1 (VCAM-1) observed in diabetic GFP-AAV2 transduced retinas, indicating that ELOVL4 levels prevented retinal vascular endothelial cell activation. As shown in Figure 5.6B, diabetes upregulated retinal levels of IL-1 $\beta$  in both GFP-AAV2 and hELOVL4-AAV2 retinas relative to control, in agreement with previous reports (1; 36). Surprisingly, however, there was an additional induction of IL-1 $\beta$  mRNA in hELOVL4 transduced retinas relative to GFP that was statistically significant. While VEGF-A mRNA was slightly decreased in hELOVL4 transduced retinas relative to control retinas, there was no statistically significant difference in VEGF-A mRNA between GFP and hELOVL4 transduced retinas. Additionally, diabetes upregulated retinal ICAM-1 levels to an equal extent in both GFP and hELOVL4 transduced retinas relative to control retinas. Overall this data suggests that intravitreal delivery of hELOVL4, but not GFP, prevented activation of retinal vascular endothelium despite increasing levels of IL-1 $\beta$  in the neural retina.

### **5.3.8 Retinal delivery of ELOVL4 alters expression of vascular tight junction components**

We next investigated whether ELOVL4-mediated changes in retinal sphingolipid metabolism prevented blood-retinal barrier dysfunction in diabetes by a mechanism that was dependent on, or exclusive of, modulation of endothelial tight junctions. mRNA levels of several components of retinal tight junctions and adherens junctions known to be compromised in diabetic retina (8; 10; 11; 14; 37; 38) were assessed by qPCR. Figure 5.7A demonstrates upregulation of vascular-associated claudin-5 mRNA in diabetic retinas that received hELOVL4-AAV2 (n=6) relative to diabetic retinas that received GFP-AAV2 (n=6) and control retinas

(n=6). Diabetes resulted in a modest decrease of ve-cadherin expression in GFP transduced retinas, which was prevented in hELOVL4 transduced retinas. Additionally, diabetes caused a slight decrease in endothelial cell-specific adhesion molecule (ESAM) mRNA in GFP-AAV2 retinas, whereas ESAM was increased 24% in hELOVL4-AAV2 retinas compared to GFP retinas. While diabetes upregulated retinal occludin mRNA (Figure 5.7B) in agreement with previous reports (11), expression of the human ELOVL4 transgene decreased retinal occludin mRNA by 21% relative to retinas expressing GFP. ZO-1 mRNA was not significantly decreased in diabetic retinas expressing GFP, yet hELOVL4-AAV2 retinas exhibited a 24% decrease in ZO-1 relative to control retinas (Figure 5.7B). No statistically significant change in mRNA abundance was observed across all groups for claudin-1 (Figure 5.7B). Overall this data suggests that ELOVL4 may counteract diabetes induced dysregulation of vascular tight junction components in general, while specifically increasing the expression of claudin-5, ve-cadherin, and ESAM. ELOVL4 may therefore be an important regulator of vascular paracellular permeability in the retina.

### **5.3.9 Retinal delivery of ELOVL4 decreases caveolin-1 expression**

To further delineate the mechanism of the ELOVL4-mediated reduction of retinal vascular permeability in diabetes, we next performed gene expression analysis by qPCR on known facilitators of retinal transcellular transport. While diabetes did not induce a significant increase in Caveolin-1a mRNA in GFP-AAV2 retinas, hELOVL4-AAV2 retinas exhibited a striking 54% decrease in caveolin-1a expression relative to control and diabetic GFP-AAV2 retinas (see Figure 5.8A.) As shown in Figure 5.8B, no statistically significant changes were

observed across all treatment groups for expression levels of vesicle-associated membrane protein-1 (VAMP-1) or VAMP-2. This data suggests that in addition to modulating paracellular permeability, ELOVL4 may also restrict the transcellular route of vascular permeability through reduction of caveolae.

#### *5.4. Discussion*

This study represents the first demonstration that fatty acid elongase ELOVL4 modulates permeability of the blood-retinal barrier in diabetic retina. AAV2 mediated normalization of ELOVL4 in the retinal vasculature of diabetic rats decreased endothelial activation and prevented early stages of vascular degeneration, as determined by an ELOVL4 driven reduction in retinal vascular permeability, despite a lack of ELOVL4 effect on ICAM-1 expression in the neural retina, and significantly increased levels of the pro-inflammatory cytokine IL-1 $\beta$  by ELOVL4. Experiments in a cell culture model of the blood-retinal barrier demonstrated that ELOVL4 activity may blunt cellular activation in response to pro-inflammatory stimuli, which could effectively shield the blood-retinal barrier from inflammatory conditions in diabetic retina. Retinal transduction with ELOVL4 also resulted in amplified expression of vascular-specific negative regulators of paracellular permeability including claudin-5, ve-cadherin, and endothelial cell-specific adhesion molecule relative to diabetic retinas transduced with GFP, supporting the notion that ELOVL4 effects were localized to the retinal vasculature as opposed to the surrounding neural retina. Transduction of diabetic retinas with ELOVL4 also reduced expression of caveolin-1, the major scaffolding protein constituent of caveolae, which may

reduce vascular transcellular permeability (11; 12). Therefore, ELOVL4 may decrease retinal vascular permeability by modulating both paracellular and transcellular routes.

Lipidomic analysis of cultured human retinal endothelial and pigment epithelial cells overexpressing hELOVL4 revealed that ELOVL4 primarily drives very long chain ceramide production in cells of the blood-retinal barrier, and does not affect VLCPUFA levels in membrane lipids of these cells. This is somewhat surprising, as to date retinal ELOVL4 function has been primarily tied to VLCPUFA synthesis (25; 39). Moreover, VLCPUFA production has been previously described in RPE cells by overexpression of a mouse ELOVL4 transgene (23). Yet, incorporation of VLCPUFA in RPE phospholipids or other lipid classes has not been previously assessed, and subtle differences in biochemical activity may exist between mouse and human ELOVL4. However, VLCPUFA are enriched in photoreceptor outer segments (24; 39), while ELOVL4 is expressed in multiple retinal layers and cell types (40). Therefore, production of VLCPUFA by ELOVL4 may be restricted to photoreceptors or other retinal neurons, while ELOVL4 mediated sphingolipid biosynthesis could predominate in other retinal cell types. Lipidomics analysis did not detect any effects of ELOVL4 on total retinal sphingolipid or phospholipid profiles. This is not surprising given that retinal capillaries account for only a small fraction of total retinal tissue, and therefore do not contribute significantly to the total retinal lipid profile. While AAV2 also localized to the RPE and choroidal blood vessels, these bodies are physically separated from the retina and therefore are not collected upon retinal isolation.

The lack of ELOVL4 mediated VLCPUFA incorporation into GPCho of retinal endothelial and epithelial cells represents the first demonstration that not all retinal ELOVL4 activity is directed toward VLCPUFA synthesis, and the novel finding that ELOVL4 impacts ceramide production in the blood-retinal barrier could be explained by studies which suggest that

ELOVL4 works in concert with ceramide synthase 3, particularly in skin and testes (41). Recent findings have demonstrated that elongase ELOVL2 is also required for VLCPUFA production (42). Retinal endothelial cells and RPE cells express ELOVL2 and elongate PUFA substrates to produce 22:6n3 via intermediate production of 24:6n3, a common precursor to both 22:6n3 and VLCPUFA (43; 44). This suggests that substrate utilization by ELOVL4 may be cell type or context specific. Both ELOVL2 and ELOVL4 are decreased in diabetic rat retina (17), therefore diabetic retina provides an excellent model for testing the VLCPUFA-independent functions of ELOVL4.

The data described in this study suggest numerous mechanisms through which normalization of ELOVL4 levels in diabetic retinal vasculature could decrease vascular permeability. Ceramides containing very long chain fatty acids have been shown to be critical lipid components of the epidermal permeability barrier, presumably due to extremely tight packing within intercellular sheets of lipid vesicles that serve to exclude water (41). While the ELOVL4-derived C26-C30 fatty acids present in ceramides of cultured blood-retinal barrier cells are considerably less elongated than those found in skin, they may serve an analogous purpose in the retinal microvasculature, although to date similar lipid vesicle sheets have not been described in retinal blood vessels.

Acids sphingomyelinase (ASM) is a central enzyme of catabolic sphingolipid metabolism, and elevated ASM expression and activity has been shown to be critical to propagation of endothelial inflammatory signals and the development of retinal vascular lesions in diabetes and other models of microvascular injury (20). In the present study, retinal ELOVL4 transfection decreased ASM expression in diabetic animals through an unknown mechanism. It is conceivable that upregulation of *de novo* very long chain ceramide synthesis by ELOVL4 has

a counter-regulatory effect on the generation of ceramide by catabolic sphingolipid metabolism. The observed downregulation of ASM in diabetic retinas transduced with ELOVL4, relative to diabetic retinas transduced with GFP, could therefore indicate uncoupling of pro-inflammatory stimuli and the vascular response to the stimuli. ASM activity has been shown to be required for endothelial expression of adhesion molecules such as VCAM-1 (19). ELOVL4 transduction completely blocked upregulation of VCAM-1 in diabetic retina despite elevating IL-1 $\beta$ , and decreased adhesion molecule expression on the vascular endothelium may prevent or reduce leukocyte adhesion (4; 45; 46). Therefore, retinal transduction with hELOVL4 may have prevented inner blood-retinal barrier breakdown by reducing leukocyte-mediated endothelial injury.

Additionally, sphingolipid metabolites such as sphingosine-1-phosphate have been shown to provide important pro-barrier signals in retinal endothelial cell culture models (47). Similarly, the activation of sphingosine kinase 2 in brain has been found to be a critical factor in the maintenance of blood-brain barrier integrity in studies of ischemic stroke (48). Vascular ELOVL4 mediated ceramide production may therefore shift the balance of sphingolipid metabolism to a barrier-promoting state. The formation of potential ceramide metabolites downstream of ELOVL4 activity were not addressed here.

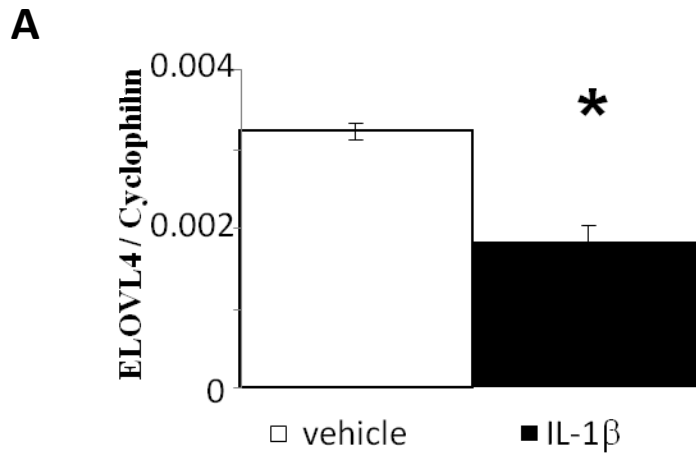
### *5.5. Conclusions*

This study demonstrated that retinal delivery of fatty acid elongase ELOVL4 prevents retinal vascular degeneration in diabetic animals by modulation of sphingolipid metabolism in cells of the blood-retinal barrier. Retinal gene delivery of ELOVL4 by capsid-modified AAV2

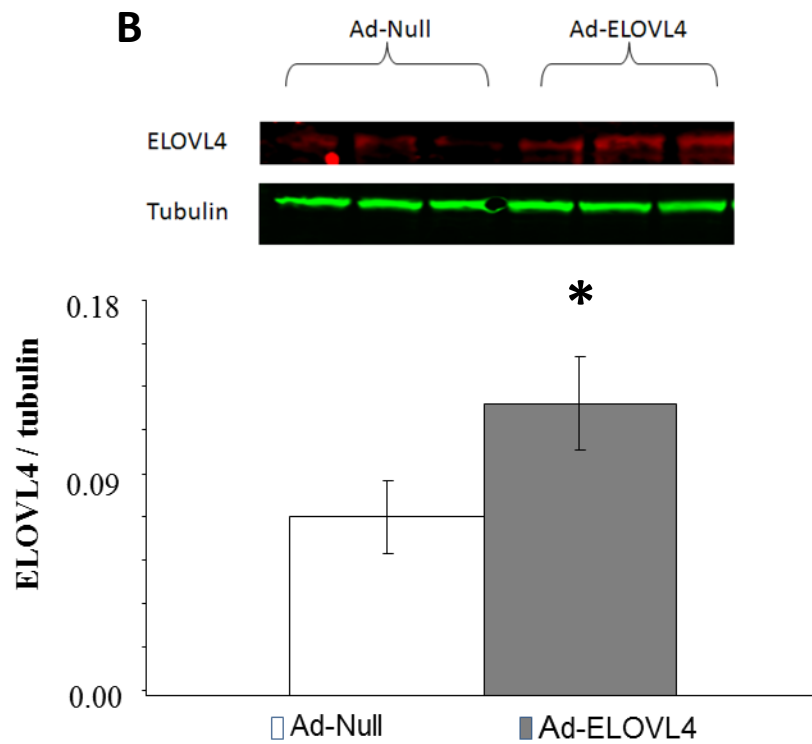
may represent a novel strategy for the prevention of diabetes induced retinal vascular lesions, and subsequent visual impairment.

Table 5.1. Animal weight gain and blood glucose concentrations.

	<b>Weight gain (g/day)</b>	<b>P value</b>	<b>Blood glucose (mg/dL)</b>	<b>P value</b>
Control (n=21)	5.00 ± 0.76	<0.00001	133.40 ± 21.96	<0.00001
Diabetic (n=40)	0.94 ± 0.98		537.45 ± 51.63	



**Figure 5.1. Inverse relationship of ELOVL4 expression and cellular activation in RPE cells.** (A) Human retinal pigment epithelial (RPE) cells were incubated with IL-1 $\beta$  (1 ng/ml) or vehicle for 48 hours. Total RNA was extracted and analyzed by qPCR. ELOVL4 expression in vehicle treated control cells is represented by white bar; ELOVL4 expression in IL-1 $\beta$  treated cells is represented by black bar.



**Figure 5.1 (cont'd).** (B) Western blot of ELOVL4 protein in RPE cells 48 hours post infection by Ad-ELOVL4 adenovirus compared to cells infected with Ad-Null control adenovirus.

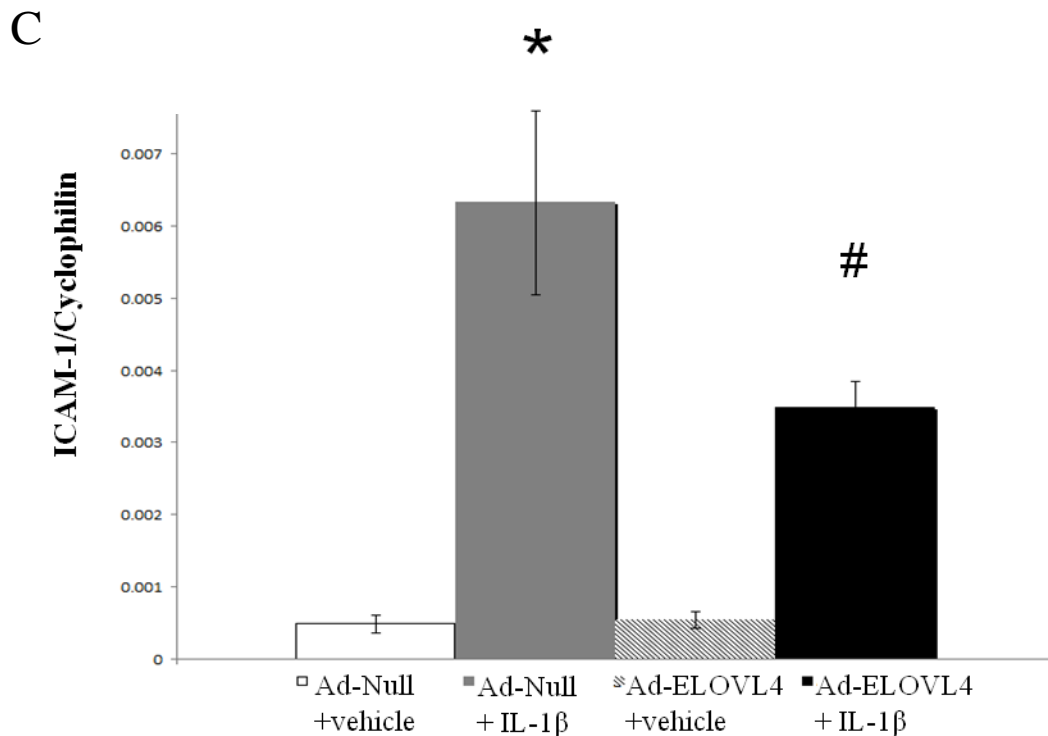


**Figure 5.1 (cont'd).**

(C) mRNA level of ICAM-1 in RPE cells infected with control Ad-Null or Ad-ELOVL4 adenovirus. Twenty four hours post infection, Ad-Null and Ad-ELOVL4 infected cells were incubated with vehicle or IL-1 $\beta$  (1ng/ml) for 48 hours. Total RNA was extracted and analyzed by quantitative real-time PCR. White bar, Ad-Null incubated with vehicle; black bar, Ad-Null incubated with IL-1 $\beta$ ; hatched bar, Ad-ELOVL4 incubated with vehicle; gray bar, Ad-ELOVL4 incubated with IL-1 $\beta$ . n=3 per treatment group. Data are presented as mean  $\pm$  SD. \* indicates statistically different from vehicle, # indicates statistically different from Ad-Null treated with IL-1 $\beta$  (P<0.05), as determined by one-way ANOVA with post-hoc Tukey test.

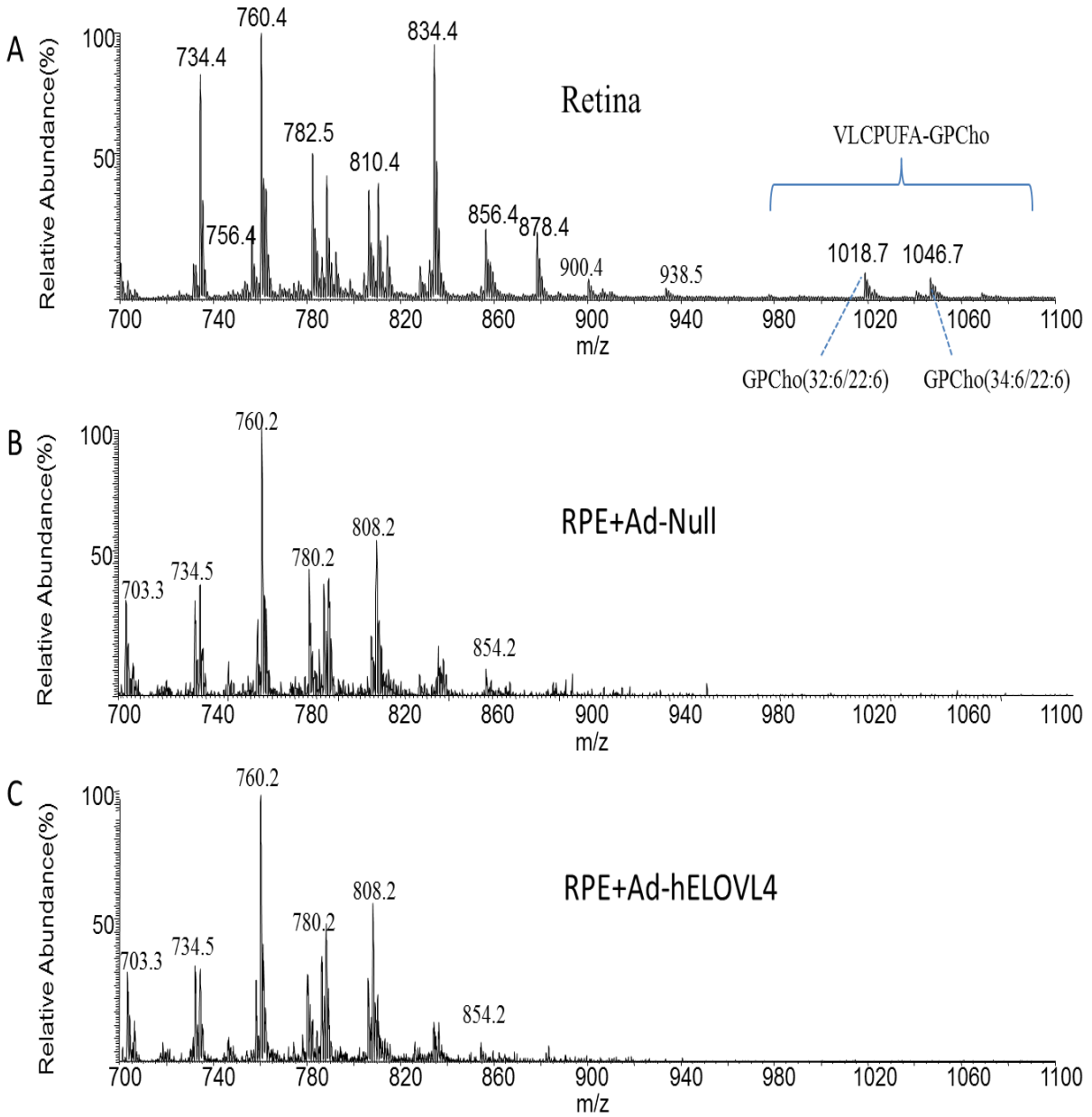
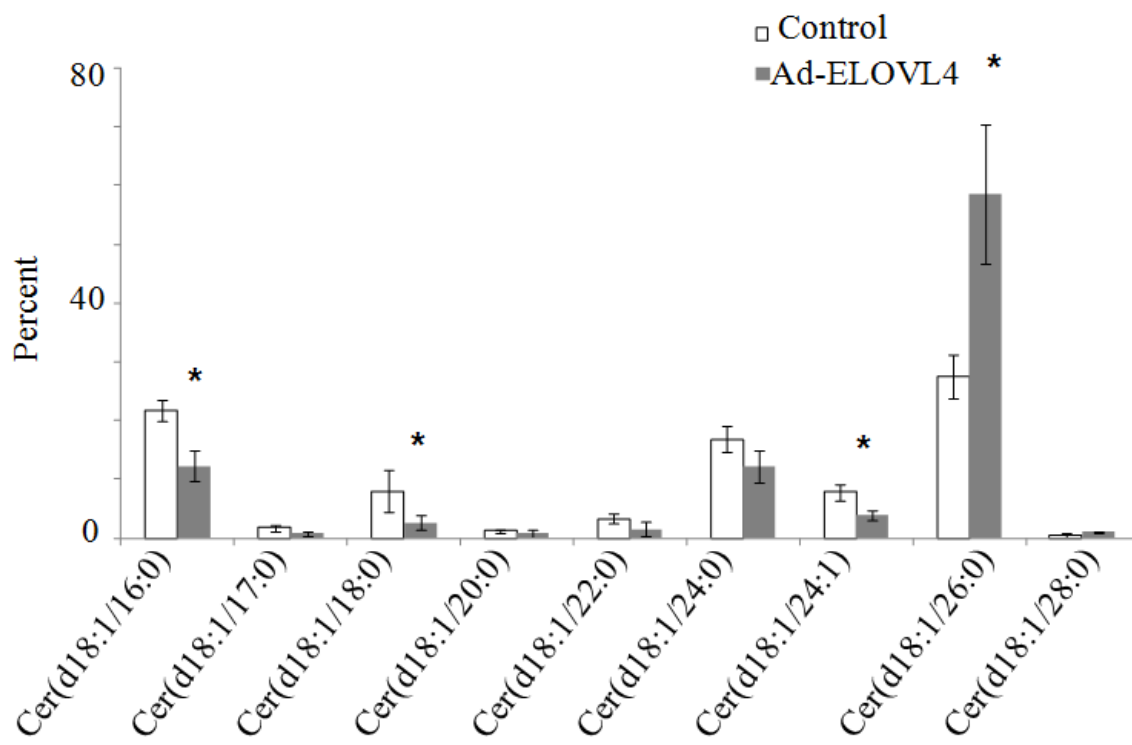
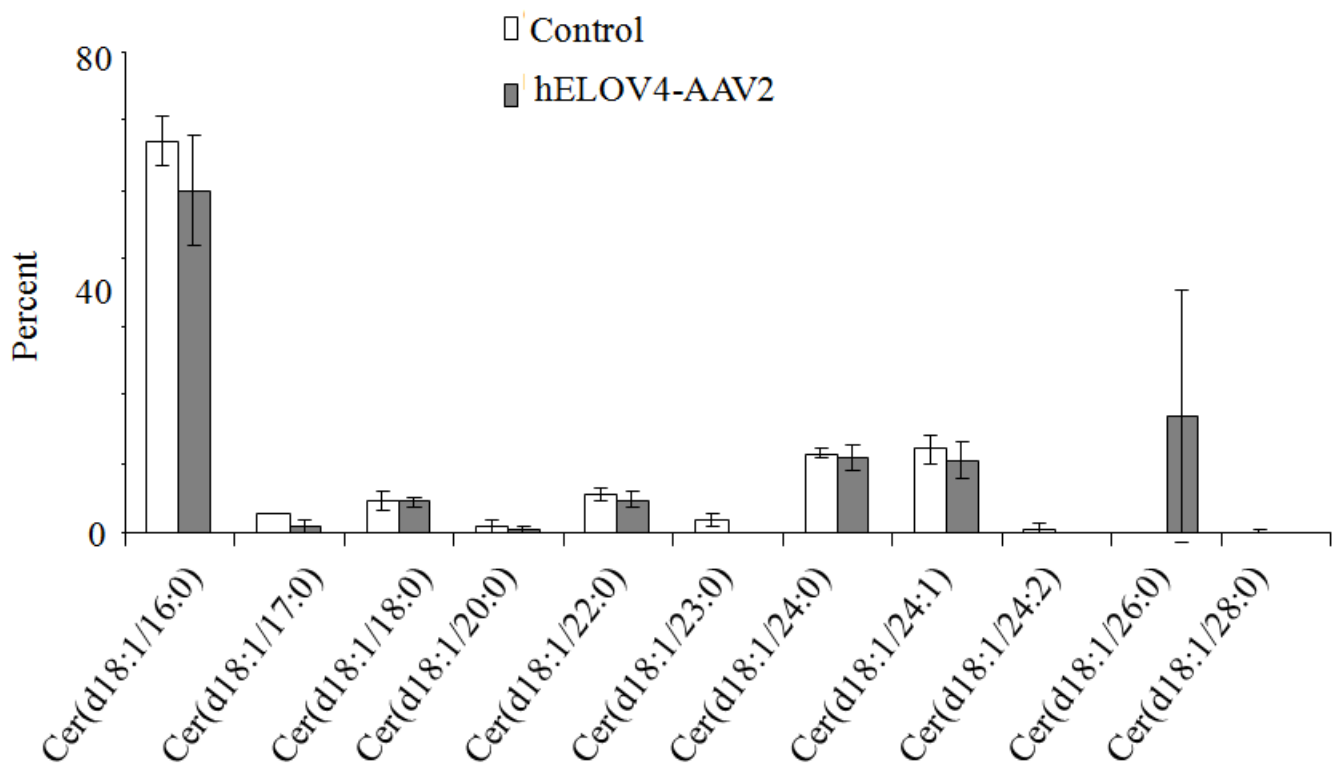


**Figure 5.2 Comparison of GPCho species containing VLCPUFA in retina and RPE cells.** (A) Mass spectrum of a rat retina lipid extract showing the most abundant VLCPUFA-GPCho typically found in retina (labeled). (B) Tandem mass spectrum of RPE GPCho lipids by precursor ion scanning of m/z 184 using a triple quadrupole mass spectrometer. RPE were infected with a Null adenovirus over a broad range of multiplicity of infection for 12 hours, and supplemented with BSA-bound 20:5n3 for 36-72 hours. (C) Tandem mass spectrum of RPE GPCho lipids by precursor ion scanning of m/z 184 using a triple quadrupole mass spectrometer. RPE were infected with Ad-ELOVL4 over a broad range of multiplicity of infection for 12 hours, and supplemented with BSA-bound 20:5n3 for 36-72 hours.



A



B

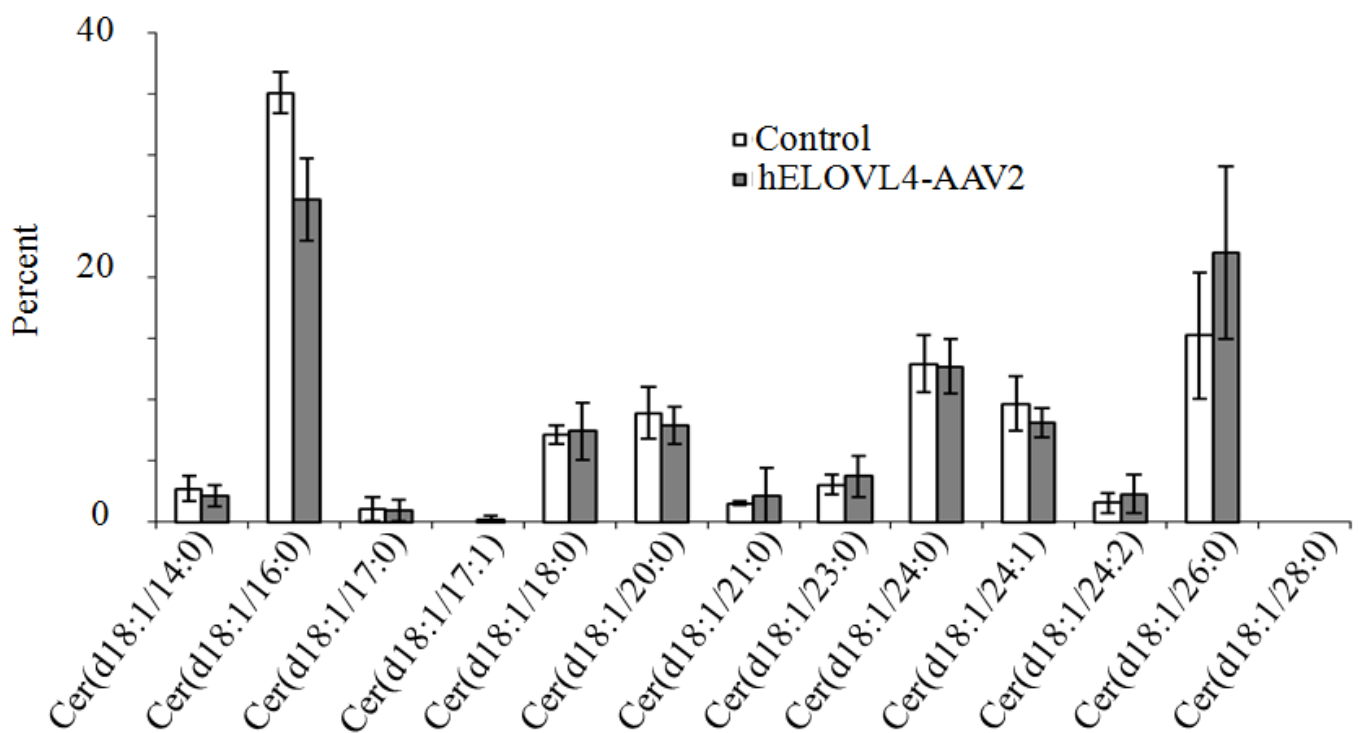


**Figure 5.3 (cont'd).** (C) Four weeks post infection, control and hELOVL4-AAV2 infected HREC were subjected to lipid extraction and ceramide analysis by positive ion mode precursor ion scanning of  $m/z$  264 using a triple quadrupole mass spectrometer.  $n=3$  per treatment group. Data are presented as mean  $\pm$  SD. \* indicates statistically significant ( $P<0.05$ ) as determined by unpaired t-test.

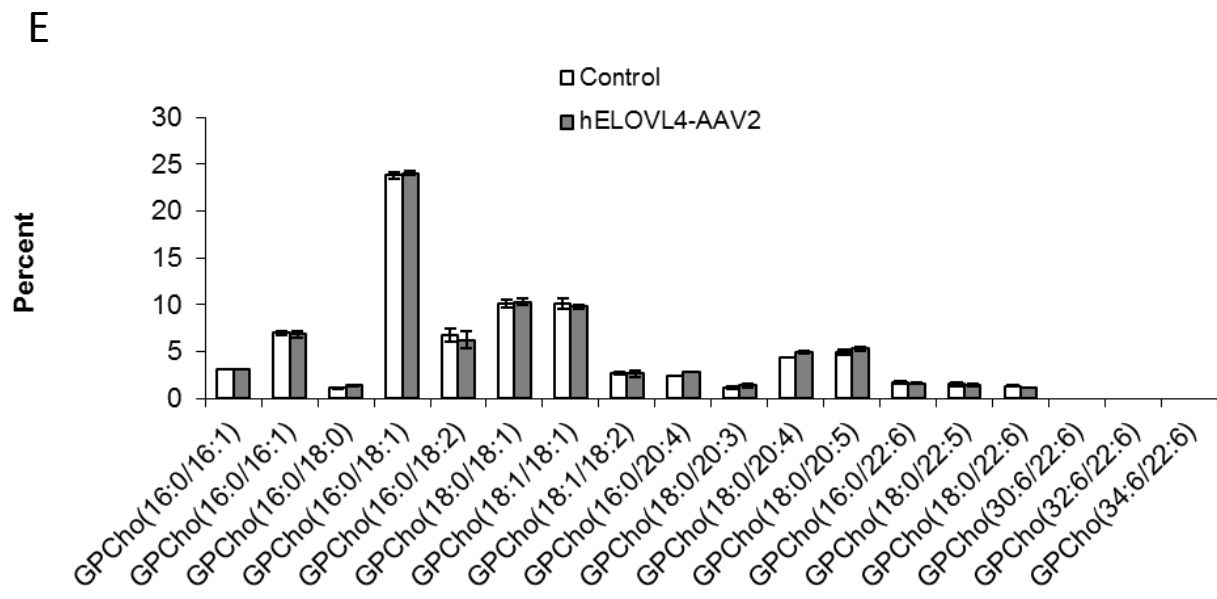
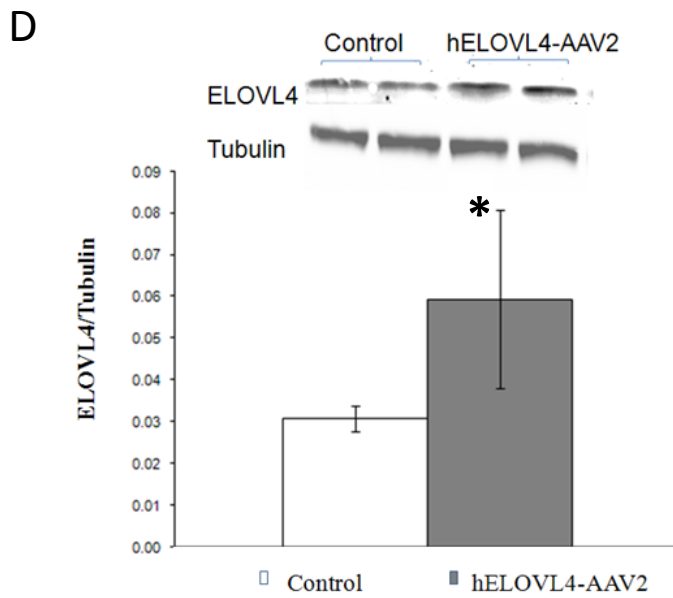


**Figure 5.3 (cont'd).** (D) Western blot of control and hELOVL4-AAV2 infected HREC four weeks post infection. (E) Control and hELOVL4-AAV2 infected HREC were supplemented with 20:5n3 for four weeks. Total lipids were extracted, and GPCho species were analyzed by positive ion mode precursor ion scanning of m/z 184 in a triple quadrupole mass spectrometer. n=3 per treatment group. Data are presented as mean  $\pm$  SD. \* indicates statistically significant ( $P < 0.05$ ) as determined by unpaired t-test.

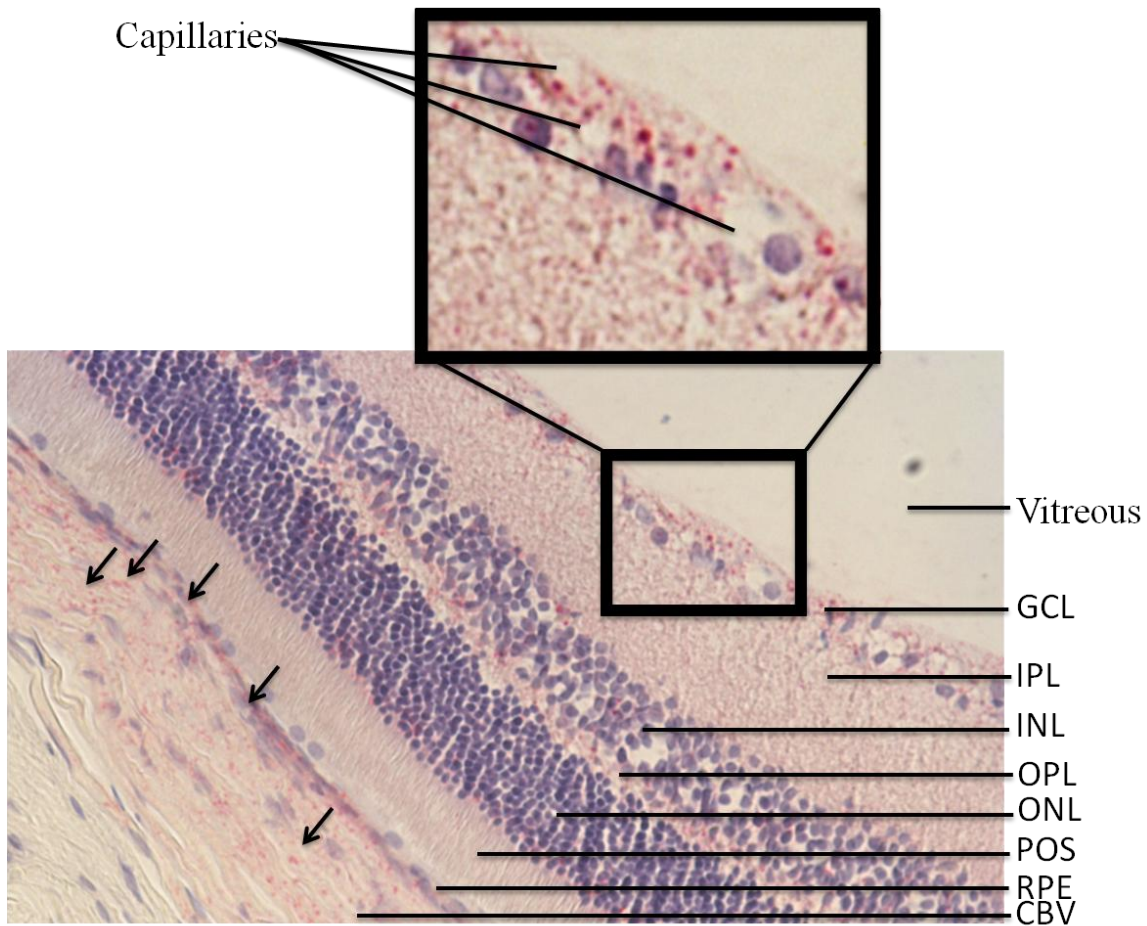


**Figure 5.4. Localization of AAV2 mut quad in diabetic retinas.** Transverse retinal sections from diabetic animals receiving intravitreal injection of GFP-AAV2 were subjected to immunohistochemical analysis to detect GFP localization. Hematoxylin stain was used to show cell nuclei. The inset illustrates anti-GFP staining (red) in close proximity to retinal capillaries in the ganglion cell layer. Arrows indicate areas of abundant GFP staining throughout the choroidal blood vessels and RPE. Punctate GFP staining is also observed in the inner and outer nuclear layers. GCL, ganglion cell layer. IPL, inner plexiform layer. INL, inner nuclear layer. OPL, outer plexiform layer. ONL, outer nuclear layer. POS, photoreceptor outer segments. RPE, retinal pigment epithelium. CBV, choroidal blood vessels. For interpretation of the references to color in this and all other figures, the reader is referred to the electronic version of this dissertation.

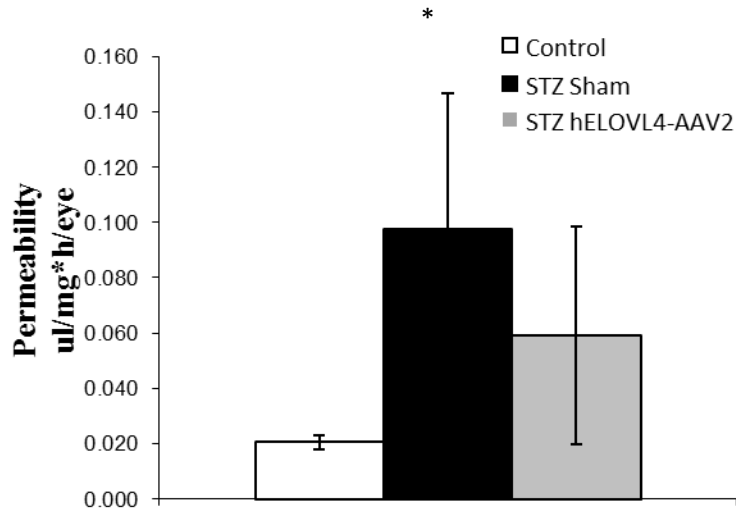


**Figure 5.5 Retinal vascular permeability in control and diabetic animals.** Extravasation of FITC-albumin was assessed in retinas from control (n=4) and STZ animals (n=4) after six to eight weeks of diabetes. STZ animals received intravitreal injection of saline vehicle in the left eye, and hELOVL4-AAV2 in the right eye after two weeks of confirmed STZ induced diabetes. Fluorescence from accumulated FITC-albumin in retina was normalized to plasma fluorescence, and the vascular permeability of each virus treated retina was compared to its matched vehicle treated retina from the same animal. Data are presented as mean  $\pm$  SD. \*  $P < 0.05$  compared to control by one-way ANOVA with post-hoc Tukey test.

A

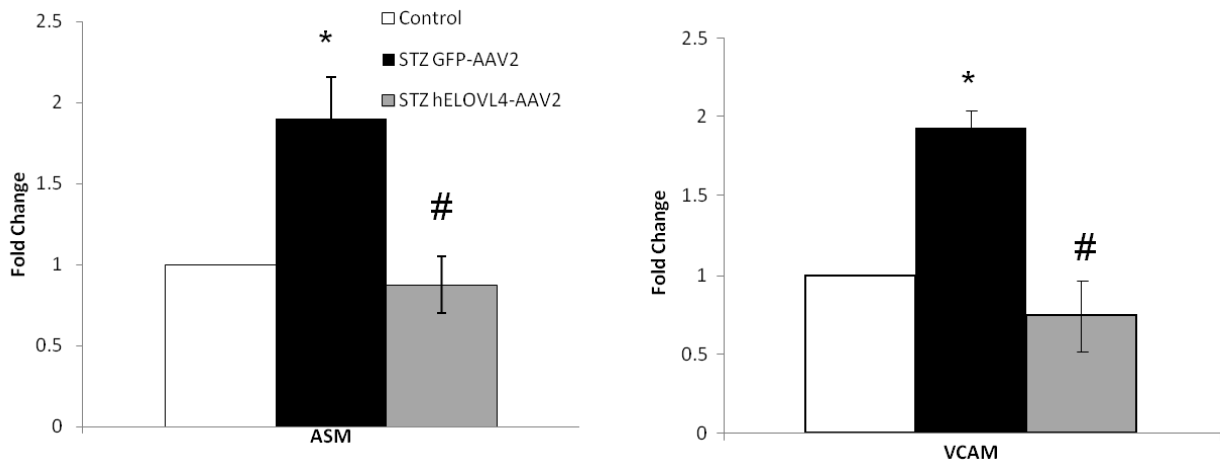


**Figure 5.6. Expression levels of inflammatory markers in retinas of control and diabetic animals.** Total RNA was extracted from retinas of control and diabetic animals after 6-8 weeks of diabetes and analyzed by qPCR. (A) Diabetes induced changes in markers of vascular activation, ASM and VCAM-1.

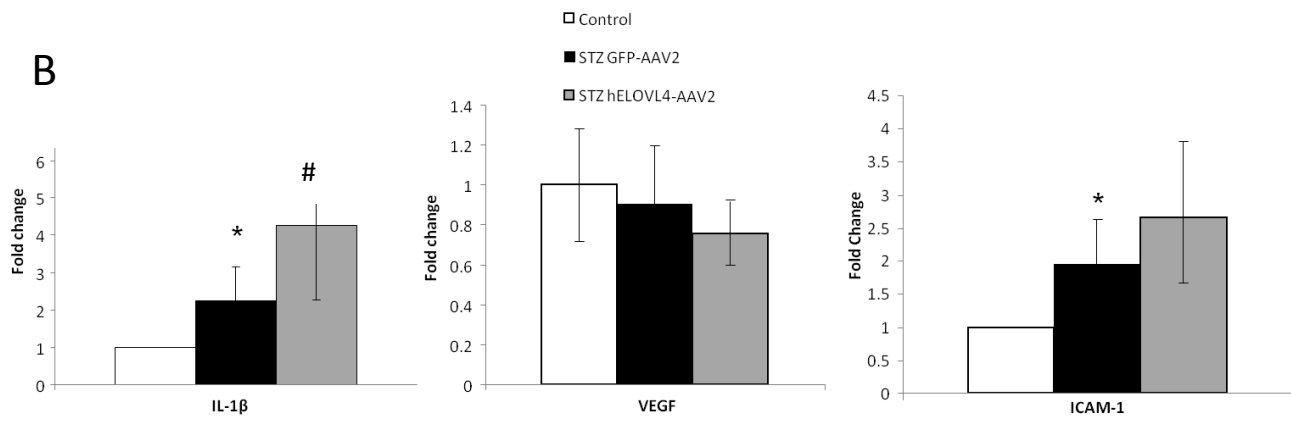


**Figure 5.6 (Continued).** (B) Markers of retinal inflammation, IL-1 $\beta$ , VEGF, and ICAM-1. n=6 retinas per treatment group. Control, white bars. STZ+GFP-AAV2, black bars. STZ+hELOVL4, gray bars. Data are presented as mean  $\pm$  SD. \* indicates statistically different from control, # indicates statistically different from STZ+GFP-AAV2 (P<0.05) as determined by one way ANOVA with post-hoc Tukey test.

A

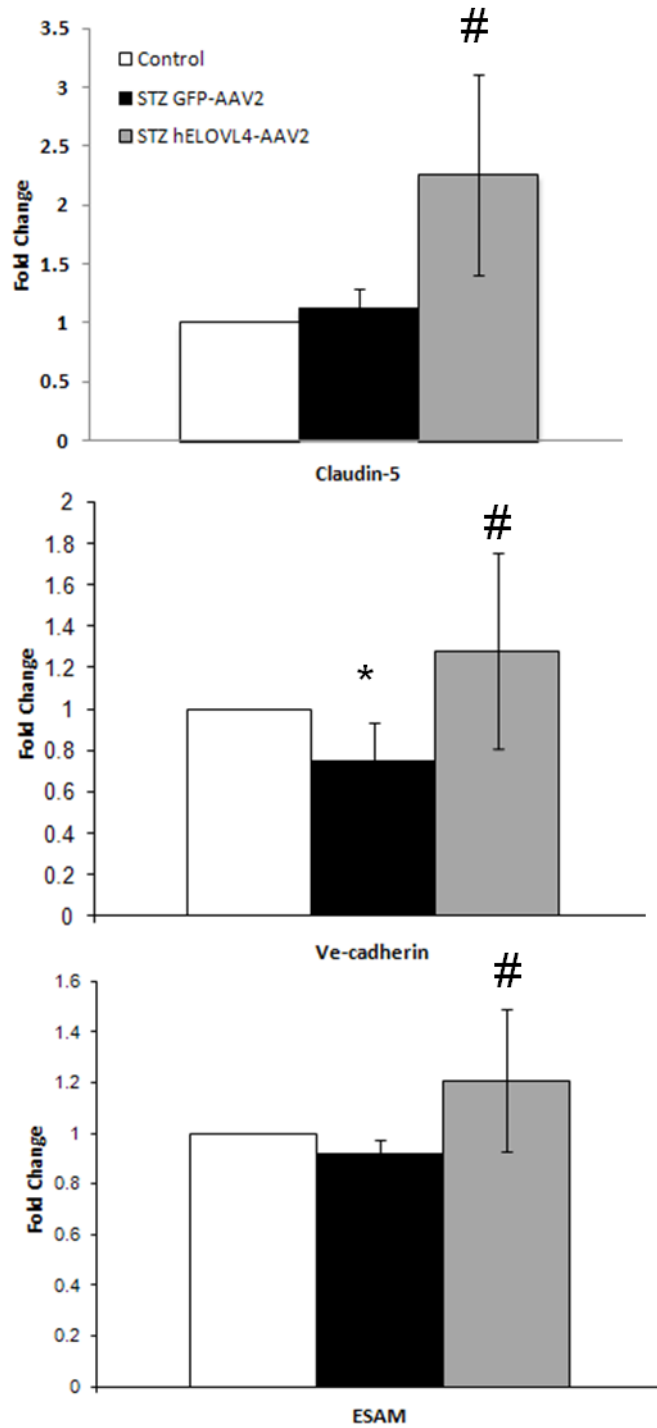


**Figure 5.7. Expression levels of blood-retinal barrier components in retinas of control and diabetic animals.** Total RNA was extracted from retinas of control and diabetic animals after 6 weeks of diabetes and analyzed by qPCR for expression of (A) Claudin-5, Ve-Cadherin, and Esam.

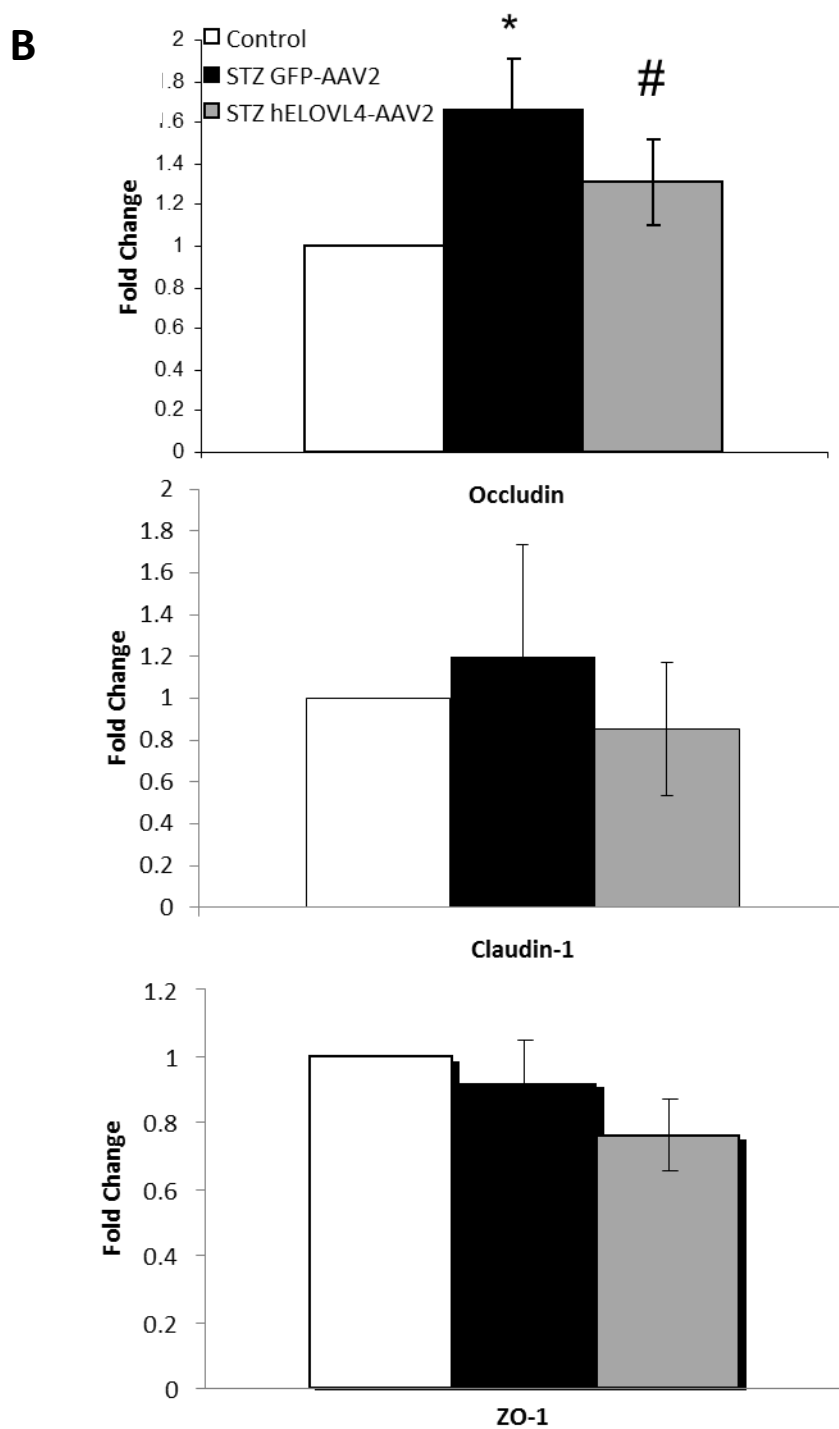


**Figure 5.7 (Continued).** (B) Occludin, Claudin-1 and ZO-1. n=6 per treatment group. Control, white bars. STZ+GFP-AAV2, black bars. STZ+hELOVL4, gray bars. Data are presented as mean  $\pm$  SD. \* indicates statistically different from control, # indicates statistically different from STZ+GFP-AAV2 ( $P < 0.05$ ) as determined by one way ANOVA with post-hoc Tukey test.

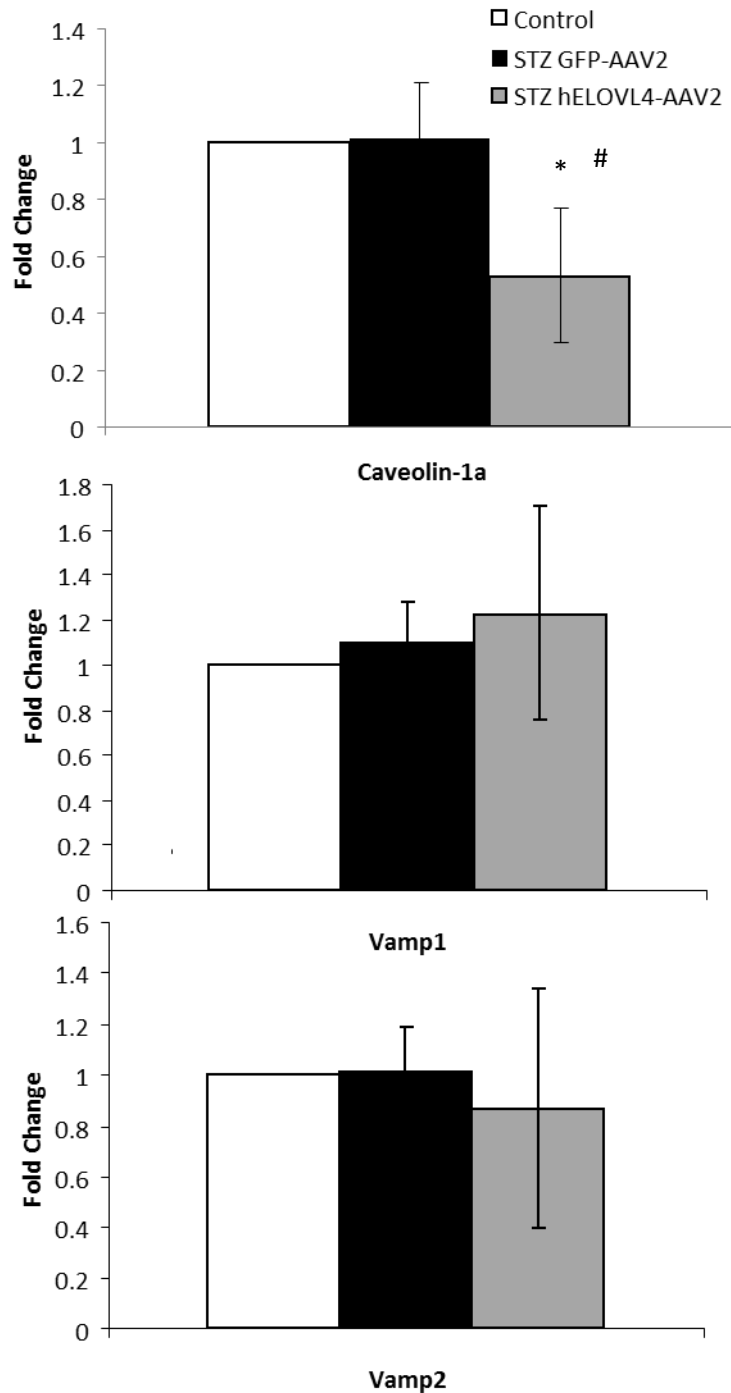


**Figure 5.8. Expression levels of transcellular transport components in retinas of control and diabetic animals.** Total RNA was extracted from retinas of control and diabetic animals after 6 weeks of diabetes and analyzed by quantitative real-time PCR for expression of caveolin-1a, vamp-1, and vamp-2. n=6 per treatment group. Control, white bars. STZ+GFP-AAV2, black bars. STZ+hELOVL4, gray bars. Data are presented as mean  $\pm$  SD. \* indicates statistically different from control, # indicates statistically different from STZ+GFP-AAV2 ( $P < 0.05$ ) as determined by one way ANOVA with post-hoc Tukey test.

## References

## 5.6 References

1. Kern TS: Contributions of inflammatory processes to the development of the early stages of diabetic retinopathy. *Exp Diabetes Res* 2007:95103, 2007.
2. Jousen AM, Poulaki V, Le ML, Koizumi K, Esser C, Janicki H, Schraermeyer U, Kociok N, Fauser S, Kirchhof B, Kern TS, Adamis AP: A central role for inflammation in the pathogenesis of diabetic retinopathy. *Faseb J*, 2004.
3. Antonetti DA, Barber AJ, Bronson SK, Freeman WM, Gardner TW, Jefferson LS, Kester M, Kimball SR, Krady JK, LaNoue KF, Norbury CC, Quinn PG, Sandirasegarane L, Simpson IA: Diabetic retinopathy: seeing beyond glucose-induced microvascular disease. *Diabetes* 55:2401-2411, 2006.
4. Jousen AM, Murata T, Tsujikawa A, Kirchhof B, Bursell SE, Adamis AP: Leukocyte-mediated endothelial cell injury and death in the diabetic retina. *Am J Pathol* 158:147-152, 2001.
5. Jousen AM, Poulaki V, Qin W, Kirchhof B, Mitsiades N, Wiegand SJ, Rudge J, Yancopoulos GD, Adamis AP: Retinal vascular endothelial growth factor induces intercellular adhesion molecule-1 and endothelial nitric oxide synthase expression and initiates early diabetic retinal leukocyte adhesion in vivo. *Am J Pathol* 160:501-509, 2002.
6. Simo R, Hernandez C: Advances in the medical treatment of diabetic retinopathy. *Diabetes Care* 32:1556-1562, 2009.
7. Antonetti DA, Lieth E, Barber AJ, Gardner TW: Molecular mechanisms of vascular permeability in diabetic retinopathy. *Semin Ophthalmol* 14:240-248, 1999.
8. Frey T, Antonetti DA: Alterations to the blood-retinal barrier in diabetes: cytokines and reactive oxygen species. *Antioxid Redox Signal* 15:1271-1284.

9. Garcia-Ramirez M, Villarroel M, Corraliza L, Hernandez C, Simo R: Measuring permeability in human retinal epithelial cells (ARPE-19): implications for the study of diabetic retinopathy. *Methods Mol Biol* 763:179-194.
10. Barber AJ, Antonetti DA: Mapping the blood vessels with paracellular permeability in the retinas of diabetic rats. *Invest Ophthalmol Vis Sci* 44:5410-5416, 2003.
11. Klaassen I, Hughes JM, Vogels IM, Schalkwijk CG, Van Noorden CJ, Schlingemann RO: Altered expression of genes related to blood-retina barrier disruption in streptozotocin-induced diabetes. *Exp Eye Res* 89:4-15, 2009.
12. Tian XF, Xia XB, Xu HZ, Xiong SQ, Jiang J: Caveolin-1 expression regulates blood-retinal barrier permeability and retinal neovascularization in oxygen-induced retinopathy. *Clin Experiment Ophthalmol* 40:e58-66.
13. Ramirez M, Wu Z, Moreno-Carranza B, Jeziorski MC, Arnold E, Diaz-Lezama N, Martinez de la Escalera G, Colosi P, Clapp C: Vasoinhibin gene transfer by adenoassociated virus type 2 protects against VEGF- and diabetes-induced retinal vasopermeability. *Invest Ophthalmol Vis Sci* 52:8944-8950.
14. Trudeau K, Roy S, Guo W, Hernandez C, Villarroel M, Simo R, Roy S: Fenofibric acid reduces fibronectin and collagen type IV overexpression in human retinal pigment epithelial cells grown in conditions mimicking the diabetic milieu: functional implications in retinal permeability. *Invest Ophthalmol Vis Sci* 52:6348-6354.
15. Runkle EA, Antonetti DA: The blood-retinal barrier: structure and functional significance. *Methods Mol Biol* 686:133-148.

16. Lyons TJ, Jenkins AJ, Zheng D, Lackland DT, McGee D, Garvey WT, Klein RL: Diabetic retinopathy and serum lipoprotein subclasses in the DCCT/EDIC cohort. *Invest Ophthalmol Vis Sci* 45:910-918, 2004.
17. Lydic TA, Tikhonenko M, Wang Y, Chen W, Opreanu M, Sochacki A, McSorley KM, Renis RL, Kern T, Jump DB, Reid GE, Busik JV: Remodeling of Retinal Fatty Acids in an Animal Model of Diabetes: a Decrease in Long Chain Polyunsaturated Fatty Acids is Associated with a Decrease in Fatty Acid Elongases Elovl2 and Elovl4. *Diabetes*, 2009.
18. Lydic TA, Renis R, Busik JV, Reid GE: Analysis of Retina and Erythrocyte Glycerophospholipid Alterations in a Rat Model of Type 1 Diabetes. *JALA Charlottesville Va* 14:383-399, 2009.
19. Opreanu M, Lydic TA, Reid GE, McSorley KM, Esselman WJ, Busik JV: Inhibition of cytokine signaling in human retinal endothelial cells through downregulation of sphingomyelinases by docosahexaenoic acid. *Invest Ophthalmol Vis Sci* 51:3253-3263.
20. Opreanu M, Tikhonenko M, Bozack S, Lydic TA, Reid GE, McSorley KM, Sochacki A, Perez GI, Esselman WJ, Kern T, Kolesnick R, Grant MB, Busik JV: The unconventional role of acid sphingomyelinase in regulation of retinal microangiopathy in diabetic human and animal models. *Diabetes* 60:2370-2378.
21. Moon YA, Shah NA, Mohapatra S, Warrington JA, Horton JD: Identification of a mammalian long chain fatty acyl elongase regulated by sterol regulatory element-binding proteins. *J Biol Chem* 276:45358-45366, 2001.
22. Ohno Y, Suto S, Yamanaka M, Mizutani Y, Mitsutake S, Igarashi Y, Sassa T, Kihara A: ELOVL1 production of C24 acyl-CoAs is linked to C24 sphingolipid synthesis. *Proc Natl Acad Sci U S A* 107:18439-18444.

23. Agbaga MP, Brush RS, Mandal MN, Henry K, Elliott MH, Anderson RE: Role of Stargardt-3 macular dystrophy protein (ELOVL4) in the biosynthesis of very long chain fatty acids. *Proc Natl Acad Sci U S A* 105:12843-12848, 2008.
24. Aveladano MI: Phospholipid species containing long and very long polyenoic fatty acids remain with rhodopsin after hexane extraction of photoreceptor membranes. *Biochemistry* 27:1229-1239, 1988.
25. McMahon A, Kedzierski W: Polyunsaturated extremely long chain C28-C36 fatty acids and retinal physiology. *Br J Ophthalmol*, 2009.
26. Aveladano MI: Long and very long polyunsaturated fatty acids of retina and spermatozoa: the whole complement of polyenoic fatty acid series. *Adv Exp Med Biol* 318:231-242, 1992.
27. Poulos A, Sharp P, Singh H, Johnson D, Fellenberg A, Pollard A: Detection of a homologous series of C26-C38 polyenoic fatty acids in the brain of patients without peroxisomes (Zellweger's syndrome). *Biochem J* 235:607-610, 1986.
28. Abcouwer SF, Lin CM, Wolpert EB, Shanmugam S, Schaefer EW, Freeman WM, Barber AJ, Antonetti DA: Effects of ischemic preconditioning and bevacizumab on apoptosis and vascular permeability following retinal ischemia-reperfusion injury. *Invest Ophthalmol Vis Sci* 51:5920-5933.
29. Vasireddy V, Vijayasathya C, Huang J, Wang XF, Jablonski MM, Petty HR, Sieving PA, Ayyagari R: Stargardt-like macular dystrophy protein ELOVL4 exerts a dominant negative effect by recruiting wild-type protein into aggresomes. *Mol Vis* 11:665-676, 2005.
30. Liu A, Chang J, Lin Y, Shen Z, Bernstein PS: Long-chain and very long-chain polyunsaturated fatty acids in ocular aging and age-related macular degeneration. *J Lipid Res* 51:3217-3229.

31. Yu M, Benham A, Logan S, Brush RS, Mandal MN, Anderson RE, Agbaga MP: ELOVL4 protein preferentially elongates 20:5n3 to very long chain PUFAs over 20:4n6 and 22:6n3. *J Lipid Res* 53:494-504.
32. Stachler MD, Bartlett JS: Mosaic vectors comprised of modified AAV1 capsid proteins for efficient vector purification and targeting to vascular endothelial cells. *Gene Ther* 13:926-931, 2006.
33. Petrs-Silva H, Dinculescu A, Li Q, Min SH, Chiodo V, Pang JJ, Zhong L, Zolotukhin S, Srivastava A, Lewin AS, Hauswirth WW: High-efficiency transduction of the mouse retina by tyrosine-mutant AAV serotype vectors. *Mol Ther* 17:463-471, 2009.
34. Ryals RC, Boye SL, Dinculescu A, Hauswirth WW, Boye SE: Quantifying transduction efficiencies of unmodified and tyrosine capsid mutant AAV vectors in vitro using two ocular cell lines. *Mol Vis* 17:1090-1102.
35. Xu X, Zhu Q, Xia X, Zhang S, Gu Q, Luo D: Blood-retinal barrier breakdown induced by activation of protein kinase C via vascular endothelial growth factor in streptozotocin-induced diabetic rats. *Curr Eye Res* 28:251-256, 2004.
36. Vincent JA, Mohr S: Inhibition of caspase-1/interleukin-1beta signaling prevents degeneration of retinal capillaries in diabetes and galactosemia. *Diabetes* 56:224-230, 2007.
37. Antonetti DA, Barber AJ, Khin S, Lieth E, Tarbell JM, Gardner TW: Vascular permeability in experimental diabetes is associated with reduced endothelial occludin content: vascular endothelial growth factor decreases occludin in retinal endothelial cells. Penn State Retina Research Group. *Diabetes* 47:1953-1959, 1998.
38. Cai J, Wu L, Qi X, Li Calzi S, Caballero S, Shaw L, Ruan Q, Grant MB, Boulton ME: PEDF regulates vascular permeability by a gamma-secretase-mediated pathway. *PLoS One* 6:e21164.

39. Harkewicz R, Du H, Tong Z, Alkuraya H, Bedell M, Sun W, Wang X, Hsu YH, Esteve-Rudd J, Hughes G, Su Z, Zhang M, Lopes VS, Molday RS, Williams DS, Dennis EA, Zhang K: Essential role of ELOVL4 in very long chain fatty acid synthesis and retinal function. *J Biol Chem*.
40. Sommer JR, Estrada JL, Collins EB, Bedell M, Alexander CA, Yang Z, Hughes G, Mir B, Gilger BC, Grob S, Wei X, Piedrahita JA, Shaw PX, Petters RM, Zhang K: Production of ELOVL4 transgenic pigs: a large animal model for Stargardt-like macular degeneration. *Br J Ophthalmol* 95:1749-1754.
41. Sandhoff R: Very long chain sphingolipids: tissue expression, function and synthesis. *FEBS Lett* 584:1907-1913.
42. Zadavec D, Tvrdek P, Guillou H, Haslam R, Kobayashi T, Napier JA, Capecchi MR, Jacobsson A: ELOVL2 controls the level of n-6 28:5 and 30:5 fatty acids in testis, a prerequisite for male fertility and sperm maturation in mice. *J Lipid Res* 52:245-255.
43. Delton-Vandenbroucke I, Grammas P, Anderson RE: Polyunsaturated fatty acid metabolism in retinal and cerebral microvascular endothelial cells. *J Lipid Res* 38:147-159, 1997.
44. Chen H, Ray J, Scarpino V, Acland GM, Aguirre GD, Anderson RE: Synthesis and release of docosahexaenoic acid by the RPE cells of prcd-affected dogs. *Invest Ophthalmol Vis Sci* 40:2418-2422, 1999.
45. Jousen AM, Poulaki V, Le ML, Koizumi K, Esser C, Janicki H, Fauser S, Kern TS, Kirchof B, Adamis AP: Long-term leukocyte-mediated vascular pathology in the diabetic retina. *Invest Ophthalmol Vis Sci* 44:U221-U221, 2003.
46. Jousen AM, Poulaki V, Le ML, Koizumi K, Esser C, Janicki H, Schraermeyer U, Kociok N, Fauser S, Kirchhof B, Kern TS, Adamis AP: A central role for inflammation in the pathogenesis of diabetic retinopathy. *Faseb J* 18:1450-1452, 2004.

47. McGuire PG, Rangasamy S, Maestas J, Das A: Pericyte-derived sphingosine 1-phosphate induces the expression of adhesion proteins and modulates the retinal endothelial cell barrier. *Arterioscler Thromb Vasc Biol* 31:e107-115.

48. Wacker BK, Freie AB, Perfater JL, Gidday JM: Junctional protein regulation by sphingosine kinase 2 contributes to blood-brain barrier protection in hypoxic preconditioning-induced cerebral ischemic tolerance. *J Cereb Blood Flow Metab*.

## Methods

*6.1 Materials and reagents*

All solvents used during extraction of lipids and saponified fatty acids were of HPLC grade and were purchased from Fisher and Sigma. Cell culture supplies (DMEM and F12 culture media, antibiotics, fetal bovine serum, and trypsin) were purchased from Invitrogen. Primary antibody against Tubulin was from BD Bioscience. The primary antibody against ELOVL4 used in Chapter IV was from Abcam; the antibody against ELOVL4 for Western blot used in Chapter V was from Protein Tech, and anti-ELOVL4 immunohistochemistry used an antibody from Sigma. IL-1 $\beta$  was purchased from Cayman Chemicals. Other reagents and supplies used and their origins are described in the following sections.

*6.2 Methods***6.2.1 Culture of HREC and RPE cells**

Primary cultures of HREC were isolated from human retinal tissue obtained from the National Disease Research Interchange in Philadelphia, PA, and grown as previously described (1). Passages 3-5 were typically used for the experiments described below. Human RPE (ARPE-19) cells were cultured as previously described (1). Experiments described below used passages 16-18.

**6.2.2 Animals and Induction of STZ diabetes.**

All procedures for the use and care of animals for laboratory research were approved by the All University Committee for Animal Use and Care at Michigan State University. Male Wistar rats weighing 237-283g were made diabetic with a single intraperitoneal injection of 65 mg STZ per kg body weight. Age matched nondiabetic control rats received a single intraperitoneal injection of citrate buffer vehicle (pH 4.5). Diabetes was confirmed by blood glucose higher than 15mM (270 mg/dL) and decrease in the body weight gain. Body weight gains and blood glucose for the control and STZ diabetic groups were monitored biweekly. Three to thirty six weeks after STZ injection the animals were sacrificed under anesthesia (Isoflurane/Vapomatic). The chest cavity was opened to expose the heart, and 5-10 ml of blood was collected by heart puncture into EDTA-containing tubes. The right atrium was carefully snapped to provide drainage and the animals expired from exsanguination.

Age or duration of diabetes of the animals used in each experiment are stated in each dissertation chapter. For each experiment, plasma, red blood cells, buffy coat, liver and eyes were recovered. Rats used in the studies described in Chapters II, IV and V were maintained on Harlan-Teklad laboratory chow (#8640) and water *ad libitum*. In Chapter III, rats were maintained on an identically formulated diet (Purified Rodent Diet #110900 from Dyets, Bethlehem, PA).

Animals used in Chapter III (3-36 weeks of diabetes) were given daily injections of 0-3 units NPH insulin, beginning two weeks after STZ injection, with the dose adjusted as needed to achieve slow weight gain while still allowing hyperglycemia in the 20-25 mM range.

### **6.2.3 Fatty acid composition of the animal diet**

The fatty acid composition of the rat chow was analyzed by reverse phase HPLC (RP-HPLC, see below) and found to be: 16:0, 20.0%; 18:0, 1.8%; 18:1n9, 21.9%; 18:2n6, 50.8%; 18:3n3, 5.6%; 18:3n6, 0.1%; 20:4n6, 0.1%; 20:5n3, 0.4%; 22:5n3, 0.1% and 22:6n3, 0.3%.

#### **6.2.4 Isolation of rat retina**

After sacrificing animals as described above, eyes were enucleated and rinsed three times in ice cold phosphate buffered saline (PBS), opened by a circumferential incision just below the ora serrata, and the anterior segment and vitreous were discarded. With the aid of a dissecting microscope, the retina was gently lifted off the eyecup using an eye spatula, weighed, and snap frozen in liquid nitrogen. Retinas were stored frozen at -80 degrees Celsius until used.

#### **6.2.5 RNA extraction**

Rat tissues were homogenized on ice in Trizol reagent (Invitrogen) using an electric tissue homogenizer, and RNA was isolated according to manufacturer instructions. Cells grown in culture were collected from cell culture plates by scraping in Trizol.

#### **6.2.6 Quantitative real time PCR and primers used in these studies**

Transcript-specific primers were designed using Primer3 software at [http://frodo.wi.mit.edu/cgi-bin/primer3/primer3\\_www.cgi](http://frodo.wi.mit.edu/cgi-bin/primer3/primer3_www.cgi). First strand cDNA was synthesized from isolated tissue or cellular RNA using the SuperScript III RNase H- Reverse Transcriptase (Invitrogen). PCR reactions were performed in triplicate on an ABI 7500 Fast Real-Time PCR system (Applied Biosystems) by combining equal amounts of 2X SYBR GreenER qPCR master mix (Invitrogen) with a mixture of gene-specific primers and diluted cDNA. Prior to use,

optimization experiments were performed to determine the sensitivity and specificity of each primer pair for a gene of interest, and gene expression analysis was subsequently performed using the optimal conditions and cDNA dilutions for each primer pair. Transcripts of interest were normalized to the abundance of cyclophilin. Relative mRNA amounts were calculated using the  $\Delta\Delta CT$  method (User Bulletin 2; Applied Biosystems). Previously unpublished gene-specific primers used in this dissertation are as follows:

Rat Elov14: GAAGTGGATGAAAGACCGAGA (sense) and GCGTTGTATGATCCCATGAA (antisense);

Rat Elov17: TGGCGTTCAGCGATCTTAC and GATGATGGTTTGTGGCAGAG;

Rat IL-6: CCAGGAAATTTGCCTATTGA and GCTCTGAATGACTCTGGCTTT;

Rat VEGF A: GCTCTCTTGGGTGCACTGG and CACCACTTCATGGGCTTTCT;

Rat ICAM-1: CCACCATCACTGTGTATTTCGTT and ACGGAGCAGCACTACTGAGA;

Human ELOVL4: GCACTCAACGACACGGTAGA and GGACCCAGCCACACAAAC;

Human ICAM-1: AGGCCACCCCAGAGGACAAC and CCCATTATGACTGCGGCTGCTA;

Human Cyclophilin: AAGGTCCCAAAGACAGCAGA and CTTGCCACCAGTGCCATTAT.

All other primers for rat elongases, desaturases, and cyclophilin have been described previously in (2). Primers for rat cytokines and acid sphingomyelinase were described in (3; 4). All primers for retinal tight junction and adherens junction genes, caveolin-1, and transcellular transport genes were previously described in (5).

### **6.2.7 Western blot analysis**

Animal tissues and cultured human cells were lysed on ice in protein lysis buffer (50 mM HEPES, pH 7.5, 150 mM NaCl, 1.5 mM MgCl<sub>2</sub>, 1 mM EGTA, 1% Triton X-100, and 10% glycerol) containing freshly added protease inhibitor cocktail (Sigma) and phosphatase inhibitors (1 mM Na<sub>3</sub>VO<sub>4</sub>, 100 μM glycerophosphate, 10 mM NaF, 1 mM Na<sub>4</sub>PPi). Protein concentration in diluted aliquots of protein lysate were measured with the Bio-Rad protein assay (Bio-Rad), according to the manufacturer's protocol, or the Qubit fluorometer (Invitrogen). Proteins were resolved on NuPAGE Novex 10% Bis-Tris polyacrylamide gels (Bio-Rad), transferred to nitrocellulose membranes, and immunoblotted using appropriate primary antibodies followed by infrared secondary antibodies (IRDye; Invitrogen, Molecular Probes). Protein bands of interest were visualized and quantified with the Odyssey infrared imaging system (LI-COR Biosciences, Lincoln, NE).

### **6.2.8 Lipid extraction from retina**

Whole or bisected retinas were placed in an ice-chilled Teflon/glass tissue grinder and homogenized on ice in 50 μL / mg tissue of 40% MeOH (prepared in water). Retina homogenates were then extracted by vortexing for 1 minute in 200 μL / mg tissue of chloroform : methanol (2:1 v / v). After centrifugation at 3000xg for 10 minutes, the lower organic phase was recovered and transferred to a new glass tube. The aqueous upper phase was then re-extracted by vortexing for 1 minute in 200 μL / mg tissue of chloroform and centrifuged as before. The lower organic phase was collected and combined with the lower phase from the first extraction. The pooled organic phases were evaporated under nitrogen. In Chapter IV and Chapter V, dried lipids were re-extracted as described above to remove contaminating aqueous-phase material, and

evaporated again under nitrogen. Dried lipid extracts were resuspended in 50  $\mu\text{L}$  / mg tissue of isopropanol:methanol:chloroform (4:2:1v/v/v) and stored under nitrogen in glass vials with Teflon-lined caps in the dark at  $-80^{\circ}\text{C}$  until further use. Acidification of lipid extracts was omitted as low pH was found to significantly alter retina lipid profiles due to destruction of plasmalogen lipid species.

### **6.2.9 Lipid extraction from liver and plasma**

50  $\mu\text{L}$  plasma or 10 mg of liver were extracted with chloroform-methanol (2:1, v:v) as described above, normalized to sample weight or volume, dried, and resuspended as described above.

### **6.2.10 Lipid extraction from erythrocytes**

Erythrocyte lipids were extracted using a modified method of Rose & Oklander (6) as follows: 100 mg of packed erythrocytes were lysed on ice for 15 minutes in 500  $\mu\text{L}$  of HPLC-grade water, then combined with 6.8 mL of 80% isopropanol, vortexed, and incubated for one hour on ice with occasional mixing. 3.2 mL of 100% chloroform was then added, and the mixture was incubated for one additional hour on ice with occasional mixing. Phases were separated by centrifuging samples for 30 minutes at 2000 x g in a swinging bucket rotor. The lower phase was collected, and the remaining aqueous phase was re-extracted as before with 3.2 mL of 100% chloroform. The lower phases were pooled, dried under nitrogen, and further dried overnight in a speedvac. Lipid extracts were resuspended in 5  $\mu\text{L}$  / mg cells of isopropanol:methanol:chloroform (4:2:1v/v/v) and stored under nitrogen in glass vials with Teflon caps in the dark at  $-80^{\circ}\text{C}$  until further use.

### 6.2.11 Lipid extraction from cultured cells

Cultured HREC and RPE cells were rinsed three times with PBS, and scraped in ice-cold 40% methanol using 250  $\mu\text{L}$  per  $1 \times 10^5$  cells. Cells were lysed by vortexing, and aliquots of cell lysate were used for determination of protein content by Bio-Rad or Qubit protein assays to confirm that equal amounts of cells were being extracted. Cell homogenates were then extracted with 2:1 chloroform:methanol as described for retina, and re-extracted to remove aqueous contaminants carried over during the extraction. Lipid extracts were resuspended in isopropanol:methanol:chloroform (4:2:1v/v/v) using 100  $\mu\text{L}$  /  $1 \times 10^5$  cells.

In some experiments (see Chapter V), specific extraction of sphingolipids from 50% of the total cellular homogenate was used to provide detailed analysis of low-abundance sphingolipids, particularly sphingomyelin. Homogenates were combined with 400  $\mu\text{L}$  of methanol and 250  $\mu\text{L}$  of chloroform and heated at 48 degrees Celsius overnight. 75  $\mu\text{L}$  of 1M potassium hydroxide (prepared in methanol) was added, and samples were heated for two hours at 37 degrees Celsius to destroy glycerolipids. Samples were neutralized with 6  $\mu\text{L}$  of glacial acetic acid, and extracted with 1.0 ml chloroform and 2.0 ml water. After vortexing and centrifugation, the lower phase was collected, and the remaining aqueous phase was re-extracted with 2.0 ml of chloroform. Samples were dried under nitrogen, and re-extracted as described for retina to remove salts added during the alkaline treatment steps. Samples were dried again under nitrogen and resuspended resuspended in isopropanol:methanol:chloroform (4:2:1v/v/v) using 100  $\mu\text{L}$  /  $1 \times 10^5$  cells in the original homogenate. The remaining 50% of the cellular homogenate

was extracted with 2:1 chloroform:methanol as described above under non-alkaline conditions. While the alkaline hydrolysis of glycerolipids enabled detailed examination of sphingomyelin molecular species, little or no differences were observed between the two extraction methods for the analysis of ceramide molecular species.

### **6.2.12 Mass spectrometry conditions for lipid analysis**

Immediately prior to analysis, aliquots of lipid extracts were further diluted in isopropanol:methanol:chloroform (4:2:1 v/v/v) containing 20 mM ammonium hydroxide or 20 mM ammonium acetate. All samples were centrifuged, then loaded into Whatman Multichem 96-well plates (Fisher Scientific) and sealed with Teflon Ultra-Thin Sealing Tape (Analytical Sales and Service). The samples were introduced to a triple quadrupole mass spectrometer (Thermo Scientific model TSQ Quantum Ultra or TSQ Vantage EMR) via a chip-based nano-electrospray ionization (nESI) source (Advion NanoMate, Ithaca, NY) operating in infusion mode using an ESI HD\_A chip, a spray voltage of 1.4 kV, a gas pressure of 0.3 psi and an air gap of 2  $\mu$ L. The ion transfer tube of the mass spectrometer was maintained at 150 °C. All MS and MS/MS spectra were acquired automatically for 2.5-10 minutes at a rate of 500 m/z per second by methods created using Xcalibur software (Thermo). In MS mode, the Q1 peak width was maintained at 0.5 Da. For neutral loss and precursor ion MS/MS scans, the peak widths of both Q1 and Q3 were maintained at 0.5 Da. For product ion scan mode MS/MS experiments, Q1 and Q3 were operated with peak widths of 1.0 Da. The Q2 collision gas pressure was set at 0.5 mtorr. Collision energies were individually optimized for each neutral loss, precursor ion or product ion scan mode MS/MS experiment of interest using commercially available lipid

standards whenever possible. A five point Gaussian smooth was applied to all spectra prior to data analysis.

### 6.2.13 Identification of lipid molecular species by mass spectrometry

Lipid species were initially identified using lipid class-specific neutral loss and precursor ion mode tandem mass spectrometry as described in Chapter II. Mass spectrum peak finding and correction for  $^{13}\text{C}$  isotope effects was performed using the Lipid Mass Spectrum Analysis (LIMSA) v.1.0 software (7) peak model fit algorithm in conjunction with an expanded user-defined database of hypothetical lipid compounds. Assignment of phospholipid acyl chain constituents was achieved by precursor ion scans to monitor for the formation of specific  $m/z$  product ions corresponding to deprotonated fatty acid anions in negative ion mode; these scans identified glycerophospholipids as  $[\text{M}-\text{H}]^-$ ,  $[\text{M}+\text{Cl}]^-$ ,  $[\text{M}+\text{CH}_3\text{CO}_2]^-$  and  $[\text{M}+\text{CH}_3\text{OCO}_2]^-$  ions. Acyl chain constituents of ceramides and other sphingolipids were confirmed where possible by product ion MS/MS analysis of  $[\text{M}+\text{H}]^+$  ions of interest. Assignment of diacylglycerol and triacylglycerol acyl chain constituents was achieved by neutral loss scans to monitor for the loss of  $m/z$  values corresponding to the loss of a fatty acid  $+\text{NH}_3$  from DG and TG  $[\text{M}+\text{NH}_4]^+$  ions in positive ion mode.

### 6.2.14 Quantitation of lipid molecular species by tandem mass spectrometry

Quantitative comparison of differences in lipid ion abundances between control and diabetic retina or erythrocyte samples was performed by two different methods. In Chapter III and Chapter IV, a ‘label free’ method was employed to quantitate GPCho, GPEtn, GPSer and GPIIns lipids identified from retina and erythrocyte extracts from age matched control and diabetic rats, 3-6 weeks post STZ injection, and GPCho and GPEtn lipids identified from retina and erythrocyte extracts from age matched control and diabetic rats, 36 weeks post STZ injection. For the label free method, lipid species were quantified by determining peak areas using the LIMSAs v.1.0 software peak model fit algorithm as described above. Where applicable, peak areas of GPEtn  $[M+H]^+$  and  $[M+Na]^+$  ions of the same lipid molecular species were summed to account for possible variability in the amount of sodium present across samples.

In the ‘internal standard method’, lipids identified from retina and erythrocyte extracts from age matched control and diabetic rats, 3-36 weeks post STZ injection, or cellular lipid extracts from HREC and RPE, were quantitated ratiometrically by comparison with the peak area of a synthetic lipid internal standard of the lipid class of interest. The LIMSAs software peak model fit algorithm was used as described above for peak finding and isotope correction, followed by automated comparison of each isotopically corrected peak area with that of the appropriate internal standard to arrive at an ‘absolute’ value for each identified lipid species. Quantitated values assigned to GPEtn molecular species were additionally corrected for the presence of GPEtn  $[M+Na]^+$  ions, when present, as described above, and ceramide molecular species were corrected for the presence of  $[M+H-H_2O]^+$  ions when present. Concentrations of synthetic internal standards employed for the analysis of specific lipid classes were typically: GPCho(14:0/14:0) (Chapter III) or GPCho(23:0/23:0) (Chapter V), 1.0  $\mu$ M; GPEtn 0.65  $\mu$ M;

GPSer(14:0/14:0), 0.65  $\mu$ M; Ceramide(d18:1/12:0) 8nM for retina lipids, 25-100 nM for HREC and RPE lipids. All synthetic internal standards were acquired from Avanti Polar Lipids. The ceramide internal standard was present in Sphingolipid Internal Standard Mix II (Avanti).

For both methods of lipid quantitation, mass spectra of each lipid extract were initially acquired at a range of different dilutions to determine the dilution range at which linearity in the response of specific lipids was observed, and to ensure that the ratio of specific lipid ion abundances compared to other lipids within the mixture, or compared to an internal standard, remained constant. However, as no attempts were made to quantitatively correct for different ESI responses of individual lipids due to concentration, acyl chain length or degree of unsaturation,(8) or to quantitatively correct for different CID-MS/MS fragmentation efficiencies as a function of precursor ion mass, we report only the relative change in the abundance of the experimentally observed lipids between the control and treatment groups, and not the absolute concentrations.

Measurement of variability introduced by the sample handling steps following lipid extraction was obtained by performing PI m/z 184 and NL m/z 87 CID-MS/MS scans on triplicate dilutions of a given lipid extract, with subsequent comparison of quantitated peak areas across the triplicate dilutions (See Chapter III). Measurement of variability introduced by the instrumentation (i.e., the ion source and mass spectrometer) was obtained by analyzing individual sample dilutions in triplicate as described above.

#### **6.2.15 Analysis of saponified fatty acids by RP-HPLC**

An aliquot of total lipids from tissues or blood fractions was saponified (0.4 N KOH in 80% methanol, 50 degrees C for 1 hr). Saponified fatty acids were acidified and extracted with 4.0 ml diethyl ether, and stored in methanol containing 1 mM butylated hydroxytoluene. Saponified free fatty acids were fractionated and quantitated by reverse phase HPLC (RP-HPLC) using a Shimadzu Prominence System. A linear gradient of 75-100% acetonitrile +0.1% acetic acid was employed over 65 minutes with a YMC J'sphere H80 reverse phase column with a flow rate of 1.0 ml/min. Fatty acids were introduced to the HPLC by injection in methanol and were detected using UV absorbance at 192 nm and evaporative light scatter as previously described (2). Authentic fatty acid standards (Nu-Chek Prep) were used to generate calibration curves for verification and quantification of fatty acids.

#### **6.2.16 Viral Vectors**

Human ELOVL4 cDNA was prepared from RNA isolated from retinal tissue as described above, and used for the construction of an E1 and E3-deleted adenoviral vector with hELOVL4 under control of the CMV promoter (Ad-ELOVL4). An empty vector (Ad-Null) adenovirus was similarly constructed without the hELOVL4 transgene. Adenoviral vectors were diluted in PBS and stored frozen at -80 degrees Celsius until used for cell culture experiments.

Human ELOVL4 or green fluorescent protein (GFP) were also engineered into self-complementary adeno-associated virus serotype 2 vectors containing four capsid Y to F mutations (AAV2 mut quad) (9). hELOVL4 and GFP were placed under control of the strong constitutive truncated chimeric CMV-chicken  $\beta$ -actin (smCBA) promoter. AAV2 mut quad vectors were diluted in Balanced Salt Solution (BSS, Alcon) and stored at -80 degrees Celsius until used for cell culture experiments.

### **6.2.17 Adenoviral infections in RPE cells**

RPE cells were seeded at densities ranging from 250,000 to 500,000 cells per well in 24 well culture plates and allowed to attach overnight in RPE cell culture medium containing 10% fetal bovine serum. The next day, growth medium was switched to RPE cell culture medium containing 2% fetal bovine serum (“infection medium”), and adenoviral particles were added to cell culture wells at multiplicities of infection (MOI) ranging from 50-20,000. Data obtained in Chapter V utilized an MOI of 100, where MOI is defined as number of viral particles per cell. Following overnight infection, cell culture media was removed and cells were washed three times with RPE cell culture medium containing 10% fetal bovine serum. Cells were then grown for 24-60 additional hours, or used for fatty acid or IL-1 $\beta$  treatments as described below.

### **6.2.18 hELOVL4-AAV2 mut quad infections in HREC**

Primary cultures of human retinal endothelial cells (HREC) were seeded at a density of  $1 \times 10^5$  cells/well in 24 well gelatin-coated cell culture plates and allowed to attach overnight. After a two hour incubation in serum-free HREC growth medium, cells were treated with hELOVL4-AAV2 mut quad at an MOI of  $1 \times 10^4$ , or BSS control, where MOI is defined as number of viral genomes/cell. Cells were infected overnight, washed three times with HREC growth medium containing 10% fetal bovine serum, and then cultured a further two to four weeks in HREC growth medium containing 10% fetal bovine serum with or without exogenously added fatty acids as described below.

### **6.2.19 Fatty acid treatments in cultured cells**

For some experiments, RPE and HREC treated with controls, Ad-ELOVL4 adenovirus, or hELOVL4-AAV2 mut quad were supplied with exogenous 20:5n3 (100  $\mu$ M) bound to BSA at a 5:1 molar ratio (as described in (3)). For RPE infected with Ad-Null or Ad-ELOVL4, 20:5n3 was added immediately following removal of virus-containing infection medium and was replenished daily until cells were harvested for lipid analysis. For HREC infected with hELOVL4-AAV2 mut quad, BSA-bound 20:5n3 was added to cell culture wells immediately after removal of virus-containing infection medium. Fresh HREC growth medium containing 100  $\mu$ M 20:5n3 was fed to cells twice per week for two to four weeks, until cells were harvested for lipid analysis. No fatty acid treatments were used in cells undergoing stimulation by pro-inflammatory cytokines (see below).

#### **6.2.20 IL-1 $\beta$ treatment in RPE cells**

Confluent RPE cells grown in 24 well culture plates with or without infection by Ad-Null or Ad-ELOVL4 were switched to RPE growth medium containing 2% fetal bovine serum and incubated overnight. The next day, IL-1 $\beta$  (1ng/ml) or PBS vehicle was added to cells and incubated overnight. Media was aspirated, fresh growth media containing IL-1 $\beta$  was added, and cells were incubated again overnight for a total of 48 hours of IL-1 $\beta$  stimulation (10). Cells were then washed three times in PBS and harvested for RNA isolation and qPCR analysis of ELOVL4 or ICAM mRNA abundance as described above.

#### **6.2.21 Intravitreal injection of AAV2 mut quad vectors in diabetic rats**

Animals were made diabetic by STZ injection as described above. After two weeks of confirmed diabetes, animals were assigned to receive intravitreal injection of GFP-AAV2 mut

quad or hELOVL4-AAV2 mut quad. Diabetic animals were anesthetized under isofluorane, and animals received 2  $\mu\text{L}$  of virus suspended in BSS at  $1 \times 10^9$  viral genomes/ $\mu\text{L}$  for a total of  $2 \times 10^9$  viral genomes delivered. Viral solutions were drawn into sterilized Hamilton 10  $\mu\text{L}$  syringes, and a sterile 30g 1/2 inch needle was used to puncture the sclera and deliver viral vectors under the lens and into the center of the vitreous cavity. For permeability assays, diabetic animals received either GFP-AAV2 mut quad or hELOVL4-AAV2 mut quad in the right eye, and a sham saline injection of BSS in the left (contralateral) eye. This was done to minimize effects of large animal-to-animal variability that were to be expected when measuring retinal vascular permeability in diabetic animals, in addition to the large degree of technical variability typically associated with the assay. Animals were maintained for an additional 4-6 weeks following intravitreal injections before being sacrificed for tissue analysis as described above, or used for assessment of retinal vascular permeability (below.)

#### **6.2.22 Assessment of retinal vascular permeability**

Control or diabetic rats receiving intravitreal injections of saline and AAV2 mut quad vectors were anesthetized under isofluorane, and injected in the tail vein with 1.0 ml of a 25 mg/ml solution of fluorescein isothiocyanate (FITC) conjugated BSA (Sigma) in sterile PBS. Animals were maintained in the dark in warm cages for two hours. Animals were quickly weighed and anesthetized again under isofluorane. The chest cavity was opened and blood was collected directly from the left ventricle into a heparinized syringe. A drop of blood was used to assess blood glucose concentration with a glucometer (AccuCheck Compact Plus), and the remainder of the blood was centrifuged to separate and collect plasma. Animals were then perfused through the left ventricle with 150 ml of a solution of 1% formaldehyde in PBS warmed

to 37 degrees Celsius. Fixed eyes were enucleated and retinas were dissected out, weighed, homogenized in lysis buffer (PBS containing 0.1% Triton X-100 and 0.1% sodium azide), centrifuged, and 200  $\mu$ L of retinal lysate was assayed on a fluorescence plate reader using excitation at 485 nm and emission at 520 nm. Retinal fluorescence per mg tissue weight was normalized to fluorescence of plasma from the same animal per hour of FITC-BSA circulation time.

### **6.2.23 Retinal histology and immunohistochemistry**

Enucleated eyes from control or diabetic rats receiving intravitreal injections of AAV2 mut quad vectors were fixed for at least 48 hours in formalin (Fisher), followed by automated vacuum infiltrating tissue processing to paraffin block. Blocks were sectioned on a rotary microtome at 4-5 microns and placed on 3-aminoalkylethoxysilane coated slides, and dried overnight at 56 degrees Celsius. Slides were de-paraffinized, hydrated with distilled water, and adjusted to pH 7.4 with TBST (Scytek Labs). All slides were stained on a Dako Autostainer (Dako Norther America) as previously described (4). Primary antibody against GFP or ELOVL4 (Sigma) was applied at an optimized dilution in normal antibody diluent (Scytek) for 1 hour, and visualized as previously described (4) with Vector Nova Red peroxidase chromagen (Vector). Slides were removed from the autostainer and counterstained with Gill 2 Hematoxylin, differentiated, dehydrated, cleared, and coverslipped with synthetic mounting medium. Color images were obtained with a Micropublisher 3.3 Megapixel Color Digital Camera.

### **6.2.24 Statistical analysis**

All data are expressed as mean  $\pm$  standard deviation. Unless otherwise stated, comparison of data from two independent groups of animals (i.e. control and diabetic) or cell culture

treatments was performed with a two-tailed T-test with significance established at  $P < 0.05$ . Comparison of three independent groups in Chapter V was performed by one-way ANOVA with post-hoc Tukey test using GraphPad Prism 4.0 software (GraphPad).

## References

### 6.3 References

1. Busik JV, Mohr S, Grant MB: Hyperglycemia-induced reactive oxygen species toxicity to endothelial cells is dependent on paracrine mediators. *Diabetes* 57:1952-1965, 2008.
2. Wang Y, Botolin D, Xu J, Christian B, Mitchell E, Jayaprakasam B, Nair MG, Peters JM, Busik JV, Olson LK, Jump DB: Regulation of hepatic fatty acid elongase and desaturase expression in diabetes and obesity. *J Lipid Res* 47:2028-2041, 2006.
3. Opreanu M, Lydic TA, Reid GE, McSorley KM, Esselman WJ, Busik JV: Inhibition of cytokine signaling in human retinal endothelial cells through downregulation of sphingomyelinases by docosahexaenoic acid. *Invest Ophthalmol Vis Sci* 51:3253-3263.
4. Opreanu M, Tikhonenko M, Bozack S, Lydic TA, Reid GE, McSorley KM, Sochacki A, Perez GI, Esselman WJ, Kern T, Kolesnick R, Grant MB, Busik JV: The unconventional role of acid sphingomyelinase in regulation of retinal microangiopathy in diabetic human and animal models. *Diabetes* 60:2370-2378.
5. Klaassen I, Hughes JM, Vogels IM, Schalkwijk CG, Van Noorden CJ, Schlingemann RO: Altered expression of genes related to blood-retina barrier disruption in streptozotocin-induced diabetes. *Exp Eye Res* 89:4-15, 2009.
6. Rose H, Oklander M: An improved method for the extraction of lipids from human erythrocytes. *J. Lipid. Res.* 6:428-431, 1965.
7. Haimi P, Uphoff A, Hermansson M, Somerharju P: Software tools for analysis of mass spectrometric lipidome data. *Anal Chem* 78:8324-8331, 2006.
8. Koivusalo M, Haimi P, Heikinheimo L, Kostainen R, Somerharju P: Quantitative determination of phospholipid compositions by ESI-MS: Effects of acyl chain length, unsaturation, and lipid concentration on instrument response. *J. Lipid Res.* 42:663-672., 2001.
9. Petrs-Silva H, Dinculescu A, Li Q, Min SH, Chiodo V, Pang JJ, Zhong L, Zolotukhin S, Srivastava A, Lewin AS, Hauswirth WW: High-efficiency transduction of the mouse retina by tyrosine-mutant AAV serotype vectors. *Mol Ther* 17:463-471, 2009.
10. Garcia-Ramirez M, Villarroel M, Corraliza L, Hernandez C, Simo R: Measuring permeability in human retinal epithelial cells (ARPE-19): implications for the study of diabetic retinopathy. *Methods Mol Biol* 763:179-194.

## Chapter VII

### Conclusions and Future Perspectives

#### *7.1 Conclusions*

The studies presented in this dissertation illustrate the feasibility and advantages of utilizing lipidomics analysis for the identification of novel pathways of lipid metabolism that contribute to disease progression. By refining and advancing “shotgun” lipidomics strategies to overcome significant limitations in the methods used for the analysis of complex lipids, we have conducted the first detailed studies of retinal lipid profiles under normal physiological conditions, and identified downregulation of fatty acid elongase ELOVL4 as an important component of aberrant retinal lipid metabolism that contributes to the earliest stages of the development of diabetic retinopathy.

We demonstrated the utility of a shotgun tandem mass spectrometry platform involving the use of multiple lipid class-specific precursor ion and neutral loss scan mode experiments to analyze diverse classes of complex lipids from normal rat retina, without the need for chromatographic separation of lipid extracts prior to analysis. We used complementary analysis of protonated or deprotonated lipid precursor ions, or their various ionic adducts, in conjunction with novel precursor ion or neutral loss scan mode MS/MS experiments to identify rat retina lipid molecular species that were not detected using MS/MS experiments often employed in lipidomics analyses. We found that this method of retinal lipid analysis enabled detailed and sensitive studies of retinal lipid molecular species and facilitated the identification of their lipid headgroups, backbones, and fatty acyl constituents. This technique enabled the compilation of

the first extensive catalog of rat retina lipid components observed under normal physiological conditions.

Furthermore, we evaluated the potential utility of a 'label free' method for quantification of lipid molecular species and compared the results to those obtained using an 'internal standard' method, and performed this comparison using lipid extracts from retina and erythrocytes. Equivalent results were obtained with each quantitative method in the analysis of retina lipid species. However, the two methods resulted in appreciable differences in the quantitation of erythrocyte lipids. The data indicated that label-free methods of lipidome quantification may be feasible when rigorous optimization of analytical parameters has first been performed.

The application of our general lipidomics approach to a rat model of type 1 diabetes enabled novel insights into the progression of diabetic retinopathy. Overall dysregulation of retina glycerophospholipid abundances was observed in diabetic animals at both 6 weeks and 36 weeks after induction of diabetes. Additionally, retina glycerophosphocholine lipids exhibited increased incorporation of the short chain polyunsaturated fatty acid linoleic acid (18:2n6) and decreased relative levels of long chain fatty acids arachidonic acid (20:4n6) and docosahexaenoic acid (22:6n3) at both 6 weeks and 36 weeks of diabetes. Subsequent studies of retina lipids from type 1 diabetic rats at 3-6 weeks of diabetes revealed additional reductions of glycerophosphocholine species containing unique 32:6n3 fatty acids.

We established that the diabetes induced aberrations of retinal lipid profiles were associated with dysregulation of retina-specific fatty acid remodeling. The expression levels of fatty acid elongases and desaturases observed in retina did not correlate with those observed in liver, and the retinal lipid profile did not correlate with plasma or liver fatty acid content.

Moreover, diabetes resulted in decreased retinal expression of fatty acid elongases ELOVL2 and ELOVL6, and induced dramatic repression of the most abundant retinal elongase, ELOVL4. No effect of diabetes was observed on retinal desaturase expression. The decrease in elongase expression in diabetic retina relative to controls was associated with increased markers of retinal inflammation, including increased levels of the cytokines IL-6 and VEGF, and the adhesion molecule ICAM-1.

AAV2 mediated gene delivery of ELOVL4 to diabetic retina revealed a previously unknown role of this elongase in maintenance of the blood-retinal barrier. ELOVL4 completely prevented diabetes induced activation of the retinal vascular endothelium, increased the expression of endothelial tight junction and adherens junction components, and decreased the expression of caveolin-1 relative to diabetic retinas transduced with green fluorescent protein. These molecular effects of ELOVL4 activity blunted a diabetes-induced increase in retinal vascular permeability, indicating that gene delivery of ELOVL4 prevented early diabetic vascular lesions. Overexpression of ELOVL4 in cell culture models of the blood-retinal barrier indicated that ELOVL4 is primarily involved in the production of ceramide species containing very long chain fatty acids, but does not affect the production of phospholipids containing very long chain polyunsaturated fatty acids in these cells. This modulation of sphingolipid metabolism by ELOVL4 was sufficient to block cellular activation in response to stimulation by the pro-inflammatory cytokine IL-1 $\beta$ , suggesting that ceramides containing ELOVL4-derived fatty acids may protect the blood retinal barrier from the damaging effects of diabetes induced retinal inflammation.

Overall, these data indicate that dysregulation of retinal lipid metabolism contributes to the pathogenesis of diabetic retinopathy by disrupting ELOVL4-mediated sphingolipid

metabolism (See Figure 7.1). Modulation of retinal very long chain sphingolipid metabolism in diabetes may represent a novel target pathway that contributes significantly to the development of diabetic visual impairment.

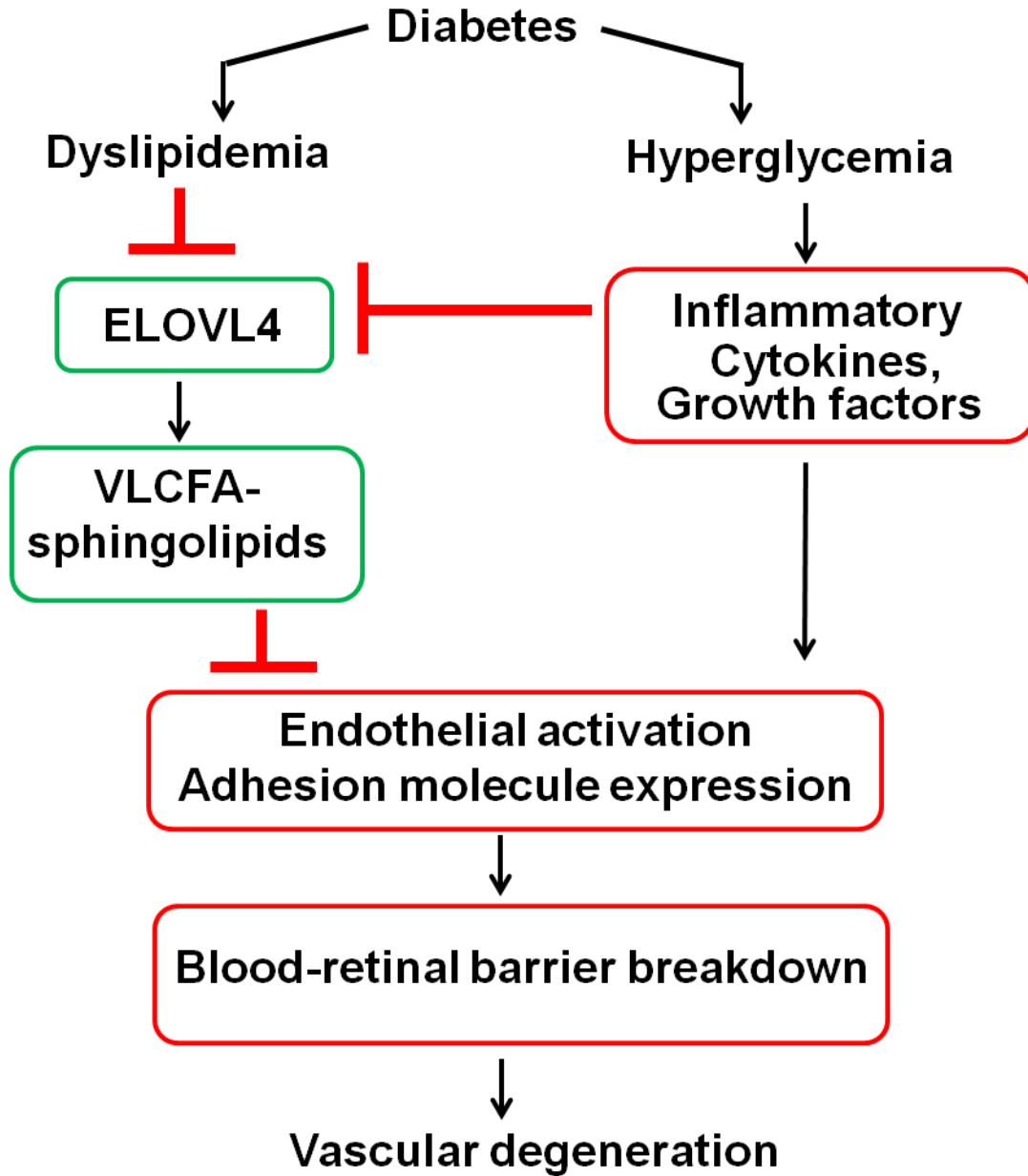


**Figure 7.1. Revised schematic of the proposed role of ELOVL4 in the development of diabetic retinal lesions.** The proposed scheme applies to cells that comprise the blood-retinal barrier, as effects of ELOVL4 activity in non-BRB cells were not addressed by the studies in this Dissertation.

## 7.2 Future Perspectives

While our initial studies of retinal lipid metabolism in diabetes encompassed both short (3-6 weeks) and long (36 weeks) durations of experimental diabetes, the experiments demonstrating a role for ELOVL4 in maintenance of vascular integrity were all performed exclusively in animals with a short duration of diabetes. While induction of vascular permeability by diabetes is an excellent marker for early retinal vascular degeneration, an important next step would be to perform similar intravitreal delivery of ELOVL4 in diabetic animals and maintain the animals for up to 8 or 9 months of diabetes. This would allow assessment of the formation of acellular degenerate capillaries in ELOVL4 transduced retinas as compared to retinas transduced with a control virus. Currently, the formation of acellular retinal capillaries represents the most advanced stage of diabetic retinopathy that can be observed in animals. Furthermore, it should be noted that retinal delivery of ELOVL4 in diabetic animals resulted upregulation of at least one pro-inflammatory cytokine, IL-1 $\beta$ , relative to diabetic retinas transduced with GFP. As the long term consequences of increased IL-1 $\beta$  in the retina could be pathological, an important next step in future ELOVL4 studies should be to delineate which retinal cell types may respond to ELOVL4 upregulation by increasing cytokine production. Perhaps a more viable long term strategy for testing the therapeutic potential of AAV2 mediated ELOVL4 normalization would include placing ELOVL4 under an endothelial (such as *ve-cadherin*) or blood-retinal barrier specific promoter (such as *zo-1* or *occludin*) in order to circumvent potential adverse effects of overexpressing ELOVL4 in certain retinal cell types.

Elucidation that ELOVL4 promotes blood retinal barrier integrity is a novel and interesting outcome of the studies presented in this dissertation. At present, however, the precise mechanism(s) of this phenomenon are not clear. Experiments in cell culture models of the blood-

retinal barrier strongly suggest that ELOVL4 plays a key role in retinal sphingolipid metabolism. Vascular and perivascular upregulation of ELOVL4 in diabetic retinas prevented upregulation of acid sphingomyelinase, an important enzyme of catabolic sphingolipid metabolism and a key responder in retinal vascular inflammatory signaling that is known to play a central role in the induction of retinal vascular damage in several models of retinal injury. It is conceivable that upregulation of *de novo* very long chain ceramide metabolism by ELOVL4 counter-regulates catabolic formation of shorter chain ceramide by acid sphingomyelinase. This idea could be tested by overexpressing or inhibiting expression of ELOVL4 or acid sphingomyelinase and assessing expression levels and/or activity of the opposing enzyme. However, it would be important to establish that C26:0 ceramide plays a cellular role distinct from that of sphingomyelinase-generated ceramide species. Perhaps this could be achieved by performing subcellular fractionation of various cellular membranes and membrane microdomains, and determining localization of the various ceramide species. At present, determining precise physiological and biochemical roles of individual ceramide molecular species remains one of the greatest challenges in the fields of sphingolipid metabolism and analysis.

Ceramides serve many cellular purposes and may be degraded to simpler sphingolipid metabolites that serve as important signaling molecules; alternatively, ceramides may function as building blocks for more complex sphingolipid molecules such as highly glycosylated sialic-acid bearing sphingolipids collectively termed gangliosides. Very long chain fatty acids have been described in retinal gangliosides through indirect methods that did not enable verification of the structures of the purported molecules. Nonetheless, gangliosides have been shown to interact with and negatively regulate the function of numerous receptors involved in cellular signaling processes, including VEGF receptor 2. Thus it is conceivable that ELOVL4 derived ceramide

species are funneled into complex gangliosides that impact signaling through the VEGF receptor, or receptors for pro-inflammatory cytokines. To test this idea, ganglioside-enriched lipid extracts from control or ELOVL4 overexpressing cells could be analyzed for ganglioside content of very long chain fatty acids. Cells could be challenged with VEGF and phosphorylation of the VEGF receptor could be monitored as a readout of receptor activity. Changes in ganglioside fatty acid content induced by ELOVL4 could then be correlated with any observed impact on VEGF receptor activity.

The apparent similarity of ELOVL4 activity in the inner and outer blood-retinal barriers suggests that ELOVL4 could be explored as a therapeutic intervention in retinal disorders beyond diabetic retinopathy. The “wet” or neovascular form of age-related macular degeneration involves impairment of the outer blood-retinal barrier with neovascular growth of choroidal blood vessels into the retina. Delivery of ELOVL4 by either subretinal or intravitreal routes could theoretically be tested for pro-barrier and anti-neovascular effects; however, the availability of appropriate animal models of this disease is currently limited.

ELOVL4 is expressed in many tissues outside of the eye. Yet the function of ELOVL4 in most tissues has not been explored. Considerable expression of ELOVL4 has been noted in brain, and brain microvascular endothelial cells form a blood-brain barrier that is absolutely required for proper brain function. Exploration of possible roles ELOVL4 in maintenance of the blood brain barrier could shed new light on factors that promote the viability of the critical partition between the brain and the systemic circulation.

A role for ELOVL4 in the endogenous production of very long chain saturated or monounsaturated fatty acids has been described in skin and, in the present study, in retinal

microvasculature and retinal pigment epithelium. However, ELOVL4 function to date has been primarily associated with production of VLCPUFA in retinal neurons and testes, and VLCPUFA have only been described in retina, testes, and brain. It is therefore very possible that ELOVL4 predominantly functions in the mediation of sphingolipid metabolism and/or production of very long chain saturated and monounsaturated fatty acids in most of the tissues in which it is expressed. This possibility opens up multiple avenues of potential future investigation of the tissue and cell-specific biochemical functions of ELOVL4, and its role in mammalian physiology.